PhD-FSTM-2025-051
The Faculty of Science, Technology
and Medicine

DISSERTATION

Defence held on 7 May 2025 in Esch-sur-Alzette to obtain the degree of

DOCTEUR DE L'UNIVERSITÉ DU LUXEMBOURG EN BIOLOGIE

by

Elle Wilson

Born on November 29th 1994 in County Durham, United Kingdom

MULTI-OMICS CHARACTERIZATION OF THE SNCA-A53T MUTATION IN PARKINSON'S DISEASE

Dissertation defence committee

Prof. Dr. Alexander Skupin (Supervisor) - *University of Luxembourg*

Prof. Dr Anne Grünewald (Chair) - *University of Luxembourg*

Prof. Dr Carole Linster (Internal Member) - *University of Luxembourg*

Prof. Dr Benno Schwikowski (External Member) - *Institut Pasteur*

Dr. Julia Fitzgerald (External Member) - *Hertie-Institute, Tubingen*

Declaration

I hereby declare that, the contents and organization of this dissertation constitute my own original work and does not compromise in any way the rights of third parties, including those relating to the security of personal data.

Elle Wilson, Wednesday 4th June, 2025

Acknowledgements

First and foremost, I would like to express my sincere gratitude to Alex for his support and guidance throughout the PhD. I am certain I could not have had a better mentor, and I am truly grateful for his advice and encouragement.

I also want to thank my colleagues in the ICS group for creating a collaborative and supportive working environment. In particular, Corrado Ameli was instrumental in developing the bioinformatics pipelines used in this project, and I greatly appreciate his help.

A special thanks to Prof. Dr. Anne Grünewald for being a member of my CET panel, providing valuable feedback during my yearly reviews, and agreeing to chair my defense. I also want to acknowledge Patrycja Mulica, Lucia Gallucci, and Ilaria Goglia from the Grünewald lab, who always took the time to offer their expertise and support, despite their own busy schedules.

I am also grateful to Prof. Dr. Benno Schwikowski for serving on my CET panel and for hosting me during my secondment at the Institut Pasteur. It was a great experience, and I had the opportunity to work with an excellent group of researchers.

I would also like to thank the other members of my PhD defense jury, Prof. Dr. Carole Linster and Dr. Julia Fitzgerald, for taking the time out of their schedules to be part of the defense panel.

Finally, I am extremely grateful to my family for their continued support.

Financial Support

This work is part of the TRANSYS Personalized Medicine Doctoral Training Unit funded by the the European Union's Horizon 2020 Research and Innovation Programme under grant agreement number 860895.

Abstract

Parkinson's disease (PD) is the second most prevalent neurodegenerative disorder in the ageing population. At the cellular level, PD is characterized by the progressive loss of midbrain dopaminergic neurons (mDA) in the substantia nigra (SN) and by the pathological accumulation of alpha-synuclein (α-syn) in surviving neurons. Alpha-synuclein is a small synaptic protein encoded by the *SNCA* gene. Although its precise role remains elusive, it is thought to promote synapse integrity and facilitate dopamine neurotransmission. Mutations in *SNCA*, such as the pathogenic *SNCA*-A53T variant, have been linked to familial PD, yet their exact contribution to disease pathogenesis remains unclear. This is partly due to the widespread effects of *SNCA* mutations, which influence a diverse range of cellular pathways, complicating efforts to define underlying disease mechanisms.

To address this challenge, we employed a longitudinal multi-omics approach to characterize *SNCA*-A53T cells at seven timepoints (days 0, 6, 15, 21, 30, 40, and 60) throughout the differentiation from induced pluripotent stem cells (iPSCs) into mature mDA neurons. In parallel, we generated mDA neurons from an age- and sex-matched control. By integrating single-cell RNA sequencing (scRNA-seq), bulk proteomics, and metabolomics, we aimed to explore how *SNCA*-A53T-induced signatures manifest over time. Additionally,

we evaluated mitochondrial bioenergetics to assess the functional consequences of the mutation.

Our results reveal that the *SNCA*-A53T mutation leads to early and progressive transcriptional and functional alterations, particularly affecting mitochondrial respiration. We identify changes in oxidative phosphorylation (OXPHOS), potentially driven by the downregulation of key regulators such as *DNAJC15* and *CHCHD2*. In addition to alterations in mitochondrial bioenergetics, we observe perturbations in calcium dynamics and mitophagy, further supporting the role of mitochondrial dysfunction in disease progression. These findings provide new insights into early molecular impairments associated with the *SNCA*-A53T mutation and highlight shared pathogenic mechanisms in PD.

Contents

List of Tables

List of Figures

Abbreviations

6-OHDA 6-hydroxydopamine

α-syn Alpha-synuclein

ALP Autophagy-lysosomal pathway

BBB Blood-brain barrier

CBD Corticobasal degeneration

CMA Chaperone-mediated autophagy

CNS Central nervous system

CSF Cerebrospinal fluid

DAP Differentially expressed protein

DaT Dopamine Transporter

DBS Deep brain stimulation

DEG Differentially expressed gene

EHT Eicosanoyl-5-hydroxytryptamide

EPS Extrapyramidal system

ERAD ER-associated degradation

ER Endoplasmic reticulum

ETC Electron transport chain

FC Fold change

GABA Gamma-aminobutyric acid

GO Gene Ontology

GPi Globus pallidus internus

GWAS Genome-wide association studies

iPSC Induced pluripotent stem cell

KEGG Kyoto encyclopedia of genes and genomes

KO Knockout

L-dopa Levodopa

LB Lewy body

LC-MS Liquid chromatography-mass spectrometry

LID Levodopa-induced dyskinesia

LN Lewy neurite

MAM Mitochondria-associated membranes

mDA Midbrain dopaminergic

MPTP 1-methyl-4-phenyl-1,2,3,6-tetrahydropyridine

MSA Multiple systems atrophy

nAChRs Nicotinic acetylcholine receptors

NAC Non-amyloid-β component

OMM Outer mitochondrial membrane

PCR Quantitative real-time PCR

PD Parkinson's disease

PSP Progressive supranuclear palsy

PTP Permeability transition pore

ROS Reactive oxygen species

SAA Seed amplification assay

scRNA-seq Single-cell RNA sequencing

SNpc Substantia nigra pars compacta

SNpr Substantia nigra pars reticulata

TBI Traumatic brain injury

ThT Thioflavin T

TH Tyrosine hydroxylase

UPR Unfolded protein response

UPS Ubiquitin-proteasome system

VAMP2 Vesicle-associated membrane protein 2

VTA Ventral tegmental area

CHAPTER 1

Introduction

Parkinson's Disease (PD) is the fastest-growing neurological condition globally, affecting around 1-2% of the population over the age of 65 [1]. At the cellular level, PD is characterized by the progressive loss of midbrain dopaminergic (mDA) neurons in the substantia nigra (SN) and by the intracellular accumulation and aggregation of alpha-synuclein (α-syn) into Lewy bodies (LBs) [2]. This neurodegenerative cascade leads to a marked depletion of striatal dopamine, resulting in the cardinal motor features of PD, including tremor, bradykinesia, rigidity, and postural instability [3]. Beyond the classical motor phenotype, PD also presents with a heterogeneous spectrum of non-motor symptoms such as cognitive decline, autonomic dysfunction, and sleep disturbances, which often precede motor dysfunction by years to decades [4, 5]. Owing to its multifactorial nature, which encompasses both genetic and environmental factors, the pathogenesis of PD is highly complex and still largely unknown. Despite intensive research efforts, there remains no treatment that can cure or halt disease progression. As such, the current therapeutic paradigm centers around alleviating motor symptoms, often by chronic dopamine replacement. Given the increasing global prevalence of PD and lack of curative therapies,

there is a pressing need to understand the biological processes that underpin disease initiation and progression. To address this challenge, we employ a multi-omics approach to investigate the PD-associated mutation *SNCA*-A53T. By combining transcriptomic, proteomic, and metabolomic analyses, we aim to identify critical drivers of disease pathology and uncover potential targets for therapeutic intervention.

1.1 Parkinson's disease: a general overview

In this chapter, the current literature on PD is introduced, with a particular focus on α-syn pathology. More specifically, Section 1.1 explores key aspects of the disease, including epidemiology, pathogenic hallmarks, clinical features, etiology, and modeling strategies. Section 1.2 then provides a comprehensive review of α-syn's role in PD pathogenesis.

1.1.1 Epidemiology

The epidemiology of PD shows pronounced variations in age, sex, geographical location, and ethnicity [6]. PD prevalence increases substantially with age, affecting approximately 1–2% of the population over the age of 65 and 4–5% of the population over the age of 85 [1, 7, 8]. Notably, only 5% of cases are diagnosed before the age of 60 [7]. For this reason, age is considered the biggest risk factor for PD development [7]. Moreover, with an increasing ageing population, it has been projected that the PD burden will exceed 12 million cases by 2040 [9].

Sex also has a significant impact on disease prevalence, as the risk of developing PD is twice as high in males as in females [10]. This disparity may be partially explained by the neuroprotective effects of estrogens [11]. It has been demonstrated that lifetime exposure to higher levels of estrogen correlates with a significantly lower PD risk in females [12]. In addition, similar PD disease rates are observed between males and post-menopausal females [10]. Despite this, females have increased mortality and accelerated disease progression compared to males [13, 14].

The incidence of PD also varies based on geographical location, with higher prevalence rates found in Europe, North America, and South America, compared to Arabic and Asian countries [15, 5]. Furthermore, it has been predicted that the PD disease burden will shift from industrialized Western nations to developing nations in the East [9].

While understanding and predicting these trends are crucial, PD epidemiological studies are often confounded by methodological limitations and by the complexity of the disease [16]. Additionally, there is a considerable lack of data from certain geographical locations such as Latin America, Southeast Asia, and Africa [17]. These factors make it challenging to provide robust predictions of the global PD burden [18, 6].

1.1.2 Pathogenic hallmarks

At the cellular level, PD is linked to a diverse range of neuropathological hallmarks reflecting its intricate pathophysiology. A principal feature of PD is the progressive degeneration of mDA neurons in the substantia nigra pars compacta (SNpc), which project to the dorsal putamen and striatum [3]. As mDA neurons are the primary site for the synthesis and release of dopamine in the central nervous system (CNS), their loss results in a substantial reduction in dopamine levels in the striatum, which in turn impairs key motor pathways [19]. By the time motor symptoms emerge, approximately 30% of mDA neurons have already been lost [20]. This figure increases to 60-80% in the advanced stages of disease, correlating with the severity of motor dysfunction and disease duration [21, 22, 20].

Dopamine is a neurotransmitter crucial for movement, learning, and attention [23]. After being synthesized in the cytosol, dopamine can interact with excitatory D1 receptors and inhibitory D2 receptors within the extrapyramidal system (EPS) [24, 25]. Key components of the EPS include the basal ganglia, which contains the globus pallidus internus (GPi) and the substantia nigra pars reticulata (SNpr) [26]. These structures form part of larger circuits in the thalamus and cortex [27].

In PD, the loss of dopamine in the striatum causes hyperactivation of the GPi and SNpr, resulting in excess gamma-aminobutyric acid (GABA) release and increased thalamic inhibition [28, 26, 22]. This in turn impairs the ability of the thalamus to activate the frontal cortex, culminating in decreased motor output [26, 29]. In addition to degeneration of dopaminergic pathways, PD pathology can also affect cholinergic, glutamatergic, adenosinergic, GABAergic, and serotonergic signaling networks [15, 30]. Dysfunction in these systems may account for the broad range of non-motor symptoms that often precede motor impairments [31, 5].

Another prominent hallmark of PD is the pathological aggregation of α-syn, a presynaptic protein that forms LBs and Lewy neurites (LNs) [2]. LBs are spherical, eosinophilic inclusions (5-25 µm in diameter) found in neuronal cell bodies [32]. LNs, on the other hand, are thread-like aggregates of α-syn found within neuronal processes [33–35]. This deposition of α-syn is central to PD, as these toxic aggregates can have a detrimental effect on physiological cellular functions (discussed in detail in Section 1.2).

The aggregation of α-syn is also fundamental to disease progression. It is thought that α-syn pathology initially begins in one location and spreads through the connectome to vulnerable regions in the nervous system [36]. Thus far, two primary models have been proposed for the propagation of α-syn pathology: the brain-first and body-first models. In the brain-first model, pathology starts in the brain, most likely in the olfactory bulb or amygdala, and subsequently spreads to the peripheral autonomic nervous system [36]. Conversely, in the body-first model, α-syn pathology starts in the peripheral nervous system and spreads to the brain stem [36]. This model is well represented in Braak's staging system, which states that in the pre-symptomatic stages of PD, Lewy pathology originates at peripheral sites, such as the gut [37, 38]. From there, it propagates via the vagus nerve and the dorsal motor nucleus of the vagus to the brainstem. As the disease progresses, LBs and LNs are detected in the SNpc, locus coeruleus, and raphe nuclei. Finally, in the advanced stage of the disease, Lewy pathology spreads to the neocortex and limbic regions, correlating with more severe motor and cognitive symptoms. Given the diversity of PD phenotypes, it is likely that pathology is initiated in a brain-first or body-first manner in different subsets of patients.

1.1.3 Clinical features

1.1.3.1 Symptoms

It is increasingly recognized that PD progresses through three distinct phases: the preclinical, prodromal, and clinical stages [39]. The preclinical phase is marked by progressive neurodegenerative pathology that precedes the emergence of clinical symptoms [40]. However, this stage remains poorly understood, and as a result, no reliable biomarkers have yet been identified to detect patients at this early point of the disease [40]. Despite this, the preclinical phase is often considered a critical therapeutic window, as interventions targeting early pathological changes may offer the greatest potential to alter disease progression [41].

Following this, the prodromal phase is characterized by the onset of non-motor symptoms, which can precede motor impairments by years or even decades [4, 5]. These symptoms include depression, cognitive decline, and urinary dysfunction, all of which are considered pre-diagnostic indicators of PD risk [42]. As it is postulated in the body-first model that PD pathology affects the peripheral autonomic nervous system, olfactory system, and structures of the lower brainstem before reaching the SN [43, 44, 37]. This may somewhat underlie the presentation of hyposmia, constipation, and sleep disorders that also develop in many patients [45, 5].

Finally, the clinical phase is characterized by the onset of hallmark motor symptoms, including bradykinesia (slowness of movement), rigidity (increased muscle tone), and resting tremors [46]. As the disease advances, postural instability frequently develops, further impacting mobility and increasing the risk of falls [46]. While the progression of functional deficits and disability is rather variable, symptoms typically progress over a period of years to decades [47]. Within 5-10 years of symptom onset, many patients experience significant gait disturbances and impairments in balance, and by 15 years, hallucinations and dementia often manifest [48, 49].

Although life expectancy is only moderately reduced compared to age-matched controls, long-term survival remains limited, with approximately 70% of patients

not surviving beyond 15 years after disease onset [50, 51]. The leading cause of mortality in PD is pneumonia, which is often secondary to aspiration caused by immobility [52]. Additionally, complications such as falls and infections contribute significantly to mortality rates [53].

1.1.3.2 Diagnosis

The diagnosis of PD is often challenging, as its clinical features overlap with atypical syndromes like multiple systems atrophy (MSA), progressive supranuclear palsy (PSP), and corticobasal degeneration (CBD) [54]. Given that there is no definitive test, PD diagnosis is largely based on the presentation of bradykinesia in combination with rigidity or resting tremor [55]. Early symptoms are often asymmetric, and the absence of atypical symptoms (e.g., cerebellar dysfunction, cortical sensory loss, vertical supranuclear palsies, or acute autonomic dysfunction) is considered indicative of a PD diagnosis [5]. Moreover, a positive response to dopamine-based treatments, such as Levodopa, can be used to further discriminate PD from other forms of parkinsonism [56, 57].

Functional and structural neuroimaging can also be used to aid diagnosis [58]. Whilst brain magnetic resonance imaging (MRI) findings are typically unremarkable in PD patients, they can be useful in excluding structural irregularities and secondary causes of parkinsonism, such as normal pressure hydrocephalus and demyelinating lesions [59, 60]. In addition, dopamine transporter (DAT) single photon emission computed tomography (SPECT) can be used to assess dopaminergic pathways *in vivo* [60]. The DAT protein plays an important role in the reuptake of dopamine from the synaptic cleft and can therefore be used to infer the extent of presynaptic dopaminergic dysfunction [61]. DaT SPECT is reported to have a specificity of 92% and sensitivity of 90% in differentiating idiopathic PD from secondary parkinsonian conditions [62, 63].

More recently, the α-synuclein seed amplification assay (α-syn-SAA) has been proposed as a promising tool for the early detection of PD [64]. This test exploits the intrinsic self-propagating nature of misfolded α-syn, which acts as a seed to template pathological conformations in native α-syn proteins [65]. In the α-syn-SAA, cerebrospinal fluid (CSF) samples are mixed with monomeric

C-terminally tagged α-syn, which serves as a substrate for any misfolded α-syn seeds present in the sample [66, 67]. The samples are then subject to alternating cycles of fibril elongation and fragmentation. After several cycles, if the sample contains aggregated α-syn, the concentration will have increased exponentially, which can be detected by amyloid-specific dyes like Thioflavin T (ThT) [66]. It has been demonstrated that the α-syn-SAA has a sensitivity ranging between 85-93% and a specificity of 95-98% for diagnosing PD [68]. However, the α-syn-SAA comes with some caveats. Firstly, the aggregation of α-syn is not exclusive to PD and occurs in other age-related neurodegenerative disorders, as well as various lysosomal and pediatric neurometabolic disorders [69–71]. Secondly, α-syn-SAA positivity correlates poorly with disease severity and progression rate [72]. As such, the α-syn-SAA should be used in conjunction with other diagnostic techniques [68].

1.1.3.3 Treatments

Treating PD symptoms effectively requires careful consideration of pharmacological options and their limitations. As dopamine itself is unable to cross the blood-brain barrier (BBB), it cannot be used to substitute depleted levels in the striatum [73]. Whilst various pharmacological options exist (outlined in Tab. 1.1), since its introduction in 1961, Levodopa (L-Dopa), a precursor of dopamine, has been the "gold standard" for treating PD-associated motor impairments [74–76].

L-Dopa is an isomer of the amino acid D, L-dihydroxyphenylalanine [77]. After crossing the BBB, L-Dopa is taken up by remaining dopaminergic neurons and converted to dopamine by the aromatic L-amino acid decarboxylase (DOPA decarboxylase) enzyme [78, 79]. To prevent peripheral breakdown and increase CNS bioavailability, L-Dopa is administered with a peripheral decarboxylase inhibitor, such as Carbidopa or Benserazide [80, 81].

During the first few years of treatment, L-Dopa is very effective in managing motor symptoms, as surviving dopaminergic neurons store exogenous dopamine and maintain normal signaling in the striatum [82]. However, long-term L-Dopa use is associated with levodopa-induced dyskinesia (LID), which refers to purposeless, involuntary movements [83]. LID occurs in approximately 80%

of PD patients, with 30% of patients experiencing it after only three years of treatment [84, 85, 82]. LID typically occurs in the advanced stages of disease, when dopaminergic neurons and dopamine transporters are severely depleted, which prevents dopamine from being stored [86]. Consequently, more dopamine is simultaneously released from each L-Dopa dose, leading to overstimulation of dopamine receptors in the putamen [87, 82]. Furthermore, the pulsatile administration of L-Dopa causes dopamine levels to fluctuate between peaks and troughs [88]. These fluctuations result in "on" periods with improved motor control and "off" periods characterized by the re-emergence of motor symptoms [89].

Type of Drug	**Brand Name(s)**	**Mode of Action**
Dopamine agonists	Pramipexole Ropinirole Rotigotine	Mimic dopamine action by directly stimulating dopamine receptors.
Monoamine Oxidase B Inhibitors (MAO-B)	Selegiline Safinamide	Inhibit MAO-B, reducing dopamine breakdown and increasing availability.
Catechol-O-Methyltransferase Inhibitors (COMT)	Tolcapone Entacapone	Inhibit COMT, prolonging levodopa's effectiveness.
Anticholinergic drugs	Trihexyphenidyl Benztropine	Block acetylcholine to restore dopamine-acetylcholine balance.
Amantadine	Symmetrel	Increases dopamine release and inhibits its reuptake.
Dopamine releasers	Apomorphine	Stimulates dopamine release and acts as a dopamine agonist.

Table 1.1 Pharmacological treatments for PD. Summary of pharmaceutical agents currently available for the treatment of PD [90].

For patients with advanced motor fluctuations who do not respond well to pharmacological treatments, deep brain stimulation (DBS) is a possible alternative [91]. During DBS, electrodes are used to deliver high-frequency stimulation to the subthalamic nucleus and GPi, which are hyperactive in PD [92, 93]. This stimulation de-synchronizes the abnormal firing of neurons in these regions [94]. Although DBS has proven effective in treating motor fluctuations, it carries the risk of post-surgical complications [95, 96]. As a result, DBS is not suitable for all patients, instead, individualized screening is used to stratify potential candidates. For instance, patients below the age of 70 years, who demonstrate a positive response to L-Dopa, are typically considered appropriate candidates [97]. Conversely, DBS is not recommended for patients with cognitive impairment, active depression, or axial dominant symptoms [97]. Intriguingly, it has also been suggested that genetic profiling can be used to estimate DBS outcomes. More specifically, phenotypes associated with the PD-linked mutations *LRRK2* and *PRKN* demonstrate more favorable outcomes than those associated with *GBA* mutations, although current evidence is still rather scarce [97].

More recently, there has been a growing interest in therapies targeting aggregated α-syn. One approach has been to use active and passive immunization strategies [98, 99]. Active immunization involves stimulating the immune system to produce antibodies against α-syn [100]. Examples of this are PD01A and PD03A developed by AFFiRiS. In phase 1 clinical trials, these synthetic peptide-based antibodies have demonstrated clear immune responses against α-syn-targeted epitopes [101]. However, neither has been evaluated in phase 2 or phase 3 clinical trials.

In contrast, passive immunization involves the direct administration of antibodies designed to target α-syn aggregates [100]. One such example is the monoclonal antibody, Prasinezumab, designed by Roche. Prasinezumab selectively binds to and inhibits the intracellular spread of α-syn, mitigating its neuronal toxicity [102]. In a multicenter, randomized, double-blind trial (PASADENA study), Prasinezumab failed to meet its primary endpoint. Despite this, post hoc analysis indicated a slower rate of disease progression in the treated cohort, prompting an extension of the trial until 2026 [100]. In parallel, a phase 2b trial (PADOVA study) was conducted to evaluate its efficacy in

slowing disease progression [103]. However, in December 2024, it was reported that the PADOVA study also failed to meet its primary endpoint [104].

Despite advancements in therapies targeting α-syn, as of yet none of the molecules tested in phase 2 trials have met their primary endpoints [100]. This highlights the challenges associated with the timing and design of treatments. PD pathology begins years before the onset of clinical symptoms, and by the time of diagnosis, extensive neuronal degeneration has already occurred [105, 100, 106]. Therefore, the majority of patients enrolled in trials may already have irreversible damage [107]. It is also possible that targeting α-syn aggregates alone may not be sufficient to alter the disease course. PD pathogenesis involves diverse pathways, and understanding the mechanisms by which α-syn impacts these pathways is crucial to therapy design [108].

1.1.4 Genetics

It is generally regarded that PD arises from a complex interplay between genetic and environmental influences [109]. Approximately 85-90% of PD cases are sporadic, with no known cause [110]. This unclear etiology makes investigating idiopathic cases very challenging. On the other hand, 10-15% of cases are attributed to genetic variants [110]. Although mutations account for only a small proportion of PD cases, much of our understanding of PD at the cellular level is based on investigating these causative genes [111]. Moreover, as monogenic and sporadic PD display a significant overlap in neuropathology and clinical features, this further exemplifies their relevance for understanding PD pathogenesis [112, 113].

Since the discovery of the first PD-related gene, *SNCA*, in 1997, over 20 causative genes have been identified [114–117]. Additionally, more than 100 genetic loci have been recognized as risk factors contributing to PD development [118, 119]. Genes associated with PD are categorized with the prefix "*PARK*" and numbered sequentially based on their order of discovery [120]. Among the genes postulated to confer disease risk, six genes have been unequivocally linked to heritable monogenic PD [120]. *SNCA (PARK1/4)* and *LRRK2 (PARK8)* are linked to autosomal-dominant forms, while mutations in *PRKN (PARK2)*,

PINK1 (PARK6), *DJ-1 (PARK7)*, and *ATP13A2 (PARK9)* underlie autosomal recessive forms [120].

Despite affecting diverse pathways, many of these mutations converge on common pathogenic hallmarks, including mitochondrial dysfunction, impaired proteostasis, and dopaminergic neuron loss. This overlap suggests common drivers of disease pathology. However, understanding how these pathways interact and their relative contribution to PD phenotypes remains a key challenge in PD research. Below a description of the most extensively studied genetic risk factors are given, alongside descriptions of their roles in these shared processes.

1.1.4.1 LRRK2 (PARK8)

Leucine-Rich Repeat Kinase 2 (*LRRK2*) mutations represent the most common known cause of late-onset PD, with a mutation frequency estimated at 2-40% in different populations [120, 121]. Patients harbouring *LRRK2* mutations typically present with a mid-to-late onset, characterized by a slow progression and milder phenotype [120, 122]. Over 50 different missense and nonsense mutations have been identified to date, with the G2019S mutation being the most frequent and well-characterized [120, 123, 124]. The *LRRK2* gene consists of 51 exons and encodes a large multidomain protein involved in cytoskeletal function, synaptic transmission, and protein expression [125, 126]. Although the precise pathogenic mechanisms of *LRRK2*-mediated PD are unknown, it is thought that hyperactivation of LRRK2 kinase activity may play a role [120]. Consistent with this, many *LRRK2* mutations occur in the catalytic domain [127, 128]. This hyperactivation is associated with impaired intracellular trafficking and perturbed mitochondrial dynamics [127, 129, 130].

1.1.4.2 SNCA (PARK1/4)

Mutations in the *SNCA* gene, which encodes α-syn, are the second most common cause of autosomal-dominant PD [131]. Collectively, they are estimated to account for 1-2% of familial cases and 0.2% of sporadic cases [131–133]. These mutations include missense variants (p.A53T, p.A30P, p.E46K, p.G51D, p.H50Q, p.A53E, and p.A53V) and increased copy numbers (duplication or

triplication of the *SNCA* locus) [134–136]. Whilst both are very rare, copy number variants are more frequent than missense variants, with 60 affected families identified to date [137]. Despite involving the same gene, the clinical phenotype can differ markedly between *SNCA* variants [138].

The p.A53T (*SNCA*-A53T) mutation, where alanine in position 53 is substituted with threonine, is often regarded as one of the most prevalent and clinically severe *SNCA* point mutations [139, 135]. On average, p.A53T carriers exhibit parkinsonian symptoms 10 years earlier than other missense variants [140, 141]. Notably, most patients harbouring the p.A53T mutation present with parkinsonian symptoms before the age of 50, which is correlated with a rapid and aggressive disease course [142]. In contrast, the p.A30P and p.E46K mutations have a later onset, typically between 50-60 years of age [142]. Patients carrying p.E46K mutations often present with severe parkinsonism and dementia, while those carrying p.A30P mutations have a milder phenotype [134]. More recently, the novel pathogenic variant p.G51D has been identified in four families [143]. This variant is of particular interest due to its early onset, which ranges from 19-60 years, and its overlapping features with MSA [144].

Genomic duplication and triplication of the *SNCA* gene also cause early-onset PD [145]. Interestingly, it has been demonstrated that gene dosage correlates with symptom onset. In a meta-analysis, patients carrying three *SNCA* copies (heterozygous *SNCA* duplication) had a mean age of onset at 44 years, whereas those with four *SNCA* copies (homozygous *SNCA* duplication, or *SNCA* triplication) had an average onset of 34 years [146, 147]. This gene dosage effect is also mirrored in the clinical phenotype, as *SNCA* triplications are associated with severe parkinsonism, accompanied by cognitive impairments [148]. In contrast, *SNCA* duplications have a more varied presentation, ranging from benign forms that resemble idiopathic PD to more aggressive, early-onset forms of disease [142].

Mutations in *SNCA* contribute to PD pathology either by directly increasing α-syn protein levels or by altering its aggregation propensity. These alterations promote the formation of toxic α-syn confirmations, which have detrimental effects on various physiological cell functions (discussed in detail in Section 1.2).

1.1.4.3 PRKN (PARK2)

Mutations in the second identified PD gene, *PRKN*, represent the most common cause of autosomal recessive PD [149, 147]. Notably, *PRKN* mutations account for up to 77% of familial cases that present before the age of 30 years [150]. *PRKN* encodes an E3 ubiquitin ligase (Parkin) that facilitates the addition of ubiquitin molecules to lysine residues on target proteins [151, 152]. This post-translational modification targets proteins for proteasomal degradation [153]. Importantly, Parkin functions in a shared signalling pathway with the PD-associated protein *PINK1* to detect and remove defective mitochondria [154]. In response to mitochondrial damage, PINK1 accumulates on the outer mitochondrial membrane (OMM), this recruits and activates cytosolic Parkin [155]. Parkin then ubiquitinates OMM proteins, triggering the selective removal of damaged mitochondria (referred to as mitophagy) [155, 156]. Mutations in *PRKN* impair the catalytic activity of the Parkin protein, which in turn affects mitochondrial quality control [157].

1.1.4.4 PINK1 (PARK6)

PTEN-induced putative kinase 1 (*PINK1*) mutations are attributed as the second leading cause of autosomal recessive early-onset PD, with mutation frequencies estimated at 1-9% [158]. The majority of these mutations are either missense or nonsense, with exon 7 harboring the largest number of identified variants [120, 159]. The *PINK1* gene encodes a 581 amino acid protein kinase, which, as mentioned, is essential for mitochondrial quality control [160]. Mutations in *PINK1* reduce the phosphorylation or kinase activity of the PINK1 protein, which compromises mitophagy [154]. This in turn leads to the accumulation of dysfunctional mitochondria, ultimately resulting in cell death [154].

1.1.4.5 DJ-1 (PARK7)

The *DJ-1* gene encodes a 189-amino-acid protein that functions as both an antioxidant and an oxidative stress sensor [161, 162]. Mutations in *DJ-1* are

associated with early-onset autosomal recessive PD [163]. Although rare, around 10 point mutations and exonic deletions have been identified, accounting for approximately 1-2% of early-onset cases [147, 164]. Many of the identified *DJ-1* variants, such as p.L166P, p.E64D, p.M26I, and p.D149A, disrupt the protein's dimeric structure, resulting in misfolding [165, 166]. This loss of function compromises its antioxidant activity, which in turn contributes to PD-associated phenotypes [167].

1.1.4.6 Other PD-linked variants

In addition to these well-established PD genes, genome-wide association studies (GWAS) have identified numerous other genes associated with an increased disease risk, such as *MAPT, GBA, NAT2, INOS2A, GAK, HLA-DRA,* and *APOE* [120]. Among these, *GBA* is one of the most well-validated PD risk genes [168]. *GBA* encodes a lysosomal enzyme β-glucocerebrosidase, which plays a crucial role in glycolipid metabolism [169]. Mutations in *GBA* cause Gaucher's disease, which results from an accumulation of glucocerebroside [170]. Strikingly, *GBA* mutations significantly increase the risk of developing PD, with studies reporting their presence in 8–14% of autopsy-confirmed PD cases [171, 172]. In addition, linkage analyses have identified numerous other genes considered potentially causative of PD (*UCHL1, OMI/HTRA2, GYGYF2, PLA2G6,* and *DNAJC13*) [173, 120]. However, as many of these variants result in phenotypes inconsistent with classical PD, the true extent of their involvement is uncertain [120]. Other PD-associated mutations include *CHCHD2, PSAP*, and *VPS35*, which occur at very low frequencies in Mendelian PD [116].

1.1.5 Environmental risk factors

The link between environmental exposures and PD was first made in 1983 with the synthetic neurotoxin, 1-methyl-4-phenyl-1,2,3,6-tetrahydropyridine (MPTP) [174]. Individuals injecting synthetic heroin contaminated with MPTP developed severe parkinsonism [175, 176]. It was later discovered that MPTP is a mitochondrial complex I inhibitor that selectively damages the nigrostriatal system [177].

Since then, it has been established that exposure to herbicides and pesticides is also linked to PD [178]. Commonly used pesticides, such as paraquat and rotenone, have both been associated with an increased disease risk [179, 180]. Using animal models, it has been established that rotenone inhibits complex I of the mitochondrial respiratory chain, leading to the selective damage of dopamine neurons in the SNpc [179, 181–183]. Whereas paraquat exposure results in the excessive generation of free radicals and oxidative stress-induced dopaminergic degeneration [184, 182, 185, 186]. These findings suggest that increased exposure to pesticides can induce neurodegeneration that closely mimics PD features. This may also somewhat explain why rural living and agricultural work are considered risk factors for PD [187–189].

In addition to environmental risk factors, lifestyle choices can also influence the risk of developing PD. Over the last 50 years, more than 40 studies have investigated the link between cigarette smoking and reduced PD prevalence [190, 46]. A large-scale study conducted in 30,000 individuals reported a 30% lower risk of PD in smokers compared with non-smokers and found that disease risk was inversely correlated with the amount of tobacco smoked [191]. Moreover, this risk was higher in current versus former smokers. It is hypothesized that this protective effect may be due to nicotine, which can activate mDA neurons through direct and indirect mechanisms [192]. More specifically, nicotine can activate nicotinic acetylcholine receptors (nAChRs) on the soma of dopaminergic neurons and can also regulate terminal dopamine signaling in the forebrain [193, 194]. However, as tobacco contains thousands of chemicals, it is difficult to decipher the extent to which each compound plays a neuroprotective role [195].

Besides cigarette smoking, coffee consumption is also associated with a reduced PD risk and slower disease progression [196, 197]. This neuroprotective effect may be linked to specific bioactive compounds in coffee. A recent study found that caffeine and eicosanoyl-5-hydroxytryptamide (EHT), two major coffee components, act synergistically to enhance the activity of protein phosphatase 2A (PP2A). This in turn dephosphorylates α-syn and protects against α-syn-mediated toxicity [198].

Whilst a variety of environmental compounds and lifestyle factors have been linked to PD, no single causative agent accounts for a large number of cases

[199]. This may be partly due to genetic heterogeneity, as individuals exposed to the same environmental factors are affected differently, resulting in disease phenotypes that are unique to individual patients [200]. This exemplifies the complex nature of PD, in which genetic background and environmental exposures contribute to disease pathology in a multi-synergic and poorly defined manner [110].

1.1.6 PD disease modeling

Given the aforementioned complexity of disease etiology, developing accurate models of PD is crucial to advancing our understanding of the disease and to developing effective treatments [201]. One major obstacle in PD research is the lack of available brain tissue [111]. Moreover, as around 60% of neurons have already been lost by the time of diagnosis, postmortem samples often represent end-stage disease [202, 111]. As it is becoming increasingly accepted that PD has a preclinical phase, beginning up to several years before clinical symptoms, it is therefore necessary to design models capable of investigating early pathophysiological cascades [203, 7, 107].

One approach commonly employed to model PD involves the administration of neurotoxins to rodents and non-human primates [204]. Local or systemic administration of neurotoxins such as 6-hydroxydopamine (6-OHDA) and MPTP disrupts complex I activity. This results in oxidative stress and a dose-dependent reduction in dopaminergic neurons in the SNpc and the putamen [205, 206, 105]. Consequently, neurotoxin administration leads to the destruction of the nigrostriatal system and motor symptoms that closely resemble those seen in human PD [176, 207].

One limitation of neurotoxin models is their ability to mimic α-syn pathology [208]. Whilst MPTP exposure has been shown to produce intraneuronal inclusions in primates, this feature is not replicated in mice [209–211]. Similarly, administration of 6-OHDA does not result in α-syn aggregates, which limits its ability to fully recapitulate the PD phenotype [212, 213]. In addition to this, the acute nature of pathology caused by neurotoxin administration does not accurately depict the progressive, age-dependent changes observed in most

patients [214, 176]. As such, these models can only be utilized to study the late, chronic, dopamine-depleted stage of the disease.

Another widely used approach for modeling PD is the use of transgenic animals, most commonly transgenic mice. This technology enables gene deletion, overexpression, and mutation *in vivo* [215]. In PD research, transgenic overexpression of autosomal dominant genes (*SNCA* and *LRRK2*) and knockout (KO) of autosomal recessive genes (*PRKN*, *PINK1*, and *DJ-1*) are commonly employed [216]. While transgenic models have broadened our overall understanding of PD, one limitation is that very few transgenic models exhibit a slow and progressive degeneration pattern [215, 217]. Furthermore, animal lines carrying the same mutation often display inconsistent phenotypes, which has been attributed to transgene insertion [218]. More recently, the MitoPark mouse model has been developed [219]. In this model, a slow and progressive SNpc degeneration is achieved through inactivation of mitochondrial transcription factor A [220]. While not without limitations, the MitoPark model is a step towards recapitulating human disease.

In addition to animal models, recent advances in iPSC technology have provided a unique tool to investigate PD. This approach involves the forced expression of Yamanaka factors (Oct3/4, Sox2, Klf4, and c-Myc) [221, 222]. These transcription factors facilitate the conversion of somatic cells into iPSCs, which have the ability to differentiate into any cell type [223]. In the case of PD, iPSCs carrying disease-associated mutations can be derived from patient fibroblasts and differentiated into mDA neurons [111, 52]. This provides an unlimited supply of disease-relevant cells while preserving the patient's original genomic background [224]. Since 2011, more than 385 iPSC neuronal cell lines have been generated from PD patients carrying different genetic mutations [110]. These studies have demonstrated the ability of iPSC models to recapitulate features of human disease such as reduced striatal dopamine release, α-syn pathology, neurodegeneration, and mitochondrial dysfunction [110]. Moreover, as patient-derived neuronal models more accurately capture the human genetic background, this in turn may increase the possibility of translational success.

1.2 Alpha-synuclein & PD

As discussed in Section 1.1, α-syn pathology is a hallmark of PD, and mutations in *SNCA*—the gene encoding α-syn—can significantly influence disease progression (Section 1.1.4.2). Given the focus of this thesis on the *SNCA*-A53T mutation, the following section will provide a detailed examination of the physiological structure and function of α-syn, the mechanisms underlying its aggregation, and the implications of these processes for PD pathology.

1.2.1 Alpha-synuclein structure & physiological function

A-syn is a small protein (14 kDa) expressed at high levels in the central and peripheral nervous systems [225, 226]. It has long been described as an intrinsically disordered monomer, meaning it lacks a fixed three-dimensional structure in aqueous solution [227, 228]. However, endogenous α-syn also exists as a folded tetramer that exhibits little to no aggregation potential [229]. These monomeric and tetrameric forms exist in dynamic equilibrium, and changes in this balance can have wide-ranging effects on aggregation propensity [230, 100].

Structurally, α-syn is composed of three regions, each having unique biological functions (Fig. 1.1) [100]. The N-terminal domain (residues 1-60) is a positively charged region, consisting of imperfect repeats that form an amphipathic helix [231–233]. This region is critical for the ability of α-syn to interact with membranes [229]. The central non-amyloid-β component (NAC) region (residues 61-95) is recognized as the most aggregation-prone portion of the protein due to its strong tendency to adopt β-sheet structures and fibrillar aggregates [234–236]. Finally, the C-terminal (residues 96-140) is a negatively charged portion of the protein, responsible for chaperone activity and Ca^{2+} binding [100, 237]. The C-terminal also contains many post-translational modification sites, which can influence aggregation dynamics and the interaction of α-syn with other cellular components [238, 239].

Although the physiological role of α-syn is not fully understood, it is thought to be involved in neurotransmitter release, vesicle trafficking, and synaptic plasticity [240, 241]. These roles are supported by its presynaptic localization [242].

Through its interaction with vesicle-associated membrane protein 2 (VAMP2), α-syn chaperones the assembly of the soluble *N*-ethylmaleimide-sensitive fusion protein attachment protein receptor (SNARE) complex [243, 244]. This assembly is crucial for exocytosis and neurotransmitter release [245]. A-syn also clusters synaptic vesicles, thereby modulating the availability of vesicles in the distal reserve pool [227, 246]. In line with this, even modest overexpression of α-syn can restrict vesicle recycling and attenuate neurotransmitter release [247].

Alongside these roles, α-syn can directly regulate dopamine neurotransmission by interacting with tyrosine hydroxylase (TH), the rate-limiting enzyme in dopamine biosynthesis [248]. *In vivo* studies have demonstrated that overexpression of endogenous α-syn diminishes TH promoter activity, leading to reductions in both TH mRNA and TH protein [249, 250]. Moreover, α-syn can restrict dopamine re-uptake through its inhibition of DAT [251].

1.2.2 Alpha-synuclein misfolding & aggregation

Under physiological conditions, α-syn is predominantly soluble and intrinsically disordered. This inherent structural flexibility is essential for its normal function but also predisposes it to misfolding and aggregation [113].

The aggregation of α-syn involves a multi-step process that occurs in distinct phases (Fig. 1.1) [252]. In the first phase of aggregation (the lag phase), native α-syn monomers assemble to form small, unstable oligomeric species [253]. Over time, these species self-associate into an aggregation-competent nucleus, which acts as a template for further misfolding [254, 57, 255–257, 235]. This is often referred to as the rate-limiting step in the aggregation process, as it is slow progressing and kinetically unfavorable [256]. In the elongation phase, oligomers grow exponentially through the continual addition of native monomers [258, 259]. This process results in the formation of protofibrils and eventually insoluble fibrils, which are large aggregates with highly ordered beta-sheet structures [35, 260]. Finally, during the stationary phase, fibril formation slows as the monomer and fibril concentration reaches equilibrium [261]. The fibrils formed during this phase represent a major constituent of LBs and LNs [262].

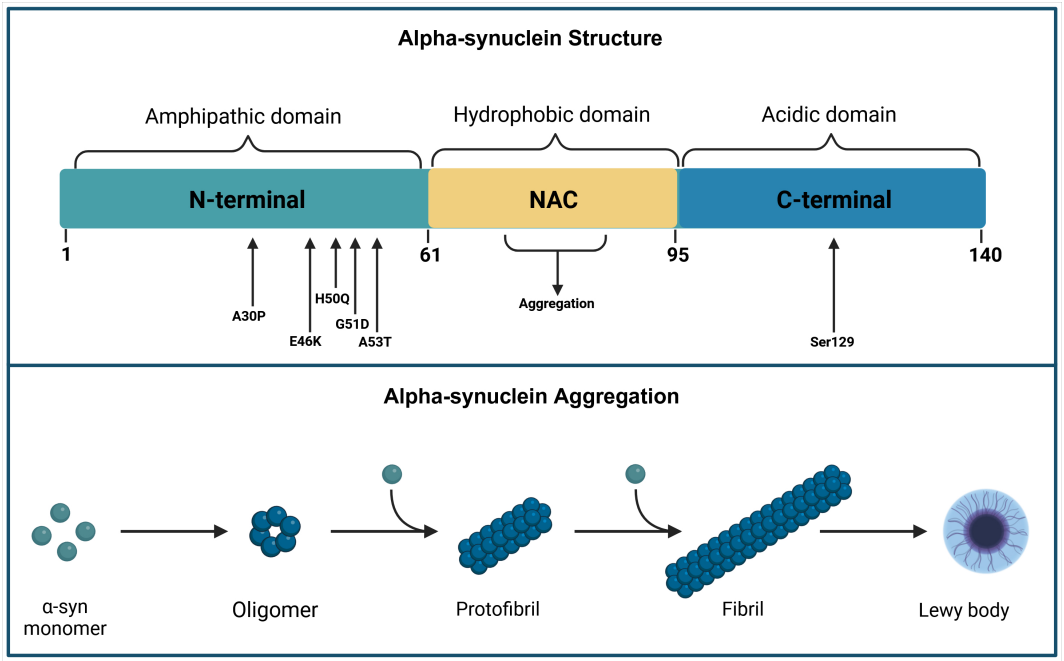

Fig. 1.1 Alpha-synuclein structure and aggregation. Simplified schematic representation of α-syn structure and aggregation dynamics, highlighting key *SNCA* variants and the primary phosphorylation site at Ser129 (created on BioRender 2025).

A plethora of intrinsic and extrinsic factors can influence this aggregation cascade [263]. Among the intrinsic factors, point mutations in the *SNCA* gene (p.A53T, p.A30P, p.E46K, p.G51D, p.H50Q, and p.A53E) have been shown to significantly alter the biophysical properties of α-syn [15]. More specifically, *SNCA* mutations can increase the aggregation rate of α-syn and influence its propensity to form oligomers or fibrils [228]. For example, the p.A53T, p.E46K, and p.H50Q mutations have been shown to increase the rate of fibril formation, whereas the p.G51D, p.A30P, and p.A53E mutations delay fibrilization [264–267, 144, 268, 269]. Genomic duplications and triplications of the *SNCA* gene can also promote aggregation, likely as a result of increased α-syn protein levels and consequent molecular crowding [270]. This crowding effect can in turn facilitate aggregation by surpassing the threshold necessary for nucleation during the lag phase [271]. Mutations in *SNCA* can also alter the interactions of α-syn with phospholipid membranes, which in turn influences its conformation and aggregation dynamics [272, 228, 273]. Variants such as p.A53P, p.A30P, and p.G51D have been shown to reduce membrane binding [266, 264, 274]. In contrast, p.E46K and p.A53T variants enhance phospholipid binding [275, 271].

Post-translational modifications can also alter the charge, size, structure, and therefore aggregation potential of α-syn [276, 277]. To date, more than 300 post-translational modifications to α-syn have been identified, including phosphorylation, ubiquitination, nitration, acetylation, glycosylation, SUMOylation, and truncation [254]. One of the most well-characterized modifications is phosphorylation at serine 129 (Ser129); approximately 90% of aggregated α-syn present in LBs is phosphorylated at Ser129 in PD brains [278]. In comparison, only 4% of total α-syn is phosphorylated at Ser129 in the brains of normal individuals [279, 280]. This modification to α-syn has been suggested to promote aggregation [278].

Alongside genetic mutations and post-translational modifications, changes in the cellular environment can also induce aggregation [281, 282]. For instance, Ca^{2+} binding to the C-terminal of α-syn causes N-terminal unfolding and aggregation-favoring conformations [283]. Similarly, at low pH, the net negative charge at the C-terminal is diminished, weakening charge-charge intramolecular repulsion [284]. This alteration causes α-syn to adopt a partially unfolded confirmation that is more susceptible to aggregation [285].

1.2.3 Toxic conformations of alpha-synuclein

Although LBs are an intrinsic feature of idiopathic and most autosomal dominant forms of PD, there is growing evidence that these insoluble inclusions are not the sole cause of disease pathogenesis [35]. In support of this, there is the observation of incidental LBs at autopsy in aged individuals without clinical symptoms of PD [286]. The presence of LBs without neurodegeneration in asymptomatic individuals is not an isolated finding and was reported in 12% of 1,200 consecutive autopsies [287]. However, it is thought that these cases may represent the preclinical stages of PD [35]. Nevertheless, evidence from familial cases also suggests that LB pathology is not the exclusive cause of neurotoxicity, as PD patients carrying the *LRRK2* G2019S mutation often display neurodegeneration in the absence of Lewy inclusions [288, 289]. Moreover, the extent of LB deposition often correlates poorly with the severity of clinical impairments [290]. In light of these findings, it is now increasingly accepted

that oligomeric forms of α-syn may be the toxic species that drive pathology [291].

Oligomers are macromolecular structures formed during the aggregation cascade [292]. Typically they are composed of a few to several monomers and range in size from 4-24 nm [35]. Oligomers are very heterogeneous and vary in terms of their structure and molecular weight [293]. Unlike fibrils, oligomers are soluble and have the ability to change conformations, which makes them highly unstable [293]. Evidence for oligomer toxicity comes from a range of experimental sources. Firstly, α-syn oligomers formed *in vitro* or through the overexpression of α-syn promote cell death in cultured neurons [294–296]. Moreover, the expression of α-syn mutants engineered to reduce fibril formation and increase oligomer formation causes toxicity in immortalized cells, dopaminergic neurons of *C. elegans*, and cultured rat neurons [297, 289]. In addition to experimental evidence, oligomers have been identified in brain extracts and CSF samples taken from PD patients [298].

While the exact reasons for the increased toxicity of α-syn oligomers are not fully understood, several explanations have been suggested [299]. As oligomers are typically small in size, they can readily diffuse into cellular structures and impair physiological functions [300]. Moreover, oligomers have a greater proportion of exposed hydrophobic surfaces compared to monomeric and fibrillar forms [301, 302]. These hydrophobic regions can directly interact with cellular membranes and impair membrane permeability [303, 304]. Finally, the transient and unstable nature of oligomers makes them highly reactive, which can enhance interactions with other cellular components [299].

Despite oligomers being recognized as the most toxic α-syn species, fibrils play a fundamental role in disease progression [305] (as introduced in Section 1.1.3.2). A plethora of *in vivo* studies have indicated that α-syn can self-propagate in a prion-like manner [254, 306]. More specifically, it has been demonstrated that in the extracellular space, fibrillar seeds can be taken up by adjacent cells through mechanisms such as endocytosis, fusion of plasma-exosomal membranes, or direct penetration of plasma membranes [254, 285, 307, 308]. Once inside neighboring cells, α-syn seeds undergo post-translational modifications that facilitate interactions with physiological α-syn monomers, thereby promoting the aggregation and spread of α-syn [254, 309, 310]. This is supported by

data showing that LB structures can propagate from the SN of PD patients to embryonic grafted neurons transplanted more than a decade earlier [311]. Furthermore, using α-syn seeds constructed from recombinant proteins or aggregate-rich lysates from PD brains, it has been observed that α-syn can spread in a prion-like fashion between neuronal cells [312–314, 262]. The hypothesis that α-syn propagates between cells is also corroborated by clinical data, in which it is observed that α-syn pathology begins in one region and subsequently spreads to other vulnerable regions [37].

1.2.4 Mechanisms of alpha-synuclein mediated toxicity

While the mechanisms of α-syn-mediated toxicity are not fully understood, cumulative evidence suggests that α-syn deposition can have wide-ranging effects on various cellular functions, including membrane stability, mitochondrial dynamics, proteostasis, endoplasmic reticulum (ER) function, inflammation, and neuronal survival. These disruptions can lead to cellular stress and impaired signalling pathways, ultimately contributing to the neurodegenerative PD phenotype. Below, some of the main mechanisms of α-syn-mediated toxicity are discussed.

1.2.4.1 Impaired membrane integrity

Membrane integrity is essential for normal cellular functions [315]. As such, any disruptions or alterations in its structure can cause significant cellular damage [316]. It has been demonstrated that oligomeric α-syn can directly penetrate cellular membranes, leading to the formation of pore-like structures that perforate the lipid bilayer [317]. This in turn increases cell permeability, causing calcium influx and cell death [317, 294]. Consistent with this, neuronal cells expressing mutant α-syn (p.A30P and p.A53T) display higher plasma membrane ion permeability, which is linked to elevated basal Ca^{2+} levels and neurodegeneration [318]. Additionally, α-syn oligomers can also stabilize and enlarge pre-existing lipid defects, which exacerbates membrane dysfunction [319].

1.2.4.2 Mitochondrial dysfunction & oxidative stress

Multiple lines of evidence suggest mitochondrial dysfunction is central to PD pathogenesis [320]. It is often regarded that α-syn aggregation and mitochondrial dysfunction exist in a vicious cycle, where pathology in one process exacerbates dysfunction in the other [321].

In postmortem PD brains, α-syn has been shown to accumulate within the mitochondrial compartment of dopaminergic neurons, leading to reduced complex I activity [322, 323]. Deficits in complex I can in turn cause the accumulation of reactive oxygen species (ROS) and oxidative stress [324]. Moreover, α-syn oligomers can promote the oxidation of the ATP synthase beta subunit and mitochondrial lipid peroxidation [325]. These events lead to the opening of the permeability transition pore (PTP), which induces mitochondrial swelling and cell death [325].

Post-translationally modified species of α-syn have also been suggested to induce mitochondrial dysfunction by perturbing protein import. More specifically, α-syn can directly bind to and inhibit TOM20, which is crucial for the translocation of proteins from the cytosol into mitochondria [326, 327]. This in turn causes mitochondrial insufficiency of respiration and oxidative stress [328].

Dynamic processes such as mitochondrial fission/fusion and quality control are also influenced by α-syn aggregation [327]. Mitochondrial fission is initiated by the recruitment of Drp1 to the OMM, and prior studies have demonstrated that the translocation of Drp1 to mitochondria is markedly increased upon α-syn overexpression [329, 330]. Supporting this, upregulation of α-syn has been shown to induce mitochondrial fragmentation and oxidation via a DRP1-dependent mechanism [331]. Additionally, exposure to exogenous α-syn directly impairs mitophagy, resulting in depolarization of the mitochondrial membrane and decreased cellular ATP [332, 333]. Intriguingly, these observations were attributed to decreased Parkin expression, suggesting a direct effect of α-syn on Parkin-dependent mitophagy [333].

1.2.4.3 Disruption of proteostasis

The autophagy-lysosomal pathway (ALP) is often regarded as the primary pathway for degrading protein aggregates [334]. The ALP includes macroautophagy and chaperone-mediated autophagy (CMA), both of which contribute to the clearance of misfolded α-syn [335]. Macroautophagy involves the formation of autophagosomes, which fuse with lysosomes to facilitate degradation [336]. In contrast, CMA involves the delivery of target proteins to lysosomes using molecular chaperones [337]. Perturbations in these pathways reduce α-syn clearance and exacerbate aggregation [338–340].

Under physiological conditions, endogenous α-syn binds to the CMA receptor LAMP-2A and is subsequently degraded by proteases [341]. However, mutant forms of α-syn exhibit a higher binding affinity for the LAMP-2A receptor, which inhibits their degradation and directly blocks CMA function [342, 338, 343]. Supporting this, reduced levels of CMA markers and accumulation of autophagosomes have been observed in experimental models of PD and in postmortem PD brains [344, 345].

The ubiquitin-proteasome system (UPS) is also essential for α-syn clearance. In this system, substrates are tagged with ubiquitin, which directs them to the proteasome for degradation [346]. Comparisons of brain samples from PD patients with healthy controls have demonstrated diminished proteasome catalytic activity and reduced levels of proteasome subunits [347]. Moreover, in experimental models oligomeric α-syn has been shown to impede UPS activity by blocking the entry of substrates to the 26S and 20S proteasome [348, 349].

1.2.4.4 Endoplasmic reticulum stress

The ER is a specialized organelle that orchestrates the synthesis, folding, and quality control of newly translated proteins [350]. Alongside this, it is also the main site of intracellular Ca^{2+} storage [351]. ER stress triggered by perturbed calcium homeostasis or oxidative stress results in the accumulation of unfolded or misfolded proteins, which in turn triggers the unfolded protein response (UPR) [352]. Activation of UPR aims to restore ER functionality by repressing protein synthesis and eliminating unfolded proteins via ER-associated

degradation (ERAD) [351]. However, chronic ER stress can result in protein accumulation and the activation of programmed cell death [353].

In mammalian culture models, overexpression of wild-type or p.A53T mutant α-syn is correlated with ER stress and UPR activity [354, 351, 355]. More specifically, α-syn accumulates in the ER lumen, where it blocks protein folding and activates the UPS [351]. Alongside this, α-syn accumulation impairs ERAD and alters ER-mitochondria calcium transfer and Golgi-ER vesicular transport [356, 357]. This culminates in severe ER and stress and neuronal loss [356].

1.2.4.5 Neuroinflammation

An increasing number of postmortem and fluid biomarker studies have revealed that neuroinflammation is a salient characteristic of PD [321]. Corroborating this, activated microglia have been shown to accumulate in the SN of postmortem PD brains [358].

Multiple lines of evidence support the ability of aggregated α-syn to activate both the innate and adaptive immune systems, which perpetuates a state of chronic inflammation [359]. Aggregated α-syn directly stimulates the release of pro-inflammatory cytokines in microglia and monocytes [360, 361]. In experimental models, the addition of aggregated α-syn to microglial cultures results in the production of pro-inflammatory modulators such as TNF-α and IL-1β [362, 363]. Additionally, oligomeric α-syn can promote inflammatory signalling by directly interacting with microglial receptors, including TLR2 and β1-integrin [364].

1.2.4.6 Selective vulnerability of mDA neurons

As mentioned, mDA neurons in the striatum are disproportionately affected in PD. This selective vulnerability may be attributed to their high energetic demands [365]. Dopaminergic neurons possess remarkably long (estimated at 4.5 meters in length) and profusely branched axons [366, 367]. Moreover, a single neuron can form between 1 and 2.4 million synapses [366, 367]. This

structure allows them to coordinate interconnected networks across the striatum but imposes a substantial energetic burden [368].

Another contributing factor is the autonomous pacemaking activity of dopaminergic neurons, which results in a sustained influx of calcium ions [369]. Unlike adjacent neurons in the ventral tegmental area (VTA), which exhibit a resistance in PD, nigral neurons have a reduced calcium buffering capacity [368]. This is evidenced by low levels of calcium-binding proteins, such as calbindin and calretinin [369]. Chronically elevated intracellular Ca^{2+} levels have been shown to promote α-syn oligomerization, leading to the formation of Ca^{2+}-permeable pores in the plasma membrane [370]. These pores further exacerbate calcium influx, setting off a self-perpetuating cycle of calcium dysregulation and toxic oligomer formation, that ultimately contributes to neuronal death [370, 294].

CHAPTER 2

Thesis Aims & Structure

2.1 Aims of the thesis

As discussed in Chapter 1, PD is a complex neurodegenerative disorder characterized by the progressive loss of mDA neurons and the pathological aggregation of α-syn. Mutations in the *SNCA* gene, including the missense variant *SNCA*-A53T, have been linked to familial PD. However, the precise mechanisms by which these mutations influence disease establishment remain poorly understood. A major challenge in elucidating their effects is that *SNCA* mutations impact diverse and often interconnected pathways (Section 1.2.4), making it difficult to determine their precise role in disease development.

To address this challenge, we conducted a longitudinal multi-omics characterization of patient-derived *SNCA*-A53T cells at seven timepoints (days 0, 6, 15, 21, 30, 40, and 60) during the differentiation from iPSCs into mature mDA neurons, using an age- and sex-matched control for comparison. In addition to transcriptomic, proteomic, and metabolomic profiling, we assessed mitochondrial function and cellular bioenergetics to explore the broader functional impact of

the *SNCA*-A53T mutation. Using this approach, we have two complementary objectives:

2.1.1 Characterize *SNCA*-A53T-driven phenotypes

By using a multi-omics approach that incorporates single-cell RNA sequencing (scRNA-seq), proteomic and metabolomic analyses, we aim to investigate how transcriptional alterations manifest at the protein level and influence metabolomic pathways, ultimately shaping the disease phenotype. We hypothesize that incorporating multiple biological levels will provide deeper insights into the multifaceted nature of *SNCA*-A53T-driven cellular phenotypes. By combining these datasets, we hope to identify dysregulated pathways and candidate genes that can be validated *in vivo*.

2.1.2 Investigate the temporal dynamics of PD

By performing a longitudinal analysis across seven developmental stages, spanning early neural differentiation to late mDA neuron maturation, we seek to investigate the emergence and progression of PD-associated impairments (Fig. 2.1). Specifically, by focusing on the initial phases of neuron development, we aim to identify early impairments that may predispose neurons to later dysfunction and contribute to disease pathology over time. Additionally, by evaluating the later stages of mDA neuron differentiation, we aim to determine the impact of *SNCA*-A53T-induced alterations on the mature neuronal phenotype. We hypothesize that this time-series approach may reveal early impairments that prime neurons for later-stage pathology. Given that PD is characterized by a preclinical phase in which pathology precedes neuronal degeneration, investigating the temporal dynamics of disease progression may uncover therapeutic targets for early intervention.

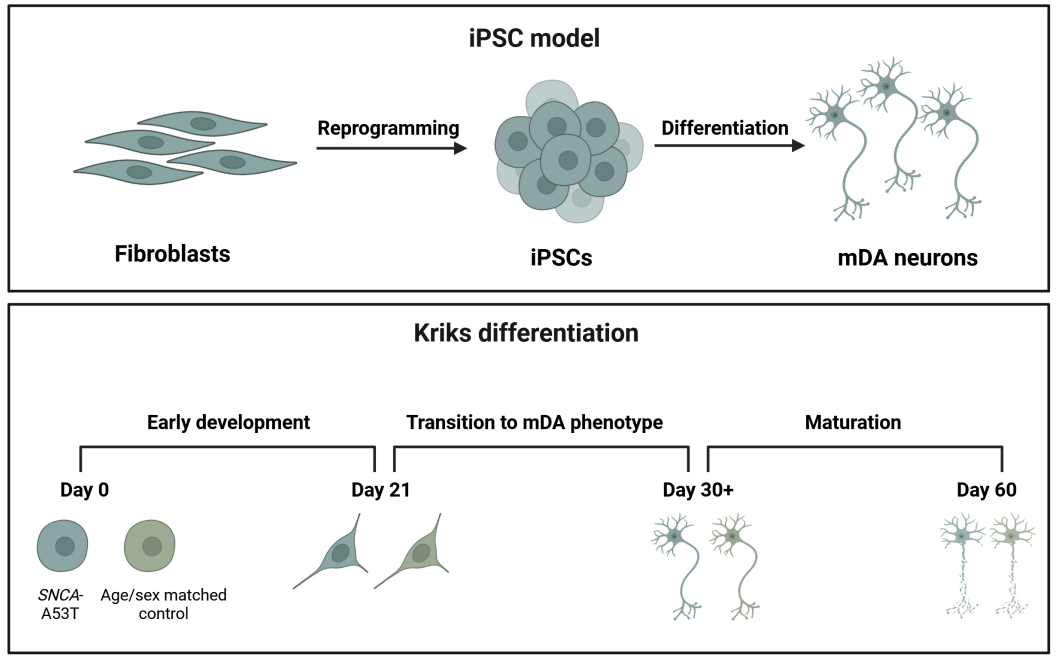

Fig. 2.1 Differentiation strategy. Schematic representation of the model and experimental strategy used in the present study. Fibroblasts from a patient carrying the *SNCA*-A53T mutation and an age- and sex-matched control are reprogrammed into iPSCs and differentiated into mature mDA neurons using the Kriks protocol. The differentiation process is evaluated across seven timepoints, capturing key transitions: days 0 to 21 represent the progression from iPSCs to neural progenitors, with mDA characteristics beginning to emerge at day 21. From day 30 onward, neurons transition from an early to a more mature mDA state (created on BioRender 2025).

2.2 Structure of the thesis

Chapter 1 introduced central themes in PD research, with a focus on the role of α-syn in disease-associated pathways. In Chapter 3, the methods used for generating and differentiating cell lines are described (Sections 3.1 - 3.2), followed by an overview of mitochondrial profiling techniques (Section 3.3), and a description of the multi-omics analysis (Section 3.4). Chapter 4 then presents the main results of the thesis, beginning with the characterization of cells from iPSCs to mDA neurons (Section 4.1), followed by the multi-omics comparison of *SNCA*-A53T and control cells (Section 4.2), and the assessment of mitochondrial function using the Seahorse metabolic assay and western blotting (Section 4.3). Chapter 5 discusses these findings in the broader scientific context

and considers their implications for future research. Finally, Chapter 6 provides the overall conclusions of the thesis.

CHAPTER 3

Materials & Methods

The methods employed for the generation of mDA neurons (Section 3.1), characterization of cell lines (Section 3.2), mitochondrial profiling (Section 3.3), and multi-omics analysis (Section 3.4) are described in the following chapter. A comprehensive list of the materials and reagents used in these analyses is provided in Appendix Tab. A.1.

3.1 Cell Culture

3.1.1 Generation & maintenance of iPSCs

iPSCs from a 51-year-old PD patient carrying the *SNCA*-A53T mutation were originally obtained from the National Institute of Neurological Disorders and Stroke (NINDS) biobank (ID: 50050). Control iPSCs were generated by the Gasser group, as previously described [371]. These cell lines were kindly gifted by the Grünewald lab at LCSB (full cell line details and karyotyping reports can be found in Appendix Tab. A.2 and Fig. A.1). Both cell lines were maintained in mTeSR-plus medium (Stem Cell Technologies) on Geltrex-coated plates (Thermo Fisher Scientific). Cells were passaged using Accutase when reaching 70% confluency at a ratio of 1:6.

3.1.2 Differentiation of iPSCs into mDA neurons

Differentiation into dopaminergic neurons was performed according to previously described protocols with minor modifications [372, 111]. Briefly, iPSCs were dissociated into single cells and plated onto 12-well plates coated with Geltrex at a density of 1.1 x 10^6 cells/well. Cells were allowed to recover in the presence of ROCK inhibitor for 8 h and then in mTeSR without ROCK inhibitor for 16 h. Following this, cells were fed 3 ml of media twice daily, corresponding to the specific day of differentiation (as outlined in Appendix Tab. A.3). To ensure that the cells were exposed to the same conditions, both the *SNCA*-A53T and control cell lines were differentiated in parallel. Different timepoints (day 0, 6, 15, 21, 30, 40, and 60) were generated by repeating the differentiation protocol on later dates.

3.2 Characterization of cell lines

3.2.1 Immunohistochemistry

Cells were cultured on 96-well plates before being fixed in 4% PFA at room temperature for 15 mins, washed three times in PBS, and permeabilized for 15 mins with 0.1% Triton-X-100. Cells were then washed three times in PBS and blocked with 2% BSA in PBS for 1 h at room temperature. After blocking, cells were incubated overnight at 4 °C with primary antibodies diluted in 2% BSA in PBS (1:500). Cells were then washed three times in PBS and incubated with species-specific secondary antibodies (anti-rabbit 647, anti-rabbit 488, and/or anti-mouse 488 antibodies) for 1 h at room temperature. Nuclei were stained using DAPI (1:1000). The following primary antibodies were used: OCT3/4 (Santa Cruz Biotechnology), TRA-1-60 (Merck), TH (Merck), MAP2 (Merck), and LMX1A (abcam). Representative images were then taken using a Zeiss Axio Observer. All antibodies used for immunohistochemistry are listed in Appendix Tab. A.4.

3.2.2 RNA extraction & quantitative real-time PCR (qPCR)

Total RNA was extracted from cell pellets using the RNeasy Mini Kit (250) (Qiagen), according to manufacturer instructions. Three biological replicates were used for each experimental condition. RNA concentration was measured through absorption at 260nm using a Nanodrop spectrophotometer (Fisher Scientific). cDNA was synthesized using the Superscript III^{TM} First-Strand Synthesis Reverse Transcriptase Kit (Invitrogen) with oligo (dT) 20 and 2 µg of total RNA, as per manufacturer instructions. To perform quantitative real-time PCR (qPCR), PowerTrack SYBR Green Master Mix (Thermo Fisher) was used and the reaction was run on a Roche lightcycler 480, with the primer annealing temperature at 60°C. Normalization of gene expression values was done using the housekeeping genes *L27* and *ACTB*. All data were exported into Prism GraphPad for plotting, and an unpaired Student's t-test was applied

for statistical analysis. Investigated genes and primer sequences are listed in Appendix Tab. A.5.

3.2.3 Flow cytometry

Flow cytometry was used to ascertain the percentage of TH, MAP2, and GFAP positive cells. For this analysis, three biological replicated were pooled for each experimental condition. On the day of collection, cells were detached using Accutase and fixed in suspension with 1% PFA for 15 min on ice. After fixation, cells were centrifuged, supernatant removed and washed twice in 4% FBS in PBS. Cells were then permeabilized with 0.1% Triton in PBS at room temperature for 15 mins. Following permeabilization, cells were washed and blocking was performed using 1% BSA in PBS for 1 h at room temperature. Cells were then centrifuged, supernatant removed and incubated in TH (1:500), MAP2 (1:500) and GFAP (1:400) primary antibodies overnight at 4°C. After primary antibody incubation, cells were centrifuged, supernatant removed and washed twice in 4% FBS in PBS. Cell pellets were then resuspended in species-specific secondary antibodies (anti-rabbit 488, anti-mouse 647, anti-rat 568, and DAPI) at a dilution of 1:500 and incubated in the dark for 1 h at room temperature. Following this, cells were washed three times in 4% FBS in PBS and filtered to remove clumps. Samples were then run on the BD LSRFortessa Cell Analyzer (BD Biosciences). The gating threshold for measured channels was determined using the control containing secondary antibody only. Once the parameters had been defined, 50,000 cell events were recorded, and data were analyzed on FlowJo. All antibodies used for flow cytometry are listed in Appendix Tab. A.4.

3.3 Mitochondrial profiling

3.3.1 Mitochondrial stress test

Mitochondrial respiration was assessed using the Seahorse XF Cell Mito Stress Kit (Agilent Technologies). Cells were seeded at a density of 100,000 cells per well in Seahorse XFe96/XPro plates. Three biological replicates, each with a minimum of 6 technical replicates, were included in the analysis. After plating, cells were allowed to recover for seven days in 5% CO2 at 37°C. On the day of analysis, growth medium was removed, and wells were washed once with Seahorse XF base medium supplemented with 10 mM glucose, 1 mM L-glutamine, and 1 mM sodium pyruvate. Plates were incubated in this medium for 1 hour in a 37°C CO2-free incubator before conducting the Mito Stress Test. The bioenergetic profile was measured by recording OCR under basal conditions and after the sequential addition of oligomycin (1.5 µM), FCCP (0.5 µM), and rotenone/antimycin A (0.5 µM) using the Seahorse XF Flux Analyzer. Values were normalized to nuclear DNA content using the CyQUANT® Cell Proliferation Assay Kit (Thermo Fisher Scientific).

The Seahorse assays were analyzed using XFe Wave software, according to manufacturer's instructions. Normalized OCR values were used to calculate various mitochondrial parameters including, basal respiration, maximal respiration, proton leak, ATP production, non-mitochondrial respiration, % spare respiratory capacity, and % coupling efficiency. All data were exported into Prism GraphPad for plotting, and an unpaired Student's t-test was applied for statistical analysis. Detailed descriptions of respiration parameter values are given in Appendix Tab. A.6.

3.3.2 Western blot

Lysates from *SNCA*-A53T and control cells were prepared in RIPA buffer supplemented with protease and phosphatase inhibitors (Thermo Fisher Scientific). Protein concentrations were measured using the Pierce™ BCA Protein Assay Kit (Thermo Fisher Scientific). Equal amounts of proteins (30 µg/lane) were

separated by NuPAGE 4–12% Bis-Tris protein gels (Thermo Fisher Scientific) and transferred onto nitrocellulose membranes (Invitrogen). After blocking with 5% milk in TBST for 1 hour at room temperature, the membranes were incubated overnight at 4 °C with primary antibodies. Following incubation, the membranes were washed three times with TBST and incubated with DyLight 680- or DyLight 800-conjugated secondary antibodies for 1 hour at room temperature. Proteins were visualized using the Odyssey Imaging System (LI-COR Biosciences). The following primary antibodies were used: Total OXPHOS Human WB Antibody Cocktail (1:500) (Abcam), which includes five monoclonal antibodies targeting NDUFB8 (complex I), SDHB (complex II), UQCRC2 (complex III), COXII (complex IV), and ATP5A (complex V). Images were acquired using the Odyssey Fc Imaging System (LI-COR). Densiometry analysis was performed using Image J software, using GAPDH as an internal control for each membrane. All antibodies used in the western blot analysis are listed in Appendix Tab. A.4.

3.4 Multi-omics analysis

3.4.1 Single-cell RNA sequencing

On the day of collection, cells were dissociated into single-cell suspensions using Accutase (Thermo Fisher Scientific). The suspension was centrifuged at 300g for 3 mins and subsequently washed twice in 2% BSA in PBS. Cells were then filtered through a 40 µm cell strainer to remove larger clumps. Cell counts and viability were determined using a Vi-CELL XR Cell Counter (Beckman Coulter). The cell concentration was then adjusted to 1.9×10^5 cells per ml by resuspending in PBS supplemented with 2% BSA. Approximately 2 ml of this final suspension was used for single-cell analysis. Subsequently, cells were processed by the Drop-Seq approach and sequenced [373, 111, 374, 375].

3.4.1.1 Microfluidics fabrication

Microfluidics devices were generated on-site using a technique based on earlier Drop-seq protocols [111, 373, 376]. For photolithography and mold preparation, a 4° silicon wafer was coated with SU-8 2050 photoresist (MicroChem) and patterned to create microchannel features 90 µm in depth. The wafer mask was subsequently silanized overnight using chlorotrimethylsilane (Sigma), before being used for the fabrication on micofluidics. To fabricate the Drop-Seq chips, silicon-based polymerization chemistry was used. In brief, a 1:10 ratio of polydimethylsiloxane (PDMS) base to cross-linker (Dow Corning) was prepared, degassed under vacuum, and poured over the patterned wafer. The PDMS layer was cured at 70 °C for 2 h. After cooling, individual PDMS monoliths were cut from the master and 1.25 mm biopsy punchers (World Precision Instruments) were used to create inlet/outlet ports. Each PDMS monolith was then plasma-treated (Harrick Plasma) and bonded to a clean glass microscope slide. To enhance droplet formation and prevent wetting, the microchannels were functionalized with 1H,1H,2H,2H-perfluorodecyltri-chlorosilane (2% v/v in FC-40 oil; Alfa Aesar/Sigma) for 5 min. Excess silane was removed by applying compressed air through the inlet and outlet ports. Finally, the chips were baked at 80 °C for 15 min to complete the hydrophobic coating process.

3.4.1.2 Drop-Seq library preparation

Single-cell encapsulation and library construction were performed following the Drop-Seq approach as previously described [111]. In brief, the adjusted cell suspension was combined with barcoded oligo(dT)-coated beads (ChemGenes Corp., USA), which were loaded at a final concentration of 180 beads/µl. Both the cell and bead suspensions were drawn into separate syringes (1.5 ml each). A micro-stirrer (VP Scientific) was used to maintain a homogeneous bead suspension throughout the experiment.

A syringe containing QX200 carrier oil (Bio-Rad) was used as the continuous phase at 11 ml/h, while the cell and bead suspensions were each infused at 2.5 ml/h to generate droplets on a microfluidic Drop-Seq chip. The emulsion was collected into a 50 ml Falcon tube until a total of 1 ml of the cell suspension had

been processed. Droplet size, consistency, and bead occupancy were monitored in real time using bright-field microscopy with an INCYTO C-Chip Disposable Hemacytometer (Thermo Fisher Scientific).

Following droplet generation, droplet breakage, bead harvesting, reverse transcription (RT), and exonuclease treatments were performed according to the standard Drop-Seq protocol (37). The RT reaction was set up in Drop-Seq lysis buffer with 1× Maxima RT buffer (Thermo Fisher Scientific), 4% Ficoll PM-400 (Sigma), 1 µM dNTP mix (Thermo Fisher Scientific), 1 U/ml RNase Inhibitor (Lucigen), 2.5 µM Template Switch Oligo, and 10 U/ml Maxima H-RT (Thermo Fisher Scientific). After Exo-I treatment, bead counts were determined using the INCYTO C-Chip hemacytometer. A total of 10,000 beads were aliquoted into 0.2 ml PCR tubes.

PCR amplification was carried out with 1× HiFi HotStart ReadyMix (Kapa Biosystems) and a 0.8 mM concentration of Template Switch PCR primer. The thermocycling program included an initial denaturation at 95°C for 3 min, followed by 4 cycles of 98 °C for 20 s, 65 °C for 45 s, 72°C for 3 min, then 9 cycles of 98 °C for 20 s, 67°C for 20 s, 72°C for 3 min, and a final extension at 72°C for 5 min. The resulting libraries were purified with 0.6× Agencourt AMPure XP beads (Beckman Coulter) and eluted in 10 µl RNase/DNase-free water. Quality and yield were assessed using an Agilent Bioanalyzer High Sensitivity DNA Chip.

3.4.1.3 Next-generation sequencing library preparation

To generate 3'scRNA-seq libraries for NGS, 600 pg of amplified cDNA was subjected to tagmentation using the Nextera XT DNA Library Preparation Kit (Illumina), following the manufacturer's instructions. The PCR protocol included an initial denaturation at 95°C for 30 s, 12 cycles of 95°C for 10 s, 55°C for 30 s, 72°C for 30 s, and a final extension at 72°C for 5 min.

The tagmented libraries were purified using two rounds of Agencourt AMPure XP beads (Beckman Coulter): first at a 0.6× ratio and then at a 1× ratio, according to the manufacturer's recommendations. The final library eluate

(10 µl) was assessed on a Bioanalyzer High Sensitivity DNA Chip (Agilent Technologies) to confirm library size distribution (400–700 bp).

Purified libraries were sequenced on an Illumina NextSeq 500 instrument. A custom Read 1 primer (GCCTGTCCGCGGAAGCAGTGGTATCAACGCAGAGTAC) at 6 pM was used to read 20 bp (comprising a 12-bp cell barcode and an 8-bp unique molecular identifier), while Read 2 proceeded for 50 bp to capture gene sequences.

3.4.1.4 Bioinformatics processing & data analysis

Raw BCL files generated from the NextSeq 500 were demultiplexed and converted to FASTQ using Illumina's bcl2fastq software. Library quality was evaluated with FastQC (Babraham Institute) to monitor per-base sequence quality (particularly for Read 2), per-base N content, per-base sequence content, and overrepresented sequences. FASTQ files were subsequently merged and converted into BAM format with Picard's FastqToSam. Finally, the Drop-Seq bioinformatics pipeline (37) was employed to map reads to the reference genome, de-multiplex cell barcodes, and generate a digital gene expression matrix for downstream analyses.

The analysis pipeline was developed under R 4.3.0. Seurat 4.4.0 was used as the main framework to import and manipulate scRNA-seq data sets [377]. For quality control, we computed common metrics that help discriminate high quality cells and transcripts, namely the percentage of mitochondrial and ribosomal expression over the whole transcriptome, the number of non-zero genes per cell and the total number of transcripts per cell. We then individually scaled these metrics by centering at 0 the mode (half.range() function from genefilter library) of each distribution and scaling (scale() function in R) in order to retain cells that were satisfying the constraints in Appendix Table A.7. We used SAVER on the corrected counts of each individual dataset to impute drop-outs – this assay was used for visualization purposes only [378]. Then, the data was log normalized using the NormalizeData function. In order to account for technical variations between samples, we found the sample with the highest mean expression across all samples to use as a scaling reference. Then, the imputed assay for each sample was normalized against reference mean. After

scaling, the data was further standardized using the ScaleData function from Seurat. We used SCT transform to stabilize the variance and prepare the data for the integration using the Seurat environment. Finally, PCA (number of principal components = 100), UMAP (number of neighbors = 100, minimum distance = 0.3) and clustering (resolution = 0.35) were performed on the integrated assay. To statistically assess differences between CTL (control) and A53T (*SNCA*-A53T) samples, we used MAST as a statistical test by setting the number of non-zero genes as a latent variable to account for differences in sequencing depth. P-values were adjusted by Bonferroni Correction (default option in Seurat) [379]. We filtered the differentially expressed genes (DEGs) by imposing an alpha level of 0.05, a log2 fold change of magnitude greater than 0.4 for DEGs per timepoint and 0.25 for persistently dysregulated genes. Genes were then ranked by calculating the sum of the absolute values of the fold changes coming from each timepoint. Note that only statistically significant dysregulated genes were taking part in the latter calculation.

3.4.1.5 Enrichment analysis

Gene-set and protein enrichment analyses were conducted using Metascape [380]. Enrichment was performed on Gene Ontology (GO) terms from the Biological Process (BP) category and Kyoto Encyclopedia of Genes and Genomes (KEGG) pathways. For each timepoint, the most statistically significant DEGs and DAPs, selected based on predefined FC cutoffs, were included in the analysis. Enriched terms were ranked by Log(q-value), and only pathway terms with a minimum of seven annotated genes were considered for analysis.

3.4.2 Proteome analysis

On the day of collection, cells were dissociated using Accutase, centrifuged at 300g for 3 mins and subsequently washed three times in PBS. Three biological replicates were used for each experimental condition. Cell pellets were lysed in a solution containing 2% sodium dodecyl sulfate, 20 mM dithiothreitol, and 50 mM tris(hydroxymethyl)amino methane hydrochloride at pH 8. After sonication, samples were boiled at 95 °C for 5 min, incubated on ice for 10 min

and centrifuged at 4 degree celsius for 15 min at 16,000×g. The supernatants were quantified by NanoDrop. Protein extracts of 10 µg were alkylated with 15 mM iodoacetamide for 30 min at room temperature in darkness. Proteins were digested overnight using the SP3 protocol (hughes) on SpeedBeads magnetic carboxylate (GE Healthcare GmbH) at 37°C with 0.2 µg of trypsin (Promega). Samples were acidified in 1% formic acid and peptides were desalted on home-made STop-And-Go-Extraction Tips (Rappsilber) using two disks of Empore C18 material (Supelco), dried by vacuum centrifugation, and reconstituted in 0.1% formic acid.

Following quantification by NanoDrop on the peptide level, 200 ng of each sample were analyzed by mass spectrometry. The HPLC system used for this project was a NanuElute 2 (Bruker Daltonics). The LC system was operated in a one-column separation set-up with an Aurora Ultimate nanoflow UHPLC column (C18, 75 µm inner diameter × 25 cm length × 1.7 µm particle size, 120 Å pore size, IonOptics) running at a flow rate of 300 nl min-1. The mobile phases A and B consisted of 0.1% formic acid in water and 0.1% formic acid in acetonitrile, respectively. The percentage of B was linearly increased from 2% to 35% in 30 min, changed to 95% within 30 s, and held constant at 95% for 6 min 46 s until a total run time of 37.27 min was reached. The eluate was directed into the timsTOF Pro (Bruker Daltonics) via a CaptiveSpray nano-electrospray ion source (Bruker Daltonics) operating in positive ion mode. The dual-TIMS analyzer operated at a fixed duty cycle of 100% using equal ramp and accumulation times of 100 ms and a ramp rate of 9.52 Hz. The diaPASEF (data-independent acquisition parallel accumulation serial fragmentation (Meier) cycle time of 0.95 s was achieved by limiting the mass range to 475-1000 Da and the mobility range to 0.85-1.27 1/K0. Every cycle consisted of 21 mass windows of 25 Da mass width. Mass selection windows as well as mobility windows did not overlap. The collision energy for collision-induced dissociation, was ramped linearly based on the measured values for 1/K0 from 20 eV at 0.6 Vs/cm2 to 59 eV at 1.6 Vs/cm2. These setting were controlled using HyStar version 6.2 and timsControl version 4.1.8.

Feature detection, peptide identification, and proteins annotation were performed with DIA_NN (version 1.8.1) using a library-free approach and the human Uniprot database (accessed June 2023). Oxidized methionine and car-

bamidomethylation on cysteine were set as modifications. The precursor mass range was set to 300-1800 Da, the precursor charge state was set to 2-4, and a peptide length of 7-30 were selected. 'Unrelated runs' and a FDR of 0.01 were chosen to reduce false identifications.

The analysis pipeline was developed under R 4.3.0. We identified and removed two outliers out of 123 replicates via means of hierarchical clustering. Imputation was performed with the R package missMDA, by using the imputePCA function separately on each individual cell-line and day of differentiation, with the parameter of number of principal components set to 2 [381]. To convert Uniprot IDs to gene symbols we used the Syngo ID conversion tool [382]. The values were then log2 normalized. To statistically assess differences between CTL and A53T cell lines we used the Limma package. Note that after the log2 normalization the distribution of the protein abundance is approximately normal [383]. P-values were adjusted with the Benjamini Hochberg procedure. We filtered the differentially abundant proteins (DAPs) by imposing an alpha level of 0.05, and a log2 fold change of magnitude greater than 1 for DAPs per timepoint and 0.5 for persistently dysregulated proteins. Proteins were then ranked by calculating the sum of the absolute values of the fold changes coming from each timepoint. Note that only statistically significant dysregulated proteins were taking part in the latter calculation.

3.4.3 Metabolome analysis

The analytical procedure for sample preparation and liquid chromatography-mass spectrometry (LC-MS) analysis was adapted from previous protocols [384]. Three biological replicates were used for each experimental condition. Briefly, cells were harvested, and metabolites were extracted using a cold methanol-water/chloroform protocol based on Bligh and Dyer. Following extraction, the samples were dried in a rotary vacuum concentrator and reconstituted in 80% acetonitrile/water. Prior to LC-MS analysis, samples were filtered to remove particulates. To account for varying cell numbers in the samples, the reconstitution volumes were adjusted proportionally based on the total number of cells extracted (100 µL per 5 million cells). This normalization ensured consistency in metabolite quantitation across samples.

LC-MS analysis was conducted using a Thermo Q Exactive HF mass spectrometer coupled with a Thermo Vanquish UHPLC system, equipped with a SeQuant ZIC-pHILIC column (5 µm particles, 2.1 × 150 mm). The gradient elution program, ionization mode, and mass detection parameters were applied as described [384]. Data acquisition and analysis were performed using Thermo TraceFinder software. To correct for analytical variations, data were sum-normalized prior to statistical analysis.

The analysis pipeline was developed under R 4.3.0. Imputation was performed with the R package missMDA, by using the imputePCA function separately on each individual cell-line and day of differentiation, with the parameter of number of principal components set to 2 [381]. To convert metabolite names to KEGG IDs we used the Metaboanalyst conversion tool [385]. The values were then log2 normalized. To statistically assess differences between CTL and A53T cell lines we used the Limma package [383]. P-values were adjusted with the Benjamini Hochberg procedure. We filtered the differentially abundant metabolites by imposing an alpha level of 0.05 and a log2 fold change of magnitude greater than 0.4.

CHAPTER 4

Results

In this chapter, the main findings of the PhD thesis are presented. Section 4.1 focuses on the characterization of cell lines, describing the differentiation from iPSCs to mature mDA neurons. Section 4.2 highlights the results of the large-scale multi-omics analysis, utilizing scRNA-seq, proteomics, and metabolomics to achieve a deep molecular phenotyping of cells carrying the *SNCA*-A53T mutation, alongside cells from an age- and sex-matched control. Section 4.3 outlines the results of functional and protein-based analyses performed to assess mitochondrial activity in *SNCA*-A53T and control neurons.

4.1 Cell line characterization

To generate mDA neurons, we differentiated iPSC lines derived from a 51-year-old female patient with a heterozygous *SNCA*-A53T (A53T) mutation and an age- and sex-matched control (CTL) using a modified version of the Kriks protocol [372, 111]. In brief, neural conversion was achieved using dual-SMAD inhibition followed by midbrain patterning using small molecule agonists of Shh, Wnt, and FGF8 signalling pathways (Methods Section 3.1.2 and Appendix Tab. A.3).

4.1.1 Confirmation of iPSC status

To validate the pluripotency of the cells and verify their capacity for differentiation, *SNCA*-A53T and control iPSC lines were stained for stemness markers POU5F1 (also known as OCT3/4) and TRA-1-60 (Fig. 4.1a and Methods Section 3.2.1). Additionally, the expression of genes indicative of a pluripotent state, including *MYC, POU5F1, USP44, TERF1*, and *POLR3G*, was quantified using scRNA-seq (Fig. 4.1b and Methods Section 3.4.1). At day 0 (iPSC stage), both cell lines exhibited robust expression of pluripotency markers, which were markedly reduced at all subsequent timepoints of the differentiation, confirming the pluripotent state of the cells prior to differentiation.

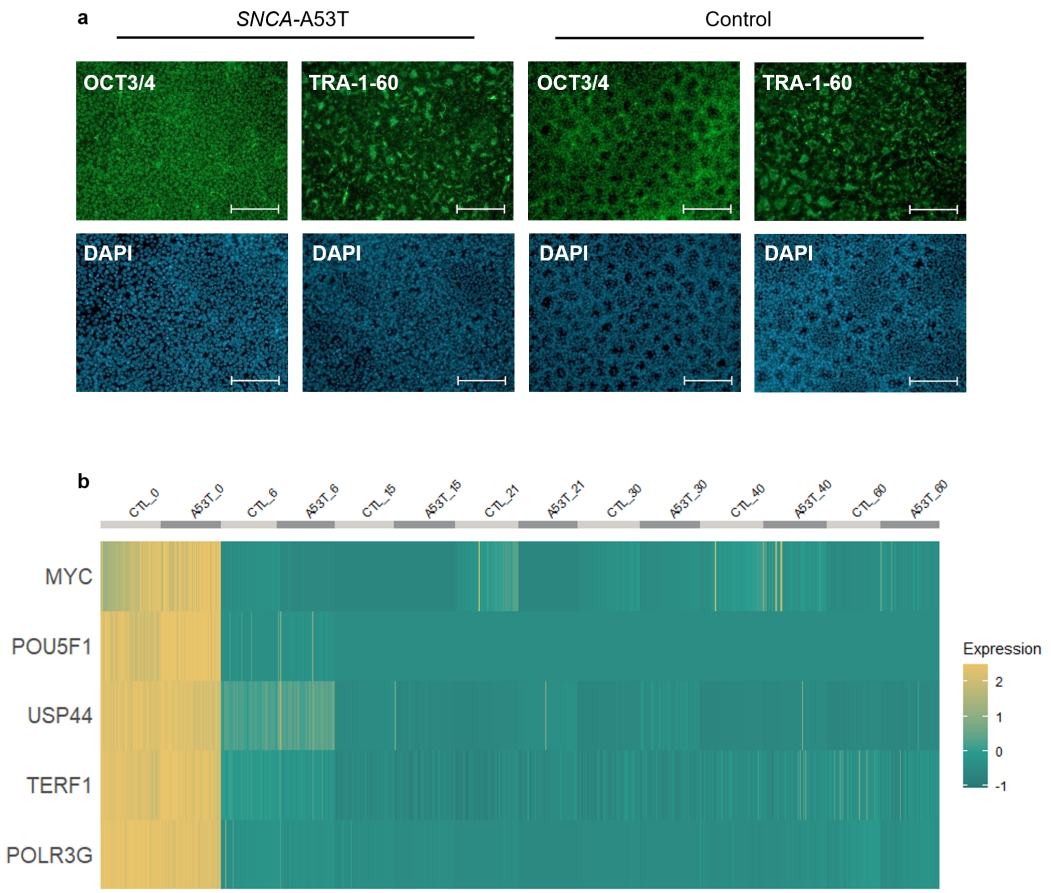

Fig. 4.1 Characterization of iPSCs. **a.** Immunofluorescent staining of *SNCA*-A53T and control cells at day 0 (iPSC stage) using iPSC markers POU5F1 (OCT3/4) and TRA-1-60. DAPI was used to stain cell nuclei as a reference. Scale bars, 200 µm. **b.** Heatmap showing robust expression of stemness markers (*MYC, POU5F1, USP44, TERF1, and POLR3G*) at day 0 compared to all other timepoints of the differentiation. Colors correlate to normalized counts (z-score, centered, and scaled) of the indicated genes. Centering and scaling was performed independently at each timepoint.

4.1.2 Validation of mDA neuron identity

To ensure the differentiation protocol recapitulated the *in vivo* developmental trajectory of mDA neurons, we identified genes essential for mDA neuron differentiation and evaluated their expression throughout development in both the *SNCA*-A53T and control lines using immunostaining, qPCR, scRNA-seq, and flow cytometry [111].

As an initial step, mDA neuron identity was confirmed by immunostaining for key mDA protein markers including TH and LMX1A, as well as the neuronal marker, MAP2 (Fig. 4.2 and Methods Section 3.2.1). At day 21, neuronal cells exhibited short processes and low mDA marker expression. In contrast, day 40 neurons displayed long axons that formed dense networks, accompanied by more pronounced expression of mDA markers. Additionally, the mRNA expression of *TH, MAP2*, and *LMX1A* was validated at day 30 and day 60 using qPCR (Fig. 4.2 and Methods Section 3.2.2). We also quantified mRNA levels of the astrocytic marker *GFAP* and found undetectable expression, confirming the absence of astrocytes in our cultures. Furthermore, we assessed *SNCA* mRNA levels using qPCR and found no significant differences in *SNCA* expression at day 30 or day 60 between *SNCA*-A53T and control cells (Fig. 4.2). This finding is consistent with literature, demonstrating that the *SNCA*-A53T mutation predominantly affects the aggregation dynamics of α-syn rather than altering the transcription of *SNCA* [386].

To characterize the developmental trajectory of the cells in greater detail, we performed scRNA-seq at seven timepoints throughout the differentiation (for full details of the scRNA-seq analysis, see Results Section 4.2.1 and Methods Section 3.4.1). Analysis of gene expression across the timepoints revealed distinct modules (Fig. 4.3). At the early stages of the differentiation (days 6 to 15), we observed the loss of iPSC markers and high expression of neural progenitor markers (*VIM, HES1, FOXA2, OTX2, LMX1A*, and *CORIN*), representing the transition of iPSCs to neuronal progenitors. From day 21 onwards, mDA-specific markers *MSX1, DDC, DCX, SYT1, SNCA, TH* and the neuronal marker *SNAP25* were identified. By day 40, these markers showed robust expression, indicating the progression to mature mDA neurons. This analysis confirmed that mDA characteristics emerge from day 21, whilst the

mature dopaminergic phenotype is evident by day 40. Notably, at days 21 and 30, differences in mDA marker expression were already evident between *SNCA*-A53T and control cells, alluding to an effect of the mutation on neuronal development.

Finally, flow cytometry was used to assess the proportion of TH-, MAP2-, and GFAP-positive cells on day 50 of the differentiation (Appendix Fig. A.2). This analysis confirmed that $\approx 74\%$ of cells expressed TH, $\approx 84\%$ expressed MAP2, and $\approx 1.6\%$ expressed GFAP across *SNCA*-A53T and control lines. These results demonstrate the high reproducibility of the differentiation protocol and support the validity of these cell populations as a relevant model for PD.

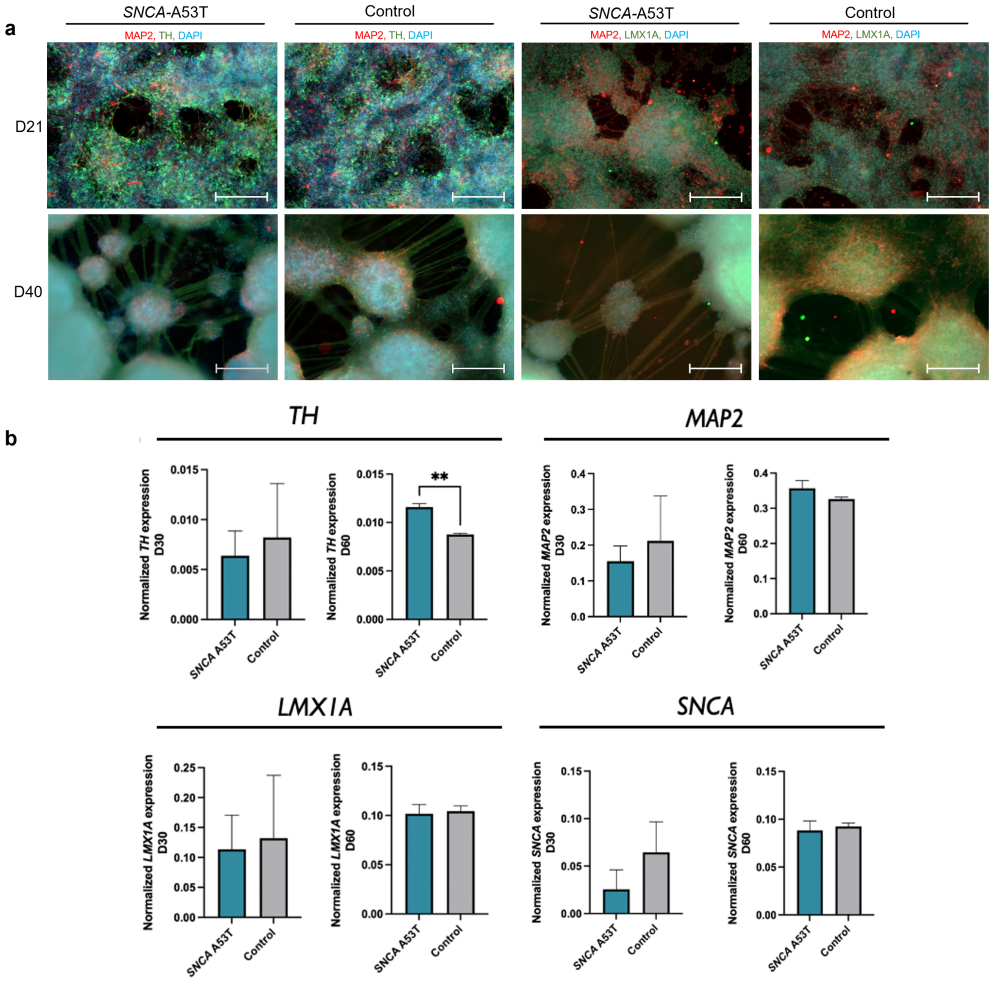

Fig. 4.2 Confirmation of mDA status. **a.** To illustrate the development of neuronal morphology and mDA status, differentiated neurons were stained at day 21 and day 40 for the mDA marker TH (green), floor plate marker LMX1A (green), and neuronal marker MAP2 (red). DAPI (blue) was used to stain cell nuclei as a reference. Scale bars, 200 µm. **b.** Quantification of *TH*, *MAP2*, *LMX1A*, and *SNCA* using real-time qPCR. Expression levels are normalized to the housekeeping genes *L27* and *ACTB* (N = 3, mean ± SEM, Student's t-test, $^{**}P < 0.005$).

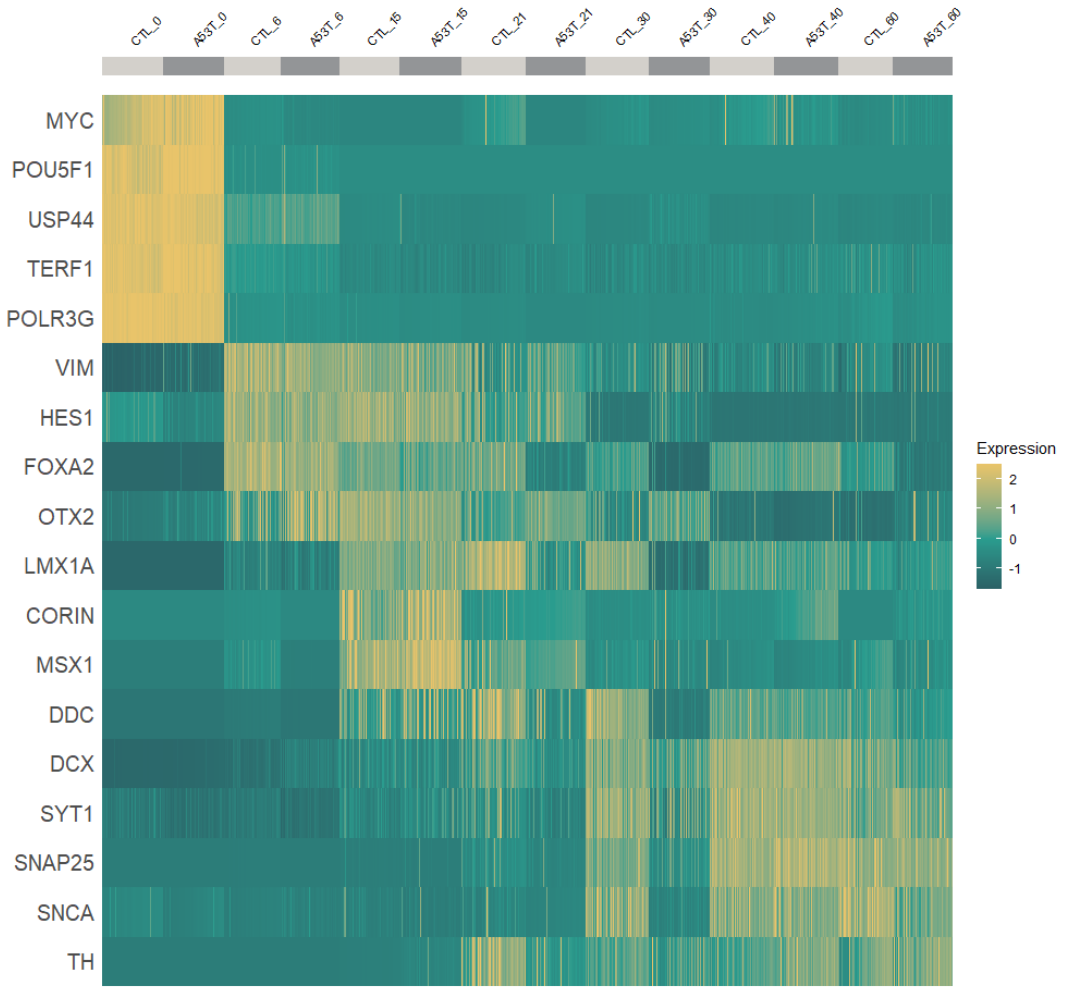

Fig. 4.3 Characterization of differentiation modules. Heatmap illustrating the transitions in gene expression from stemness markers (*MYC, POU5F1, USP44, TERF1*, and *POLR3G*), to genes associated with mDA differentiation (*VIM, HES1, FOXA2, OTX2, LMX1A*, and *CORIN*), and finally to the expression of mature mDA markers (*MSX1, DDC, DCX, SYT1, SNCA*, and *TH*) and the neuronal marker *SNAP25*. Colors correlate to normalized counts (z-score, centered, and scaled) of the indicated genes. Centering and scaling was performed independently at each timepoint.

4.2 Multi-omics analysis of *SNCA*-A53T and control cells

To investigate disease mechanisms linked to the *SNCA*-A53T mutation, we performed droplet-based scRNA-seq, bulk proteomics, and untargeted metabolomics (LC-MS) on *SNCA*-A53T and control cells at seven timepoints throughout mDA neuron differentiation (D0, D6, D15, D21, D30, D40, and D60). Each timepoint served as an independent biological replicate. Replicates were initiated on different days using cells of varying passage numbers to account for biological variability and minimize batch effects.

4.2.1 scRNA-seq analysis

To identify transcriptional pathways affected by the *SNCA*-A53T mutation, we employed scRNA-seq using the Drop-seq method at days 0, 6, 15, 21, 30, 40, and 60 (Methods Section 3.4.1). This approach allowed us to track dynamic changes in gene expression throughout the differentiation at a single-cell resolution [373, 111].

4.2.1.1 UMAP visualization of clusters based on differentiation stage

After preprocessing and quality filtering (Methods 3.4.1.4), a total of 33,063 cells and 19,695 genes were included in our analysis. Using the Louvain modularity algorithm, we identified seven distinct clusters of cells based on shared phenotypic features (Fig. 4.4). UMAP dimensionality reduction demonstrated that clustering was primarily driven by developmental stage, with *SNCA*-A53T and control lines grouping together according to the day of differentiation. These results indicate that gene expression profiles were largely comparable between *SNCA*-A53T and control, and that both cell lines followed similar differentiation trajectories. However, at day 30, *SNCA*-A53T and control clusters exhibited a small degree of separation, further suggesting developmental alterations associated with the *SNCA*-A53T mutation.

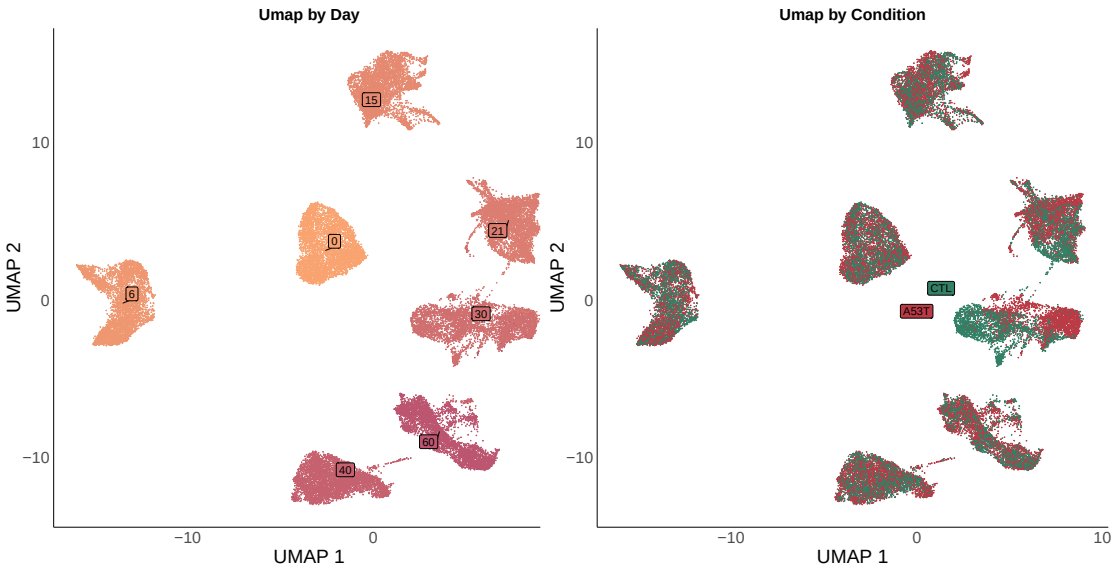

Fig. 4.4 UMAP embeddings by day and condition. UMAP projections illustrate that *SNCA*-A53T and control cells cluster based on the day of differentiation, indicating comparable developmental trajectories. At day 30, reduced overlap between the two populations suggests transcriptional differences between *SNCA*-A53T and control cells.

4.2.1.2 Transcriptional dysregulation of bioenergetic pathways in *SNCA*-A53T mutant cells

As an initial step, we sought to investigate the impact of the *SNCA*-A53T mutation on neuronal development and to determine the onset of PD-associated impairments. To this end, we identified the top differentially expressed genes (DEGs) between *SNCA*-A53T and control cells at each timepoint of the differentiation (adjusted p values ($p_{\text{adj}} < 0.05$ and $|\text{FC}|>0.4$). For the full list of DEGs, see Appendix Section A.1.

Using this approach, we detected a total of 2502 DEGs across the seven timepoints (Fig. 4.5). Interestingly, the highest number of DEGs was observed at days 21 and 30, corresponding to the transition from early-stage progenitors to more mature dopaminergic neurons. This may reflect the activation of transcriptional pathways that facilitate the adaptations necessary for mDA neuron maturation. However, this transition period may also be when cells are

most vulnerable to the deleterious effects of the *SNCA*-A53T mutation. This is supported by the transcriptional divergence observed between *SNCA*-A53T and control cells in the UMAP projections at day 30 (Fig. 4.4).

In contrast, fewer DEGs were identified at days 40 and 60, suggesting that gene expression differences stabilized as neurons matured. At these later timepoints, we also noted a decline in the number of detected genes per cell and the overall number of genes with at least one read. This reduction may be influenced by *in vitro* culture conditions, as prolonged maintenance can affect cell viability [387]. Additionally, isolating aged neurons for scRNA-seq is technically challenging due to their complex morphologies, which may contribute to the weaker transcriptomic phenotype observed at the later stages.

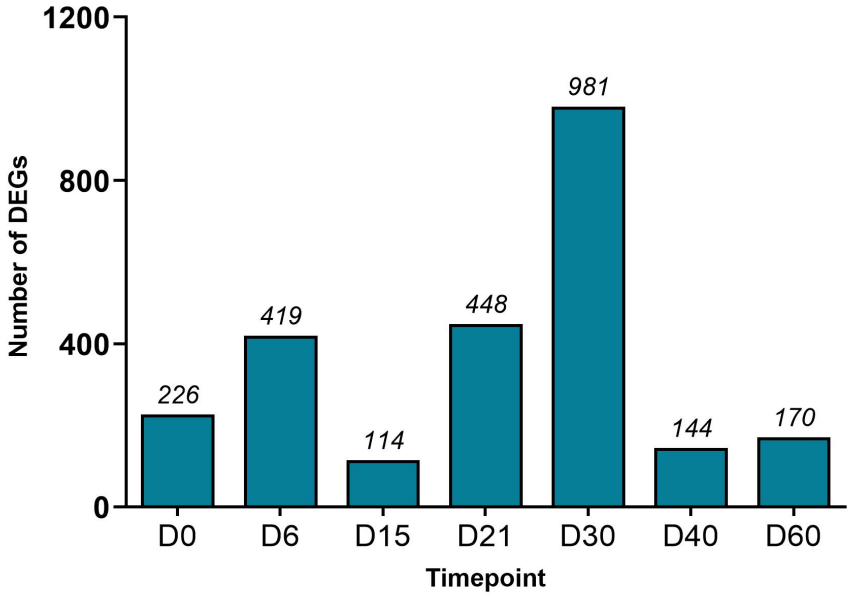

Fig. 4.5 DEGs per timepoint. Number of DEGs identified between *SNCA*-A53T and control cells at each timepoint of the differentiation ($p_{\text{adj}} < 0.05$ and $|\text{FC}|>0.4$). At day 30, a peak in DEGs was observed, potentially indicating a phase in mDA development when the cells are most vulnerable to the effects of the *SNCA*-A53T mutation.

Next, we explored the functional annotations of the DEGs using Metascape to perform GO (biological processes) and KEGG pathway enrichment analyses (Tab. 4.1 and Methods Section 3.4.1.5). Using this approach, we aimed to identify the biological processes and pathways disrupted by the *SNCA*-A53T mutation and to determine the development stages at which these impairments first emerge.

The enrichment analyses revealed transcriptional dysregulation in critical processes associated with PD pathology including mitochondrial function, oxidative phosphorylation (OXPHOS), and neuronal development (Tab. 4.1). In line with this, PD emerged as an enriched term at multiple timepoints of the differentiation, including the early stages of development. These findings suggest that PD-associated impairments manifest prior to the maturation of mDA neurons.

The highest number of PD-associated genes was identified at days 21 (29 genes) and 30 (43 genes) (Appendix Tab. A.8), supporting the notion that the *SNCA*-A53T mutation exerts a strong effect during the conversion to the mDA phenotype. Within the PD annotations, we identified genes involved in the cellular response to stress (Fig. 4.6). For instance, genes associated with protein degradation (*PSMA1, PSMA3,* and *UBA52*) and oxidative stress (*SOD1* and *TXN*) were upregulated in *SNCA*-A53T cells at multiple timepoints. Interestingly, we also observed a downregulation of genes encoding calmodulin proteins (*CALM1* and *CALM2*), which play a pivotal role in buffering intracellular calcium. This observation aligns with evidence implicating defective calcium homeostasis as a driver of PD pathogenesis [388].

Another key finding was the enrichment of pathways related to mitochondrial function, specifically OXPHOS, at the earliest stages of the differentiation (days 0, 6, and 15) (Tab. 4.1). Interestingly, many of the genes identified in the PD annotations were also OXPHOS genes, further implicating mitochondrial dysfunction as an important event in *SNCA*-A53T mediated pathology (Appendix Tab. A.8). Throughout the differentiation, *SNCA*-A53T cells predominantly exhibited overexpression of genes encoding respiratory chain complexes. Specifically, this included subunits and assembly factors of complex I (e.g., *NDUFA13, MT-ND5*, and *MT-ND1*), complex III (e.g., *UQCRB* and *UQCRH*), complex

IV (*e.g., COX7C, COX6B1*, and *COX5A*), and complex V (e.g., *ATP5MC2* and *MT-ATP6*) (Fig. 4.6).

In addition, terms related to neuron differentiation were enriched from day 21 onward (Tab. 4.1). Notably, we observed a downregulation of genes associated with neuron projection in *SNCA*-A53T cells at day 21, and to a greater extent at day 30 (Fig. 4.7). This included genes involved in dopaminergic neuron development, such as *NRP1, NR4A2 (Nurr1), GAP43, DDC, MAP2, LMX1A, NEFL*, and *FOXA2*. These changes may contribute to the subtle separation of *SNCA*-A53T and control clusters in the UMAP projections (Fig. 4.4). Overall, these findings again support an effect of the *SNCA*-A53T mutation on the neurodevelopmental trajectory of mDA neurons.

Day	Top KEGG annotations	Top GO annotations
0	Diabetic cardiomyopathy	Oxidative phosphorylation
	Oxidative phosphorylation	Generation of precursor metabolites
	Prions disease	Aerobic respiration
6	Alzheimer's disease	Head & brain development
	Parkinson's disease	Purine metabolic process
	Amyotrophic lateral sclerosis	Oxidative phosphorylation
15	Oxidative phosphorylation	Thermogenesis
	Aerobic respiration	Diabetic cardiomyopathy
	Cellular respiration	Parkinson's disease
21	Parkinson's disease	Brain development
	Alzheimer's disease	Reg. of neuron projection
	Huntington disease	Neuron projection development
30	Parkinson's disease	Neuron projection development
	Neurodegeneration	Neuron morphogenesis
	Dopaminergic synapse	PM bounded cell projection
40	No KEGG annotations	Brain & head development
		Forebrain development
		Cell projection morphogenesis
60	Neurodegeneration	Brain & head development
	Alzheimer's disease	Neuron projection development
	Parkinson's disease	Axon development

Table 4.1 DEG enrichment analyses. Top KEGG and GO annotations for DEGs between *SNCA*-A53T and control at each timepoint of the differentiation ($p_{\text{adj}} < 0.05$ and |FC|>0.4).

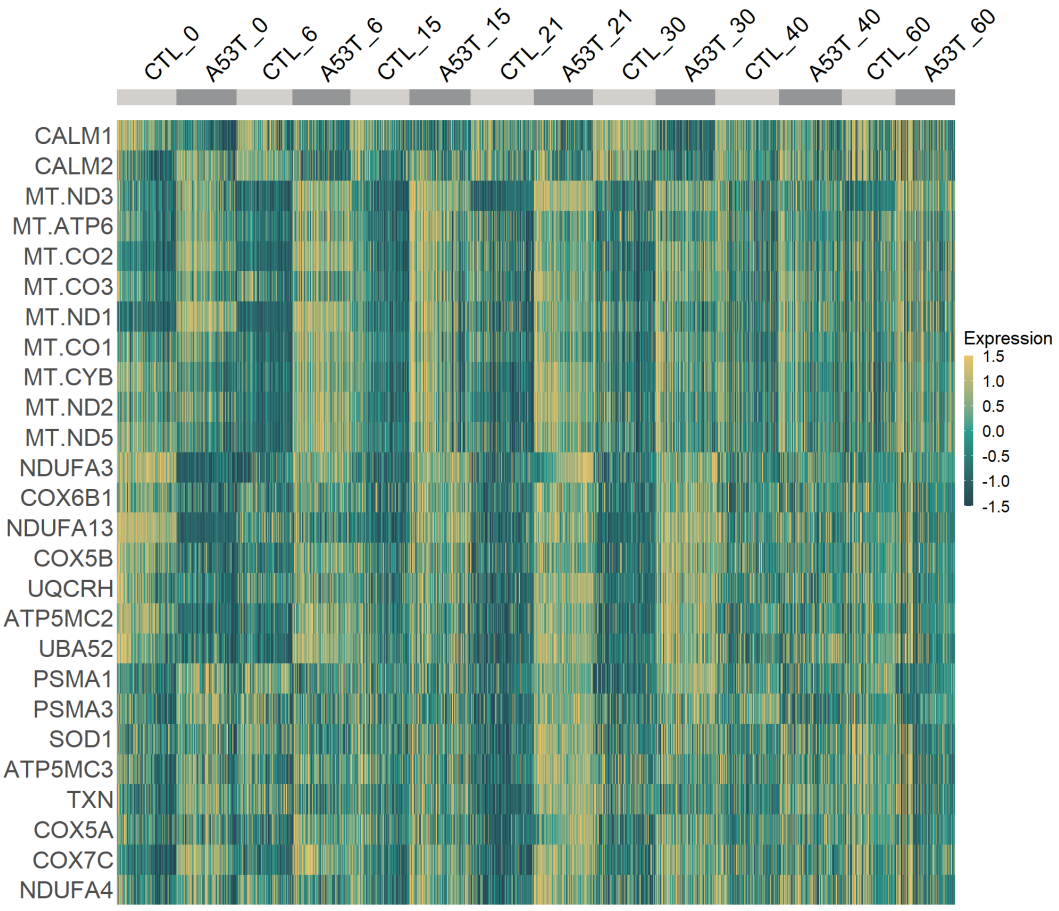

Fig. 4.6 Dysregulated PD-associated genes. Heatmap for selected OXPHOS and cell stress genes identified within the PD annotations that where differentially expressed between *SNCA*-A53T and control cells at multiple timepoints of the differentiation ($p_{\text{adj}} < 0.05$ and |FC|>0.4). Colors correlate to normalized counts (z-score, centered, and scaled) of the indicated genes. Centering and scaling was performed independently at each timepoint.

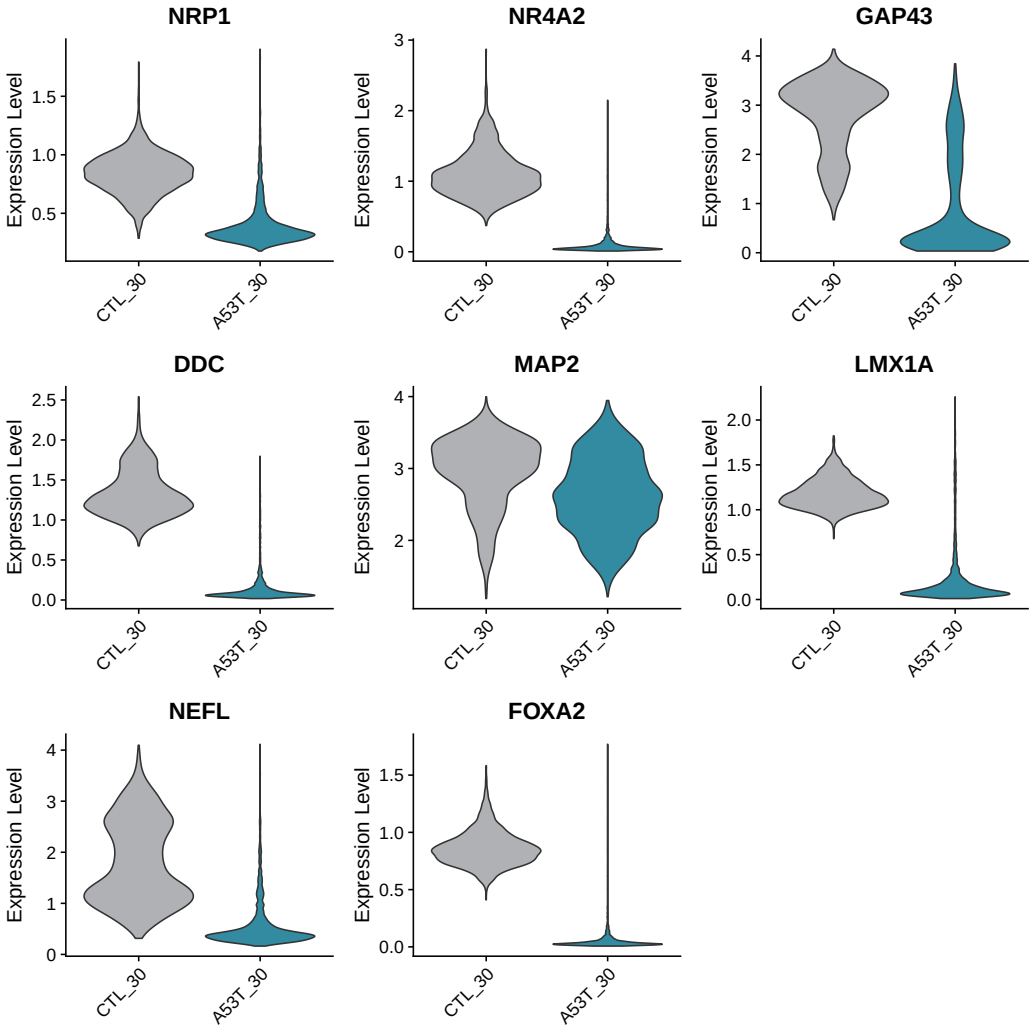

Fig. 4.7 Downregulation of genes associated with mDA neuron identity. Violin plots showing the downregulation of genes associated with mDA neuron identity and development in *SNCA*-A53T at day 30 of the differentiation ($p_{\text{adj}} < 0.05$ and |FC|>0.4).

4.2.1.3 Persistently dysregulated genes converge on mitochondrial function

Expanding on the timepoint-specific analysis, we next sought to identify genes that were persistently dysregulated throughout the differentiation. These genes are influenced by the presence of the *SNCA*-A53T mutation regardless of cell state and thus likely reflect genes that participate in systemic PD pathology. For this purpose, we focused on genes that were dysregulated in the same direction (upregulated or downregulated) at five or more timepoints of the differentiation ($p_{\text{adj}} < 0.05$ and fold change |FC|>0.25).

Using this approach, we identified a network of 56 dysregulated genes (31 consistently upregulated and 25 consistently downregulated) (Fig. 4.8 and Appendix Tab. A.10). Interestingly, many of the persistently dysregulated genes aligned with the temporal disruptions observed in the timepoint-specific analysis. Again we observed a strong representation of genes crucial for mitochondrial dynamics, cellular stress responses, and neuronal differentiation.

For instance, OXPHOS genes, including *MT-CO1*, *MT-CO2* (subunits of complex IV), and *MT-ND3* (a subunit of complex I), were consistently overexpressed in *SNCA*-A53T cells (Fig. 4.9). Similarly, genes involved in mitochondrial protein synthesis (*MT-RNR1*) and import (*TIMM10*) were also persistently upregulated. In contrast to this, key mitochondrial regulators such as *CHCHD2* and *DNAJC15* were underexpressed throughout the differentiation (Fig. 4.9). Notably, mutations in *CHCHD2* have been linked to both familial and sporadic PD [389].

Alongside this, *SNCA*-A53T cells also exhibited a persistent upregulation of genes associated with protein quality control (*CLU, PSMD10*, and *USP11*), oxidative stress (*FTL* and *S100A6*), DNA repair (*DDX11, MORF4L2*, and *ZNF506*), and apoptosis (*STK26, BEX2*, and *BEX3*) (Fig. 4.8). Many of these pathways are frequently implicated in PD pathology (as discussed in Section 1.2.4). As such, our findings further highlight the broad cellular stress response in *SNCA*-A53T cells, suggesting that dysregulation across multiple systems contributes to disease pathogenesis.

Finally, we observed the dysregulation of genes involved in various aspects of neuronal development. More specifically, genes associated with dopamine neuron survival (*PBX1*) and identity (*LM03, MAP2,* and *NR2F1*) were consistently downregulated in *SNCA*-A53T cells (Fig. 4.8). Intriguingly, *NR2F1* has recently been demonstrated to interact with the PD mutation *LRRK2*-G2019S, to accelerate dopaminergic differentiation [390]. Therefore, its dysregulation in *SNCA*-A53T cells may suggest shared mechanisms of pathology.

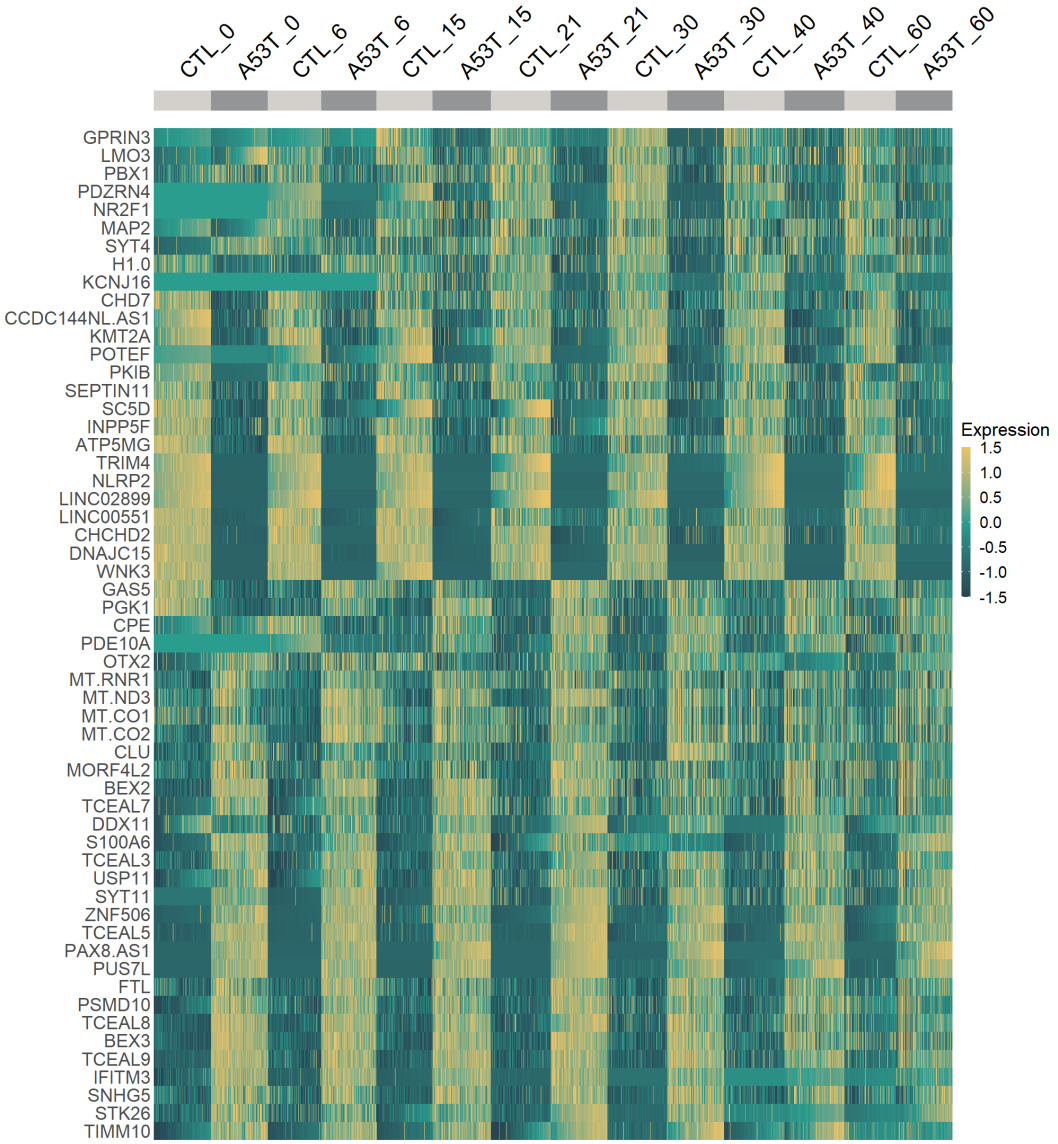

Fig. 4.8 Persistently dysregulated genes. Heatmap showing genes dysregulated between *SNCA*-A53T and control cells at five or more timepoints of the differentiation ($p_{\text{adj}} < 0.05$ and fold change |FC|>0.25). Colors correlate to normalized counts (z-score, centered, and scaled) of the indicated genes. Centering and scaling was performed independently at each timepoint.

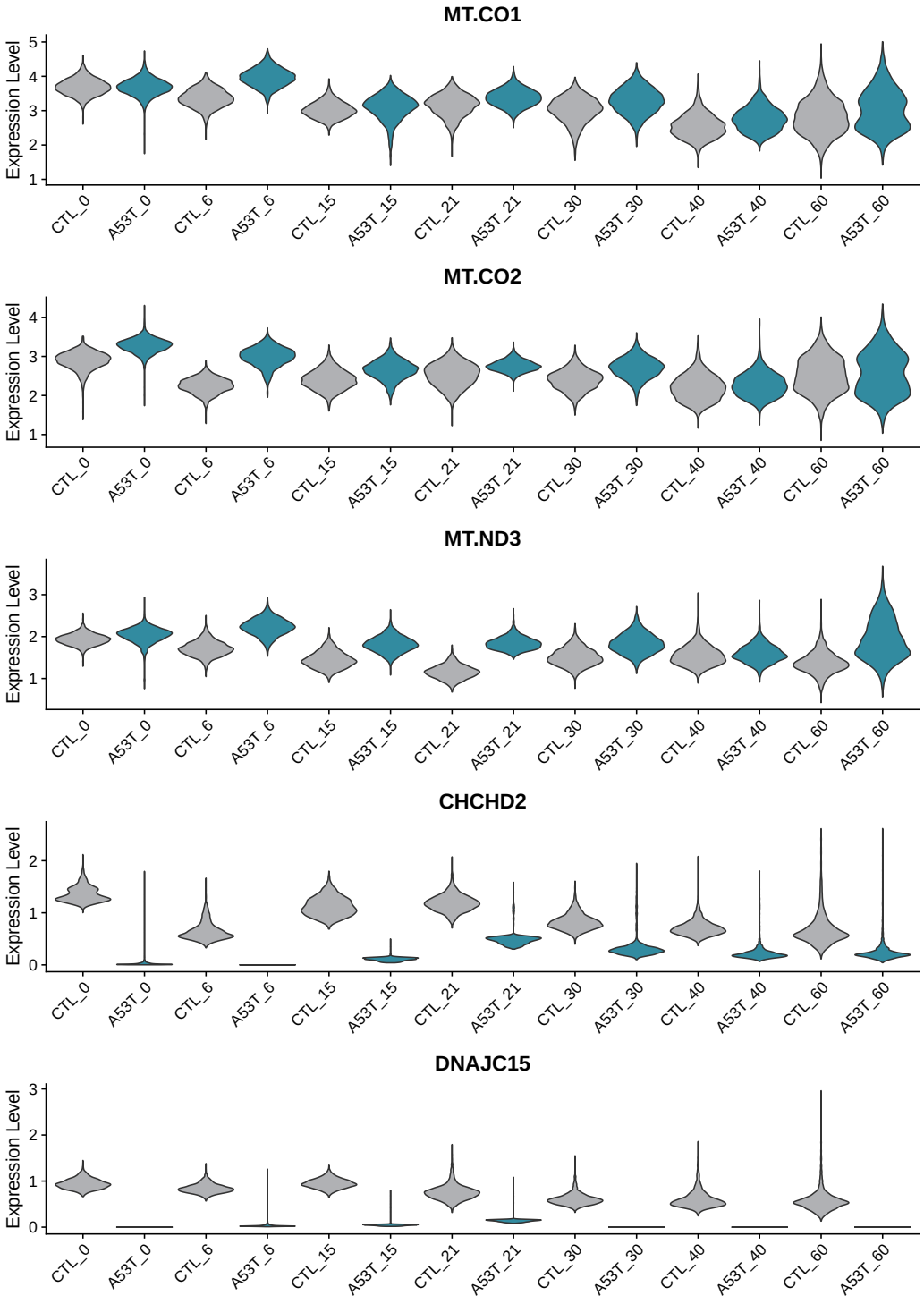

Fig. 4.9 Persistently dysregulated mitochondrial-related genes. Violin plots of selected mitochondrial-related genes persistently dysregulated in *SNCA*-A53T cells throughout the differentiation ($p_{\text{adj}} < 0.05$ and $|\text{FC}|>0.25$).

4.2.2 Proteomic analysis

To investigate how the identified transcriptional alterations manifest at the protein level, we performed bulk proteomics on *SNCA*-A53T and control cells at days 0, 6, 15, 21, 30, 40, and 60 of the differentiation, in parallel with scRNA-seq analysis (Methods Section 3.4.2). This approach enabled us to track proteomic changes throughout neuronal development, whilst providing insights into how *SNCA*-A53T-driven transcriptional alterations translate into protein-level phenotypes.

4.2.2.1 Proteomic alterations extend into late maturation

Analogous to our transcriptomic approach, we first identified the top differentially abundant proteins (DAPs) at each timepoint of the differentiation ($p_{\text{adj}} < 0.05$ and $|\text{FC}|>1$) (Fig. 4.10). For the full list of DAPs, see Appendix Section A.2.

Similar to the transcriptomic dataset, we observed a high number of DAPs at day 30, confirming that transcriptional alterations are reflected at the protein level (Fig. 4.10). However, unlike the transcriptomic analysis, where fewer DEGs were detected at later differentiation stages, proteomic alterations persisted into the mature neuronal phenotype. Notably, we observed 518 DAPs at day 40, indicating that differences between *SNCA*-A53T and control cells become more pronounced as cells mature into differentiated mDA neurons. These findings suggest that molecular alterations not only arise early in neuronal development but also persist into later maturation stages, potentially contributing to PD progression.

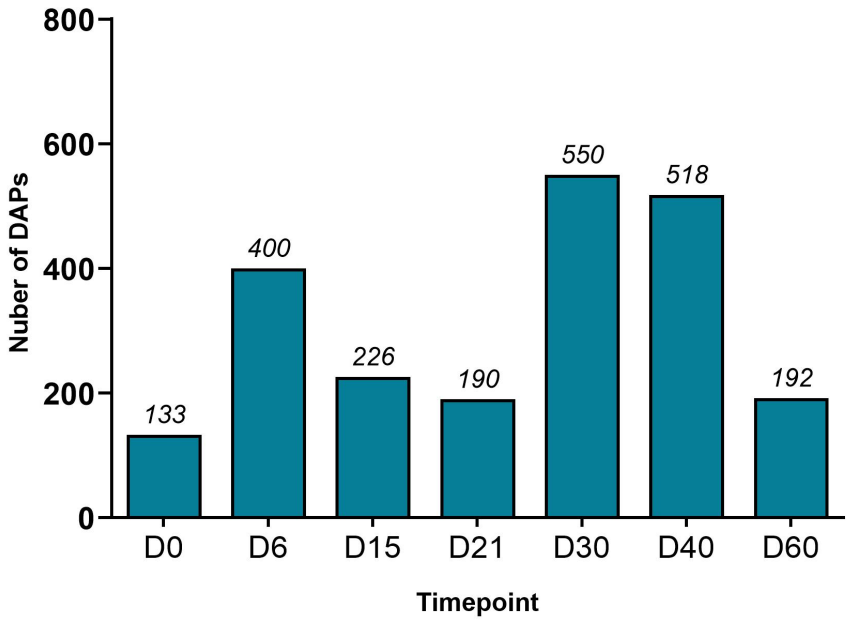

Fig. 4.10 DAPs per timepoint. Number of DAPs between *SNCA*-A53T and control cells at each timepoint of the differentiation ($p_{\text{adj}} < 0.05$ and |FC|>1). The number of DAPs exhibits peaks at days 30 and 40, suggesting that *SNCA*-A53T-induced alterations affect maturing mDA neurons.

After identifying the DAPs at each timepoint, we performed enrichment analyses using Metascape to identify proteomic pathways impacted by the *SNCA*-A53T mutation at each stage of differentiation (Methods Section 3.4.1.5). Interestingly, PD consistently emerged as an enriched KEGG pathway across all seven timepoints of the DAP analysis (Tab. 4.2). Dysregulation of proteasome components (PSMA2, PSMC5, and PSMC1) and upregulation of VDAC proteins (VDAC1, VDAC2, and VDAC3) were common to multiple timepoints, suggesting persistent alterations in both proteostasis and mitochondrial function in *SNCA*-A53T cells (Fig. 4.11). Likewise, we again observed that proteins central to the assembly of electron transport chain (ETC) complexes (ATP5F1E, NDUFB1, NDUFB5, UQCRFS1, COX1, and ATP5FD1) were dysregulated in *SNCA*-A53T cells at multiple timepoints of the differentiation (Fig. 4.11).

The most pronounced phenotype occurred at day 40, characterized by the highest number of PD-related proteins (32 proteins) (Appendix Tab. A.9). Unique to this timepoint was the strong representation of proteins involved in cytoskeletal organization and axonal transport (Fig. 4.11). More specifically, we observed a significant upregulation of tubulin proteins, including TUBB6, TUBB2A, TUBB4B, TUBB, and TUBB4A in *SNCA*-A53T cells, suggesting altered microtubule dynamics.

Interestingly, cytoplasmic translation also appeared as an enriched GO term at days 0, 6, 40, and 60 of the differentiation (Tab. 4.2). Overall, we identified 42 proteins within this annotation, with the majority being upregulated in *SNCA*-A53T cells (see Appendix Fig. A.3). Many of these were RPL proteins of the 60S ribosomal subunit and RPS proteins of the 40S ribosomal subunit. This aligns with growing evidence implicating aberrant translation in PD pathogenesis [391]. Similar mechanisms have been reported in *LRRK2*- and *DJ-1*-associated pathology, where translational upregulation promotes disease progression, likely by upregulating pathogenic translational targets [392, 393]. Notably, inhibition of translation has been shown to protect dopaminergic neurons from degeneration, further highlighting its potential relevance as a therapeutic target in PD [392].

Enrichment of the DAPs at each timepoint also revealed terms associated with other neurodegenerative pathologies such as Huntington's disease, amyotrophic lateral sclerosis, and prion disease (Tab. 4.2). We identified a significant overlap in the proteins identified within these annotations and those identified in the PD annotations. Many of these disorders display similar pathogenic features to PD, including protein aggregation, mitochondrial dysfunction, and progressive degenerative pathology. As such, there may be convergent mechanisms of cellular dysfunction between these diseases. Our findings may therefore have a broader relevance to other neurodegenerative pathologies.

Day	Top KEGG annotations	Top GO annotations
0	Influenza A Parkinson's disease	Alcohol metabolic process Cytoplasmic translation Cellular respiration
6	Amyotrophic lateral sclerosis Pathways of neurodegeneration Huntington's disease Parkinson's disease	Cytoplasmic translation Translation Purine nucleotide metabolic process
15	Prion disease Parkinson's disease Thermogenesis	Membrane organization Regulation of transferase activity Oxidative phosphorylation
21	Amyotrophic lateral sclerosis Prion disease Pathways of neurodegeneration Huntington's disease Parkinson's disease	Heterochromatin formation Projection organization Plasma membrane projection
30	Cytoskeleton in muscle cells Ribosome Parkinson's disease	Neuron projection development Neuron projection morphogenesis Plasma membrane projection
40	Amyotrophic lateral sclerosis Pathways of neurodegeneration Parkinson's Disease	Cytoplasmic translation Membrane organization Purine ribonucleotide metabolism
60	Ribosome Parkinson's disease Covid 19	Regulation of spindle organization Cytoplasmic translation Reg. of mitotic spindle organization

Table 4.2 DAP enrichment analyses. Top KEGG and GO annotations for DAPs between *SNCA*-A53T and control at each timepoint of the differentiation ($p_{\text{adj}} < 0.05$ and $|\text{FC}|>1$).

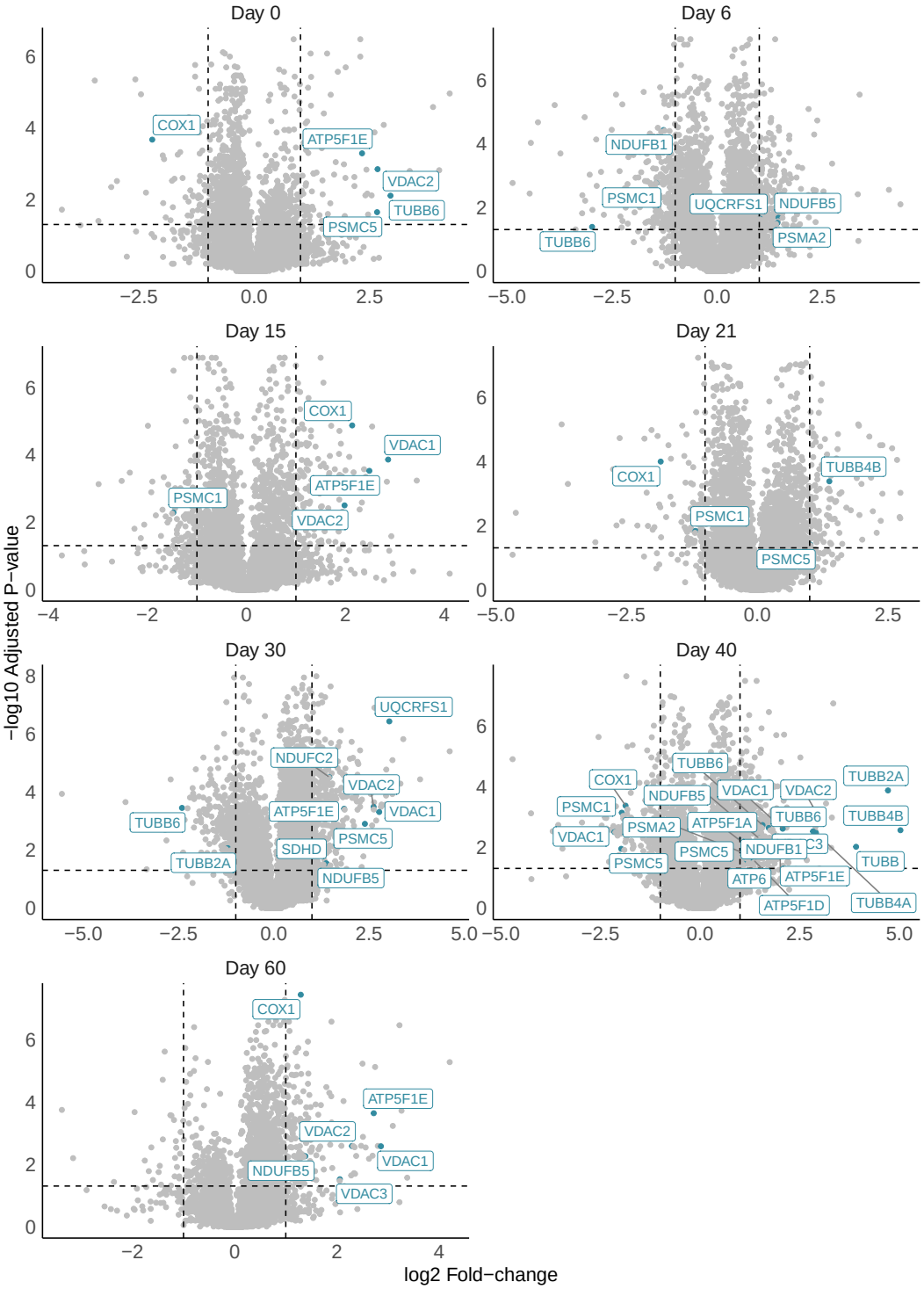

Fig. 4.11 Dysregulated PD-associated proteins. Volcano plots of selected PD-associated proteins that were dysregulated between *SNCA*-A53T and control cells at multiple timepoints of the differentiation ($p_{\text{adj}} < 0.05$ and $|\text{FC}|>1$). Horizontal dashed line marks stastistical significance.

4.2.2.2 Proteomics confirms the mitochondrial phenotype in *SNCA*-A53T cells

Following this timepoint-wise analysis, we investigated proteins that were systemically altered by the *SNCA*-A53T mutation. Specifically, we focused on proteins that were dysregulated in the same direction across five or more timepoints of the differentiation ($p_{\text{adj}} < 0.05$ and |FC|>0.5). This revealed a total of 71 DAPs, including 44 that were persistently upregulated and 27 that were persistently downregulated in *SNCA*-A53T cells (Fig. 4.12 and Appendix Tab. A.11).

Similar to the persistently dysregulated genes, proteins involved in OXPHOS were consistently altered. *SNCA*-A53T cells exhibited an upregulation of proteins associated with ETC complex biogenesis (DMAC2, UQCRFS1, ATP5F1E, and SCO2), possibly reflecting a compensatory response to cellular stress (Fig. 4.13). In line with this, proteins involved in mitochondrial turnover (FKBP8) and mtDNA repair (LIG3) were upregulated, whereas proteins involved in respiratory chain regulation (CHCHD2) and oxidative stress defense (CAT) were downregulated throughout differentiation in *SNCA*-A53T cells (Fig. 4.13 and Fig. 4.12).

Beyond this, PGK1, a pivotal glycolytic enzyme, was also persistently upregulated in *SNCA*-A53T cells (Fig. 4.12). This potentially reflects an adaptive response to mitochondrial dysfunction and suggests broader metabolic impairments beyond OXPHOS. Recently, Terazosin, a PGK1 activator, has been shown to confer neuroprotection in multiple PD models. Suggesting PGK1 activity is a crucial leverage point in neuronal bioenergetic control [394].

We also observed that proteins crucial for regulating mitochondrial calcium dynamics, namely VDAC2, Miro1 (*RHOT1*), and EMRE (*SMDT1*), were upregulated throughout the differentiation in *SNCA*-A53T cells (Fig. 4.13). These proteins work in a coordinated manner to shuttle Ca^{2+} across mitochondrial membranes. Consistent with our findings, previous studies have reported that PD-associated mutations can influence the levels and turnover of Ca^{2+} transport proteins [395]. This in turn can have detrimental effects on mDA neurons, which are already primed for calcium dysfunction due to their lower Ca^{2+} buffering capacity (as outlined in Section 1.2.4.6).

Another notable finding was the downregulation of HPCAL1 and CDH2 in *SNCA*-A53T cells (Fig. 4.12). Recent studies have shown that HPCAL1 mediates ferroptosis through its interaction with CDH2, suggesting that the simultaneous downregulation of these proteins may alter the susceptibility of *SNCA*-A53T cells to ferroptotic cell death [396].

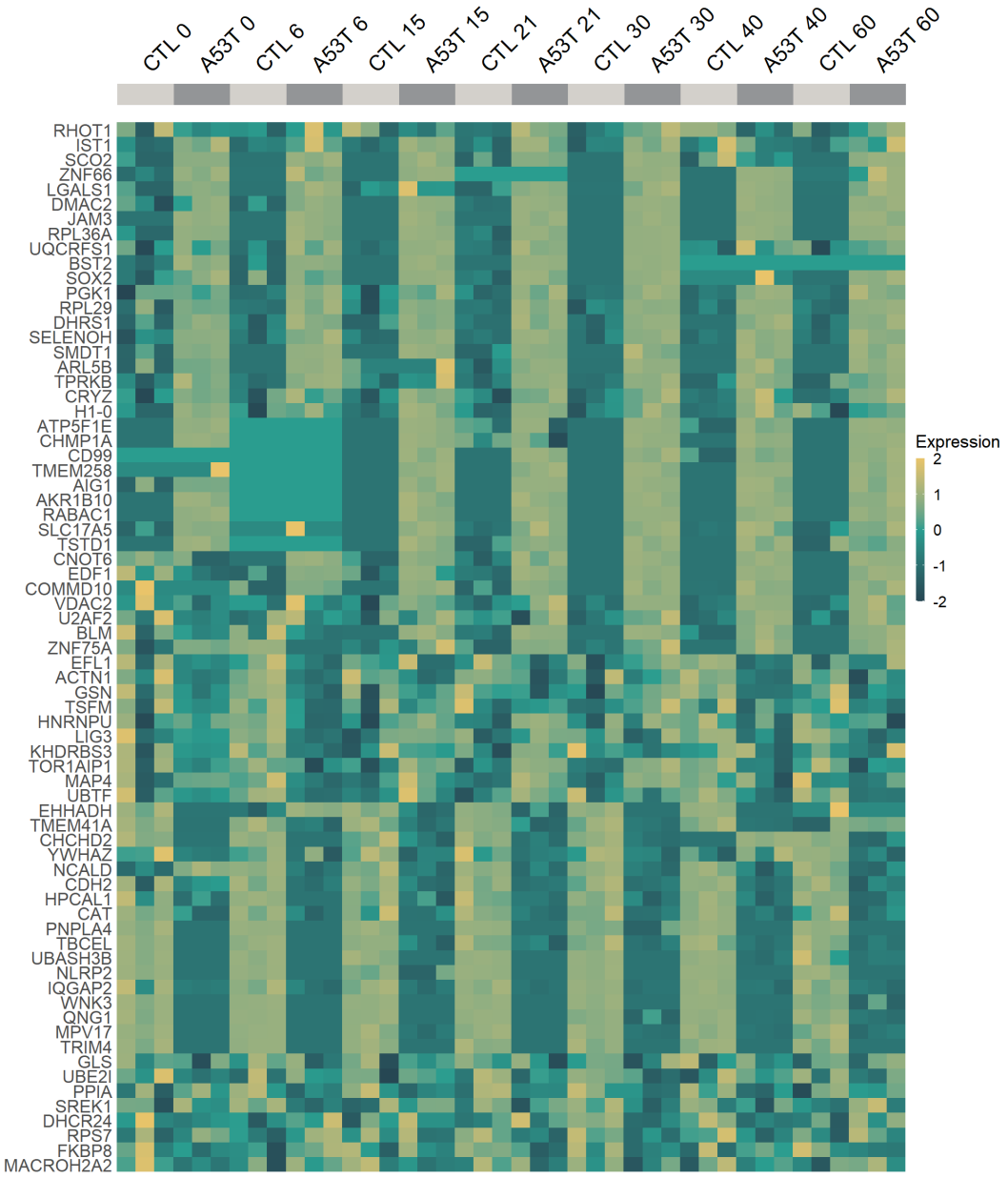

Fig. 4.12 Persistently dysregulated proteins. Heatmap showing proteins dysregulated between *SNCA*-A53T and control cells at five or more timepoints of the differentiation ($p_{\text{adj}} < 0.05$ and $|\text{FC}|>0.5$). Colors correlate to normalized counts (z-score, centered, and scaled) of the indicated proteins. Centering and scaling was performed independently at each timepoint.

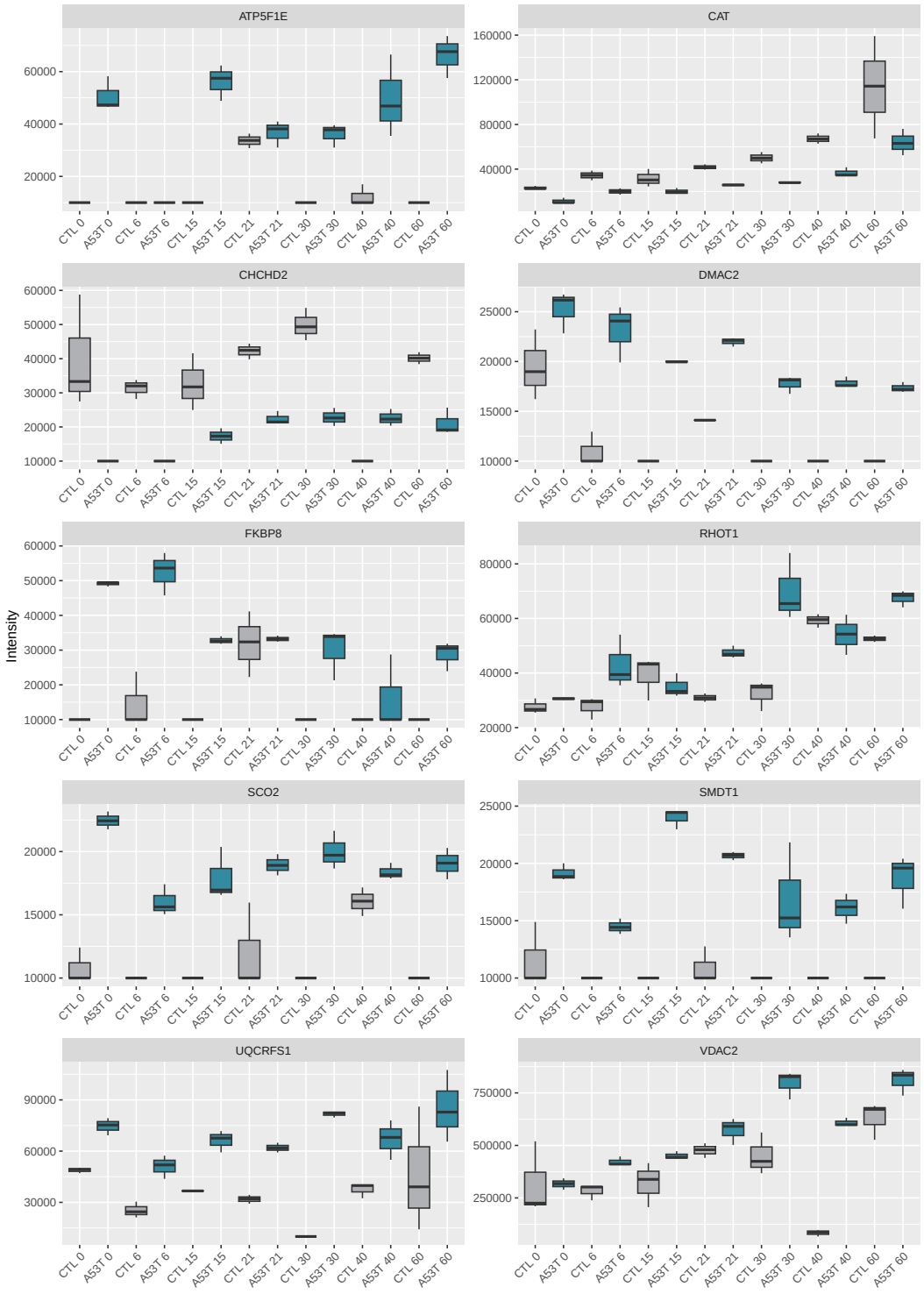

Fig. 4.13 Persistently dysregulated mitochondrial- and calcium-related proteins. Boxplots for selected proteins involved in mitochondrial function and calcium dynamics persistently dysregulated between *SNCA*-A53T and control cells at five or more timepoints of the differentiation ($p_{\text{adj}} < 0.05$ and |FC|>0.5).

4.2.3 Overlap between transcriptomic & proteomic datasets

As similar biological pathways were altered in both the transcriptomic and proteomic analyses, we sought to characterize this overlap in greater detail and to determine the extent to which the transcriptional alterations are mirrored in the proteome. To this end, we identified DEGs and DAPs that were shared at each timepoint of the differentiation. To adopt a stringent approach, we applied the same thresholds used for the previous analyses (DEGs, ($p_{\text{adj}} < 0.05$ and |FC|>0.4) and (DAPs, ($p_{\text{adj}} < 0.05$ and |FC|>1) (Fig. 4.14). In doing so, we aimed to retain biologically meaningful changes whilst minimizing noise.

Interestingly, we observed the greatest overlap during the critical transition periods of the differentiation (Fig. 4.14). For example, at day 6 (5.1%), during the transition from pluripotency to early neural progenitors, and at days 21 (6.9%) and 30 (10.8%), during the transition from early to more mature mDA phenotypes. These findings suggest a degree of concordance between mRNA and protein changes at key developmental phases. However, we observed a smaller overlap (<2.6%) at all other timepoints of the differentiation. These findings draw parallels with other studies in which only a minimal correlation is observed between mRNA and protein measurements in multi-omics datasets [397]. However, due to factors like post-translational regulation, protein/mRNA stability, and temporal delays, estimating this overlap is somewhat approximative [293].

Based on this analysis, we then ranked the DEGs and DAPs by their absolute sum (see Methods Section 3.4.1.4) to identify the most s trongly dysregulated genes and proteins common to both datasets. By prioritizing genes with significant transcriptional changes and their corresponding proteins with altered abundance, we aimed to identify key drivers of disease. As components dysregulated at both the transcriptomic and proteomic levels may represent critical regulatory hubs, acting as entry points for early pathology or promoting downstream neurodegeneration.

This approach revealed a core network of seven genes that were consistently dysregulated at both the transcriptomic and proteomic levels at a minimum

of four timepoints (Appendix Fig. A.4 and Fig. A.5). This network included *GPC3, BST2*, and *DLK1*, which were predominantly overexpressed, as well as *CHCHD2, WNK3, NLRP2*, and *QNG1*, which were underexpressed in *SNCA*-A53T cells. Interestingly, many of these genes have previously been identified in pathways closely linked to PD. More specifically, *NLRP2* and *BST2* are involved in neuroinflammation, while *WNK3* and *QNG1* play roles in neuroprotection. Additionally, several of these genes, including *CHCHD2, GPC3*, and *DLK1*, have been shown to interact with other PD-associated mutations, suggesting common pathogenic mechanisms [398, 111].

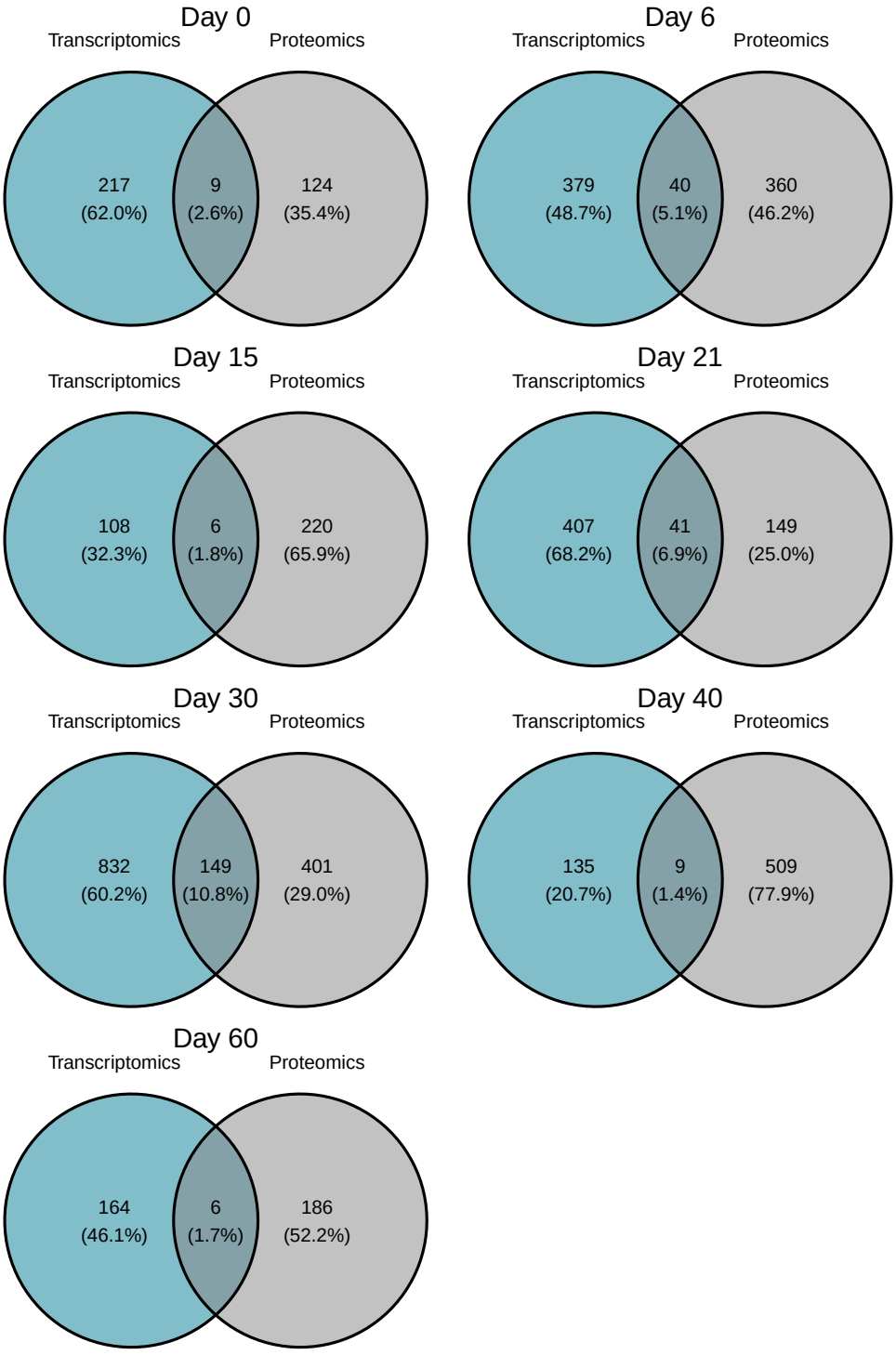

Fig. 4.14 Overlap between DEGs and DAPs. Venn diagrams showing overlap between DEGs and DAPs at each timepoint of the differentiation (DEGs, ($p_{\text{adj}} < 0.05$ and |FC|>0.4) and (DAPs, ($p_{\text{adj}} < 0.05$ and |FC|>1).

4.2.4 Metabolomic analysis

To explore how the identified transcriptomic and proteomic alterations influence the metabolome, we performed LC-MS-based metabolomics at days 0, 6, 15, 21, 30, 40 and 60 (Methods Section 3.4.3). Using this approach, we sought to investigate how these molecular changes affect cellular metabolism and gain deeper insights into their functional consequences.

4.2.4.1 Early alterations in energy metabolism in *SNCA*-A53T cells

Using this technique, we identified 80 metabolites that were differentially abundant between *SNCA*-A53T and control cells across the seven timepoints ($p_{\text{adj}} < 0.05$ and |FC|>0.4). For the full list of differentially abundant metabolites, see Appendix Section A.4.

We observed the highest number of differentially abundant metabolites during the early stages of differentiation (days 0, 6, and 15) (Fig. 4.15). In contrast, only a few metabolites showed differential abundance between *SNCA*-A53T and control cells at days 21 and 30, with none detected at later time points.

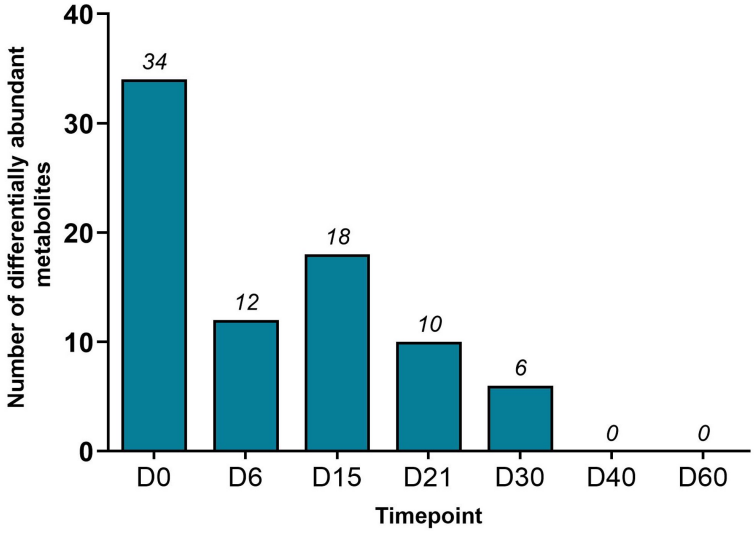

Fig. 4.15 Differentially abundant metabolites per timepoint. Number of differentially abundant metabolites between *SNCA*-A53T and control cells at each timepoint of the differentiation ($p_{\text{adj}} < 0.05$ and |FC|>0.4).

In *SNCA*-A53T cells, we observed distinct alterations in metabolites related to energy production in the early differentiation period (Fig. 4.16). At day 0, the levels of adenosine triphosphate (ATP), adenosine diphosphate (ADP), and adenosine monophosphate (AMP) were significantly lower in *SNCA*-A53T cells compared to control, which may reflect impaired energy production or increased utilization at the early stages of development. Similarly, glycolytic intermediates such as glucose-6-phosphate and fructose-1,6-bisphosphate were also decreased in *SNCA*-A53T cells, suggesting potential alterations in glycolytic flux.

Moreover, at day 6, several TCA cycle metabolites, including citric acid, fumaric acid, malic acid, and pyruvic acid (which links acetyl-CoA to the TCA cycle), were also significantly lower in *SNCA*-A53T cells, further highlighting differences in energy metabolism compared to control (Fig. 4.16).

To investigate these trends, we utilized the proteomics data to assess the expression levels of enzymes involved in the TCA cycle and glycolysis. While we didn't observe any discernible trends at the earlier timepoints, a marked increase in proteins encoding TCA cycle enzymes was observed at day 30 in *SNCA*-A53T cells (Fig. 4.17).

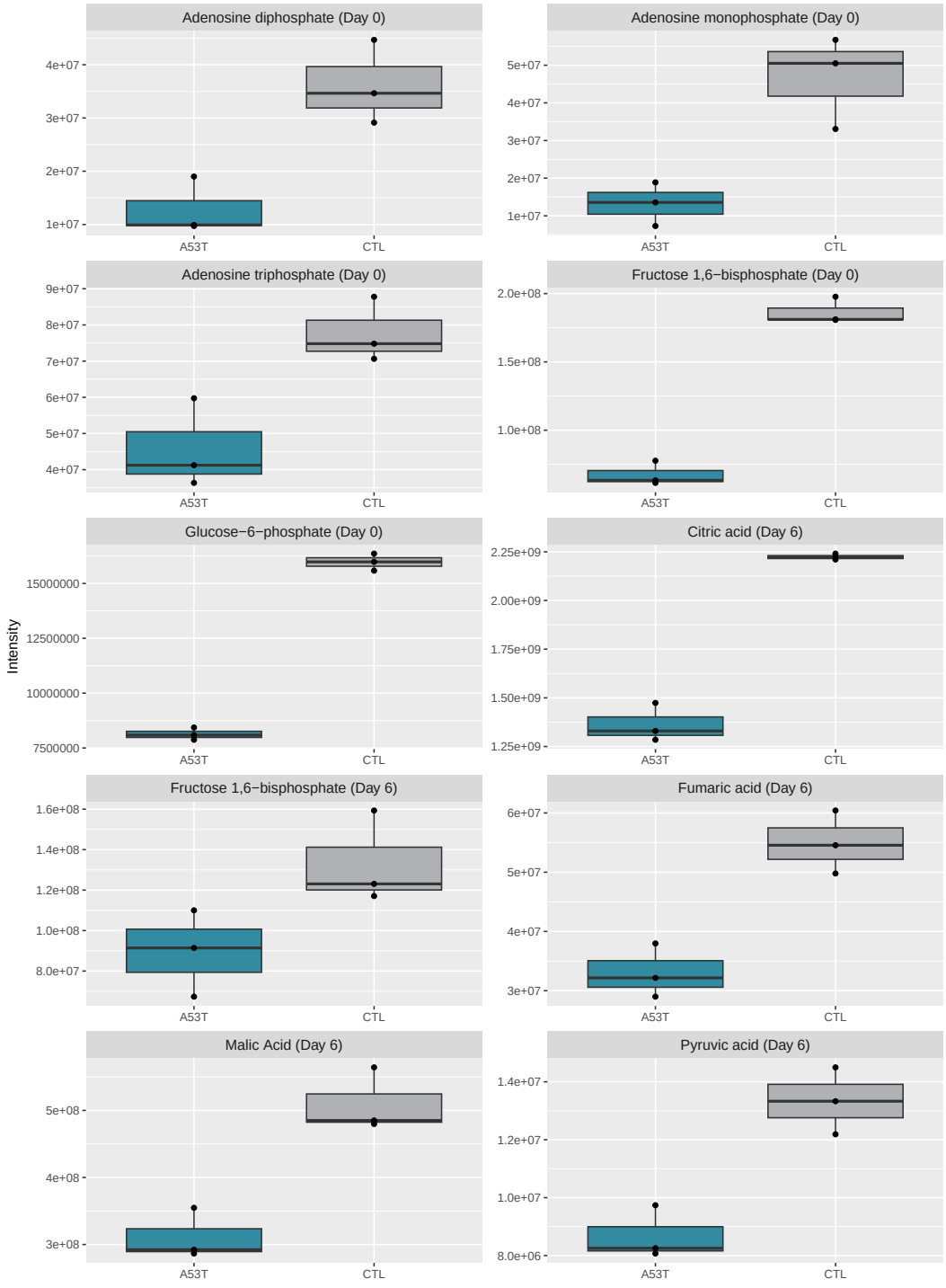

Fig. 4.16 Differentially abundant bioenergetic metabolites. Boxplots of differentially abundant energy metabolites, TCA cycle intermediates, and glycolytic intermediates between *SNCA*-A53T and control cells at the early differentiation timepoints ($p_{\text{adj}} < 0.05$ and $|\text{FC}|>0.4$).

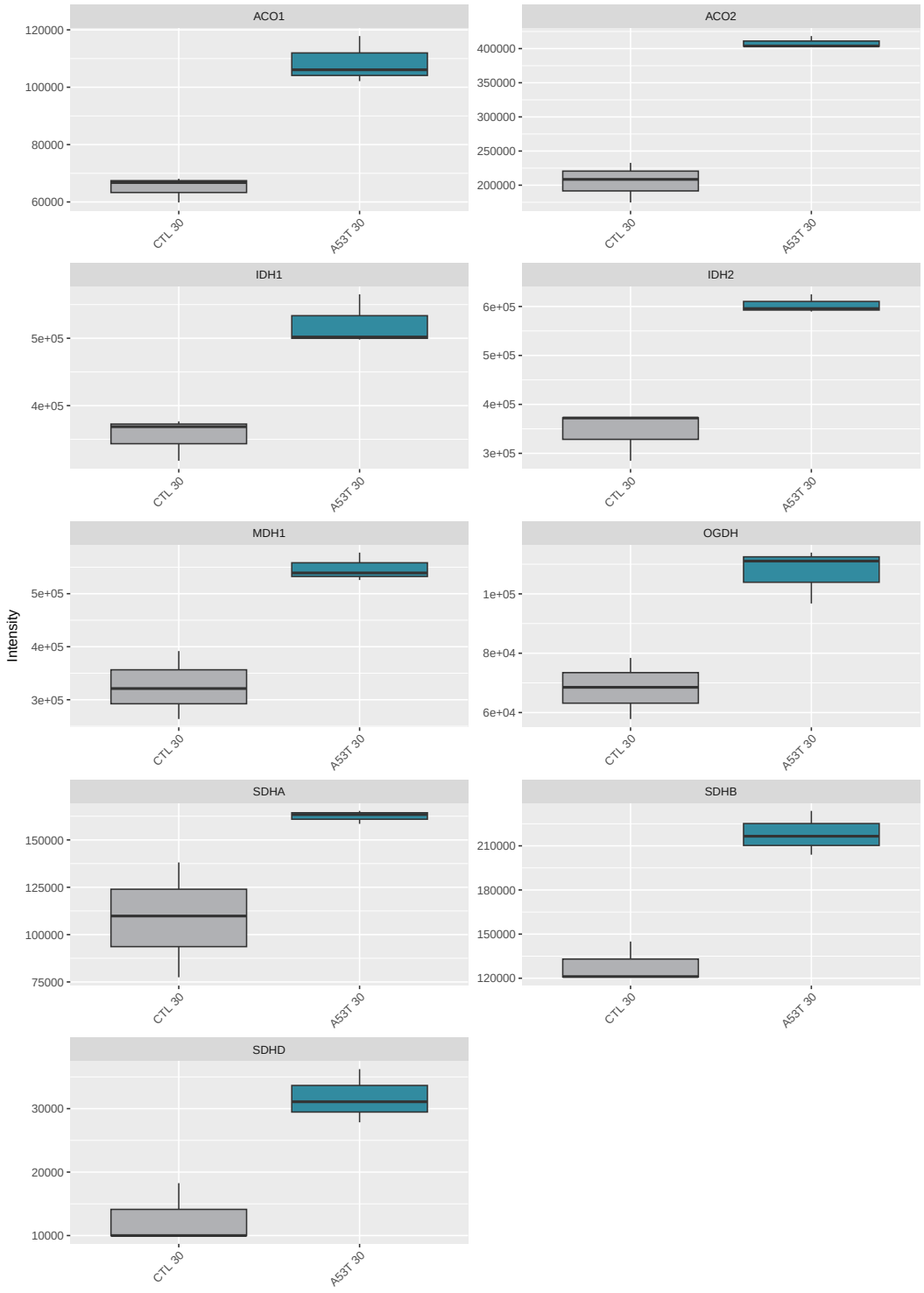

Fig. 4.17 Upregulated TCA cycle enzymes. TCA cycle enzymes identified as upregulated in *SNCA*-A53T cells at day 30 by proteomic analysis ($p_{\text{adj}} < 0.05$ and |FC|>1).

4.3 Mitochondrial function and protein expression analyses

As the multi-omics analysis revealed alterations in genes and proteins associated with mitochondrial dynamics and cellular respiration in *SNCA*-A53T cells, we sought to investigate these findings at a functional level. For this, we used the Seahorse XFe96 Flux Analyzer platform to assess the bioenergetic status of *SNCA*-A53T and control cells at days 15, 30, and 40 of the differentiation (Fig. 4.19). For detailed descriptions of the respiration parameters, see Methods Section 3.3.1 and Appendix Tab. A.6.

Briefly, oxygen consumption rate (OCR) and extracellular acidification rate (ECAR) were measured before and after the sequential injection of three key respiration modulators: the ATP synthase inhibitor oligomycin, the ETC uncoupler FCCP, and the complex I and III inhibitors rotenone and antimycin A. This enables the estimation of various respiration parameters, which can be used to determine the bioenergetic status and overall health of mitochondria [183].

4.3.1 Elevated respiratory parameters in *SNCA*-A53T cells

Using this approach, we determined that at day 15, the respiratory profiles between *SNCA*-A53T and control cells were largely comparable, with most respiration parameters showing no significant differences between the two groups (Fig. 4.19). The only exception was spare respiratory capacity, which was significantly higher in *SNCA*-A53T cells.

In contrast, at day 30, all measured respiration parameters (basal respiration, maximal respiration, ATP production, non-mitochondrial oxygen consumption, spare respiratory capacity, and coupling efficiency) apart from proton leak were significantly higher in *SNCA*-A53T compared to the control line (Fig. 4.19). This overall increase in mitochondrial function may reflect a compensatory response to altered energy metabolism or cellular stress.

Similarly, at day 40, maximal respiration, non-mitochondrial oxygen consumption, and spare respiratory capacity were significantly higher in *SNCA*-A53T cells (Fig. 4.19). In addition, although not statistically significant, at day 40, proton leak was higher and coupling efficiency was lower in *SNCA*-A53T cells compared to control. This may reflect a progression towards mitochondrial inefficiency and impaired energy utilization as cells acquire a mature mDA phenotype.

To further investigate these metabolic changes, we assessed the dependence of the cells on OXPHOS and glycolysis using the OCR/ECAR ratio (Appendix Fig. A.6). At day 15, both *SNCA*-A53T and control cells displayed a stronger dependence on glycolysis as indicated by a lower OCR/ECAR ratio. This reliance on glycolysis may contribute to the lack of observable differences in mitochondrial respiration at this stage. In contrast, at day 30 both *SNCA*-A53T and control cells exhibited a shift in metabolism from glycolysis to OXPHOS, as evidenced by a higher OCR/ECAR ratio. Of note, at day 40, *SNCA*-A53T cells exhibited a higher OCR/ECAR ratio compared to control cells, suggesting a greater reliance on OXPHOS as a primary energy pathway. These findings align with the metabolic reprogramming that occurs during differentiation, where iPSCs transition from glycolysis to OXPHOS to meet the ATP demands required for neuronal activity [399].

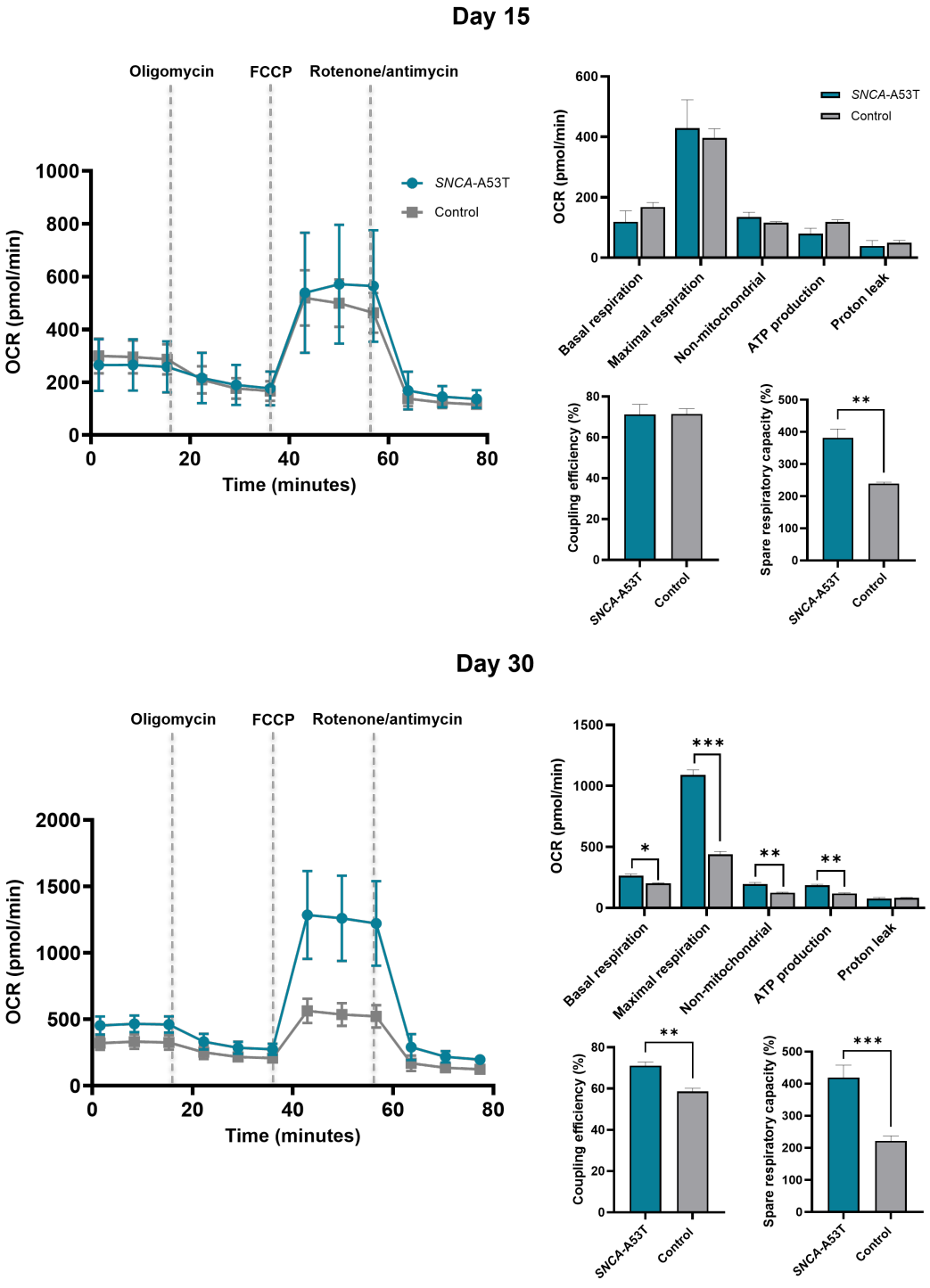
Day 15
Oligomycin
FCCP
Rotenone/antimycin
OCR (pmol/min)
Time (minutes)
SNCA-A53T
Control
Basal respiration
Maximal respiration
Non-mitochondrial
ATP production
Proton leak
Coupling efficiency (%)
Spare respiratory capacity (%)
Day 30
Oligomycin
FCCP
Rotenone/antimycin
OCR (pmol/min)
Time (minutes)
SNCA-A53T
Control
Basal respiration
Maximal respiration
Non-mitochondrial
ATP production
Proton leak
Coupling efficiency (%)
Spare respiratory capacity (%)

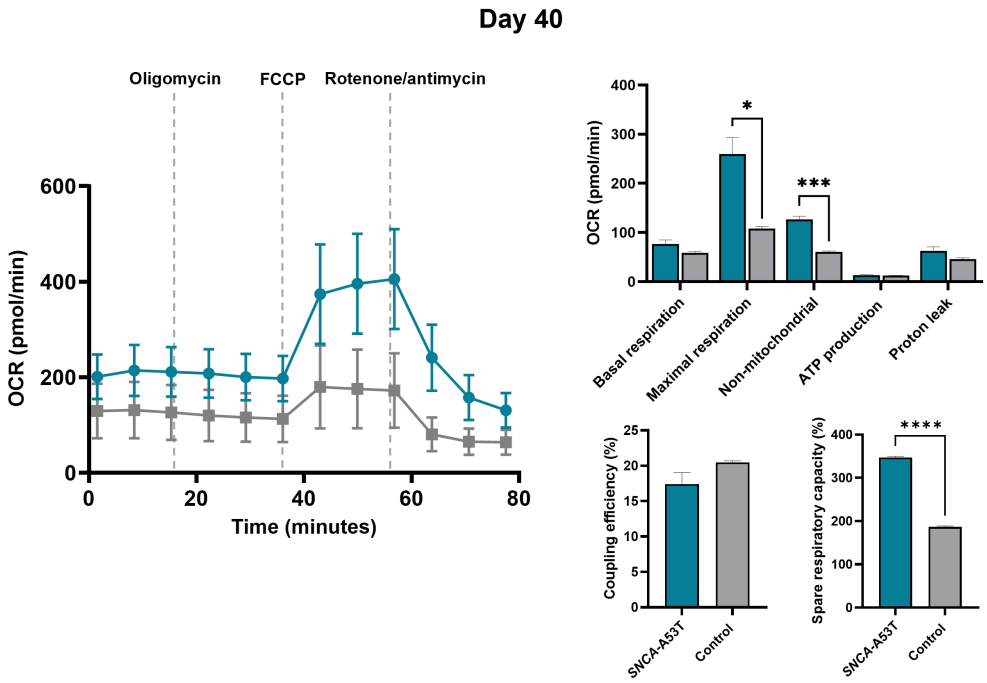

Fig. 4.19 Respiratory flux profiles. Oxygen consumption rates (OCRs) and mitochondrial respiration parameters for *SNCA*-A53T and control cells at days 15, 30, and 40 of the differentiation. All OCR readings were normalized to DNA content (N = 3, mean ± SEM, Student's t-test, *P<0.05, **P<0.01, ***P<0.001, ****P<0.0001).

4.3.2 Increased ETC complex expression in *SNCA*-A53T cells

Given that *SNCA*-A53T cells exhibited altered respiratory profiles and the multi-omics analysis highlighted a strong representation of ETC complex genes, we further investigated these findings by examining the protein levels of ETC complexes I-V (Methods Section 3.3.2). Western blot analysis was performed using an antibody cocktail that detects OXPHOS subunits, including NDUFB8 (complex I), SDHB (complex II), UQCRC2 (complex III), COXII (complex IV), and ATP5A (complex V) (Fig. 4.20 and Appendix Fig. A.7).

Interestingly, we observed increased complex I (NDUFB8) and complex IV (COXII) levels in *SNCA*-A53T cells at days 15, 30, and 40, while protein expression of complex II, complex III, and complex V was comparable between the two cell lines. These changes in ETC complex expression may contribute to the enhanced mitochondrial respiration observed at days 30 and 40 (Fig. 4.19) and further support the upregulation of ETC complex genes and proteins observed in the multi-omics analysis.

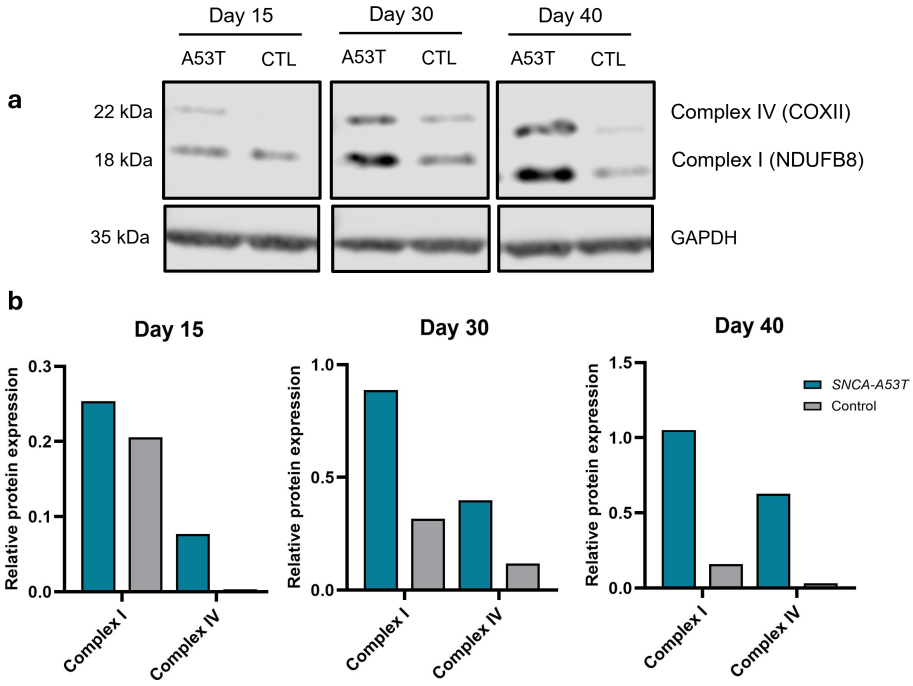

Fig. 4.20 Increased ETC complex expression. Western blot analysis showing increased expression of complex I and complex IV subunits in *SNCA*-A53T cells compared to control cells at days 15, 30, and 40 of the differentiation. **a**. Imaged western blot membrane. **b**. Quantification of band intensity, normalized to GAPDH.

CHAPTER 5

Discussion

PD is a complex neurodegenerative disorder, with a multifactorial etiology encompassing both genetic and environmental factors. The pathological aggregation of α-syn is a defining hallmark of PD and is strongly linked to mutations in the *SNCA* gene. Among these, the *SNCA*-A53T mutation is associated with early-onset, aggressive forms of the disease. However, due to the intricate nature of *SNCA*-associated dysfunction, which spans interconnected molecular pathways, the precise contribution of *SNCA* mutations to the development and establishment of the PD phenotype remains unclear.

To address this open question, we conducted a longitudinal multi-omics analysis at seven key timepoints during the differentiation of patient-derived *SNCA*-A53T iPSCs into mature mDA neurons, using an age- and sex-matched healthy control for comparison. By combining transcriptomic, proteomic, and metabolomic analyses, we provide a comprehensive, systems-level insight into *SNCA*-A53T-related cellular phenotypes across different layers of biological regulation. These molecular analyses are complemented by functional assays of mitochondrial bioenergetics.

Importantly, by employing a time-series approach encompassing both early and late stages of neuronal differentiation, we not only identify key pathways disrupted by the *SNCA*-A53T mutation but also assess the onset and progression of these alterations. This is of particular relevance given the limited understanding of the early, preclinical stages of PD. Our approach, therefore, facilitates the identification of early PD mechanisms and explores how mutation-induced changes evolve over time.

5.1 Longitudinal characterization reveals early PD-associated impairments

To investigate the transcriptional and proteomic signatures associated with the *SNCA*-A53T mutation, we employed two complementary approaches. First, we examined how the mutation impacts cells during neuronal development by assessing timepoint-specific alterations in gene and protein expression. Specifically, we aimed to determine whether PD-associated impairments emerge early in mDA neuron differentiation or only once cells acquire a more mature neuronal phenotype. To achieve this, we identified the top DEGs and DAPs at each timepoint and performed functional enrichment analyses to uncover biological processes disrupted at each stage. We then complemented this by identifying genes and proteins that were persistently dysregulated across development, revealing core features of *SNCA*-A53T pathology. In particular, we focused on genes and proteins dysregulated in the same direction across at least five timepoints.

Our findings indicate that PD-related alterations emerge early during neuronal differentiation and persist throughout maturation. PD appeared as an enriched term at multiple stages, including the earliest timepoints, in both the DEG and DAP analyses (Fig. 4.1 and Fig. 4.2). While PD is traditionally thought of as an age-related disorder, our findings suggest that neurodevelopmental disruptions may also play a role in disease pathogenesis. Increasing evidence indicates that such early disturbances could impact neuronal viability and resilience to stressors, potentially predisposing mDA neurons to neurodegeneration over time [400]. Notably, we observed the highest number of PD-associated DEGs at

day 30 and DAPs at day 40, suggesting that while these molecular signatures are present early in development, they become more pronounced as the cells acquire an mDA phenotype.

Moreover, our complementary approaches identified consistent themes in the biological processes potentially affected by the *SNCA*-A53T mutation. Both timepoint-specific analyses and the investigation of persistently dysregulated genes and proteins highlighted key differences between *SNCA*-A53T and control cells in processes such as cellular respiration, calcium homeostasis, cellular stress responses, and neuronal development. Given this overlap, we will discuss these processes in an integrated manner to provide a more comprehensive overview.

5.2 Altered bioenergetics

A key finding from our analysis was the widespread dysregulation of genes and proteins linked to mitochondrial function, and more specifically to the assembly and biogenesis of ETC complexes. The timepoint-specific analyses revealed upregulation of both nuclear- and mitochondrially-encoded ETC subunits in *SNCA*-A53T cells at multiple stages of the differentiation (Fig. 4.6). In line with this, OXPHOS appeared as an enriched pathway at days 0, 6, and 15 of the DEG analysis, highlighting early differences in cellular metabolism (Fig. 4.1).

Similarly, analyses of the persistently dysregulated genes and proteins revealed a sustained elevation in assembly factors and subunits of complex I (DMAC2 and *MT-ND3*), complex III (UQCRFS1), complex IV (*MT-CO1*, *MT-CO2*, and SCO2), and complex V (ATP5F1E) (Fig. 4.9 and Fig. 4.13). These findings were also corroborated by an increased expression of complex I (NDUFB8) and IV (COXII) at days 15, 30, and 40 using western blot (Fig. 4.20).

ETC complexes form an essential component of mitochondrial OXPHOS, directly contributing to ATP production [401]. During aerobic respiration, these multi-domain enzymes transfer electrons from electron donors (NADH and FADH2) to electron acceptors via redox reactions [402]. This electron flow is coupled to the transfer of protons (H^+) across the inner mitochondrial

membrane (IMM), which generates an electrochemical proton gradient that drives the production of ATP via ATP synthase [403].

Given this coupling of ETC complex expression and mitochondrial respiration, we assessed whether the upregulation of ETC components leads to functional changes in mitochondrial bioenergetics using the Seahorse metabolic assay (Fig. 4.19). Interestingly, at day 15, *SNCA*-A53T and control cells displayed comparable bioenergetic profiles, although this may be due to a greater reliance on glycolysis at the earlier stages of the differentiation, which can obscure differences in OXPHOS. In contrast, at day 30, all mitochondrial respiration parameters, apart from proton leak, were significantly higher in *SNCA*-A53T cells compared to control cells. Meanwhile, at day 40, *SNCA*-A53T cells exhibited significantly higher maximal respiration, non-mitochondrial oxygen consumption, and spare respiratory capacity compared to control cells. However, based on the OCR profile at day 40, the oligomycin concentration used may not have been sufficient to fully block ATP-linked respiration, suggesting that a higher concentration could have provided a clearer distinction in mitochondrial function.

Intriguingly, our findings are contrary to those of previous studies, demonstrating that *SNCA*-A53T iPSC-derived dopamine neurons display impaired bioenergetic profiles, characterized by reduced respiration and diminished spare respiratory capacity [386]. Moreover, in the broader context of PD, respiratory chain dysfunction has been identified as a common feature of both idiopathic and familial PD. In postmortem studies of PD brains and experimental models, the functional capacity and protein levels of complex I, the first complex of the ETC, are markedly reduced, which is associated with decreased ATP production [404–407]. Additionally, impairments in complex III have also been noted in cells derived from PD patients, whilst reports on complex II, IV, and V have been inconsistent [408].

Several possible explanations may account for the observed increase in ETC components and may also somewhat reconcile the discrepancy between our findings and those of previous studies. One possibility is that the upregulation of ETC components and subsequent increase in mitochondrial bioenergetics reflects a compensatory response to early alterations in energy metabolism. Supporting this notion, metabolomic analyses revealed a reduction in key energy

substrates in *SNCA*-A53T cells at the early stages of the differentiation (Fig. 4.16). More specifically, at day 0, ATP, ADP, and AMP levels were significantly lower in *SNCA*-A53T cells compared to controls. This was accompanied by reduced levels of glycolytic and TCA cycle intermediates at both days 0 and 6, reflecting global differences in energy metabolism. In support of this, alongside upregulation of ETC complex genes, we also observed the persistent upregulation of PGK1 in *SNCA*-A53T cells, which is the first ATP-producing enzyme of glycolysis (Fig. 4.12).

However, it is worth noting that although we observed increased expression of ETC complex components and enhanced mitochondrial respiration at day 30, these changes were not accompanied by corresponding increases in TCA cycle metabolites or ATP. This could indicate an increased turnover of TCA cycle intermediates and heightened energy demand in *SNCA*-A53T cells. In support of this, proteomic analysis at day 30 confirmed an upregulation of multiple TCA cycle enzymes, suggesting a potential increase in TCA cycle flux that may contribute to enhanced mitochondrial respiration (Fig. 4.17). However, as LC-MS-based metabolomics provides only a static snapshot of metabolite concentrations, it may not fully capture dynamic changes in metabolic activity. To better resolve this, future studies utilizing metabolic flux analysis with stable isotope tracing would be valuable [409].

Taken together, these findings suggest that early alterations in energy metabolism in *SNCA*-A53T cells may promote the compensatory upregulation of ETC components, which becomes functionally evident as the cells transition to a greater reliance on mitochondrial respiration.

A possible factor contributing to the dysregulation of energy metabolism, and more specifically mitochondrial respiration is the altered expression of genes critical for respiratory chain function, namely *CHCHD2* and *DNAJC15*. *CHCHD2* was consistently downregulated in *SNCA*-A53T cells at both the transcriptomic and proteomic levels (Fig. 4.9 and Fig. 4.13). As a member of the coiled-coil-helix-coiled-coil-helix (CHCH) domain protein family, CHCHD2 is critical for mitochondrial respiration and redox regulation [410]. Interestingly, mutations in *CHCHD2* have been associated with autosomal dominant PD and are also proposed as a risk factor for sporadic disease [411, 389]. In the nucleus, CHCHD2 functions as a transcription factor for COX412 (a subunit

of complex IV), and CHCHD2 itself [412, 412]. Upon translocation to the intermembrane space (IMS), CHCHD2 binds to MISC1, cytochrome c, and COX, thereby stabilizing complex IV and maintaining electron flow through the transport chain [413].

Loss of *CHCHD2* reduces subunits of complexes I, IV, and V, impairing ATP production [414]. However, this depletion can also trigger compensatory increases in mitochondrial respiration. More specifically, *CHCHD2* KO has been shown to increase basal respiration, maximal respiration, and ATP-coupled oxygen consumption, likely as an acute response to mitigate respiratory chain dysfunction [415]. Thus, *SNCA*-A53T cells may compensate for reduced CHCHD2 by upregulating ETC complex biogenesis to sustain efficient electron flow and ATP production. In line with this, it is well established that mitochondria possess a large reserve capacity, meaning that even in the presence of significant OXPHOS defects, cells can maintain ATP production [416].

Another important factor that may contribute to the observed increase in mitochondrial respiration in *SNCA*-A53T cells is the downregulation of *DNAJC15*, identified at the transcriptomic level (Fig. 4.9). *DNAJC15* encodes a co-chaperone that functions as a negative regulator of the ETC; more specifically, it preferentially interacts with complex I to impair the formation of supercomplexes [417]. Thus, reductions in DNAJC15 result in increased oxidative respiration and mitochondrial ATP production [417]. Moreover, as a subunit of the TIMM23 translocase, DNAJC15 plays an important role in importing OXPHOS-related proteins into mitochondria, meaning its downregulation could further impact mitochondrial respiration [418].

It is also possible that the alterations in ETC complex expression reflect an underlying impairment in mitochondrial quality control. Unlike nuclear DNA (nDNA), which exists in two copies per cell, mitochondrial DNA (mtDNA) is present in thousands of copies, and its abundance is tightly linked to mitochondrial content and number [419]. Since mtDNA encodes 13 essential ETC subunits, an increase in mitochondrial abundance can directly elevate ETC subunit levels [401].

Supporting this, our dataset showed a strong representation of ETC subunits encoded by the mitochondrial genome (Fig. 4.6). Moreover, at day 0 and day 6 of differentiation, *SNCA*-A53T cells exhibited a higher percentage of mitochondrial transcripts compared to control cells (Supplementary Fig. A.8). To assess whether the increased expression of mitochondrially-encoded ETC subunits simply reflected this higher mitochondrial transcript percentage, we incorporated mitochondrial transcript abundance as a latent variable in our statistical analysis. This revealed that mitochondrial percentage did not significantly influence the upregulation of these subunits. However, this does not fully exclude a role for mitochondrial quality control in their increased expression.

Mitochondrial homeostasis is achieved through an orchestrated balance of mitochondrial biogenesis and mitochondrial clearance via mitophagy [420]. While we did not detect upregulation of key mitochondrial biogenesis regulators (e.g., TFAM, PGC-1α, PGC-1β, NRF-1, and NRF-2) in *SNCA*-A53T cells, we did observe an increased expression of mitophagy-associated proteins [420]. More specifically, Miro1 (*RHOT1*), VDAC1, and FKBP8 were upregulated in *SNCA*-A53T cells at multiple timepoints throughout the differentiation (Fig. 4.13 and Fig. 4.11).

Miro1 (*RHOT1*) is a OMM protein required for the initiation and progression of PINK1/Parkin-mediated mitophagy [421, 422]. In Drosophila models, its overexpression delays the clearance of defective mitochondria, thereby promoting dopaminergic degeneration [423]. Similarly, VDAC1 also serves as an essential Parkin substrate, whilst FKBP8 facilitates the recruitment of LC3A to depolarized mitochondria, aiding their degradation [424, 425]. In line with our findings, mounting evidence suggests the *SNCA*-A53T mutation can adversely impact mitochondrial function and disrupt the mitochondrial clearance process [426]. *In vitro* analyses have demonstrated both impaired and enhanced mitophagy associated with the *SNCA*-A53T mutation [426]. Therefore, it is possible that perturbations in mitophagy could also contribute to the observed alterations in energy metabolism in *SNCA*-A53T cells.

Taken together, we hypothesize that the increase in ETC complex subunits and assembly factors may represent a compensatory response to respiratory chain impairment or reflect broader disruptions in mitochondrial homeostasis. Indeed, these mechanisms are not mutually exclusive and may collectively contribute to

the altered mitochondrial phenotype observed in *SNCA*-A53T cells. Given the complex interplay between cellular metabolism, respiratory chain regulation, and mitochondrial turnover, further studies are needed to clarify the precise mechanisms underlying these alterations.

5.3 Disrupted calcium homeostasis

In addition to being a primary source of cellular energy, mitochondria play an essential role in intracellular calcium buffering [423]. Calcium ions act as second messengers that regulate numerous physiological functions, necessitating tight control over cytosolic calcium concentrations [423]. Growing evidence has implicated increased Ca^{2+} influx and defective Ca^{2+} storage in PD pathogenesis, with elevated calcium levels linked to increased disease susceptibility [427, 428].

Consistent with these findings, mitochondrial calcium proteins, including Miro1 (*RHOT1*), EMRE (*SMDT1*), and VDAC1-3, were upregulated in *SNCA*-A53T cells at multiple stages of the differentiation (Fig. 4.13 and Fig. 4.11). While each having their own disparate functions, these proteins work in a coordinated manner to regulate calcium homeostasis [423].

Beyond its role in mitochondrial quality control, Miro1 (*RHOT1*) is also essential for calcium buffering [423, 429]. In response to elevated cytosolic calcium levels, Ca^{2+} binds to the EF-hand domains of Miro1 [423]. This induces a conformational change that dissociates mitochondria from the cytoskeleton, facilitating their deposition at sites requiring ATP and Ca^{2+} buffering [430]. Notably, Miro1 overexpression has been linked to enhanced mitochondrial Ca^{2+} uptake, potentially mediated through interactions with the mitochondrial calcium uniporter (MCU) complex [423].

In agreement with this, EMRE (*SMDT1*), an essential subunit of the MCU, was also upregulated in *SNCA*-A53T cells. Given that the MCU facilitates Ca^{2+} entry into the mitochondrial matrix, the concurrent elevation of Miro1 and EMRE indicates a potential dysregulation of calcium homeostasis [431]. This is further supported by the increase of VDAC proteins, which regulate calcium transfer between the ER and mitochondria.

The simultaneous upregulation of these proteins in *SNCA*-A53T cells may greatly alter the distribution and concentration of intracellular calcium, which can in turn lead to mitochondrial stress and subsequent dysfunction. Adding another layer of complexity, increased mitochondrial Ca^{2+} uptake can also enhance mitochondrial respiration by activating TCA cycle dehydrogenases [432, 433]. This interplay between calcium dynamics and metabolism may also contribute to the enhanced mitochondrial respiratory profile observed in *SNCA*-A53T cells.

5.4 Increased cellular stress

Our analysis also revealed widespread dysregulation of genes and proteins involved in cellular stress response pathways, including protein quality control, oxidative stress defense, DNA repair, and apoptosis, in *SNCA*-A53T cells (Fig. 4.6 and Fig. 4.8).

Specifically, we observed an upregulation of genes involved in protein degradation, including those encoding subunits of the 20S proteasome (*PSMD10, PSMA1*, and *PSMA3*) and components of the ubiquitin-mediated degradation pathway (*UBA52* and *USP11*), suggesting increased proteotoxic stress (Fig. 4.6 and Fig. 4.8) [347, 434]. While we did not directly assess α-syn aggregation, the upregulation of these pathways may reflect an increased aggregation burden, given the known propensity of *SNCA*-A53T to promote α-syn misfolding.

Consistent with this, *CLU*, a molecular chaperone involved in proteostasis, was also persistently overexpressed in *SNCA*-A53T cells (Fig. 4.8). Notably, increased CLU protein levels have been detected in the plasma and CSF of PD patients [435]. CLU has also been linked to the spread of pathological α-syn, as it limits astrocytic uptake and promotes its extracellular accumulation [436].

Beyond proteostasis, we identified dysregulation of genes and proteins involved in antioxidant defense, including *SOD1* and CAT, which are critical for managing ROS. *SOD1* was overexpressed at days 21 and 30, potentially reflecting a compensatory response to increased mitochondrial respiration, as it plays a key role in mitigating superoxide production during OXPHOS (Fig. 4.6) [437]. In

contrast, CAT was persistently downregulated throughout the differentiation (Fig. 4.12). This finding is consistent with reports of reduced catalase activity in PD, where its deficiency has been implicated in oxidative damage [438]. While these represent just a few examples, they suggest an overall increase in cellular stress in *SNCA*-A53T cells.

5.5 Delayed mDA neuron differentiation

An additional observation from our work was the pronounced downregulation of genes essential for establishing and maintaining mDA neuron identity in *SNCA*-A53T cells, particularly at day 30 (Fig. 4.7). This included early developmental regulators such as *LMX1A* and *FOXA2*, as well as *NR4A2* (*Nurr1*), *NRP1*, *DDC*, *NEFL* and *GAP43*, which are required for the later stages of neuronal maturation [439, 440]. Many of these genes continue to be expressed into adulthood, where they play essential roles in neuronal maintenance and survival [441]. For instance, loss of *NR42A* expression during early development results in the absence of midbrain neurons, whereas its downregulation in adulthood is associated with decreased striatal dopamine [442]. Similarly, reduced expression of *GAP43*, a mediator of neuronal maturation, has been linked to a diminished regenerative capacity of dopaminergic neurons in the SNpc of PD patients [443].

At least four independent studies have previously demonstrated the reduced differentiation potential of neuronal cells derived from PD patients, which has been suggested to reflect a neurodevelopmental aspect of PD pathology [442, 444–446, 110, 447]. However, flow cytometry, at day 50, revealed a similar proportion of TH/MAP2 positive neurons between *SNCA*-A53T and control cells, suggesting that the *SNCA*-A53T mutation most likely delays mDA maturation, rather than reducing the final yield of mature mDA neurons (Results Section 4.1.2 and Supplementary Fig. A.2).

5.6 Trancriptiomic & proteomic overlap

As many of the genes and proteins that were dysregulated at specific stages of development or persistently dysregulated throughout development converged on shared biological functions, we investigated the true extent of their overlap by identifying the shared DEGs and DAPs for each timepoint (Fig. 4.14) Interestingly, we observed the highest overlap at days 6, 21, and 30, suggesting coordination in transcriptional and proteomic changes during the critical transition periods of the differentiation. Yet, we observed a smaller overlap ($<$2.6%) at all other timepoints of the differentiation.

An underlying assumption in many biological studies is the concordance of transcript and protein levels during the transfer of information from DNA to phenotype [448]. However, it is becoming increasingly accepted that the relationship between mRNA expression and protein abundance is not linear [397]. Our findings therefore support the notion that a direct one-to-one relationship between gene expression and protein levels is not always evident [449, 450]. Nevertheless, we observed a substantial overlap in dysregulated pathways based on the transcriptomic and proteomic analyses, which reinforces the importance of using a multi-omics approach. Such an approach is crucial for capturing the complexity of biological regulation and uncovering phenotypes that cannot be deciphered from mRNA and protein expression alone.

5.7 Core dysregulated genes

To gain further insights into the transcriptomic and proteomic overlap, we ranked the DEGs and DAPs by their absolute sum. Using this approach, we identified a core set of seven genes and their corresponding proteins that were strongly dysregulated at both biological levels (Supplementary Fig. A.4 and Fig. A.5). This list included *GPC3, DLK1* and *BST2,* which were overexpressed, and *CHCHD2, WNK3, NLRP2,* and *QNG1*, which were underexpressed in *SNCA*-A53T cells. Intriguingly, many of these genes are associated with pathways integral to PD, including inflammatory signaling, mitochondrial function, and

neuronal survival, supporting their potential involvement in disease-relevant processes.

Among these genes, *NLRP2* and *BST2* play well-established roles in inflammatory signaling. *BST2* encodes a transmembrane protein that is integral to the innate immune response [451]. In contrast, NLRP2 functions as a component of the inflammasome, a multi-domain complex that senses intracellular stress and regulates inflammatory pathways [452].

Chronic inflammasome activation is a prominent feature of PD pathology and is primarily linked to NLRP3, a close relative of NLRP2 [453]. While NLRP3's involvement is well documented, much less is known about how NLRP2 contributes to disease onset [454]. Interestingly, studies suggest that NLRP2 overexpression suppresses NF-κB activation, serving as a regulatory checkpoint to prevent excessive inflammation [455, 456]. This raises the possibility that NLRP2 downregulation could exacerbate inflammatory responses.

Beyond inflammation, a number of the identified genes have previously been linked to neuroprotection, including *WNK3* and *QNG1*. WNK3 is a protein kinase known to inhibit apoptosis through sequestration of procaspase 3 [457]. Its overexpression has been shown to mitigate neuronal loss and promote cell survival in traumatic brain injury (TBI) models, suggesting its downregulation could increase susceptibility to apoptotic stimuli [458, 459]. Alternatively, QNG1 is involved in the salvage and recycling of queuine, a precursor of queosine, which has been shown to confer neuroprotective effects in PD models [460]. Notably, queosine depletion has been associated with mitochondrial dysfunction, further implicating QNG1 in PD-relevant alterations [461].

Importantly, a number of the core dysregulated genes have also been directly associated with other genetic forms of PD. For example, *DLK1*, encodes a member of the delta/notch protein family involved in mDA neuron development. Recently, DLK1 was identified as a differentially expressed protein in *LRRK2*, *GBA*, and idiopathic patient cohorts in a large-scale protogenomic study [462]. Moreover, in rodent models, DLK1 is upregulated in response to neuron loss, suggesting it may serve as a marker of degeneration [463].

Similarly, *GPC3* has been linked to PD through its interaction with *DJ-1* and has also been identified as a dysregulated gene within the *PINK1* network

[398, 111]. *GPC3* encodes a proteoglycan involved in cell proliferation and apoptosis [464]. Whilst its role has been extensively studied in cancer, its involvement in PD remains largely unexplored [465, 466]. Intriguingly, GPC3 is known to influence both Wnt and SHH signaling pathways, which are essential for the specification and proliferation of neural progenitors during mDA neuron differentiation. Dysregulation of these pathways has been linked to reduced mDA neuron survival and PD development, suggesting a potential mechanism through which GPC3 may contribute to disease pathogenesis [467–470].

As previously mentioned, *CHCHD2* is a causative PD gene [471]. Its expression is significantly reduced in postmortem PD brains and in animal models; however, this reduction does not correlate with motor or cognitive impairments, implying that it represents an early event in the disease process [135]. Supporting this, *CHCHD2* mRNA levels are also significantly reduced in erythrocytes, a phenomenon that also takes place in the early stages of disease [410]. Despite *CHCHD2* being downregulated at almost all timepoints in our transcriptomic and proteomic datasets, this reduction was most pronounced in the early stages of differentiation, as indicated by a stronger fold change (Supplementary Fig. A.10 and Fig. A.11). Therefore, our results may support the notion that CHCHD2 serves as an early biomarker for PD [135].

Notably, in an analogous longitudinal multi-omics study conducted by our group on the PD-associated mutation *PINK1*-ILE368ASN, *CHCHD2* was also identified as one of the most strongly and consistently dysregulated genes [472]. The fact that *CHCHD2* is prominently affected across two distinct PD-associated mutations and throughout differentiation suggests it may play a fundamental role in disease pathology.

The convergence of these core dysregulated genes and proteins in key PD-associated pathways suggests that distinct PD mutations feed into the same pathogenic routes and that pathology, to some extent, may be driven by shared mechanisms. Therefore, our findings again underscore the value of a multi-omics approach in identifying potential disease drivers and molecular hubs, which may have a broader relevance across the PD spectrum.

5.8 Limitations

Whilst our study has provided a comprehensive insight into *SNCA*-A53T driven cellular dynamics, it is accompanied by some limitations.

One key aspect not fully addressed in our work is the contribution of α-syn aggregation to the observed cellular alterations. By employing a multi-scale omics analysis, our aim was to adopt a less biased and more data-driven approach that goes beyond the scope of the well-established role of *SNCA*-A53T mediated aggregation. While *SNCA* gene expression was largely comparable between *SNCA*-A53T and control cells throughout the differentiation, we did not quantitatively assess α-syn aggregation. Therefore, future experiments will focus on directly examining aggregation dynamics to determine whether the observed alterations are, at least partly, attributable to the effects of *SNCA*-A53T mediated aggregates. This is of particular relevance given that pathologic α-syn has been shown to interact with many of the genes and proteins identified in our analysis.

Additionally, our study prioritized a deep phenotypic characterization of two cell lines rather than a broader, less detailed assessment across a larger number of cell lines. While this approach enabled a more comprehensive insight into *SNCA*-A53T-driven alterations, it may have also reduced the statistical power of the subsequent analysis. To address this, we have since performed a follow-up study using iPSCs from a second patient heterozygous for the *SNCA*-A53T mutation, alongside a corresponding isogenic control. This experiment followed the same differentiation protocol to generate mDA neurons but was performed on a more focused scale, with scRNA-seq and proteomics conducted at days 0, 15, 21, 30, and 40 of the differentiation. By including a second patient-derived *SNCA*-A53T cell line, we aim to validate the reproducibility of our findings across different patients. Moreover, the incorporation of an isogenic control serves to minimize genetic variability between patient and control cell lines, thereby lowering the threshold for detection of disease-related phenotypes [110]. Once the analysis of this dataset is complete, we will compare the findings with the current study to narrow down key targets for follow-up investigations.

Beyond these, another limitation may lie in the choice of model system. While the degeneration of mDA neurons is pivotal to PD progression, growing evidence has implicated other neural cell types such as astrocytes, microglia, and oligodendrocytes in PD pathogenesis [473]. Therefore, focusing solely on mDA-related pathology may neglect non-cell autonomous interactions that are fundamental to the disease process [473]. Although 2D culture models, like the one used in the present study, offer valuable insights into cell-specific perturbations, they lack the spatial organization of the human brain, potentially limiting the complexity of PD-relevant phenotypes captured. To address these challenges, more advanced 3D culture systems could be employed in future research. One such example is midbrain organoids, which are 3D structures derived from iPSCs or isolated organ progenitors [474]. Importantly, midbrain organoids contain various CNS-relevant cell types and thus more accurately mimic the architecture and function of the brain [474]. Providing a more physiologically relevant model that is able to capture the complex interactions between different PD-associated cell types.

5.9 Future work

Our findings have identified key disruptions that may be central to PD pathology, including alterations in mitochondrial function and calcium dynamics. While these changes suggest potential mechanisms driving disease progression, further research will be important to determine how they contribute to pathological phenotypes.

An essential next step will be to further characterize the mitochondrial phenotype associated with the *SNCA*-A53T mutation, using both structural and functional analyses. We have already initiated this process by acquiring electron microscopy images of *SNCA*-A53T and control cells and are currently developing a pipeline for their analysis. This will allow us to examine mitochondrial morphology in detail, which is particularly relevant given that *CHCHD2*, one of the most dysregulated genes identified in our analysis, is known to regulate mitochondrial ultrastructure.

Moreover, as our findings point to the potential dysregulation of mitophagy, it would be beneficial to probe this further. Assessing autophagic flux by measuring LC3-II and p62 levels in the presence and absence of bafilomycin A1 would help determine whether mitophagic degradation is altered [423]. Additionally, western blot analysis of PINK1 and Parkin could provide insight into upstream mitophagy signaling. To distinguish whether the observed increase in ETC components reflects changes in mitochondrial biogenesis or turnover, evaluating mitochondrial mass through TOM20 levels would also be important.

Another key aspect that should be addressed is determining whether the observed increase in calcium transport proteins leads to functionally relevant impairments. More specifically, it will be important to clarify if elevated Miro1 (*RHOT1*), EMRE (*SMDT1*) and VDAC leads to increased baseline mitochondrial calcium levels and whether these effects are exacerbated following physiological stimulation. If these effects are confirmed, it will also be of value to assess whether they can be attenuated by pharmacological inhibition of MCU and VDAC.

Finally, given the interplay between mitochondrial function and calcium homeostasis, it may also be valuable to investigate mitochondria-associated membranes (MAMs), which are responsible for the functional tethering between the ER and mitochondria [475]. MAMs play a critical role in calcium transfer, mitochondrial dynamics, and mitophagy and may therefore represent a point of convergence linking the disruptions we observe. Exploring whether MAM integrity and function are altered in *SNCA*-A53T cells could provide further valuable mechanistic insights.

.

CHAPTER 6

Conclusion

Our work provides novel insights into the molecular signatures associated with the *SNCA*-A53T mutation, demonstrating that PD-related transcriptional and functional alterations arise early in development. Through a longitudinal multi-omics approach, we identify disruptions in mitochondrial respiration in *SNCA*-A53T cells, potentially driven, at least in part, by the downregulation of key respiratory chain regulators, including *DNAJC15* and *CHCHD2*. Given that *CHCHD2* is also strongly dysregulated in *PINK1* mutant cells, its altered expression across distinct genetic backgrounds suggests a broader role in disease pathogenesis.

Beyond alterations in mitochondrial respiration, our findings reveal more extensive mitochondrial dysfunction, including disrupted calcium homeostasis and perturbed mitophagy, further supporting the central role of mitochondrial impairment in PD.

Additionally, we define a core set of seven dysregulated genes, several of which have been implicated in other genetic forms of PD. The convergence of these molecular alterations suggests that distinct genetic risk factors may

ultimately impact overlapping cellular processes, reinforcing the presence of shared pathogenic mechanisms in PD.

In summary, this study highlights the utility of a multi-omics approach in dissecting the complex phenotypic landscape of PD, where multiple interrelated pathways drive disease progression. Importantly, the identification of early molecular disruptions may aid in understanding the preclinical phase of PD, offering potential markers for early intervention. Taken together, our findings contribute to a broader mechanistic understanding of PD pathogenesis.

References

[1] Raja Mehanna, Suzanne Moore, J. Gabriel Hou, Aliya I. Sarwar, and Eugene C. Lai. Comparing clinical features of young onset, middle onset and late onset Parkinson's disease. *Parkinsonism & Related Disorders*, 20(5):530–534, May 2014. Publisher: Elsevier.

[2] Moeko Noguchi-Shinohara and Kenjiro Ono. The Mechanisms of the Roles of α-Synuclein, Amyloid-β, and Tau Protein in the Lewy Body Diseases: Pathogenesis, Early Detection, and Therapeutics. *International Journal of Molecular Sciences*, 24(12):10215, June 2023.

[3] Sairam Ramesh and Arosh S. Perera Molligoda Arachchige. Depletion of dopamine in Parkinson's disease and relevant therapeutic options: A review of the literature. *AIMS Neuroscience*, 10(3):200–231, August 2023.

[4] Tien K. Khoo, Alison J. Yarnall, Gordon W. Duncan, Shirley Coleman, John T. O'Brien, David J. Brooks, Roger A. Barker, and David J. Burn. The spectrum of nonmotor symptoms in early Parkinson disease. *Neurology*, 80(3):276–281, January 2013.

[5] Antonina Kouli, Kelli M. Torsney, and Wei-Li Kuan. Parkinson's Disease: Etiology, Neuropathology, and Pathogenesis. In Thomas B. Stoker and Julia C. Greenland, editors, *Parkinson's Disease: Pathogenesis and Clinical Aspects*. Codon Publications, Brisbane (AU), 2018.

[6] Yoav Ben-Shlomo, Sirwan Darweesh, Jorge Llibre-Guerra, Connie Marras, Marta San Luciano, and Caroline Tanner. The epidemiology of Parkinson's disease. *The Lancet*, 403(10423):283–292, January 2024. Publisher: Elsevier.

[7] Amy Reeve, Eve Simcox, and Doug Turnbull. Ageing and Parkinson's disease: Why is advancing age the biggest risk factor? *Ageing Research Reviews*, 14(100):19–30, March 2014.

[8] Lonneke ML de Lau and Monique MB Breteler. Epidemiology of Parkinson's disease. *The Lancet Neurology*, 5(6):525–535, June 2006. Publisher: Elsevier.

[9] E R Dorsey, R Constantinescu, J P Thompson, K M Biglan, R G Holloway, K Kieburtz, F J Marshall, B M Ravina, G Schifitto, A Siderowf, and C M Tanner. Projected number of people with CME Parkinson disease in the most.

[10] Silvia Cerri, Liudmila Mus, and Fabio Blandini. Parkinson's Disease in Women and Men: What's the Difference? *Journal of Parkinson's Disease*, 9(3):501–515, January 2019. Publisher: IOS Press.

[11] Jose L. Labandeira-Garcia, Ana I. Rodriguez-Perez, Rita Valenzuela, Maria A. Costa-Besada, and Maria J. Guerra. Menopause and Parkinson's disease. Interaction between estrogens and brain renin-angiotensin system in dopaminergic degeneration. *Frontiers in Neuroendocrinology*, 43:44–59, October 2016.

[12] N. M. Gatto, D. Deapen, S. Stoyanoff, R. Pinder, S. Narayan, Y. Bordelon, and B. Ritz. Lifetime exposure to estrogens and Parkinson's disease in California teachers. *Parkinsonism & Related Disorders*, 20(11):1149–1156, November 2014.

[13] Nabila Dahodwala, Qinglin Pei, and Peter Schmidt. Sex Differences in the Clinical Progression of Parkinson's Disease. *Journal of obstetric, gynecologic, and neonatal nursing : JOGNN / NAACOG*, 45(5):749–756, 2016.

[14] Shilpa C. Rao, Yadi Li, Brittany Lapin, Sreya Pattipati, Kamalini Ghosh Galvelis, Anna Naito, Nicolas Gutierrez, Thiago Peixoto Leal, Amira Salim, Philippe A. Salles, Maria De Leon, and Ignacio F. Mata. Association of women-specific health factors in the severity of Parkinson's disease. *npj Parkinson's Disease*, 9(1):1–16, June 2023. Publisher: Nature Publishing Group.

[15] Lorraine V. Kalia, Jonathan M. Brotchie, and Susan H. Fox. Novel nondopaminergic targets for motor features of Parkinson's disease: Review of recent trials. *Movement Disorders*, 28(2):131–144, 2013. _eprint: https://onlinelibrary.wiley.com/doi/pdf/10.1002/mds.25273.

[16] Brage Brakedal, Lilah Toker, Kristoffer Haugarvoll, and Charalampos Tzoulis. A nationwide study of the incidence, prevalence and mortality of Parkinson's disease in the Norwegian population. *npj Parkinson's Disease*, 8(1):1–8, March 2022. Publisher: Nature Publishing Group.

[17] Artur Francisco Schumacher-Schuh, Andrei Bieger, Olaitan Okunoye, Kin Ying Mok, Shen-Yang Lim, Soraya Bardien, Azlina Ahmad-Annuar, Bruno Lopes Santos-Lobato, Matheus Zschornack Strelow, Mohamed Salama, Shilpa C. Rao, Yared Zenebe Zewde, Saiesha Dindayal, Jihan Azar, Lingappa Kukkle Prashanth, Roopa Rajan, Alastair J. Noyce, Njideka Okubadejo, Mie Rizig, Suzanne Lesage, Ignacio Fernandez Mata, and Global Parkinson's Genetics Program (GP2). Underrepresented Populations in Parkinson's Genetics Research: Current Landscape and Future Directions. *Movement Disorders: Official Journal of the Movement Disorder Society*, 37(8):1593–1604, August 2022.

[18] Nikolas Grotewold and Roger L. Albin. Update: Descriptive epidemiology of Parkinson disease. *Parkinsonism & Related Disorders*, 120:106000, March 2024.

[19] Jennifer Sally Samson, Anuradha Ramesh, and Venkatachalam Deepa Parvathi. Development of Midbrain Dopaminergic Neurons and the Advantage of Using hiPSCs as a Model System to Study Parkinson's Disease. *Neuroscience*, 546:1–19, May 2024.

[20] Sandrine Greffard, Marc Verny, Anne-Marie Bonnet, Jean-Yves Beinis, Claude Gallinari, Sylvie Meaume, François Piette, Jean-Jacques Hauw, and Charles Duyckaerts. Motor Score of the Unified Parkinson Disease Rating Scale as a Good Predictor of Lewy Body–Associated Neuronal Loss in the Substantia Nigra. *Archives of Neurology*, 63(4):584–588, April 2006.

[21] Hsiao-Chun Cheng, Christina M. Ulane, and Robert E. Burke. Clinical Progression in Parkinson's Disease and the Neurobiology of Axons. *Annals of neurology*, 67(6):715–725, June 2010.

[22] Mengmeng Wang, King-Hwa Ling, Jun Jie Tan, and Cheng-Biao Lu. Development and Differentiation of Midbrain Dopaminergic Neuron: From Bench to Bedside. *Cells*, 9(6):1489, June 2020.

[23] Breana Channer, Stephanie M. Matt, Emily A. Nickoloff-Bybel, Vasiliki Pappa, Yash Agarwal, Jason Wickman, and Peter J. Gaskill. Dopamine, Immunity, and Disease. *Pharmacological Reviews*, 75(1):62–158, January 2023.

[24] Angel Toval, Daniel Garrigos, Yevheniy Kutsenko, Miroljub Popović, Bruno Ribeiro Do-Couto, Nicanor Morales-Delgado, Kuei Y. Tseng, and José Luis Ferran. Dopaminergic Modulation of Forced Running Performance in Adolescent Rats: Role of Striatal D1 and Extra-striatal D2 Dopamine Receptors. *Molecular Neurobiology*, 58(4):1782–1791, 2021.

[25] Saad Latif, Muhammad Jahangeer, Dure Maknoon Razia, Mehvish Ashiq, Abdul Ghaffar, Muhammad Akram, Aicha El Allam, Abdelhakim Bouyahya, Larisa Garipova, Mohammad Ali Shariati, Muthu

Thiruvengadam, and Mohammad Azam Ansari. Dopamine in Parkinson's disease. *Clinica Chimica Acta; International Journal of Clinical Chemistry*, 522:114–126, November 2021.

[26] George DeMaagd and Ashok Philip. Parkinson's Disease and Its Management. *Pharmacy and Therapeutics*, 40(8):504–532, August 2015.

[27] José L. Lanciego, Natasha Luquin, and José A. Obeso. Functional neuroanatomy of the basal ganglia. *Cold Spring Harbor Perspectives in Medicine*, 2(12):a009621, December 2012.

[28] Matthew M. McGregor and Alexandra B. Nelson. Circuit Mechanisms of Parkinson's Disease. *Neuron*, 101(6):1042–1056, March 2019.

[29] Emanuela Formaggio, Maria Rubega, Jessica Rupil, Angelo Antonini, Stefano Masiero, Gianna Maria Toffolo, and Alessandra Del Felice. Reduced Effective Connectivity in the Motor Cortex in Parkinson's Disease. *Brain Sciences*, 11(9):1200, September 2021.

[30] Ana Muñoz, Andrea Lopez-Lopez, Carmen M. Labandeira, and Jose L. Labandeira-Garcia. Interactions Between the Serotonergic and Other Neurotransmitter Systems in the Basal Ganglia: Role in Parkinson's Disease and Adverse Effects of L-DOPA. *Frontiers in Neuroanatomy*, 14:26, June 2020.

[31] K. Ray Chaudhuri, Daniel G. Healy, Anthony H. V. Schapira, and National Institute for Clinical Excellence. Non-motor symptoms of Parkinson's disease: diagnosis and management. *The Lancet. Neurology*, 5(3):235–245, March 2006.

[32] Maria Grazia Spillantini, R. Anthony Crowther, Ross Jakes, Masato Hasegawa, and Michel Goedert. α-Synuclein in filamentous inclusions of Lewy bodies from Parkinson's disease and dementia with Lewy bodies. *Proceedings of the National Academy of Sciences of the United States of America*, 95(11):6469–6473, May 1998.

[33] Tomoya Kon, Masahiko Tomiyama, and Koichi Wakabayashi. Neuropathology of Lewy body disease: Clinicopathological crosstalk between typical and atypical cases. *Neuropathology: Official Journal of the Japanese Society of Neuropathology*, 40(1):30–39, February 2020.

[34] Clifford W. Shults. Lewy bodies. *Proceedings of the National Academy of Sciences of the United States of America*, 103(6):1661–1668, February 2006.

[35] Lorraine V. Kalia, Suneil K. Kalia, Pamela J. McLean, Andres M. Lozano, and Anthony E. Lang. α-Synuclein oligomers and clinical implications for Parkinson disease. *Annals of neurology*, 73(2):155, December 2012.

[36] Zhiheng Xu, Tianyu Hu, Chenqin Xu, Xiaoniu Liang, Shiyu Li, Yimin Sun, Fengtao Liu, Jian Wang, and Yilin Tang. Disease progression in proposed brain-first and body-first Parkinson's disease subtypes. *npj Parkinson's Disease*, 10(1):1–5, June 2024. Publisher: Nature Publishing Group.

[37] Heiko Braak, Kelly Del Tredici, Udo Rüb, Rob A. I. de Vos, Ernst N. H. Jansen Steur, and Eva Braak. Staging of brain pathology related to sporadic Parkinson's disease. *Neurobiology of Aging*, 24(2):197–211, 2003.

[38] Heiko Braak, Estifanos Ghebremedhin, Udo Rüb, Hansjürgen Bratzke, and Kelly Del Tredici. Stages in the development of Parkinson's disease-related pathology. *Cell and Tissue Research*, 318(1):121–134, October 2004.

[39] Lisanne J. Dommershuijsen, Agnita J. W. Boon, and M. Kamran Ikram. Probing the Pre-diagnostic Phase of Parkinson's Disease in Population-Based Studies. *Frontiers in Neurology*, 12:702502, July 2021.

[40] Daniela Berg, Per Borghammer, Seyed-Mohammad Fereshtehnejad, Sebastian Heinzel, Jacob Horsager, Eva Schaeffer, and Ronald B. Postuma. Prodromal Parkinson disease subtypes - key to understanding heterogeneity. *Nature Reviews. Neurology*, 17(6):349–361, June 2021.

[41] Yuncheng Wu, Weidong Le, and Joseph Jankovic. Preclinical Biomarkers of Parkinson Disease. *Archives of Neurology*, 68(1):22–30, January 2011.

[42] Anette Schrag, Zacharias Anastasiou, Gareth Ambler, Alastair Noyce, and Kate Walters. Predicting diagnosis of Parkinson's disease: A risk algorithm based on primary care presentations. *Movement Disorders*, 34(4):480–486, April 2019.

[43] Cécilia Tremblay, Jie Mei, and Johannes Frasnelli. Olfactory bulb surroundings can help to distinguish Parkinson's disease from non-parkinsonian olfactory dysfunction. *NeuroImage: Clinical*, 28:102457, January 2020.

[44] Chengxiao Ma, Wen Zhang, and Maohong Cao. Role of the Peripheral Nervous System in PD Pathology, Diagnosis, and Treatment. *Frontiers in Neuroscience*, 15:598457, April 2021.

[45] Pauline Dodet, Marion Houot, Smaranda Leu-Semenescu, Jean-Christophe Corvol, Stéphane Lehéricy, Graziella Mangone, Marie Vidailhet, Emmanuel Roze, and Isabelle Arnulf. Sleep disorders in Parkinson's disease, an early and multiple problem. *npj Parkinson's Disease*, 10(1):1–11, February 2024. Publisher: Nature Publishing Group.

[46] Priyadarshi Prajjwal, Herson S Flores Sanga, Kirtish Acharya, Tamara Tango, Jobby John, Rene S.C. Rodriguez, Mohammed Dheyaa Marsool Marsool, Mukhamed Sulaimanov, Aneeqa Ahmed, and Omniat A.

Hussin. Parkinson's disease updates: Addressing the pathophysiology, risk factors, genetics, diagnosis, along with the medical and surgical treatment. *Annals of Medicine and Surgery*, 85(10):4887–4902, August 2023.

[47] J. Eric Ahlskog. Parkinson's disease progression is multifaceted: Evidence for the underlying benchmarks. *Parkinsonism & Related Disorders*, 121:106037, April 2024.

[48] Philippe Rizek, Niraj Kumar, and Mandar S. Jog. An update on the diagnosis and treatment of Parkinson disease. *CMAJ : Canadian Medical Association Journal*, 188(16):1157–1165, November 2016.

[49] Werner Poewe. Clinical measures of progression in Parkinson's disease. *Movement Disorders: Official Journal of the Movement Disorder Society*, 24 Suppl 2:S671–676, 2009.

[50] J. H. Bower, D. M. Maraganore, S. K. McDonnell, and W. A. Rocca. Incidence and distribution of parkinsonism in Olmsted County, Minnesota, 1976-1990. *Neurology*, 52(6):1214–1220, April 1999.

[51] Johan Lokk and Ahmad Delbari. Clinical aspects of palliative care in advanced Parkinson's disease. *BMC Palliative Care*, 11:20, October 2012.

[52] Lisanne J. Dommershuijsen, Sirwan K. L. Darweesh, Yoav Ben-Shlomo, Benzi M. Kluger, and Bastiaan R. Bloem. The elephant in the room: critical reflections on mortality rates among individuals with Parkinson's disease. *npj Parkinson's Disease*, 9(1):1–5, October 2023. Publisher: Nature Publishing Group.

[53] Sze-Ee Soh, Jennifer L. McGinley, Jennifer J. Watts, Robert Iansek, Anna T. Murphy, Hylton B. Menz, Frances Huxham, and Meg E. Morris. Determinants of health-related quality of life in people with Parkinson's disease: a path analysis. *Quality of Life Research*, 22(7):1543–1553, September 2013.

[54] Eduardo Tolosa, Alicia Garrido, Sonja W. Scholz, and Werner Poewe. Challenges in the diagnosis of Parkinson's disease. *The Lancet. Neurology*, 20(5):385–397, May 2021.

[55] Christopher W. Hess and Mark Hallett. The Phenomenology of Parkinson's Disease. *Seminars in neurology*, 37(2):109–117, April 2017.

[56] S. S. Lövdal, G. Carli, B. Orso, M. Biehl, D. Arnaldi, P. Mattioli, A. Janzen, E. Sittig, S. Morbelli, J. Booij, W. H. Oertel, K. L. Leenders, and S. K. Meles. Investigating the aspect of asymmetry in brain-first versus body-first Parkinson's disease. *npj Parkinson's Disease*, 10(1):1–10, March 2024. Publisher: Nature Publishing Group.

[57] Diego Santos-García, Teresa de Deus Fonticoba, Carlos Cores Bartolomé, María J. Feal Painceiras, Iago García Díaz, María Cristina Íñiguez Alvarado, Jose Manuel Paz, Silvia Jesús, Marina Cosgaya, Juan García Caldentey, Nuria Caballol, Ines Legarda, Isabel González Aramburu, Maria A. Ávila Rivera, Víctor Gómez Mayordomo, Lydia Vela, Sonia Escalante, Zebenzui Mendoza, Juan C. Martínez Castrillo, Pilar Sánchez Alonso, Maria G. Alonso Losada, Nuria López Ariztegui, Darrian McAfee, Pablo Martinez-Martin, and Pablo Mir. Response to levodopa in Parkinson's disease over time. A 4-year follow-up study. *Parkinsonism & Related Disorders*, 116:105852, November 2023.

[58] G. Kägi, K. P. Bhatia, and E. Tolosa. The role of DAT-SPECT in movement disorders. *Journal of Neurology, Neurosurgery & Psychiatry*, 81(1):5–12, January 2010. Publisher: BMJ Publishing Group Ltd Section: Review.

[59] Lydia Chougar, Nadya Pyatigorskaya, Bertrand Degos, David Grabli, and Stéphane Lehéricy. The Role of Magnetic Resonance Imaging for the Diagnosis of Atypical Parkinsonism. *Frontiers in Neurology*, 11:665, July 2020.

[60] Renato P. Munhoz, Vitor Tumas, José Luiz Pedroso, and Laura Silveira-Moriyama. The clinical diagnosis of Parkinson's disease. *Arquivos de Neuro-Psiquiatria*, 82(6):1–10, February 2024.

[61] Ümit Özgür AKDEMİR, Ayşe BORA TOKÇAER, and Lütfiye Özlem ATAY1. Dopamine transporter SPECT imaging in Parkinson's disease and parkinsonian disorders. *Turkish Journal of Medical Sciences*, 51(2):400–410, April 2021.

[62] F. Brigo, A. Matinella, R. Erro, and M. Tinazzi. [^{123}I]FP-CIT SPECT (DaTSCAN) may be a useful tool to differentiate between Parkinson's disease and vascular or drug-induced parkinsonisms: a meta-analysis. *European Journal of Neurology*, 21(11):1369–e90, 2014. _eprint: https://onlinelibrary.wiley.com/doi/pdf/10.1111/ene.12444.

[63] Kaki Tsang and Richard Walker. Dopamine transporter single photon emission computed tomography (DaT-SPECT) use in the diagnosis and clinical management of parkinsonism: an 8-year retrospective study. *Journal of Neurology*, 270(5):2550–2558, May 2023.

[64] Luis Concha-Marambio, Carly M. Farris, Bret Holguin, Yihua Ma, John Seibyl, Marco J. Russo, Un J. Kang, Samantha J. Hutten, Kalpana Merchant, Mohammad Shahnawaz, and Claudio Soto. Seed Amplification Assay to Diagnose Early Parkinson's and Predict Dopaminergic Deficit Progression. *Movement Disorders*, 36(10):2444–2446, 2021. _eprint: https://onlinelibrary.wiley.com/doi/pdf/10.1002/mds.28715.

[65] Luis Concha-Marambio, Sandra Pritzkow, Mohammad Shahnawaz, Carly M. Farris, and Claudio Soto. Seed amplification assay for the detection of pathologic alpha-synuclein aggregates in cerebrospinal fluid. *Nature Protocols*, 18(4):1179–1196, April 2023. Publisher: Nature Publishing Group.

[66] Bárbara Fernandes Gomes, Carly M. Farris, Yihua Ma, Luis Concha-Marambio, Russ Lebovitz, Bengt Nellgård, Keti Dalla, Julius Constantinescu, Radu Constantinescu, Johan Gobom, Ulf Andreasson, Henrik Zetterberg, and Kaj Blennow. α-Synuclein seed amplification assay as a diagnostic tool for parkinsonian disorders. *Parkinsonism & Related Disorders*, 117:105807, December 2023.

[67] Yaoyun Kuang, Hengxu Mao, Tingting Gan, Wenyuan Guo, Wei Dai, Weimeng Huang, Zhuohua Wu, Hongyan Li, Xiaoyun Huang, Xinling Yang, and Ping-Yi Xu. A skin-specific α-Synuclein seeding amplification assay for diagnosing Parkinson's disease. *npj Parkinson's Disease*, 10(1):1–12, July 2024. Publisher: Nature Publishing Group.

[68] Alberto J. Espay, Andrew J. Lees, Francisco Cardoso, Steven J. Frucht, Daniel Erskine, Ivette M. Sandoval, Luis Daniel Bernal-Conde, Andrea Sturchio, Alberto Imarisio, Christian Hoffmann, Kora T. Montemagno, Dragomir Milovanovic, Glenda M. Halliday, and Fredric P. Manfredsson. The α-synuclein seed amplification assay: Interpreting a test of Parkinson's pathology. *Parkinsonism & Related Disorders*, 131:107256, February 2025.

[69] Johannes Levin, Simone Baiardi, Corinne Quadalti, Marcello Rossi, Angela Mammana, Jonathan Vöglein, Alexander Bernhardt, Richard J. Perrin, Mathias Jucker, Oliver Preische, Anna Hofmann, Günter U. Höglinger, Nigel J. Cairns, Erin E. Franklin, Patricio Chrem, Carlos Cruchaga, Sarah B. Berman, Jasmeer P. Chhatwal, Alisha Daniels, Gregory S. Day, Natalie S. Ryan, Alison M. Goate, Brian A. Gordon, Edward D. Huey, Laura Ibanez, Celeste M. Karch, Jae-Hong Lee, Jorge Llibre-Guerra, Francisco Lopera, Colin L. Masters, John C. Morris, James M. Noble, Alan E. Renton, Jee Hoon Roh, Matthew P. Frosch, C. Dirk Keene, Catriona McLean, Raquel Sanchez-Valle, Peter R. Schofield, Charlene Supnet-Bell, Chengjie Xiong, Armin Giese, Oskar Hansson, Randall J. Bateman, Eric McDade, Dominantly Inherited Alzheimer Network, and Piero Parchi. α-Synuclein seed amplification assay detects Lewy body co-pathology in autosomal dominant Alzheimer's disease late in the disease course and dependent on Lewy pathology burden. *Alzheimer's & Dementia*, 20(6):4351–4365, 2024. _eprint: https://onlinelibrary.wiley.com/doi/pdf/10.1002/alz.13818.

[70] Coro Paisán-Ruiz, Abi Li, Susanne A. Schneider, Janice L. Holton, Robert Johnson, Desmond Kidd, Jeremy Chataway, Kailash P. Bhatia, Andrew J. Lees, John Hardy, Tamas Revesz, and Henry Houlden. Widespread

Lewy body and tau accumulation in childhood and adult onset dystonia-parkinsonism cases with *PLA2G6* mutations. *Neurobiology of Aging*, 33(4):814–823, April 2012.

[71] Christopher Hatton, Simona S. Ghanem, David J. Koss, Ilham Y. Abdi, Elizabeth Gibbons, Rita Guerreiro, Jose Bras, International DLB Genetics Consortium, Lauren Walker, Ellen Gelpi, Wendy Heywood, Tiago F. Outeiro, Johannes Attems, Robert McFarland, Rob Forsyth, Omar M. El-Agnaf, and Daniel Erskine. Prion-like α-synuclein pathology in the brain of infants with Krabbe disease. *Brain*, 145(4):1257–1263, April 2022.

[72] Andrew Siderowf, Luis Concha-Marambio, David-Erick Lafontant, Carly M Farris, Yihua Ma, Paula A Urenia, Hieu Nguyen, Roy N Alcalay, Lana M Chahine, Tatiana Foroud, Douglas Galasko, Karl Kieburtz, Kalpana Merchant, Brit Mollenhauer, Kathleen L Poston, John Seibyl, Tanya Simuni, Caroline M Tanner, Daniel Weintraub, Aleksandar Videnovic, Seung Ho Choi, Ryan Kurth, Chelsea Caspell-Garcia, Christopher S Coffey, Mark Frasier, Luis M A Oliveira, Samantha J Hutten, Todd Sherer, Kenneth Marek, and Claudio Soto. Assessment of heterogeneity among participants in the Parkinson's Progression Markers Initiative cohort using α-synuclein seed amplification: a cross-sectional study. *The Lancet Neurology*, 22(5):407–417, May 2023.

[73] R. M. Pinder. Possible Dopamine Derivatives capable of Crossing the Blood-Brain Barrier in relation to Parkinsonism. *Nature*, 228(5269):358–358, October 1970. Publisher: Nature Publishing Group.

[74] Federico Paolini Paoletti, Nicola Tambasco, and Lucilla Parnetti. Levodopa treatment in Parkinson's disease: earlier or later? *Annals of Translational Medicine*, 7(Suppl 6):S189, September 2019.

[75] Karolina Poplawska-Domaszewicz, Lucia Batzu, Cristian Falup-Pecurariu, and K. Ray Chaudhuri. Subcutaneous Levodopa: A New Engine for the Vintage Molecule. *Neurology and Therapy*, 13(4):1055–1068, August 2024.

[76] R. G. Cury, R. Galhardoni, E. T. Fonoff, S. Perez Lloret, M. G. Dos Santos Ghilardi, E. R. Barbosa, M. J. Teixeira, and D. Ciampi de Andrade. Sensory abnormalities and pain in Parkinson disease and its modulation by treatment of motor symptoms. *European Journal of Pain (London, England)*, 20(2):151–165, February 2016.

[77] Oleh Hornykiewicz. A brief history of levodopa. *Journal of Neurology*, 257(Suppl 2):S249–252, November 2010.

[78] Maria Hadjiconstantinou and Norton H. Neff. Enhancing Aromatic L-amino Acid Decarboxylase Activity: Implications for L-DOPA Treatment in Parkinson's Disease. *CNS Neuroscience & Therapeutics*, 14(4):340–351, November 2008.

[79] A Münchau and K P Bhatia. Pharmacological treatment of Parkinson's disease. *Postgraduate Medical Journal*, 76(900):602–610, October 2000.

[80] Robert A. Hauser, Michel Panisset, Giovanni Abbruzzese, Linda Mancione, Nalina Dronamraju, Algirdas Kakarieka, and FIRST-STEP Study Group. Double-blind trial of levodopa/carbidopa/entacapone versus levodopa/carbidopa in early Parkinson's disease. *Movement Disorders: Official Journal of the Movement Disorder Society*, 24(4):541–550, March 2009.

[81] Eduardo Tolosa, Basilio Hernández, Gurutz Linazasoro, Juan José López-Lozano, Pablo Mir, José Marey, and Jaime Kulisevsky. Efficacy of levodopa/carbidopa/entacapone versus levodopa/carbidopa in patients with early Parkinson's disease experiencing mild wearing-off: a randomised, double-blind trial. *Journal of Neural Transmission (Vienna, Austria: 1996)*, 121(4):357–366, April 2014.

[82] Destany K. Kwon, Mohit Kwatra, Jing Wang, and Han Seok Ko. Levodopa-Induced Dyskinesia in Parkinson's Disease: Pathogenesis and Emerging Treatment Strategies. *Cells*, 11(23):3736, January 2022. Number: 23 Publisher: Multidisciplinary Digital Publishing Institute.

[83] J. Guridi, R. González-Redondo, and J. A. Obeso. Clinical features, pathophysiology, and treatment of levodopa-induced dyskinesias in Parkinson's disease. *Parkinson's Disease*, 2012:943159, 2012.

[84] Pierpaolo Turcano, Michelle M. Mielke, James H. Bower, Joseph E. Parisi, Jeremy K. Cutsforth-Gregory, J. Eric Ahlskog, and Rodolfo Savica. Levodopa-induced dyskinesia in Parkinson disease. *Neurology*, 91(24):e2238–e2243, December 2018. Publisher: Wolters Kluwer.

[85] J. E. Ahlskog and M. D. Muenter. Frequency of levodopa-related dyskinesias and motor fluctuations as estimated from the cumulative literature. *Movement Disorders: Official Journal of the Movement Disorder Society*, 16(3):448–458, May 2001.

[86] Dag Nyholm. The rationale for continuous dopaminergic stimulation in advanced Parkinson's disease. *Parkinsonism & Related Disorders*, 13:S13–S17, September 2007.

[87] Hanna S. Lindgren, Daniel R. Andersson, Sören Lagerkvist, Hans Nissbrandt, and M. Angela Cenci. l-DOPA-induced dopamine efflux in the striatum and the substantia nigra in a rat model of Parkinson's disease: temporal and quantitative relationship to the expression of dyskinesia. *Journal of Neurochemistry*, 112(6):1465–1476, 2010. _eprint: https://onlinelibrary.wiley.com/doi/pdf/10.1111/j.1471-4159.2009.06556.x.

[88] Thomas Müller and Hans Michael Thiede. Bound, free, and total L-dopa measurement in plasma of Parkinson's disease patients. *Journal of Neural Transmission (Vienna, Austria: 1996)*, 126(11):1417–1420, November 2019.

[89] M. Angela Cenci. Presynaptic Mechanisms of l-DOPA-Induced Dyskinesia: The Findings, the Debate, and the Therapeutic Implications. *Frontiers in Neurology*, 5, December 2014. Publisher: Frontiers.

[90] Insha Zahoor, Amrina Shafi, and Ehtishamul Haq. Pharmacological Treatment of Parkinson's Disease. In Thomas B. Stoker and Julia C. Greenland, editors, *Parkinson's Disease: Pathogenesis and Clinical Aspects*. Codon Publications, Brisbane (AU), 2018.

[91] Marwan Hariz and Patric Blomstedt. Deep brain stimulation for Parkinson's disease. *Journal of Internal Medicine*, 292(5):764–778, 2022. _eprint: https://onlinelibrary.wiley.com/doi/pdf/10.1111/joim.13541.

[92] Matthew D. Johnson, Svjetlana Miocinovic, Cameron C. McIntyre, and Jerrold L. Vitek. Mechanisms and targets of deep brain stimulation in movement disorders. *Neurotherapeutics*, 5(2):294–308, April 2008.

[93] Honglong Pei, Zhenghan Wu, Li Ma, Jun Wang, Jinghui Li, Xin Geng, Yanghong Zou, Mou Zhang, Renli Qi, and Hualin Yu. Deep Brain Stimulation Mechanisms in Parkinson's Disease: Immediate and Long-Term Effects. *Journal of Integrative Neuroscience*, 23(6):114, June 2024. Number: 6 Publisher: IMR Press.

[94] Charles J. Wilson, Bryce Beverlin, and Theoden Netoff. Chaotic desynchronization as the therapeutic mechanism of deep brain stimulation. *Frontiers in Systems Neuroscience*, 5:50, 2011.

[95] Viviana Torres, Kirsys Del Giudice, Pedro Roldán, Jordi Rumià, Esteban Muñoz, Ana Cámara, Yaroslau Compta, Almudena Sánchez-Gómez, and Francesc Valldeoriola. Image-guided programming deep brain stimulation improves clinical outcomes in patients with Parkinson's disease. *npj Parkinson's Disease*, 10(1):1–9, January 2024. Publisher: Nature Publishing Group.

[96] Alan D. Dorval, Alexis M. Kuncel, Merrill J. Birdno, Dennis A. Turner, and Warren M. Grill. Deep Brain Stimulation Alleviates Parkinsonian Bradykinesia by Regularizing Pallidal Activity. *Journal of Neurophysiology*, 104(2):911–921, August 2010.

[97] Johanne Ligaard, Julia Sannæs, and Lasse Pihlstrøm. Deep brain stimulation and genetic variability in Parkinson's disease: a review of the literature. *npj Parkinson's Disease*, 5(1):1–10, September 2019. Publisher: Nature Publishing Group.

[98] David Baggett, Alex Olson, and Mayur S. Parmar. Novel approaches targeting α-Synuclein for Parkinson's Disease: Current progress and future directions for the disease-modifying therapies. *Brain Disorders*, 16:100163, December 2024.

[99] Sindhu Menon, Sabrina Armstrong, Amir Hamzeh, Naomi P. Visanji, Sergio Pablo Sardi, and Anurag Tandon. Alpha-Synuclein Targeting Therapeutics for Parkinson's Disease and Related Synucleinopathies. *Frontiers in Neurology*, 13:852003, May 2022.

[100] Paolo Calabresi, Alessandro Mechelli, Giuseppina Natale, Laura Volpicelli-Daley, Giulia Di Lazzaro, and Veronica Ghiglieri. Alpha-synuclein in Parkinson's disease and other synucleinopathies: from overt neurodegeneration back to early synaptic dysfunction. *Cell Death & Disease*, 14(3):176, March 2023.

[101] Wassilios G. Meissner, Anne Pavy-Le Traon, Alexandra Foubert-Samier, Gergana Galabova, Monique Galitzky, Alexandra Kutzelnigg, Brice Laurens, Petra Lührs, Rossella Medori, Patrice Péran, Umberto Sabatini, Sylvain Vergnet, Dieter Volc, Werner Poewe, Achim Schneeberger, Günther Staffler, Olivier Rascol, and AFF009 Study Investigators. A Phase 1 Randomized Trial of Specific Active α-Synuclein Immunotherapies PD01A and PD03A in Multiple System Atrophy. *Movement Disorders: Official Journal of the Movement Disorder Society*, 35(11):1957–1965, November 2020.

[102] Gennaro Pagano, Kirsten I. Taylor, Judith Anzures-Cabrera, Maddalena Marchesi, Tanya Simuni, Kenneth Marek, Ronald B. Postuma, Nicola Pavese, Fabrizio Stocchi, Jean-Philippe Azulay, Brit Mollenhauer, Lydia López-Manzanares, David S. Russell, James T. Boyd, Anthony P. Nicholas, María R. Luquin, Robert A. Hauser, Thomas Gasser, Werner Poewe, Benedicte Ricci, Anne Boulay, Annamarie Vogt, Frank G. Boess, Juergen Dukart, Giulia D'Urso, Rebecca Finch, Stefano Zanigni, Annabelle Monnet, Nathalie Pross, Andrea Hahn, Hanno Svoboda, Markus Britschgi, Florian Lipsmeier, Ekaterina Volkova-Volkmar, Michael Lindemann, Sebastian Dziadek, Štefan Holiga, Daria Rukina, Thomas Kustermann, Geoffrey A. Kerchner, Paulo Fontoura, Daniel Umbricht, Rachelle Doody, Tania Nikolcheva, and Azad Bonni. Trial of Prasinezumab in Early-Stage Parkinson's Disease. *New England Journal of Medicine*, 387(5):421–432, August 2022. Publisher: Massachusetts Medical Society _eprint: https://www.nejm.org/doi/pdf/10.1056/NEJMoa2202867.

[103] Gennaro Pagano, Kirsten I. Taylor, Judith Anzures Cabrera, Tanya Simuni, Kenneth Marek, Ronald B. Postuma, Nicola Pavese, Fabrizio Stocchi, Kathrin Brockmann, Hanno Svoboda, Dylan Trundell, Annabelle Monnet, Rachelle Doody, Paulo Fontoura, Geoffrey A. Kerchner, Patrik Brundin, Tania Nikolcheva, and Azad Bonni. Prasinezumab slows motor progression in rapidly progressing early-stage Parkinson's disease. *Nature*

Medicine, 30(4):1096–1103, April 2024. Publisher: Nature Publishing Group.

[104] Tania Nikolcheva, Gennaro Pagano, Nathalie Pross, Tanya Simuni, Kenneth Marek, Ronald B. Postuma, Nicola Pavese, Fabrizio Stocchi, Klaus Seppi, Annabelle Monnet, Nima Shariati, Benedicte Ricci, Loes Rutten-Jacobs, Gesine Respondek, Thomas Kustermann, Kirsten I. Taylor, Dylan Trundell, Paulo Fontoura, Rachelle Doody, Hanno Svoboda, and Azad Bonni. A Phase IIb, Multicenter, Randomized, Double-blind, Placebo-controlled Study to Evaluate the Efficacy and Safety of Intravenous Prasinezumab in Early-stage Parkinson's disease (PADOVA): Rationale, Design, and Baseline Data. *Parkinsonism & Related Disorders*, page 107257, December 2024.

[105] William Dauer and Serge Przedborski. Parkinson's Disease: Mechanisms and Models. *Neuron*, 39(6):889–909, September 2003. Publisher: Elsevier.

[106] Soania Mathur and Jon Stamford. Bringing Advanced Therapies for Parkinson's Disease to the Clinic: The Patient's Perspective. *Journal of Parkinson's Disease*, 11(s2):S141–S145, January 2021. Publisher: IOS Press.

[107] David P. Breen and Anthony E. Lang. Tracking the course of prodromal Parkinson's disease. *Brain: A Journal of Neurology*, 140(2):259–262, February 2017.

[108] Poul Henning Jensen, Michael G. Schlossmacher, and Leonidas Stefanis. Who Ever Said It Would Be Easy? Reflecting on Two Clinical Trials Targeting α-Synuclein. *Movement Disorders*, 38(3):378–384, 2023. _eprint: https://onlinelibrary.wiley.com/doi/pdf/10.1002/mds.29318.

[109] Shirley Yin-Yu Pang, Philip Wing-Lok Ho, Hui-Fang Liu, Chi-Ting Leung, Lingfei Li, Eunice Eun Seo Chang, David Boyer Ramsden, and Shu-Leong Ho. The interplay of aging, genetics and environmental factors in the pathogenesis of Parkinson's disease. *Translational Neurodegeneration*, 8(1):23, August 2019.

[110] Jenne Tran, Helena Anastacio, and Cedric Bardy. Genetic predispositions of Parkinson's disease revealed in patient-derived brain cells. *NPJ Parkinson's Disease*, 6:8, April 2020.

[111] Gabriela Novak, Dimitrios Kyriakis, Kamil Grzyb, Michela Bernini, Sophie Rodius, Gunnar Dittmar, Steven Finkbeiner, and Alexander Skupin. Single-cell transcriptomics of human iPSC differentiation dynamics reveal a core molecular network of Parkinson's disease. *Communications Biology*, 5:49, January 2022.

[112] Xylena Reed, Sara Bandrés-Ciga, Cornelis Blauwendraat, and Mark R. Cookson. The role of monogenic genes in idiopathic Parkinson's disease. *Neurobiology of disease*, 124:230–239, April 2019.

[113] Chou Chai and Kah-Leong Lim. Genetic Insights into Sporadic Parkinson's Disease Pathogenesis. *Current Genomics*, 14(8):486–501, December 2013.

[114] Mihael H. Polymeropoulos, Christian Lavedan, Elisabeth Leroy, Susan E. Ide, Anindya Dehejia, Amalia Dutra, Brian Pike, Holly Root, Jeffrey Rubenstein, Rebecca Boyer, Edward S. Stenroos, Settara Chandrasekharappa, Aglaia Athanassiadou, Theodore Papapetropoulos, William G. Johnson, Alice M. Lazzarini, Roger C. Duvoisin, Giuseppe Di Iorio, Lawrence I. Golbe, and Robert L. Nussbaum. Mutation in the α-Synuclein Gene Identified in Families with Parkinson's Disease. *Science*, 276(5321):2045–2047, June 1997. Publisher: American Association for the Advancement of Science.

[115] Takuya Konno, Owen A. Ross, Andreas Puschmann, Dennis W. Dickson, and Zbigniew K. Wszolek. Autosomal dominant Parkinson's disease caused by *SNCA* duplications. *Parkinsonism & Related Disorders*, 22:S1–S6, January 2016.

[116] Manabu Funayama, Kenya Nishioka, Yuanzhe Li, and Nobutaka Hattori. Molecular genetics of Parkinson's disease: Contributions and global trends. *Journal of Human Genetics*, 68(3):125–130, March 2023.

[117] Yun Joong Kim, Kiyong Kim, Heonwoo Lee, Junbeom Jeon, Jinwoo Lee, and Jeehee Yoon. The Protein-Protein Interaction Network of Hereditary Parkinsonism Genes Is a Hierarchical Scale-Free Network. *Yonsei Medical Journal*, 63(8):724–734, August 2022.

[118] Lara M. Lange, Catalina Cerquera-Cleves, Marijn Schipper, Georgia Panagiotaropoulou, Alice Braun, Julia Kraft, Swapnil Awasthi, Nathaniel Bell, Danielle Posthuma, Stephan Ripke, Cornelis Blauwendraat, and Karl Heilbron. Prioritizing Parkinson's disease risk genes in genome-wide association loci, December 2024. Pages: 2024.12.13.24318996.

[119] Marzieh Khani, Catalina Cerquera-Cleves, Mariam Kekenadze, Peter Wild Crea, Andrew B. Singleton, and Sara Bandres-Ciga. Towards a Global View of Parkinson's Disease Genetics. *Annals of Neurology*, 95(5):831–842, 2024. _eprint: https://onlinelibrary.wiley.com/doi/pdf/10.1002/ana.26905.

[120] Christine Klein and Ana Westenberger. Genetics of Parkinson's Disease. *Cold Spring Harbor Perspectives in Medicine*, 2(1):a008888, January 2012.

[121] Alexis Brice. Genetics of Parkinson's disease: LRRK2 on the rise. *Brain: A Journal of Neurology*, 128(Pt 12):2760–2762, December 2005.

[122] Jean-Marc Taymans, Matt Fell, Tim Greenamyre, Warren D. Hirst, Adamantios Mamais, Shalini Padmanabhan, Inga Peter, Hardy Rideout, and Avner Thaler. Perspective on the current state of the LRRK2 field. *npj*

Parkinson's Disease, 9(1):1–9, July 2023. Publisher: Nature Publishing Group.

[123] Qin Rui, Haibo Ni, Di Li, Rong Gao, and Gang Chen. The Role of LRRK2 in Neurodegeneration of Parkinson Disease. *Current Neuropharmacology*, 16(9):1348–1357, November 2018.

[124] Karen Nuytemans, Jessie Theuns, Marc Cruts, and Christine Van Broeckhoven. Genetic etiology of Parkinson disease associated with mutations in the SNCA, PARK2, PINK1, PARK7, and LRRK2 genes: a mutation update. *Human Mutation*, 31(7):763–780, 2010. _eprint: https://onlinelibrary.wiley.com/doi/pdf/10.1002/humu.21277.

[125] Ga Ram Jeong and Byoung Dae Lee. Pathological Functions of LRRK2 in Parkinson's Disease. *Cells*, 9(12):2565, November 2020.

[126] Di Fonzo A, Tassorelli C, De Mari M, Chien Hf, Ferreira J, Rohé Cf, Riboldazzi G, Antonini A, Albani G, Mauro A, Marconi R, Abbruzzese G, Lopiano L, Fincati E, Guidi M, Marini P, Stocchi F, Onofrj M, Toni V, Tinazzi M, Fabbrini G, Lamberti P, Vanacore N, Meco G, Leitner P, Uitti Rj, Wszolek Zk, Gasser T, Simons Ej, Breedveld Gj, Goldwurm S, Pezzoli G, Sampaio C, Barbosa E, Martignoni E, Oostra Ba, and Bonifati V. Comprehensive analysis of the LRRK2 gene in sixty families with Parkinson's disease. *European journal of human genetics : EJHG*, 14(3), March 2006. Publisher: Eur J Hum Genet.

[127] David MacLeod, Julia Dowman, Rachel Hammond, Thomas Leete, Keiichi Inoue, and Asa Abeliovich. The Familial Parkinsonism Gene LRRK2 Regulates Neurite Process Morphology. *Neuron*, 52(4):587–593, November 2006. Publisher: Elsevier.

[128] Xiaojuan Zhang and Arjan Kortholt. LRRK2 Structure-Based Activation Mechanism and Pathogenesis. *Biomolecules*, 13(4):612, March 2023.

[129] C. Alexander Boecker, Juliet Goldsmith, Dan Dou, Gregory G. Cajka, and Erika L. F. Holzbaur. Increased LRRK2 kinase activity alters neuronal autophagy by disrupting the axonal transport of autophagosomes. *Current Biology*, 31(10):2140–2154.e6, May 2021. Publisher: Elsevier.

[130] Xinglong Wang, Michael H. Yan, Hisashi Fujioka, Jun Liu, Amy Wilson-Delfosse, Shu G. Chen, George Perry, Gemma Casadesus, and Xiongwei Zhu. LRRK2 regulates mitochondrial dynamics and function through direct interaction with DLP1. *Human Molecular Genetics*, 21(9):1931–1944, May 2012.

[131] Suzanne Lesage, Marion Houot, Graziella Mangone, Christelle Tesson, Hélène Bertrand, Sylvie Forlani, Mathieu Anheim, Christine Brefel-Courbon, Emmanuel Broussolle, Stéphane Thobois, Philippe Damier, Franck Durif, Emmanuel Roze, François Tison, David Grabli, Fabienne

Ory-Magne, Bertrand Degos, François Viallet, Florence Cormier-Dequaire, Anne-Marie Ouvrard-Hernandez, Marie Vidailhet, Ebba Lohmann, Andrew Singleton, Jean-Christophe Corvol, Alexis Brice, and for the French Parkinson disease Genetics Study Group(PDG). Genetic and Phenotypic Basis of Autosomal Dominant Parkinson's Disease in a Large Multi-Center Cohort. *Frontiers in Neurology*, 11, July 2020. Publisher: Frontiers.

[132] N. Brueggemann, P. Odin, A. Gruenewald, V. Tadic, J. Hagenah, G. Seidel, K. Lohmann, C. Klein, and A. Djarmati. α-Synuclein gene duplication is present in sporadic Parkinson disease. *Neurology*, 71(16):1294–1294, October 2008. Publisher: Wolters Kluwer.

[133] A. Lunati, S. Lesage, and A. Brice. The genetic landscape of Parkinson's disease. *Revue Neurologique*, 174(9):628–643, November 2018.

[134] Luca Magistrelli, Elena Contaldi, and Cristoforo Comi. The Impact of SNCA Variations and Its Product Alpha-Synuclein on Non-Motor Features of Parkinson's Disease. *Life*, 11(8):804, August 2021.

[135] Hui Liu, Christos Koros, Timo Strohäker, Claudia Schulte, Maria Bozi, Stefanos Varvaresos, Alain Ibáñez de Opakua, Athina Maria Simitsi, Anastasia Bougea, Konstantinos Voumvourakis, Matina Maniati, Sokratis G. Papageorgiou, Ann-Kathrin Hauser, Stefan Becker, Markus Zweckstetter, Leonidas Stefanis, and Thomas Gasser. A Novel SNCA A30G Mutation Causes Familial Parkinsons Disease. *Movement Disorders*, 36(7):1624–1633, 2021. _eprint: https://onlinelibrary.wiley.com/doi/pdf/10.1002/mds.28534.

[136] Sokhna Haissatou Diaw, Max Borsche, Linn Streubel-Gallasch, Marija Dulovic-Mahlow, Julia Hermes, Insa Lenz, Philip Seibler, Christine Klein, Norbert Brüggemann, Melissa Vos, and Katja Lohmann. Characterization of the pathogenic α-Synuclein Variant V15A in Parkinson´s disease. *npj Parkinson's Disease*, 9(1):1–11, October 2023. Publisher: Nature Publishing Group.

[137] Cornelis Blauwendraat, Mary B. Makarious, Hampton L. Leonard, Sara Bandres-Ciga, Hirotaka Iwaki, Mike A. Nalls, Alastair J. Noyce, and Andrew B. Singleton. A population scale analysis of rare SNCA variation in the UK Biobank. *Neurobiology of disease*, 148:105182, January 2021.

[138] K. Markopoulou, D. W. Dickson, R. D. McComb, Z. K. Wszolek, L. Katechalidou, L. Avery, M. S. Stansbury, and B. A. Chase. Clinical, neuropathological and genotypic variability in SNCA A53T familial Parkinson's disease. *Acta Neuropathologica*, 116(1):25–35, July 2008.

[139] Tommi Kilpeläinen, Ulrika H. Julku, Reinis Svarcbahs, and Timo T. Myöhänen. Behavioural and dopaminergic changes in double mutated human A30P*A53T alpha-synuclein transgenic mouse model of Parkinson´s disease. *Scientific Reports*, 9(1):17382, November 2019. Publisher: Nature Publishing Group.

[140] Joanne Trinh, Florentine M.J. Zeldenrust, Jana Huang, Meike Kasten, Susen Schaake, Sonja Petkovic, Harutyun Madoev, Anne Grünewald, Shahad Almuammar, Inke R. König, Christina M. Lill, Katja Lohmann, Christine Klein, and Connie Marras. Genotype-phenotype relations for the Parkinson's disease genes SNCA, LRRK2, VPS35: MDSGene systematic review. *Movement Disorders*, 33(12):1857–1870, 2018. _eprint: https://onlinelibrary.wiley.com/doi/pdf/10.1002/mds.27527.

[141] Meike Kasten and Christine Klein. The many faces of alpha-synuclein mutations. *Movement Disorders: Official Journal of the Movement Disorder Society*, 28(6):697–701, June 2013.

[142] Simona Petrucci, Monia Ginevrino, and Enza Maria Valente. Phenotypic spectrum of alpha-synuclein mutations: New insights from patients and cellular models. *Parkinsonism & Related Disorders*, 22:S16–S20, January 2016. Publisher: Elsevier.

[143] Heather H. C. Lau, Ivan Martinez-Valbuena, Raphaella W. L. So, Surabhi Mehra, Nicholas R. G. Silver, Alison Mao, Erica Stuart, Cian Schmitt-Ulms, Bradley T. Hyman, Martin Ingelsson, Gabor G. Kovacs, and Joel C. Watts. The G51D SNCA mutation generates a slowly progressive α-synuclein strain in early-onset Parkinson's disease. *Acta Neuropathologica Communications*, 11(1):72, May 2023.

[144] Suzanne Lesage, Mathieu Anheim, Franck Letournel, Luc Bousset, Aurélie Honoré, Nelly Rozas, Laura Pieri, Karine Madiona, Alexandra Dürr, Ronald Melki, Christophe Verny, Alexis Brice, and for the French Parkinson's Disease Genetics Study Group. G51D α-synuclein mutation causes a novel Parkinsonian–pyramidal syndrome. *Annals of Neurology*, 73(4):459–471, 2013. _eprint: https://onlinelibrary.wiley.com/doi/pdf/10.1002/ana.23894.

[145] Ruo-Nan Duan, Gui-Yu Liu, Yin-Lian Han, Pei-Zheng Li, Bo-Han Zhang, and Yi-Ming Liu. Characterization of Multiplication in Parkinson's Disease: 2 New Cases and Evaluation of the Literature. *Movement Disorders Clinical Practice*, 10(10):1536–1541, 2023. _eprint: https://onlinelibrary.wiley.com/doi/pdf/10.1002/mdc3.13852.

[146] Adam Book, Ilaria Guella, Tara Candido, Alexis Brice, Nobutaka Hattori, Beomseok Jeon, Matthew J. Farrer, and SNCA Multiplication Investigators of the GEoPD Consortium. A Meta-Analysis of α-Synuclein Multiplication in Familial Parkinsonism. *Frontiers in Neurology*, 9, December 2018. Publisher: Frontiers.

[147] Fangzhi Jia, Avi Fellner, and Kishore Raj Kumar. Monogenic Parkinson's Disease: Genotype, Phenotype, Pathophysiology, and Genetic Testing. *Genes*, 13(3):471, March 2022.

[148] Isabel Wurster, Corinne Quadalti, Marcello Rossi, Ann-Kathrin Hauser, Christian Deuschle, Claudia Schulte, Katharina Waniek, Ingolf Lachmann, Christian la Fougere, Kathrin Doppler, Thomas Gasser, Benjamin Bender, Piero Parchi, and Kathrin Brockmann. Linking the phenotype of SNCA Triplication with PET-MRI imaging pattern and alpha-synuclein CSF seeding. *npj Parkinson's Disease*, 8(1):1–8, September 2022. Publisher: Nature Publishing Group.

[149] Magali Periquet, Morwena Latouche, Ebba Lohmann, Nina Rawal, Giuseppe De Michele, Sylvain Ricard, Hélio Teive, Valérie Fraix, Marie Vidailhet, David Nicholl, Paolo Barone, Nick W. Wood, Salmo Raskin, Jean-François Deleuze, Yves Agid, Alexandra Dürr, Alexis Brice, French Parkinson's Disease Genetics Study Group, and European Consortium on Genetic Susceptibility in Parkinson's Disease. Parkin mutations are frequent in patients with isolated early-onset parkinsonism. *Brain: A Journal of Neurology*, 126(Pt 6):1271–1278, June 2003.

[150] C. B. Lücking, A. Dürr, V. Bonifati, J. Vaughan, G. De Michele, T. Gasser, B. S. Harhangi, G. Meco, P. Denèfle, N. W. Wood, Y. Agid, A. Brice, French Parkinson's Disease Genetics Study Group, and European Consortium on Genetic Susceptibility in Parkinson's Disease. Association between early-onset Parkinson's disease and mutations in the parkin gene. *The New England Journal of Medicine*, 342(21):1560–1567, May 2000.

[151] Iryna Kamienieva, Jerzy Duszyński, and Joanna Szczepanowska. Multitasking guardian of mitochondrial quality: Parkin function and Parkinson's disease. *Translational Neurodegeneration*, 10(1):5, January 2021.

[152] Liliane Glauser, Sarah Sonnay, Klodjan Stafa, and Darren J. Moore. Parkin promotes the ubiquitination and degradation of the mitochondrial fusion factor mitofusin 1. *Journal of Neurochemistry*, 118(4):636–645, August 2011.

[153] B. E. Riley, J. C. Lougheed, K. Callaway, M. Velasquez, E. Brecht, L. Nguyen, T. Shaler, D. Walker, Y. Yang, K. Regnstrom, L. Diep, Z. Zhang, S. Chiou, M. Bova, D. R. Artis, N. Yao, J. Baker, T. Yednock, and J. A. Johnston. Structure and function of Parkin E3 ubiquitin ligase reveals aspects of RING and HECT ligases. *Nature Communications*, 4:1982, 2013.

[154] Peter M. J. Quinn, Paula I. Moreira, António Francisco Ambrósio, and C. Henrique Alves. PINK1/PARKIN signalling in neurodegeneration and neuroinflammation. *Acta Neuropathologica Communications*, 8(1):189, November 2020.

[155] Alicia M. Pickrell and Richard J. Youle. The roles of PINK1, parkin, and mitochondrial fidelity in Parkinson's disease. *Neuron*, 85(2):257–273, January 2015.

[156] Shouliang Wang, Haijiao Long, Lianjie Hou, Baorong Feng, Zihong Ma, Ying Wu, Yu Zeng, Jiahao Cai, Da-wei Zhang, and Guojun Zhao. The mitophagy pathway and its implications in human diseases. *Signal Transduction and Targeted Therapy*, 8(1):1–28, August 2023. Publisher: Nature Publishing Group.

[157] Julian P. Wagner, Véronique Sauvé, Anshu Saran, and Kalle Gehring. Structural basis for the pathogenicity of parkin catalytic domain mutants. *Journal of Biological Chemistry*, 301(1):108051, January 2025.

[158] Enza Maria Valente, Patrick M. Abou-Sleiman, Viviana Caputo, Miratul M. K. Muqit, Kirsten Harvey, Suzana Gispert, Zeeshan Ali, Domenico Del Turco, Anna Rita Bentivoglio, Daniel G Healy, Alberto Albanese, Robert Nussbaum, Rafael González-Maldonado, Thomas Deller, Sergio Salvi, Pietro Cortelli, William P. Gilks, David S. Latchman, Robert J. Harvey, Bruno Dallapiccola, Georg Auburger, and Nicholas W. Wood. Hereditary Early-Onset Parkinson's Disease Caused by Mutations in PINK1. *Science*, 304(5674):1158–1160, May 2004. Publisher: American Association for the Advancement of Science.

[159] Joanna Siuda, Barbara Jasinska-Myga, Magdalena Boczarska-Jedynak, Grzegorz Opala, Fabienne C. Fiesel, Elisabeth L. Moussaud-Lamodière, Leslie A. Scarffe, Valina L. Dawson, Owen A. Ross, Wolfdieter Springer, Ted M. Dawson, and Zbigniew K. Wszolek. Early-onset Parkinson's disease due to PINK1 p.Q456X mutation–clinical and functional study. *Parkinsonism & Related Disorders*, 20(11):1274–1278, November 2014.

[160] Preston Ge, Valina L. Dawson, and Ted M. Dawson. PINK1 and Parkin mitochondrial quality control: a source of regional vulnerability in Parkinson's disease. *Molecular Neurodegeneration*, 15(1):20, March 2020.

[161] Mariaelena Repici and Flaviano Giorgini. DJ-1 in Parkinson's Disease: Clinical Insights and Therapeutic Perspectives. *Journal of Clinical Medicine*, 8(9):1377, September 2019.

[162] Rosa M. Canet-Avilés, Mark A. Wilson, David W. Miller, Rili Ahmad, Chris McLendon, Sourav Bandyopadhyay, Melisa J. Baptista, Dagmar Ringe, Gregory A. Petsko, and Mark R. Cookson. The Parkinson's disease protein DJ-1 is neuroprotective due to cysteine-sulfinic acid-driven mitochondrial localization. *Proceedings of the National Academy of Sciences*, 101(24):9103–9108, June 2004. Publisher: Proceedings of the National Academy of Sciences.

[163] Stéphanie Baulac, Matthew J. LaVoie, Jennifer Strahle, Michael G. Schlossmacher, and Weiming Xia. Dimerization of Parkinson's disease-causing DJ-1 and formation of high molecular weight complexes in human brain. *Molecular and Cellular Neuroscience*, 27(3):236–246, November 2004.

[164] Nathan Pankratz, Michael W. Pauciulo, Veronika E. Elsaesser, Diane K. Marek, Cheryl A. Halter, Joanne Wojcieszek, Alice Rudolph, Clifford W. Shults, Tatiana Foroud, and William C. Nichols. Mutations in *DJ-1* are rare in familial Parkinson disease. *Neuroscience Letters*, 408(3):209–213, November 2006.

[165] Kazuko Takahashi-Niki, Takeshi Niki, Takahiro Taira, Sanae M. M Iguchi-Ariga, and Hiroyoshi Ariga. Reduced anti-oxidative stress activities of DJ-1 mutants found in Parkinson's disease patients. *Biochemical and Biophysical Research Communications*, 320(2):389–397, July 2004.

[166] Maria G. Macedo, Burcu Anar, Iraad F. Bronner, Milena Cannella, Ferdinando Squitieri, Vincenzo Bonifati, André Hoogeveen, Peter Heutink, and Patrizia Rizzu. The DJ-1L166P mutant protein associated with early onset Parkinson's disease is unstable and forms higher-order protein complexes. *Human Molecular Genetics*, 12(21):2807–2816, November 2003.

[167] Raymond H. Kim, Patrice D. Smith, Hossein Aleyasin, Shawn Hayley, Matthew P. Mount, Scott Pownall, Andrew Wakeham, Annick J. You-Ten, Suneil K. Kalia, Patrick Horne, David Westaway, Andres M. Lozano, Hymie Anisman, David S. Park, and Tak W. Mak. Hypersensitivity of DJ-1-deficient mice to 1-methyl-4-phenyl-1,2,3,6-tetrahydropyrindine (MPTP) and oxidative stress. *Proceedings of the National Academy of Sciences*, 102(14):5215–5220, April 2005. Publisher: Proceedings of the National Academy of Sciences.

[168] Laura Smith and Anthony H. V. Schapira. GBA Variants and Parkinson Disease: Mechanisms and Treatments. *Cells*, 11(8):1261, April 2022.

[169] Giulietta M. Riboldi and Alessio B. Di Fonzo. GBA, Gaucher Disease, and Parkinson's Disease: From Genetic to Clinic to New Therapeutic Approaches. *Cells*, 8(4):364, April 2019.

[170] Jérôme Stirnemann, Nadia Belmatoug, Fabrice Camou, Christine Serratrice, Roseline Froissart, Catherine Caillaud, Thierry Levade, Leonardo Astudillo, Jacques Serratrice, Anaïs Brassier, Christian Rose, Thierry Billette de Villemeur, and Marc G. Berger. A Review of Gaucher Disease Pathophysiology, Clinical Presentation and Treatments. *International Journal of Molecular Sciences*, 18(2):441, February 2017.

[171] O. Goker-Alpan, R. Schiffmann, M. E. LaMarca, R. L. Nussbaum, A. McInerney-Leo, and E. Sidransky. Parkinsonism among Gaucher disease carriers. *Journal of Medical Genetics*, 41(12):937–940, December 2004. Publisher: BMJ Publishing Group Ltd Section: Short report.

[172] Alicia Lwin, Eduard Orvisky, Ozlem Goker-Alpan, Mary E LaMarca, and Ellen Sidransky. Glucocerebrosidase mutations in subjects with parkinsonism. *Molecular Genetics and Metabolism*, 81(1):70–73, January 2004.

[173] Prabhjyot Saini, Uladzislau Rudakou, Eric Yu, Jennifer A. Ruskey, Farnaz Asayesh, Sandra B. Laurent, Dan Spiegelman, Stanley Fahn, Cheryl Waters, Oury Monchi, Yves Dauvilliers, Nicolas Dupré, Lior Greenbaum, Sharon Hassin-Baer, Alberto J. Espay, Guy A. Rouleau, Roy N. Alcalay, Edward A. Fon, Ronald B. Postuma, and Ziv Gan-Or. Association study of *DNAJC13*, *UCHL1*, *HTRA2*, *GIGYF2*, and *EIF4G1* with Parkinson's disease. *Neurobiology of Aging*, 100:119.e7–119.e13, April 2021.

[174] Richard Jay Smeyne and Vernice Jackson-Lewis. The MPTP model of Parkinson's disease. *Molecular Brain Research*, 134(1):57–66, March 2005.

[175] J. W. Langston, P. Ballard, J. W. Tetrud, and I. Irwin. Chronic Parkinsonism in humans due to a product of meperidine-analog synthesis. *Science (New York, N.Y.)*, 219(4587):979–980, February 1983.

[176] Sohaila AlShimemeri, Daniel G. Di Luca, and Susan H. Fox. MPTP Parkinsonism and Implications for Understanding Parkinson's Disease. *Movement Disorders Clinical Practice*, 9(1):42–47, September 2021.

[177] Won-Seok Choi, Shane E. Kruse, Richard D. Palmiter, and Zhengui Xia. Mitochondrial complex I inhibition is not required for dopaminergic neuron death induced by rotenone, MPP+, or paraquat. *Proceedings of the National Academy of Sciences of the United States of America*, 105(39):15136–15141, September 2008.

[178] Dana B Hancock, Eden R Martin, Gregory M Mayhew, Jeffrey M Stajich, Rita Jewett, Mark A Stacy, Burton L Scott, Jeffery M Vance, and William K Scott. Pesticide exposure and risk of Parkinson's disease: A family-based case-control study. *BMC Neurology*, 8:6, March 2008.

[179] Caroline M. Tanner, Freya Kamel, G. Webster Ross, Jane A. Hoppin, Samuel M. Goldman, Monica Korell, Connie Marras, Grace S. Bhudhikanok, Meike Kasten, Anabel R. Chade, Kathleen Comyns, Marie Barber Richards, Cheryl Meng, Benjamin Priestley, Hubert H. Fernandez, Franca Cambi, David M. Umbach, Aaron Blair, Dale P. Sandler, and J. William Langston. Rotenone, Paraquat, and Parkinson's Disease. *Environmental Health Perspectives*, 119(6):866–872, June 2011.

[180] Fangjie Cao, Christopher L. Souders II, Veronica Perez-Rodriguez, and Christopher J. Martyniuk. Elucidating Conserved Transcriptional Networks Underlying Pesticide Exposure and Parkinson's Disease: A Focus on Chemicals of Epidemiological Relevance. *Frontiers in Genetics*, 9, January 2019. Publisher: Frontiers.

[181] Sabrina Heinz, Alexius Freyberger, Bettina Lawrenz, Ludwig Schladt, Gabriele Schmuck, and Heidrun Ellinger-Ziegelbauer. Mechanistic Investigations of the Mitochondrial Complex I Inhibitor Rotenone in the Context of Pharmacological and Safety Evaluation. *Scientific Reports*, 7(1):45465, April 2017. Publisher: Nature Publishing Group.

[182] Todd B. Sherer, Jin-Ho Kim, Ranjita Betarbet, and J. Timothy Greenamyre. Subcutaneous Rotenone Exposure Causes Highly Selective Dopaminergic Degeneration and α-Synuclein Aggregation. *Experimental Neurology*, 179(1):9–16, January 2003.

[183] Nianyu Li, Kathy Ragheb, Gretchen Lawler, Jennie Sturgis, Bartek Rajwa, J. Andres Melendez, and J. Paul Robinson. Mitochondrial complex I inhibitor rotenone induces apoptosis through enhancing mitochondrial reactive oxygen species production. *The Journal of Biological Chemistry*, 278(10):8516–8525, March 2003.

[184] Claire Henchcliffe and M. Flint Beal. Mitochondrial biology and oxidative stress in Parkinson disease pathogenesis. *Nature Clinical Practice. Neurology*, 4(11):600–609, November 2008.

[185] Amber D. Van Laar, Katherine R. Webb, Matthew T. Keeney, Victor S. Van Laar, Alevtina Zharikov, Edward A. Burton, Teresa G. Hastings, Kelly E. Glajch, Warren D. Hirst, J. Timothy Greenamyre, and Emily M. Rocha. Transient exposure to rotenone causes degeneration and progressive parkinsonian motor deficits, neuroinflammation, and synucleinopathy. *npj Parkinson's Disease*, 9(1):1–9, August 2023. Publisher: Nature Publishing Group.

[186] Alison L. McCormack, Jennifer G. Atienza, Louisa C. Johnston, Julie K. Andersen, Susan Vu, and Donato A. Di Monte. Role of oxidative stress in paraquat-induced dopaminergic cell degeneration. *Journal of Neurochemistry*, 93(4):1030–1037, May 2005.

[187] J. M. Gorell, C. C. Johnson, B. A. Rybicki, E. L. Peterson, and R. J. Richardson. The risk of Parkinson's disease with exposure to pesticides, farming, well water, and rural living. *Neurology*, 50(5):1346–1350, May 1998.

[188] F. Kamel, Cm Tanner, Dm Umbach, Ja Hoppin, McR Alavanja, A. Blair, K. Comyns, Sm Goldman, M. Korell, Jw Langston, Gw Ross, and Dp Sandler. Pesticide exposure and self-reported Parkinson's disease in the agricultural health study. *American Journal of Epidemiology*, 165(4):364–374, February 2007.

[189] Camille Pouchieu, Clément Piel, Camille Carles, Anne Gruber, Catherine Helmer, Séverine Tual, Elisabeth Marcotullio, Pierre Lebailly, and Isabelle Baldi. Pesticide use in agriculture and Parkinson's disease in the AGRICAN cohort study. *International Journal of Epidemiology*, 47(1):299–310, February 2018.

[190] Kenneth N. Rose, Michael A. Schwarzschild, and Stephen N. Gomperts. Clearing the Smoke: What Protects Smokers from Parkinson's Disease? *Movement Disorders*, 39(2):267–272, 2024. _eprint: https://onlinelibrary.wiley.com/doi/pdf/10.1002/mds.29707.

[191] Benjamin Mappin-Kasirer, Hongchao Pan, Sarah Lewington, Jennifer Kizza, Richard Gray, Robert Clarke, and Richard Peto. Tobacco smoking and the risk of Parkinson disease. *Neurology*, 94(20):e2132–e2138, May 2020. Publisher: Wolters Kluwer.

[192] Manivannan Subramaniyan and John A. Dani. Dopaminergic and cholinergic learning mechanisms in nicotine addiction. *Annals of the New York Academy of Sciences*, 1349(1):46–63, September 2015.

[193] Chao Wang, Cheng Zhou, Tao Guo, Peiyu Huang, Xiaojun Xu, and Minming Zhang. Association between cigarette smoking and Parkinson's disease: a neuroimaging study. *Therapeutic Advances in Neurological Disorders*, 15:17562864221092566, January 2022. Publisher: SAGE Publications Ltd STM.

[194] Maryka Quik, Kathryn O'Leary, and Caroline M. Tanner. Nicotine and Parkinson's disease; implications for therapy. *Movement disorders : official journal of the Movement Disorder Society*, 23(12):1641–1652, September 2008.

[195] Nikodem Grzesiak. The causal direction in the association between Parkinson's disease and cigarette or nicotine use, July 2017.

[196] G. Webster Ross, Robert D. Abbott, Helen Petrovitch, David M. Morens, Andrew Grandinetti, Ko-Hui Tung, Caroline M. Tanner, Kamal H. Masaki, Patricia L. Blanchette, J. David Curb, Jordan S. Popper, and Lon R. White. Association of Coffee and Caffeine Intake With the Risk of Parkinson Disease. *JAMA*, 283(20):2674–2679, May 2000.

[197] K. Sääksjärvi, P. Knekt, H. Rissanen, M. A. Laaksonen, A. Reunanen, and S. Männistö. Prospective study of coffee consumption and risk of Parkinson's disease. *European Journal of Clinical Nutrition*, 62(7):908–915, July 2008. Publisher: Nature Publishing Group.

[198] Run Yan, Jie Zhang, Hye-Jin Park, Eun S. Park, Stephanie Oh, Haiyan Zheng, Eunsung Junn, Michael Voronkov, Jeffry B. Stock, and M. Maral Mouradian. Synergistic neuroprotection by coffee components eicosanoyl-5-hydroxytryptamide and caffeine in models of Parkinson's disease and DLB. *Proceedings of the National Academy of Sciences of the United States of America*, 115(51):E12053–E12062, December 2018.

[199] Cannon Jr and Greenamyre Jt. Gene-environment interactions in Parkinson's disease: specific evidence in humans and mammalian models. *Neurobiology of disease*, 57, September 2013. Publisher: Neurobiol Dis.

[200] Nicole Ball, Wei-Peng Teo, Shaneel Chandra, and James Chapman. Parkinson's Disease and the Environment. *Frontiers in Neurology*, 10, March 2019. Publisher: Frontiers.

[201] Gaia Skibinski and Steven Finkbeiner. Drug discovery in Parkinson's disease—Update and developments in the use of cellular models. *International journal of high throughput screening*, 2011(2):15–25, June 2011.

[202] Andreas Hartmann. Postmortem studies in Parkinson's disease. *Dialogues in Clinical Neuroscience*, 6(3):281–293, September 2004.

[203] Richard Nathaniel Rees, Alastair John Noyce, and Anette Schrag. The prodromes of Parkinson's disease. *The European Journal of Neuroscience*, 49(3):320–327, February 2019.

[204] Thilaga Thirugnanam and Kirankumar Santhakumar. Chemically induced models of Parkinson's disease. *Comparative Biochemistry and Physiology Part C: Toxicology & Pharmacology*, 252:109213, February 2022.

[205] S. Przedborski, M. Levivier, H. Jiang, M. Ferreira, V. Jackson-Lewis, D. Donaldson, and D. M. Togasaki. Dose-dependent lesions of the dopaminergic nigrostriatal pathway induced by intrastriatal injection of 6-hydroxydopamine. *Neuroscience*, 67(3):631–647, August 1995.

[206] Gloria E. Meredith and David J. Rademacher. MPTP Mouse Models of Parkinson's Disease: An Update. *Journal of Parkinson's disease*, 1(1):19–33, January 2011.

[207] E. Maruthi Prasad and Shih-Ya Hung. Behavioral Tests in Neurotoxin-Induced Animal Models of Parkinson's Disease. *Antioxidants*, 9(10):1007, October 2020.

[208] Shyh Jenn Chia, Eng-King Tan, and Yin-Xia Chao. Historical Perspective: Models of Parkinson's Disease. *International Journal of Molecular Sciences*, 21(7):2464, April 2020.

[209] Mohamed El-Gamal, Mohamed Salama, Lyndsey E. Collins-Praino, Irina Baetu, Ahmed M. Fathalla, Amira M. Soliman, Wael Mohamed, and Ahmed A. Moustafa. Neurotoxin-Induced Rodent Models of Parkinson's Disease: Benefits and Drawbacks. *Neurotoxicity Research*, 39(3):897–923, June 2021.

[210] Lysia S. Forno, J. William Langston, Louis E. DeLanney, Ian Irwin, and George A. Ricaurte. Locus ceruleus lesions and eosinophilic inclusions in MPTP-treated monkeys. *Annals of Neurology*, 20(4):449–455, 1986. _eprint: https://onlinelibrary.wiley.com/doi/pdf/10.1002/ana.410200403.

[211] Mika Shimoji, Li Zhang, Allen S. Mandir, Valina L. Dawson, and Ted M. Dawson. Absence of inclusion body formation in the MPTP mouse model of Parkinson's disease. *Molecular Brain Research*, 134(1):103–108, March 2005.

[212] D. Hernandez-Baltazar, L. M. Zavala-Flores, and A. Villanueva-Olivo. The 6-hydroxydopamine model and parkinsonian pathophysiology: Novel findings in an older model. *Neurología (English Edition)*, 32(8):533–539, October 2017. Publisher: Elsevier.

[213] Débora Masini, Carina Plewnia, Maëlle Bertho, Nicolas Scalbert, Vittorio Caggiano, and Gilberto Fisone. A Guide to the Generation of a 6-Hydroxydopamine Mouse Model of Parkinson's Disease for the Study of Non-Motor Symptoms. *Biomedicines*, 9(6):598, May 2021.

[214] Kim Tieu. A Guide to Neurotoxic Animal Models of Parkinson's Disease. *Cold Spring Harbor Perspectives in Medicine:*, 1(1):a009316, September 2011.

[215] Donna M Crabtree and Jianhua Zhang. Genetically engineered mouse models of Parkinson's disease. *Brain Research Bulletin*, 88(1):13–32, May 2012.

[216] Ted M. Dawson, Han Seok Ko, and Valina L. Dawson. Genetic animal models of Parkinson's disease. *Neuron*, 66(5):646–661, June 2010.

[217] Michael J. Beckstead and Rebecca D. Howell. Progressive parkinsonism due to mitochondrial impairment: Lessons from the MitoPark mouse model. *Experimental Neurology*, 341:113707, July 2021.

[218] Javier Blesa and Serge Przedborski. Parkinson's disease: animal models and dopaminergic cell vulnerability. *Frontiers in Neuroanatomy*, 8:155, 2014.

[219] Mats I. Ekstrand, Mügen Terzioglu, Dagmar Galter, Shunwei Zhu, Christoph Hofstetter, Eva Lindqvist, Sebastian Thams, Anita Bergstrand, Fredrik Sterky Hansson, Aleksandra Trifunovic, Barry Hoffer, Staffan Cullheim, Abdul H. Mohammed, Lars Olson, and Nils-Göran Larsson. Progressive parkinsonism in mice with respiratory-chain-deficient dopamine neurons. *Proceedings of the National Academy of Sciences of the United States of America*, 104(4):1325–1330, January 2007.

[220] Sui He, Qin Ru, Lin Chen, Guodong Xu, and Yuxiang Wu. Advances in animal models of Parkinson's disease. *Brain Research Bulletin*, 215:111024, September 2024.

[221] Kazutoshi Takahashi, Koji Tanabe, Mari Ohnuki, Megumi Narita, Tomoko Ichisaka, Kiichiro Tomoda, and Shinya Yamanaka. Induction of pluripotent stem cells from adult human fibroblasts by defined factors. *Cell*, 131(5):861–872, November 2007.

[222] Jonas Cerneckis, Hongxia Cai, and Yanhong Shi. Induced pluripotent stem cells (iPSCs): molecular mechanisms of induction and applications. *Signal Transduction and Targeted Therapy*, 9(1):1–26, April 2024. Publisher: Nature Publishing Group.

[223] Ninuo Xia, Pengbo Zhang, Fang Fang, Zhengyuan Wang, Megan Rothstein, Benjamin Angulo, Rosaria Chiang, James Taylor, and Renee A. Reijo Pera. Transcriptional comparison of human induced and primary midbrain dopaminergic neurons. *Scientific Reports*, 6(1):20270, February 2016. Publisher: Nature Publishing Group.

[224] Jara M. Baena-Montes, Sahar Avazzadeh, and Leo R. Quinlan. α-synuclein pathogenesis in hiPSC models of Parkinson's disease. *Neuronal Signaling*, 5(2):NS20210021, June 2021.

[225] Liancai Mu, Stanislaw Sobotka, Jingming Chen, Hungxi Su, Ira Sanders, Charles H. Adler, Holly A. Shill, John N. Caviness, Johan E. Samanta, and Thomas G. Beach. α-Synuclein Pathology and Axonal Degeneration of the Peripheral Motor Nerves Innervating Pharyngeal Muscles in Parkinson's Disease. *Journal of neuropathology and experimental neurology*, 72(2):119–129, February 2013.

[226] Yunying Yang and Zhentao Zhang. α-Synuclein pathology from the body to the brain: so many seeds so close to the central soil. *Neural Regeneration Research*, 19(7):1463–1472, November 2023.

[227] Virginia Gao, Juan A. Briano, Lauren E. Komer, and Jacqueline Burré. Functional and Pathological Effects of α-Synuclein on Synaptic SNARE Complexes. *Journal of molecular biology*, 435(1):167714, January 2023.

[228] Richard M. Meade, David P. Fairlie, and Jody M. Mason. Alpha-synuclein structure and Parkinson's disease – lessons and emerging principles. *Molecular Neurodegeneration*, 14(1):29, July 2019.

[229] Tim Bartels, Joanna G. Choi, and Dennis J. Selkoe. α-Synuclein occurs physiologically as a helically folded tetramer that resists aggregation. *Nature*, 477(7362):107–110, September 2011. Publisher: Nature Publishing Group.

[230] Heather R. Lucas and Ricardo D. Fernández. Navigating the dynamic landscape of alpha-synuclein morphology: a review of the physiologically relevant tetrameric conformation. *Neural Regeneration Research*, 15(3):407, September 2019.

[231] Katherina Vamvaca, Michael J. Volles, and Peter T. Lansbury. The First N-terminal Amino Acids of α-Synuclein Are Essential for α-Helical Structure Formation In Vitro and Membrane Binding in Yeast. *Journal of molecular biology*, 389(2):413–424, June 2009.

[232] Leonid Breydo, Jessica W. Wu, and Vladimir N. Uversky. A-synuclein misfolding and Parkinson's disease. *Biochimica Et Biophysica Acta*, 1822(2):261–285, February 2012.

[233] Matteo Runfola, Alfonso De Simone, Michele Vendruscolo, Christopher M. Dobson, and Giuliana Fusco. The N-terminal Acetylation of α-Synuclein Changes the Affinity for Lipid Membranes but not the Structural Properties of the Bound State. *Scientific Reports*, 10(1):204, January 2020. Publisher: Nature Publishing Group.

[234] Marco Bisaglia, Alessandra Trolio, Massimo Bellanda, Elisabetta Bergantino, Luigi Bubacco, and Stefano Mammi. Structure and topology of the non-amyloid-β component fragment of human α-synuclein bound to micelles: Implications for the aggregation process. *Protein Science : A Publication of the Protein Society*, 15(6):1408–1416, June 2006.

[235] Tulika Srivastava, Ritu Raj, Amit Dubey, Dinesh Kumar, Rajnish K. Chaturvedi, Sandeep K. Sharma, and Smriti Priya. Fast kinetics of environmentally induced α-synuclein aggregation mediated by structural alteration in NAC region and result in structure dependent cytotoxicity. *Scientific Reports*, 10(1):18412, October 2020. Publisher: Nature Publishing Group.

[236] Edward Pajarillo, Asha Rizor, Jayden Lee, Michael Aschner, and Eunsook Lee. The role of posttranslational modifications of α-synuclein and LRRK2 in Parkinson's disease: Potential contributions of environmental factors. *Biochimica et Biophysica Acta (BBA) - Molecular Basis of Disease*, 1865(8):1992–2000, August 2019.

[237] M. S. Nielsen, H. Vorum, E. Lindersson, and P. H. Jensen. Ca2+ binding to alpha-synuclein regulates ligand binding and oligomerization. *The Journal of Biological Chemistry*, 276(25):22680–22684, June 2001.

[238] Mirva Hejjaoui, Sara Butterfield, Bruno Fauvet, Filip Vercruysse, Jia Cui, Igor Dikiy, Michel Prudent, Diana Olschewski, Yan Zhang, David Eliezer, and Hilal A. Lashuel. Elucidating the role of C-terminal post-translational modifications using protein semisynthesis strategies: α-synuclein phosphorylation at tyrosine 125. *Journal of the American Chemical Society*, 134(11):5196–5210, March 2012.

[239] Nelson de Oliveira Manzanza, Lucia Sedlackova, and Raj N. Kalaria. Alpha-Synuclein Post-translational Modifications: Implications for Pathogenesis of Lewy Body Disorders. *Frontiers in Aging Neuroscience*, 13:690293, June 2021.

[240] Jacob Bendor, Todd Logan, and Robert H. Edwards. The Function of α-Synuclein. *Neuron*, 79(6):10.1016/j.neuron.2013.09.004, September 2013.

[241] Furong Cheng, Giorgio Vivacqua, and Shun Yu. The role of α-synuclein in neurotransmission and synaptic plasticity. *Journal of Chemical Neuroanatomy*, 42(4):242–248, December 2011.

[242] Robert E. Burke and Karen O'Malley. Axon Degeneration in Parkinson's Disease. *Experimental neurology*, 246:72–83, August 2013.

[243] Janin Lautenschläger, Clemens F. Kaminski, and Gabriele S. Kaminski Schierle. α-Synuclein – Regulator of Exocytosis, Endocytosis, or Both? *Trends in Cell Biology*, 27(7):468–479, July 2017. Publisher: Elsevier.

[244] Jacqueline Burré. The Synaptic Function of α-Synuclein. *Journal of Parkinson's Disease*, 5(4):699–713, 2015.

[245] Neeliyath A. Ramakrishnan, Marian J. Drescher, and Dennis G. Drescher. The SNARE complex in neuronal and sensory cells. *Molecular and cellular neurosciences*, 50(1):58–69, May 2012.

[246] Diane D. Murphy, Susan M. Rueter, John Q. Trojanowski, and Virginia M.-Y. Lee. Synucleins Are Developmentally Expressed, and α-Synuclein Regulates the Size of the Presynaptic Vesicular Pool in Primary Hippocampal Neurons. *Journal of Neuroscience*, 20(9):3214–3220, May 2000. Publisher: Society for Neuroscience Section: ARTICLE.

[247] Kristin E. Larsen, Yvonne Schmitz, Matthew D. Troyer, Eugene Mosharov, Paula Dietrich, Abrar Z. Quazi, Magali Savalle, Venu Nemani, Farrukh A. Chaudhry, Robert H. Edwards, Leonidas Stefanis, and David Sulzer. Alpha-synuclein overexpression in PC12 and chromaffin cells impairs catecholamine release by interfering with a late step in exocytosis. *The Journal of Neuroscience: The Official Journal of the Society for Neuroscience*, 26(46):11915–11922, November 2006.

[248] Ruth G. Perez, Jack C. Waymire, Eva Lin, Jen J. Liu, Fengli Guo, and Michael J. Zigmond. A Role for α-Synuclein in the Regulation of Dopamine Biosynthesis. *Journal of Neuroscience*, 22(8):3090–3099, April 2002. Publisher: Society for Neuroscience Section: ARTICLE.

[249] Melisa J. Baptista, Casey O'Farrell, Sneha Daya, Rili Ahmad, David W. Miller, John Hardy, Matthew J. Farrer, and Mark R. Cookson. Co-ordinate transcriptional regulation of dopamine synthesis genes by α-synuclein in human neuroblastoma cell lines. *Journal of Neurochemistry*, 85(4):957–968, 2003. _eprint: https://onlinelibrary.wiley.com/doi/pdf/10.1046/j.1471-4159.2003.01742.x.

[250] Nan Gao, Yao-Hua Li, Xin Li, Shun Yu, Gui-Lian Fu, and Biao Chen. Effect of α-synuclein on the promoter activity of tyrosine hydroxylase gene. *Neuroscience Bulletin*, 23(1):53–57, December 2007.

[251] Christophe Wersinger and Anita Sidhu. Attenuation of dopamine transporter activity by alpha-synuclein. *Neuroscience Letters*, 340(3):189–192, April 2003.

[252] Semanti Mukherjee, Arunima Sakunthala, Laxmikant Gadhe, Manisha Poudyal, Ajay Singh Sawner, Pradeep Kadu, and Samir K. Maji. Liquid-liquid Phase Separation of α-Synuclein: A New Mechanistic Insight for α-Synuclein Aggregation Associated with Parkinson's Disease Pathogenesis. *Journal of Molecular Biology*, 435(1):167713, January 2023.

[253] Xi Li, Chunhua Dong, Marion Hoffmann, Craig R. Garen, Leonardo M. Cortez, Nils O. Petersen, and Michael T. Woodside. Early stages of aggregation of engineered α-synuclein monomers and oligomers in solution. *Scientific Reports*, 9:1734, February 2019.

[254] Asad Jan, Nádia Pereira Gonçalves, Christian Bjerggaard Vaegter, Poul Henning Jensen, and Nelson Ferreira. The Prion-Like Spreading of Alpha-Synuclein in Parkinson's Disease: Update on Models and Hypotheses. *International Journal of Molecular Sciences*, 22(15):8338, August 2021.

[255] Beate Winner, Roberto Jappelli, Samir K. Maji, Paula A. Desplats, Leah Boyer, Stefan Aigner, Claudia Hetzer, Thomas Loher, Marçal Vilar, Silvia Campioni, Christos Tzitzilonis, Alice Soragni, Sebastian Jessberger, Helena Mira, Antonella Consiglio, Emiley Pham, Eliezer Masliah, Fred H. Gage, and Roland Riek. In vivo demonstration that α-synuclein oligomers are toxic. *Proceedings of the National Academy of Sciences*, 108(10):4194–4199, March 2011. Publisher: Proceedings of the National Academy of Sciences.

[256] Samuel Peña-Díaz, Javier García-Pardo, and Salvador Ventura. Development of Small Molecules Targeting α-Synuclein Aggregation: A Promising Strategy to Treat Parkinson's Disease. *Pharmaceutics*, 15(3):839, March 2023.

[257] Kreesan Reddy and Birger Victor Dieriks. Multiple system atrophy: α-Synuclein strains at the neuron-oligodendrocyte crossroad. *Molecular Neurodegeneration*, 17(1):77, November 2022.

[258] Animesh Mondal, Sandip Dolui, Sukhamoy Dhabal, Ashish Bhattacharjee, and Nakul C. Maiti. Structure Specific Neuro-toxicity of α-Synuclein Oligomer, October 2020. Pages: 2020.10.11.334979 Section: New Results.

[259] Alexander K. Buell, Céline Galvagnion, Ricardo Gaspar, Emma Sparr, Michele Vendruscolo, Tuomas P. J. Knowles, Sara Linse, and Christopher M. Dobson. Solution conditions determine the relative importance of nucleation and growth processes in α-synuclein aggregation. *Proceedings of the National Academy of Sciences of the United States of America*, 111(21):7671–7676, May 2014.

[260] Anahita Khammari, Seyed Shahriar Arab, and Mohammad Reza Ejtehadi. The hot sites of α-synuclein in amyloid fibril formation. *Scientific Reports*, 10(1):12175, July 2020. Publisher: Nature Publishing Group.

[261] Surabhi Mehra, Sahil Ahlawat, Harish Kumar, Debalina Datta, Ambuja Navalkar, Nitu Singh, Komal Patel, Laxmikant Gadhe, Pradeep Kadu, Rakesh Kumar, Narendra N. Jha, Arunima Sakunthala, Ajay S. Sawner, Ranjith Padinhateeri, Jayant B. Udgaonkar, Vipin Agarwal, and Samir K. Maji. α-Synuclein Aggregation Intermediates form Fibril Polymorphs with Distinct Prion-like Properties. *Journal of Molecular Biology*, 434(19):167761, October 2022.

[262] Kelvin C. Luk, Cheng Song, Patrick O'Brien, Anna Stieber, Jonathan R. Branch, Kurt R. Brunden, John Q. Trojanowski, and Virginia M.-Y. Lee. Exogenous α-synuclein fibrils seed the formation of Lewy body-like intracellular inclusions in cultured cells. *Proceedings of the National Academy of Sciences*, 106(47):20051–20056, November 2009. Publisher: Proceedings of the National Academy of Sciences.

[263] Alma Karen Lomeli-Lepe, Jose Luis Castañeda-Cabral, and Silvia Josefina López-Pérez. Synucleinopathies: Intrinsic and Extrinsic Factors. *Cell Biochemistry and Biophysics*, 81(3):427–442, September 2023.

[264] Mohamed-Bilal Fares, Nadine Ait-Bouziad, Igor Dikiy, Martial K. Mbefo, Ana Jovičić, Aoife Kiely, Janice L. Holton, Seung-Jae Lee, Aaron D. Gitler, David Eliezer, and Hilal A. Lashuel. The novel Parkinson's disease linked mutation G51D attenuates in vitro aggregation and membrane binding of α-synuclein, and enhances its secretion and nuclear localization in cells. *Human Molecular Genetics*, 23(17):4491–4509, September 2014.

[265] R. KRUGER. Ala 30 Pro mutation in the gene encoding α synuclein in Parkinson disease. *Nat. Genet.*, 18:106–108, 1998.

[266] Dhiman Ghosh, Shruti Sahay, Priyatosh Ranjan, Shimul Salot, Ganesh M. Mohite, Pradeep K. Singh, Saumya Dwivedi, Edmund Carvalho, Rinti Banerjee, Ashutosh Kumar, and Samir K. Maji. The Newly Discovered Parkinson's Disease Associated Finnish Mutation (A53E) Attenuates α-Synuclein Aggregation and Membrane Binding. *Biochemistry*, 53(41):6419–6421, October 2014. Publisher: American Chemical Society.

[267] Nicola J. Rutherford, Brenda D. Moore, Todd E. Golde, and Benoit I. Giasson. Divergent effects of the H50Q and G51D SNCA mutations on the aggregation of α-synuclein. *Journal of Neurochemistry*, 131(6):859–867, 2014. _eprint: https://onlinelibrary.wiley.com/doi/pdf/10.1111/jnc.12806.

[268] Eric A. Greenbaum, Charles L. Graves, Amanda J. Mishizen-Eberz, Michael A. Lupoli, David R. Lynch, S. Walter Englander, Paul H. Axelsen, and Benoit I. Giasson. The E46K Mutation in α-Synuclein Increases Amyloid Fibril Formation *. *Journal of Biological Chemistry*, 280(9):7800–7807, March 2005. Publisher: Elsevier.

[269] L. C. Serpell, J. Berriman, R. Jakes, M. Goedert, and R. A. Crowther. Fiber diffraction of synthetic alpha-synuclein filaments shows amyloid-like

cross-beta conformation. *Proceedings of the National Academy of Sciences of the United States of America*, 97(9):4897–4902, April 2000.

[270] Allen P. Minton. Influence of macromolecular crowding upon the stability and state of association of proteins: Predictions and observations. *Journal of Pharmaceutical Sciences*, 94(8):1668–1675, August 2005.

[271] Istvan Horvath, Ranjeet Kumar, and Pernilla Wittung-Stafshede. Macromolecular crowding modulates α-synuclein amyloid fiber growth. *Biophysical Journal*, 120(16):3374–3381, August 2021.

[272] Thibault Viennet, Michael M. Wördehoff, Boran Uluca, Chetan Poojari, Hamed Shaykhalishahi, Dieter Willbold, Birgit Strodel, Henrike Heise, Alexander K. Buell, Wolfgang Hoyer, and Manuel Etzkorn. Structural insights from lipid-bilayer nanodiscs link α-Synuclein membrane-binding modes to amyloid fibril formation. *Communications Biology*, 1(1):1–12, May 2018. Publisher: Nature Publishing Group.

[273] Min Zhu, Jie Li, and Anthony L. Fink. The Association of α-Synuclein with Membranes Affects Bilayer Structure, Stability, and Fibril Formation*. *Journal of Biological Chemistry*, 278(41):40186–40197, October 2003.

[274] Euijung Jo, Nola Fuller, R. Peter Rand, Peter St George-Hyslop, and Paul E. Fraser. Defective membrane interactions of familial Parkinson's disease mutant A30P alpha-synuclein. *Journal of Molecular Biology*, 315(4):799–807, January 2002.

[275] Woong Choi, Shahin Zibaee, Ross Jakes, Louise C. Serpell, Bazbek Davletov, R. Anthony Crowther, and Michel Goedert. Mutation E46K increases phospholipid binding and assembly into filaments of human α-synuclein. *FEBS Letters*, 576(3):363–368, October 2004.

[276] Zaina Khan and Yoo Jin Jung. The effects of post-translational modifications on alpha-synuclein aggregation and immune cell activation in Parkinson's disease. *Exploration of Neuroprotective Therapy*, 3(5):281–298, October 2023. Number: 5 Publisher: Open Exploration.

[277] Katrin Beyer. Alpha-synuclein structure, posttranslational modification and alternative splicing as aggregation enhancers. *Acta Neuropathologica*, 112(3):237–251, September 2006.

[278] Hideo Fujiwara, Masato Hasegawa, Naoshi Dohmae, Akiko Kawashima, Eliezer Masliah, Matthew S. Goldberg, Jie Shen, Koji Takio, and Takeshi Iwatsubo. alpha-Synuclein is phosphorylated in synucleinopathy lesions. *Nature Cell Biology*, 4(2):160–164, February 2002.

[279] John P. Anderson, Donald E. Walker, Jason M. Goldstein, Rian de Laat, Kelly Banducci, Russell J. Caccavello, Robin Barbour, Jiping Huang, Kristin Kling, Michael Lee, Linnea Diep, Pamela S. Keim, Xiaofeng Shen,

Tim Chataway, Michael G. Schlossmacher, Peter Seubert, Dale Schenk, Sukanto Sinha, Wei Ping Gai, and Tamie J. Chilcote. Phosphorylation of Ser-129 Is the Dominant Pathological Modification of α-Synuclein in Familial and Sporadic Lewy Body Disease *. *Journal of Biological Chemistry*, 281(40):29739–29752, October 2006. Publisher: Elsevier.

[280] Shigeki Arawaka, Hiroyasu Sato, Asuka Sasaki, Shingo Koyama, and Takeo Kato. Mechanisms underlying extensive Ser129-phosphorylation in α-synuclein aggregates. *Acta Neuropathologica Communications*, 5(1):48, June 2017.

[281] Anna Villar-Piqué, Tomás Lopes da Fonseca, and Tiago Fleming Outeiro. Structure, function and toxicity of alpha-synuclein: the Bermuda triangle in synucleinopathies. *Journal of Neurochemistry*, 139(S1):240–255, 2016. _eprint: https://onlinelibrary.wiley.com/doi/pdf/10.1111/jnc.13249.

[282] Neeleema Seetaloo, Maria Zacharopoulou, Amberley D. Stephens, Gabriele S. Kaminski Schierle, and Jonathan J. Phillips. Millisecond Hydrogen/Deuterium-Exchange Mass Spectrometry Approach to Correlate Local Structure and Aggregation in α-Synuclein. *Analytical Chemistry*, 94(48):16711–16719, December 2022.

[283] Amberley D. Stephens, Maria Zacharopoulou, Rani Moons, Giuliana Fusco, Neeleema Seetaloo, Anass Chiki, Philippa J. Woodhams, Ioanna Mela, Hilal A. Lashuel, Jonathan J. Phillips, Alfonso De Simone, Frank Sobott, and Gabriele S. Kaminski Schierle. Extent of N-terminus exposure of monomeric alpha-synuclein determines its aggregation propensity. *Nature Communications*, 11(1):2820, June 2020. Publisher: Nature Publishing Group.

[284] Andrei Surguchov and Alexei Surguchev. Synucleins: New Data on Misfolding, Aggregation and Role in Diseases. *Biomedicines*, 10(12):3241, December 2022.

[285] Cai Zhang, Yunshan Pei, Zeting Zhang, Lingling Xu, Xiaoli Liu, Ling Jiang, Gary J. Pielak, Xin Zhou, Maili Liu, and Conggang Li. C-terminal truncation modulates α-Synuclein's cytotoxicity and aggregation by promoting the interactions with membrane and chaperone. *Communications Biology*, 5(1):798, August 2022.

[286] L. S. Forno. Concentric Hyalin Intraneuronal Inclusions of Lewy Type in the Brains of Elderly Persons (50 Incidental Cases): Relationship to Parkinsonism. *Journal of the American Geriatrics Society*, 17(6):557–575, 1969. _eprint: https://onlinelibrary.wiley.com/doi/pdf/10.1111/j.1532-5415.1969.tb01316.x.

[287] Yuko Saito, Nyoka N. Ruberu, Motoji Sawabe, Tomio Arai, Hirohito Kazama, Takayuki Hosoi, Hiroshi Yamanouchi, and Shigeo Murayama. Lewy body-related alpha-synucleinopathy in aging. *Journal of Neuropathology and Experimental Neurology*, 63(7):742–749, July 2004.

[288] Mark R Cookson, John Hardy, and Patrick A Lewis. Genetic Neuropathology of Parkinson's Disease. *International Journal of Clinical and Experimental Pathology*, 1(3):217–231, January 2008.

[289] Nora Bengoa-Vergniory, Rosalind F. Roberts, Richard Wade-Martins, and Javier Alegre-Abarrategui. Alpha-synuclein oligomers: a new hope. *Acta Neuropathologica*, 134(6):819–838, December 2017.

[290] C. Colosimo, A. J. Hughes, L. Kilford, and A. J. Lees. Lewy body cortical involvement may not always predict dementia in Parkinson's disease. *Journal of Neurology, Neurosurgery, and Psychiatry*, 74(7):852–856, July 2003.

[291] Roberta Cascella, Alessandra Bigi, Nunilo Cremades, and Cristina Cecchi. Effects of oligomer toxicity, fibril toxicity and fibril spreading in synucleinopathies. *Cellular and Molecular Life Sciences: CMLS*, 79(3):174, March 2022.

[292] Samir Negi, Navneet Khurana, and Navneet Duggal. The misfolding mystery: α-synuclein and the pathogenesis of Parkinson's disease. *Neurochemistry International*, 177:105760, July 2024.

[293] Xiao-yu Du, Xi-xiu Xie, and Rui-tian Liu. The Role of α-Synuclein Oligomers in Parkinson's Disease. *International Journal of Molecular Sciences*, 21(22):8645, November 2020.

[294] Karin M. Danzer, Dorothea Haasen, Anne R. Karow, Simon Moussaud, Matthias Habeck, Armin Giese, Hans Kretzschmar, Bastian Hengerer, and Marcus Kostka. Different Species of α-Synuclein Oligomers Induce Calcium Influx and Seeding. *Journal of Neuroscience*, 27(34):9220–9232, August 2007. Publisher: Society for Neuroscience Section: Articles.

[295] Thomas Näsström, Therese Fagerqvist, Mikael Barbu, Mikael Karlsson, Fredrik Nikolajeff, Alex Kasrayan, Monica Ekberg, Lars Lannfelt, Martin Ingelsson, and Joakim Bergström. The lipid peroxidation products 4-oxo-2-nonenal and 4-hydroxy-2-nonenal promote the formation of α-synuclein oligomers with distinct biochemical, morphological, and functional properties. *Free Radical Biology and Medicine*, 50(3):428–437, February 2011.

[296] Leo Chen, Jinghua Jin, Jeanne Davis, Yong Zhou, Yan Wang, Jun Liu, Paul J. Lockhart, and Jing Zhang. Oligomeric alpha-synuclein inhibits tubulin polymerization. *Biochemical and Biophysical Research Communications*, 356(3):548–553, May 2007.

[297] Damla Pinar Karpinar, Madhu Babu Gajula Balija, Sebastian Kügler, Felipe Opazo, Nasrollah Rezaei-Ghaleh, Nora Wender, Hai-Young Kim, Grit Taschenberger, Björn H Falkenburger, Henrike Heise, Ashutosh Kumar, Dietmar Riedel, Lars Fichtner, Aaron Voigt, Gerhard H Braus,

Karin Giller, Stefan Becker, Alf Herzig, Marc Baldus, Herbert Jäckle, Stefan Eimer, Jörg B Schulz, Christian Griesinger, and Markus Zweckstetter. Pre-fibrillar α-synuclein variants with impaired β-structure increase neurotoxicity in Parkinson's disease models. *The EMBO Journal*, 28(20):3256–3268, October 2009. Num Pages: 3268 Publisher: John Wiley & Sons, Ltd.

[298] T. Tokuda, M.M. Qureshi, M.T. Ardah, S. Varghese, S.A.S. Shehab, T. Kasai, N. Ishigami, A. Tamaoka, M. Nakagawa, and O.M.A. El-Agnaf. Detection of elevated levels of α-synuclein oligomers in CSF from patients with Parkinson disease. *Neurology*, 75(20):1766–1770, November 2010. Publisher: Wolters Kluwer.

[299] Meenakshi Verma, Abhishek Vats, and Vibha Taneja. Toxic species in amyloid disorders: Oligomers or mature fibrils. *Annals of Indian Academy of Neurology*, 18(2):138, June 2015.

[300] M. P. Lambert, A. K. Barlow, B. A. Chromy, C. Edwards, R. Freed, M. Liosatos, T. E. Morgan, I. Rozovsky, B. Trommer, K. L. Viola, P. Wals, C. Zhang, C. E. Finch, G. A. Krafft, and W. L. Klein. Diffusible, nonfibrillar ligands derived from Abeta1-42 are potent central nervous system neurotoxins. *Proceedings of the National Academy of Sciences of the United States of America*, 95(11):6448–6453, May 1998.

[301] Anant K. Paravastu, Richard D. Leapman, Wai-Ming Yau, and Robert Tycko. Molecular structural basis for polymorphism in Alzheimer's β-amyloid fibrils. *Proceedings of the National Academy of Sciences*, 105(47):18349–18354, November 2008. Publisher: Proceedings of the National Academy of Sciences.

[302] Kapur B. Dhami, Sanjib Karki, Antanisha Parks, Cameron G. Nichols, and Michael R. Nichols. Development of β-sheet structure in Aβ aggregation intermediates diminishes exposed hydrophobic surface area and enhances proinflammatory activity. *Biochimica et Biophysica Acta (BBA) - Proteins and Proteomics*, 1870(9):140817, September 2022.

[303] Marija Vidović and Milena G. Rikalovic. Alpha-Synuclein Aggregation Pathway in Parkinson's Disease: Current Status and Novel Therapeutic Approaches. *Cells*, 11(11):1732, May 2022.

[304] Giuliana Fusco, Serene W. Chen, Philip T. F. Williamson, Roberta Cascella, Michele Perni, James A. Jarvis, Cristina Cecchi, Michele Vendruscolo, Fabrizio Chiti, Nunilo Cremades, Liming Ying, Christopher M. Dobson, and Alfonso De Simone. Structural basis of membrane disruption and cellular toxicity by α-synuclein oligomers. *Science (New York, N.Y.)*, 358(6369):1440–1443, December 2017.

[305] Wolfgang P. Ruf, Joao L. Meirelles, and Karin M. Danzer. Spreading of alpha-synuclein between different cell types. *Behavioural Brain Research*, 436:114059, January 2023.

[306] Jessica Y. Vargas, Clara Grudina, and Chiara Zurzolo. The prion-like spreading of α-synuclein: From *in vitro* to *in vivo* models of Parkinson's disease. *Ageing Research Reviews*, 50:89–101, March 2019.

[307] Norihito Uemura, Hisashi Yagi, Maiko T. Uemura, Hodaka Yamakado, and Ryosuke Takahashi. Limited spread of pathology within the brainstem of α-synuclein BAC transgenic mice inoculated with preformed fibrils into the gastrointestinal tract. *Neuroscience Letters*, 716:134651, January 2020.

[308] Xiaobo Mao, Michael Tianhao Ou, Senthilkumar S. Karuppagounder, Tae-In Kam, Xiling Yin, Yulan Xiong, Preston Ge, George Essien Umanah, Saurav Brahmachari, Joo-Ho Shin, Ho Chul Kang, Jianmin Zhang, Jinchong Xu, Rong Chen, Hyejin Park, Shaida A. Andrabi, Sung Ung Kang, Rafaella Araújo Gonçalves, Yu Liang, Shu Zhang, Chen Qi, Sharon Lam, James A. Keiler, Joel Tyson, Donghoon Kim, Nikhil Panicker, Seung Pil Yun, Creg J. Workman, Dario A. A. Vignali, Valina L. Dawson, Han Seok Ko, and Ted M. Dawson. Pathological α-synuclein transmission initiated by binding lymphocyte-activation gene 3. *Science (New York, N.Y.)*, 353(6307):aah3374, September 2016.

[309] Chao Peng, John Q. Trojanowski, and Virginia M.-Y. Lee. Protein transmission in neurodegenerative disease. *Nature Reviews. Neurology*, 16(4):199–212, April 2020.

[310] Mohamed Bilal Fares, Somanath Jagannath, and Hilal A. Lashuel. Publisher Correction: Reverse engineering Lewy bodies: how far have we come and how far can we go? *Nature Reviews Neuroscience*, 22(4):256–256, April 2021. Publisher: Nature Publishing Group.

[311] Jeffrey H. Kordower, Yaping Chu, Robert A. Hauser, Thomas B. Freeman, and C. Warren Olanow. Lewy body-like pathology in long-term embryonic nigral transplants in Parkinson's disease. *Nature Medicine*, 14(5):504–506, May 2008.

[312] Nelson Ferreira, Hjalte Gram, Zachary A. Sorrentino, Emil Gregersen, Sissel Ida Schmidt, Lasse Reimer, Cristine Betzer, Clara Perez-Gozalbo, Marjo Beltoja, Madhu Nagaraj, Jie Wang, Jan S. Nowak, Mingdong Dong, Katarina Willén, Ersoy Cholak, Kaare Bjerregaard-Andersen, Nicolas Mendez, Prakruti Rabadia, Mohammad Shahnawaz, Claudio Soto, Daniel E. Otzen, Ümit Akbey, Morten Meyer, Benoit I. Giasson, Marina Romero-Ramos, and Poul Henning Jensen. Multiple system atrophy-associated oligodendroglial protein p25α stimulates formation of novel α-synuclein strain with enhanced neurodegenerative potential. *Acta Neuropathologica*, 142(1):87–115, July 2021.

[313] Sara Elfarrash, Nanna Møller Jensen, Nelson Ferreira, Cristine Betzer, Jervis Vermal Thevathasan, Robin Diekmann, Mohamed Adel, Nisreen Mansour Omar, Mohamed Z. Boraie, Sabry Gad, Jonas Ries, Deniz

Kirik, Sadegh Nabavi, and Poul Henning Jensen. Organotypic slice culture model demonstrates inter-neuronal spreading of alpha-synuclein aggregates. *Acta Neuropathologica Communications*, 7(1):213, December 2019.

[314] Amanda N. Sacino, Mieu Brooks, Michael A. Thomas, Alex B. McKinney, Sooyeon Lee, Robert W. Regenhardt, Nicholas H. McGarvey, Jacob I. Ayers, Lucia Notterpek, David R. Borchelt, Todd E. Golde, and Benoit I. Giasson. Intramuscular injection of α-synuclein induces CNS α-synuclein pathology and a rapid-onset motor phenotype in transgenic mice. *Proceedings of the National Academy of Sciences*, 111(29):10732–10737, July 2014. Publisher: Proceedings of the National Academy of Sciences.

[315] Masoud Jelokhani-Niaraki. Membrane Proteins: Structure, Function and Motion. *International Journal of Molecular Sciences*, 24(1):468, December 2022.

[316] Caroline Barisch, Joost C. M. Holthuis, and Katia Cosentino. Membrane damage and repair: a thin line between life and death. *Biological Chemistry*, 404(5):467–490, April 2023.

[317] Igor F. Tsigelny, Yuriy Sharikov, Wolfgang Wrasidlo, Tania Gonzalez, Paula A. Desplats, Leslie Crews, Brian Spencer, and Eliezer Masliah. Role of α-synuclein penetration into the membrane in the mechanisms of oligomer pore formation. *The FEBS journal*, 279(6):1000–1013, March 2012.

[318] Katsutoshi Furukawa, Michiko Matsuzaki-Kobayashi, Takafumi Hasegawa, Akio Kikuchi, Naoto Sugeno, Yasuto Itoyama, Yue Wang, Pamela J. Yao, Ittai Bushlin, and Atsushi Takeda. Plasma membrane ion permeability induced by mutant alpha-synuclein contributes to the degeneration of neural cells. *Journal of Neurochemistry*, 97(4):1071–1077, May 2006.

[319] Himanshu Chaudhary, Aditya Iyer, Vinod Subramaniam, and Mireille M. A. E. Claessens. α-Synuclein Oligomers Stabilize Pre-Existing Defects in Supported Bilayers and Propagate Membrane Damage in a Fractal-Like Pattern. *Langmuir*, 32(45):11827–11836, November 2016. Publisher: American Chemical Society.

[320] A. H. V. Schapira. Mitochondrial dysfunction in Parkinson's disease. *Cell Death & Differentiation*, 14(7):1261–1266, July 2007. Publisher: Nature Publishing Group.

[321] Werner Poewe, Klaus Seppi, Caroline M. Tanner, Glenda M. Halliday, Patrik Brundin, Jens Volkmann, Anette-Eleonore Schrag, and Anthony E. Lang. Parkinson disease. *Nature Reviews Disease Primers*, 3(1):1–21, March 2017. Publisher: Nature Publishing Group.

[322] Latha Devi, Vijayendran Raghavendran, Badanavalu M. Prabhu, Narayan G. Avadhani, and Hindupur K. Anandatheerthavarada. Mitochondrial Import and Accumulation of α-Synuclein Impair Complex I in Human Dopaminergic Neuronal Cultures and Parkinson Disease Brain *. *Journal of Biological Chemistry*, 283(14):9089–9100, April 2008. Publisher: Elsevier.

[323] Shankar J. Chinta, Jyothi K. Mallajosyula, Anand Rane, and Julie K. Andersen. Mitochondrial α-synuclein accumulation impairs complex I function in dopaminergic neurons and results in increased mitophagy in vivo. *Neuroscience Letters*, 486(3):235–239, December 2010.

[324] Ken Nakamura. α-Synuclein and Mitochondria: Partners in Crime? *Neurotherapeutics*, 10(3):391–399, July 2013.

[325] Marthe H. R. Ludtmann, Plamena R. Angelova, Mathew H. Horrocks, Minee L. Choi, Margarida Rodrigues, Artyom Y. Baev, Alexey V. Berezhnov, Zhi Yao, Daniel Little, Blerida Banushi, Afnan Saleh Al-Menhali, Rohan T. Ranasinghe, Daniel R. Whiten, Ratsuda Yapom, Karamjit Singh Dolt, Michael J. Devine, Paul Gissen, Tilo Kunath, Morana Jaganjac, Evgeny V. Pavlov, David Klenerman, Andrey Y. Abramov, and Sonia Gandhi. α-synuclein oligomers interact with ATP synthase and open the permeability transition pore in Parkinson's disease. *Nature Communications*, 9(1):2293, June 2018.

[326] Briana R. De Miranda, Emily M. Rocha, Sandra L. Castro, and J. Timothy Greenamyre. Protection from α-Synuclein induced dopaminergic neurodegeneration by overexpression of the mitochondrial import receptor TOM20. *npj Parkinson's Disease*, 6(1):1–10, December 2020. Publisher: Nature Publishing Group.

[327] Naomi J. Thorne and David A. Tumbarello. The relationship of alpha-synuclein to mitochondrial dynamics and quality control. *Frontiers in Molecular Neuroscience*, 15:947191, August 2022.

[328] Roberto Di Maio, Paul J. Barrett, Eric K. Hoffman, Caitlyn W. Barrett, Alevtina Zharikov, Anupom Borah, Xiaoping Hu, Jennifer McCoy, Charleen T. Chu, Edward A. Burton, Teresa G. Hastings, and J. Timothy Greenamyre. α-Synuclein binds to TOM20 and inhibits mitochondrial protein import in Parkinson's disease. *Science Translational Medicine*, 8(342):342ra78, June 2016.

[329] Ya-Xing Gui, Xin-Yi Wang, Wen-Yan Kang, Ying-Jie Zhang, Yu Zhang, Yong Zhou, Thomas J. Quinn, Jun Liu, and Sheng-Di Chen. Extracellular signal-regulated kinase is involved in alpha-synuclein-induced mitochondrial dynamic disorders by regulating dynamin-like protein 1. *Neurobiology of Aging*, 33(12):2841–2854, December 2012.

[330] Richard J. Youle and Alexander M. van der Bliek. Mitochondrial fission, fusion, and stress. *Science (New York, N.Y.)*, 337(6098):1062–1065, August 2012.

[331] Thomas J. Krzystek, Rupkatha Banerjee, Layne Thurston, JianQiao Huang, Kelsey Swinter, Saad Navid Rahman, Tomas L. Falzone, and Shermali Gunawardena. Differential mitochondrial roles for α-synuclein in DRP1-dependent fission and PINK1/Parkin-mediated oxidation. *Cell Death & Disease*, 12(9):796, August 2021.

[332] Anna Wilkaniec, Anna M. Lenkiewicz, Grzegorz A. Czapski, Henryk M. Jęśko, Wojciech Hilgier, Robert Brodzik, Magdalena Gąssowska-Dobrowolska, Carsten Culmsee, and Agata Adamczyk. Extracellular Alpha-Synuclein Oligomers Induce Parkin S-Nitrosylation: Relevance to Sporadic Parkinson's Disease Etiopathology. *Molecular Neurobiology*, 56(1):125–140, January 2019.

[333] Anna Wilkaniec, Anna M. Lenkiewicz, Lidia Babiec, Emilia Murawska, Henryk M. Jęśko, Magdalena Cieślik, Carsten Culmsee, and Agata Adamczyk. Exogenous Alpha-Synuclein Evoked Parkin Downregulation Promotes Mitochondrial Dysfunction in Neuronal Cells. Implications for Parkinson's Disease Pathology. *Frontiers in Aging Neuroscience*, 13, February 2021. Publisher: Frontiers.

[334] Michela Deleidi and Walter Maetzler. Protein Clearance Mechanisms of Alpha-Synuclein and Amyloid-Beta in Lewy Body Disorders. *International Journal of Alzheimer's Disease*, 2012(1):391438, 2012. _eprint: https://onlinelibrary.wiley.com/doi/pdf/10.1155/2012/391438.

[335] Luis M. A. Oliveira, Thomas Gasser, Robert Edwards, Markus Zweckstetter, Ronald Melki, Leonidas Stefanis, Hilal A. Lashuel, David Sulzer, Kostas Vekrellis, Glenda M. Halliday, Julianna J. Tomlinson, Michael Schlossmacher, Poul Henning Jensen, Julia Schulze-Hentrich, Olaf Riess, Warren D. Hirst, Omar El-Agnaf, Brit Mollenhauer, Peter Lansbury, and Tiago F. Outeiro. Alpha-synuclein research: defining strategic moves in the battle against Parkinson's disease. *npj Parkinson's Disease*, 7(1):1–23, July 2021. Publisher: Nature Publishing Group.

[336] Willa Wen-You Yim and Noboru Mizushima. Lysosome biology in autophagy. *Cell Discovery*, 6(1):1–12, February 2020. Publisher: Nature Publishing Group.

[337] Eloy Bejarano and Ana Maria Cuervo. Chaperone-Mediated Autophagy. *Proceedings of the American Thoracic Society*, 7(1):29–39, February 2010.

[338] Marta Martinez-Vicente, Zsolt Talloczy, Susmita Kaushik, Ashish C. Massey, Joseph Mazzulli, Eugene V. Mosharov, Roberto Hodara, Ross Fredenburg, Du-Chu Wu, Antonia Follenzi, William Dauer, Serge Przedborski, Harry Ischiropoulos, Peter T. Lansbury, David Sulzer, and

Ana Maria Cuervo. Dopamine-modified α-synuclein blocks chaperone-mediated autophagy. *The Journal of Clinical Investigation*, 118(2):777–788, February 2008.

[339] Benjamin H.M. Hunn, Siv Vingill, Sarah Threlfell, Javier Alegre-Abarrategui, Morgane Magdelyns, Thierry Deltheil, Nora Bengoa-Vergniory, Peter L. Oliver, Milena Cioroch, Natalie M. Doig, David M. Bannerman, Stephanie J. Cragg, and Richard Wade-Martins. Impairment of Macroautophagy in Dopamine Neurons Has Opposing Effects on Parkinsonian Pathology and Behavior. *Cell Reports*, 29(4):920–931.e7, October 2019.

[340] Gessica Sala, Daniele Marinig, Alessandro Arosio, and Carlo Ferrarese. Role of Chaperone-Mediated Autophagy Dysfunctions in the Pathogenesis of Parkinson's Disease. *Frontiers in Molecular Neuroscience*, 9, December 2016. Publisher: Frontiers.

[341] Kristen A. Malkus and Harry Ischiropoulos. Regional deficiencies in chaperone-mediated autophagy underlie α-synuclein aggregation and neurodegeneration. *Neurobiology of Disease*, 46(3):732–744, June 2012.

[342] Ana Maria Cuervo, Leonidas Stefanis, Ross Fredenburg, Peter T. Lansbury, and David Sulzer. Impaired Degradation of Mutant α-Synuclein by Chaperone-Mediated Autophagy. *Science*, 305(5688):1292–1295, August 2004. Publisher: American Association for the Advancement of Science.

[343] Armin Bayati and Peter S. McPherson. Alpha-synuclein, autophagy-lysosomal pathway, and Lewy bodies: Mutations, propagation, aggregation, and the formation of inclusions. *The Journal of Biological Chemistry*, 300(10):107742, September 2024.

[344] Yaping Chu, Hemraj Dodiya, Patrick Aebischer, C. Warren Olanow, and Jeffrey H. Kordower. Alterations in lysosomal and proteasomal markers in Parkinson's disease: Relationship to alpha-synuclein inclusions. *Neurobiology of Disease*, 35(3):385–398, September 2009.

[345] P. Anglade, S. Vyas, F. Javoy-Agid, M. T. Herrero, P. P. Michel, J. Marquez, A. Mouatt-Prigent, M. Ruberg, E. C. Hirsch, and Y. Agid. Apoptosis and autophagy in nigral neurons of patients with Parkinson's disease. *Histology and Histopathology*, 12(1):25–31, January 1997.

[346] Takashi Nonaka and Masato Hasegawa. A Cellular Model To Monitor Proteasome Dysfunction by α-Synuclein. *Biochemistry*, 48(33):8014–8022, August 2009. Publisher: American Chemical Society.

[347] Chris McKinnon, Mitchell L. De Snoo, Elise Gondard, Clemens Neudorfer, Hien Chau, Sophie G. Ngana, Darren M. O'Hara, Jonathan M. Brotchie, James B. Koprich, Andres M. Lozano, Lorraine V. Kalia, and Suneil K. Kalia. Early-onset impairment of the ubiquitin-proteasome system in

dopaminergic neurons caused by α-synuclein. *Acta Neuropathologica Communications*, 8(1):17, February 2020.

[348] Evangelia Emmanouilidou, Leonidas Stefanis, and Kostas Vekrellis. Cell-produced α-synuclein oligomers are targeted to, and impair, the 26S proteasome. *Neurobiology of Aging*, 31(6):953–968, June 2010.

[349] Evo Lindersson, Rasmus Beedholm, Peter Højrup, Torben Moos, WeiPing Gai, Klavs B. Hendil, and Poul H. Jensen. Proteasomal Inhibition by α-Synuclein Filaments and Oligomers *. *Journal of Biological Chemistry*, 279(13):12924–12934, March 2004. Publisher: Elsevier.

[350] Miao Wang and Randal J. Kaufman. Protein misfolding in the endoplasmic reticulum as a conduit to human disease. *Nature*, 529(7586):326–335, January 2016.

[351] Emanuela Colla, Philippe Coune, Ying Liu, Olga Pletnikova, Juan C Troncoso, Takeshi Iwatsubo, Bernard L. Schneider, and Michael K. Lee. Endoplasmic Reticulum Stress Is Important for the Manifestations of α-Synucleinopathy In Vivo. *The Journal of Neuroscience*, 32(10):3306–3320, March 2012.

[352] Aitor Almanza, Antonio Carlesso, Chetan Chintha, Stuart Creedican, Dimitrios Doultsinos, Brian Leuzzi, Andreia Luís, Nicole McCarthy, Luigi Montibeller, Sanket More, Alexandra Papaioannou, Franziska Püschel, Maria Livia Sassano, Josip Skoko, Patrizia Agostinis, Jackie de Belleroche, Leif A. Eriksson, Simone Fulda, Adrienne M. Gorman, Sandra Healy, Andrey Kozlov, Cristina Muñoz-Pinedo, Markus Rehm, Eric Chevet, and Afshin Samali. Endoplasmic reticulum stress signalling – from basic mechanisms to clinical applications. *The Febs Journal*, 286(2):241–278, January 2019.

[353] Eva Szegezdi, Susan E Logue, Adrienne M Gorman, and Afshin Samali. Mediators of endoplasmic reticulum stress-induced apoptosis. *EMBO Reports*, 7(9):880–885, September 2006.

[354] Wanli W. Smith, Haibing Jiang, Zhong Pei, Yuji Tanaka, Hokuto Morita, Akira Sawa, Valina L. Dawson, Ted M. Dawson, and Christopher A. Ross. Endoplasmic reticulum stress and mitochondrial cell death pathways mediate A53T mutant alpha-synuclein-induced toxicity. *Human Molecular Genetics*, 14(24):3801–3811, December 2005.

[355] Michele Bellucci, Francesca De Marchis, and Andrea Pompa. The endoplasmic reticulum is a hub to sort proteins toward unconventional traffic pathways and endosymbiotic organelles. *Journal of Experimental Botany*, 69(1):7–20, December 2017.

[356] Antony A. Cooper, Aaron D. Gitler, Anil Cashikar, Cole M. Haynes, Kathryn J. Hill, Bhupinder Bhullar, Kangning Liu, Kexiang Xu, Katherine E. Strathearn, Fang Liu, Songsong Cao, Kim A. Caldwell, Guy A.

Caldwell, Gerald Marsischky, Richard D. Kolodner, Joshua LaBaer, Jean-Christophe Rochet, Nancy M. Bonini, and Susan Lindquist. α-Synuclein Blocks ER-Golgi Traffic and Rab1 Rescues Neuron Loss in Parkinson's Models. *Science*, 313(5785):324–328, July 2006. Publisher: American Association for the Advancement of Science.

[357] Natalia Siwecka, Kamil Saramowicz, Grzegorz Galita, Wioletta Rozpędek-Kamińska, and Ireneusz Majsterek. Inhibition of Protein Aggregation and Endoplasmic Reticulum Stress as a Targeted Therapy for α-Synucleinopathy. *Pharmaceutics*, 15(8):2051, August 2023. Number: 8 Publisher: Multidisciplinary Digital Publishing Institute.

[358] P. L. McGeer, S. Itagaki, B. E. Boyes, and E. G. McGeer. Reactive microglia are positive for HLA-DR in the substantia nigra of Parkinson's and Alzheimer's disease brains. *Neurology*, 38(8):1285–1285, August 1988. Publisher: Wolters Kluwer.

[359] Heather E. Allen Reish and David G. Standaert. Role of α-synuclein in inducing innate and adaptive immunity in Parkinson disease. *Journal of Parkinson's Disease*, 5(1):1–19, 2015.

[360] Federica Piancone, Marina Saresella, Francesca La Rosa, Ivana Marventano, Mario Meloni, Jorge Navarro, and Mario Clerici. Inflammatory Responses to Monomeric and Aggregated α-Synuclein in Peripheral Blood of Parkinson Disease Patients. *Frontiers in Neuroscience*, 15:639646, March 2021.

[361] Lydia Alvarez-Erviti, Yvonne Couch, Jill Richardson, J. Mark Cooper, and Matthew J. A. Wood. Alpha-synuclein release by neurons activates the inflammatory response in a microglial cell line. *Neuroscience Research*, 69(4):337–342, April 2011.

[362] Yvonne Couch, Lydia Alvarez-Erviti, Nicola R. Sibson, Matthew JA Wood, and Daniel C. Anthony. The acute inflammatory response to intranigral α-synuclein differs significantly from intranigral lipopolysaccharide and is exacerbated by peripheral inflammation. *Journal of Neuroinflammation*, 8(1):166, November 2011.

[363] He-Jin Lee, Ji-Eun Suk, Christina Patrick, Eun-Jin Bae, Ji-Hoon Cho, Sangchul Rho, Daehee Hwang, Eliezer Masliah, and Seung-Jae Lee. Direct transfer of alpha-synuclein from neuron to astroglia causes inflammatory responses in synucleinopathies. *The Journal of Biological Chemistry*, 285(12):9262–9272, March 2010.

[364] Changyoun Kim, Eun-Deok Cho, Hyung-Koo Kim, Sungyong You, He-Jin Lee, Daehee Hwang, and Seung-Jae Lee. β1-integrin-dependent migration of microglia in response to neuron-released α-synuclein. *Experimental & Molecular Medicine*, 46(4):e91, April 2014.

[365] Xóchitl Flores-Ponce and Iván Velasco. Dopaminergic neuron metabolism: relevance for understanding Parkinson's disease. *Metabolomics*, 20(6):116, 2024.

[366] Eleftheria Kyriaki Pissadaki and J. Paul Bolam. The energy cost of action potential propagation in dopamine neurons: clues to susceptibility in Parkinson's disease. *Frontiers in Computational Neuroscience*, 7, March 2013. Publisher: Frontiers.

[367] J. Paul Bolam and Eleftheria K. Pissadaki. Living on the edge with too many mouths to feed: why dopamine neurons die. *Movement Disorders: Official Journal of the Movement Disorder Society*, 27(12):1478–1483, October 2012.

[368] Mortimer Mamelak. Parkinson's Disease, the Dopaminergic Neuron and Gammahydroxybutyrate. *Neurology and Therapy*, 7(1):5–11, January 2018.

[369] D. James Surmeier, Paul T. Schumacker, Jaime D. Guzman, Ema Ilijic, Ben Yang, and Enrico Zampese. Calcium and Parkinson's disease. *Biochemical and Biophysical Research Communications*, 483(4):1013–1019, February 2017.

[370] Plamena R. Angelova, Marthe H. R. Ludtmann, Mathew H. Horrocks, Alexander Negoda, Nunilo Cremades, David Klenerman, Christopher M. Dobson, Nicholas W. Wood, Evgeny V. Pavlov, Sonia Gandhi, and Andrey Y. Abramov. Ca2+ is a key factor in α-synuclein-induced neurotoxicity. *Journal of Cell Science*, 129(9):1792–1801, May 2016.

[371] Peter Reinhardt, Michael Glatza, Kathrin Hemmer, Yaroslav Tsytsyura, Cora S. Thiel, Susanne Höing, Sören Moritz, Juan A. Parga, Lydia Wagner, Jan M. Bruder, Guangming Wu, Benjamin Schmid, Albrecht Röpke, Jürgen Klingauf, Jens C. Schwamborn, Thomas Gasser, Hans R. Schöler, and Jared Sterneckert. Derivation and Expansion Using Only Small Molecules of Human Neural Progenitors for Neurodegenerative Disease Modeling. *PLoS ONE*, 8(3):e59252, March 2013.

[372] Sonja Kriks, Jae-Won Shim, Jinghua Piao, Yosif M. Ganat, Dustin R. Wakeman, Zhong Xie, Luis Carrillo-Reid, Gordon Auyeung, Chris Antonacci, Amanda Buch, Lichuan Yang, M. Flint Beal, D. James Surmeier, Jeffrey H. Kordower, Viviane Tabar, and Lorenz Studer. Dopamine neurons derived from human ES cells efficiently engraft in animal models of Parkinson's disease. *Nature*, 480(7378):547–551, December 2011. Publisher: Nature Publishing Group.

[373] Evan Z. Macosko, Anindita Basu, Rahul Satija, James Nemesh, Karthik Shekhar, Melissa Goldman, Itay Tirosh, Allison R. Bialas, Nolan Kamitaki, Emily M. Martersteck, John J. Trombetta, David A. Weitz, Joshua R.

Sanes, Alex K. Shalek, Aviv Regev, and Steven A. McCarroll. Highly Parallel Genome-wide Expression Profiling of Individual Cells Using Nanoliter Droplets. *Cell*, 161(5):1202–1214, May 2015. Publisher: Elsevier.

[374] Carole Sousa, Anna Golebiewska, Suresh K Poovathingal, Tony Kaoma, Yolanda Pires-Afonso, Silvia Martina, Djalil Coowar, Francisco Azuaje, Alexander Skupin, Rudi Balling, Knut Biber, Simone P Niclou, and Alessandro Michelucci. Single-cell transcriptomics reveals distinct inflammation-induced microglia signatures. *EMBO reports*, 19(11):e46171, November 2018. Publisher: John Wiley & Sons, Ltd.

[375] Cole Trapnell, Davide Cacchiarelli, Jonna Grimsby, Prapti Pokharel, Shuqiang Li, Michael Morse, Niall J. Lennon, Kenneth J. Livak, Tarjei S. Mikkelsen, and John L. Rinn. The dynamics and regulators of cell fate decisions are revealed by pseudotemporal ordering of single cells. *Nature Biotechnology*, 32(4):381–386, April 2014. Publisher: Nature Publishing Group.

[376] Anne Dirkse, Anna Golebiewska, Thomas Buder, Petr V. Nazarov, Arnaud Muller, Suresh Poovathingal, Nicolaas H. C. Brons, Sonia Leite, Nicolas Sauvageot, Dzjemma Sarkisjan, Mathieu Seyfrid, Sabrina Fritah, Daniel Stieber, Alessandro Michelucci, Frank Hertel, Christel Herold-Mende, Francisco Azuaje, Alexander Skupin, Rolf Bjerkvig, Andreas Deutsch, Anja Voss-Böhme, and Simone P. Niclou. Stem cell-associated heterogeneity in Glioblastoma results from intrinsic tumor plasticity shaped by the microenvironment. *Nature Communications*, 10(1):1787, April 2019. Publisher: Nature Publishing Group.

[377] Yuhan Hao, Stephanie Hao, Erica Andersen-Nissen, William M. Mauck, Shiwei Zheng, Andrew Butler, Maddie J. Lee, Aaron J. Wilk, Charlotte Darby, Michael Zager, Paul Hoffman, Marlon Stoeckius, Efthymia Papalexi, Eleni P. Mimitou, Jaison Jain, Avi Srivastava, Tim Stuart, Lamar M. Fleming, Bertrand Yeung, Angela J. Rogers, Juliana M. McElrath, Catherine A. Blish, Raphael Gottardo, Peter Smibert, and Rahul Satija. Integrated analysis of multimodal single-cell data. *Cell*, 184(13):3573–3587.e29, June 2021.

[378] Mo Huang, Jingshu Wang, Eduardo Torre, Hannah Dueck, Sydney Shaffer, Roberto Bonasio, John I. Murray, Arjun Raj, Mingyao Li, and Nancy R. Zhang. SAVER: gene expression recovery for single-cell RNA sequencing. *Nature Methods*, 15(7):539–542, July 2018.

[379] Greg Finak, Andrew McDavid, Masanao Yajima, Jingyuan Deng, Vivian Gersuk, Alex K. Shalek, Chloe K. Slichter, Hannah W. Miller, M. Juliana McElrath, Martin Prlic, Peter S. Linsley, and Raphael Gottardo. MAST: a flexible statistical framework for assessing transcriptional changes and characterizing heterogeneity in single-cell RNA sequencing data. *Genome Biology*, 16(1):278, December 2015.

[380] Yingyao Zhou, Bin Zhou, Lars Pache, Max Chang, Alireza Hadj Khodabakhshi, Olga Tanaseichuk, Christopher Benner, and Sumit K. Chanda. Metascape provides a biologist-oriented resource for the analysis of systems-level datasets. *Nature Communications*, 10(1):1523, April 2019. Publisher: Nature Publishing Group.

[381] Julie Josse and François Husson. missMDA: A Package for Handling Missing Values in Multivariate Data Analysis. *Journal of Statistical Software*, 70:1–31, April 2016.

[382] Frank Koopmans, Pim van Nierop, Maria Andres-Alonso, Andrea Byrnes, Tony Cijsouw, Marcelo P. Coba, L. Niels Cornelisse, Ryan J. Farrell, Hana L. Goldschmidt, Daniel P. Howrigan, Natasha K. Hussain, Cordelia Imig, Arthur P. H. de Jong, Hwajin Jung, Mahdokht Kohansalnodehi, Barbara Kramarz, Noa Lipstein, Ruth C. Lovering, Harold MacGillavry, Vittoria Mariano, Huaiyu Mi, Momchil Ninov, David Osumi-Sutherland, Rainer Pielot, Karl-Heinz Smalla, Haiming Tang, Katherine Tashman, Ruud F. G. Toonen, Chiara Verpelli, Rita Reig-Viader, Kyoko Watanabe, Jan van Weering, Tilmann Achsel, Ghazaleh Ashrafi, Nimra Asi, Tyler C. Brown, Pietro De Camilli, Marc Feuermann, Rebecca E. Foulger, Pascale Gaudet, Anoushka Joglekar, Alexandros Kanellopoulos, Robert Malenka, Roger A. Nicoll, Camila Pulido, Jaime de Juan-Sanz, Morgan Sheng, Thomas C. Südhof, Hagen U. Tilgner, Claudia Bagni, Àlex Bayés, Thomas Biederer, Nils Brose, John Jia En Chua, Daniela C. Dieterich, Eckart D. Gundelfinger, Casper Hoogenraad, Richard L. Huganir, Reinhard Jahn, Pascal S. Kaeser, Eunjoon Kim, Michael R. Kreutz, Peter S. McPherson, Ben M. Neale, Vincent O'Connor, Danielle Posthuma, Timothy A. Ryan, Carlo Sala, Guoping Feng, Steven E. Hyman, Paul D. Thomas, August B. Smit, and Matthijs Verhage. SynGO: An Evidence-Based, Expert-Curated Knowledge Base for the Synapse. *Neuron*, 103(2):217–234.e4, July 2019.

[383] Matthew E. Ritchie, Belinda Phipson, Di Wu, Yifang Hu, Charity W. Law, Wei Shi, and Gordon K. Smyth. limma powers differential expression analyses for RNA-sequencing and microarray studies. *Nucleic Acids Research*, 43(7):e47, April 2015.

[384] Adhish S. Walvekar, Marc Warmoes, Dean Cheung, Tim Sikora, Najmesadat Seyedkatouli, Gemma Gomez-Giro, Sebastian Perrone, Lisa Dengler, François Unger, Bruno F. R. Santos, Floriane Gavotto, Xiangyi Dong, Julia Becker-Kettern, Yong-Jun Kwon, Christian Jäger, Jens C. Schwamborn, Nicole J. Van Bergen, John Christodoulou, and Carole L. Linster. Failure to repair damaged NAD(P)H blocks de novo serine synthesis in human cells. *Cellular & Molecular Biology Letters*, 30(1):3, January 2025.

[385] Zhiqiang Pang, Jasmine Chong, Shuzhao Li, and Jianguo Xia. MetaboAnalystR 3.0: Toward an Optimized Workflow for Global Metabolomics. *Metabolites*, 10(5):186, May 2020.

[386] Federico Zambon, Marta Cherubini, Hugo J R Fernandes, Charmaine Lang, Brent J Ryan, Viola Volpato, Nora Bengoa-Vergniory, Siv Vingill, Moustafa Attar, Heather D E Booth, Walther Haenseler, Jane Vowles, Rory Bowden, Caleb Webber, Sally A Cowley, and Richard Wade-Martins. Cellular α-synuclein pathology is associated with bioenergetic dysfunction in Parkinson's iPSC-derived dopamine neurons. *Human Molecular Genetics*, 28(12):2001–2013, June 2019.

[387] Valentina Gilmozzi, Giovanna Gentile, Diana A. Riekschnitz, Michael Von Troyer, Alexandros A. Lavdas, Emanuela Kerschbamer, Christian X. Weichenberger, Marcelo D. Rosato-Siri, Simona Casarosa, Luciano Conti, Peter P. Pramstaller, Andrew A. Hicks, Irene Pichler, and Alessandra Zanon. Generation of hiPSC-Derived Functional Dopaminergic Neurons in Alginate-Based 3D Culture. *Frontiers in Cell and Developmental Biology*, 9, August 2021. Publisher: Frontiers.

[388] Shinae Jung, Yuhyun Chung, Yunsoo Lee, Yangsin Lee, Jin Won Cho, Eun-Joo Shin, Hyoung-Chun Kim, and Young J. Oh. Buffering of cytosolic calcium plays a neuroprotective role by preserving the autophagy-lysosome pathway during MPP+-induced neuronal death. *Cell Death Discovery*, 5(1):1–15, August 2019. Publisher: Nature Publishing Group.

[389] Chang-He Shi, Cheng-Yuan Mao, Shu-Yu Zhang, Jing Yang, Bo Song, Ping Wu, Chuan-Tao Zuo, Yu-Tao Liu, Yan Ji, Zhi-Hua Yang, Jun Wu, Zheng-Ping Zhuang, and Yu-Ming Xu. CHCHD2 gene mutations in familial and sporadic Parkinson's disease. *Neurobiology of Aging*, 38:217.e9–217.e13, February 2016.

[390] Jonas Walter, Silvia Bolognin, Suresh K. Poovathingal, Stefano Magni, Deborah Gérard, Paul M. A. Antony, Sarah L. Nickels, Luis Salamanca, Emanuel Berger, Lisa M. Smits, Kamil Grzyb, Rita Perfeito, Fredrik Hoel, Xiaobing Qing, Jochen Ohnmacht, Michele Bertacchi, Javier Jarazo, Tomasz Ignac, Anna S. Monzel, Laura Gonzalez-Cano, Rejko Krüger, Thomas Sauter, Michèle Studer, Luis Pereira de Almeida, Karl J. Tronstad, Lasse Sinkkonen, Alexander Skupin, and Jens C. Schwamborn. The Parkinson's-disease-associated mutation LRRK2-G2019S alters dopaminergic differentiation dynamics via NR2F1. *Cell Reports*, 37(3):109864, October 2021.

[391] Ian Martin. Decoding Parkinson's Disease Pathogenesis: The Role of Deregulated mRNA Translation. *Journal of Parkinson's Disease*, 6(1):17–27, 2016.

[392] Luke S. Tain, Heather Mortiboys, Ran N. Tao, Elena Ziviani, Oliver Bandmann, and Alexander J. Whitworth. Rapamycin activation of 4E-BP prevents parkinsonian dopaminergic neuron loss. *Nature Neuroscience*, 12(9):1129–1135, September 2009. Publisher: Nature Publishing Group.

[393] Hugo J. R. Fernandes, Nikolaos Patikas, Stefanie Foskolou, Sarah F. Field, Jong-Eun Park, Meg L. Byrne, Andrew R. Bassett, and Emmanouil Metzakopian. Single-Cell Transcriptomics of Parkinson's Disease Human In Vitro Models Reveals Dopamine Neuron-Specific Stress Responses. *Cell Reports*, 33(2), October 2020. Publisher: Elsevier.

[394] Alexandros C. Kokotos, Aldana M. Antoniazzi, Santiago R. Unda, Myung Soo Ko, Daehun Park, David Eliezer, Michael G. Kaplitt, Pietro De Camilli, and Timothy A. Ryan. Phosphoglycerate kinase is a central leverage point in Parkinson's Disease driven neuronal metabolic deficits. *bioRxiv*, page 2023.10.10.561760, October 2023.

[395] Jingxian Zhang, Qingqing Shen, Yue Ma, Lin Liu, Wenting Jia, Leilei Chen, and Junxia Xie. Calcium Homeostasis in Parkinson's Disease: From Pathology to Treatment. *Neuroscience Bulletin*, 38(10):1267–1270, June 2022.

[396] Xin Chen, Xinxin Song, Jingbo Li, Ruoxi Zhang, Chunhua Yu, Zhuan Zhou, Jiao Liu, Siyan Liao, Daniel J. Klionsky, Guido Kroemer, Jinbao Liu, Daolin Tang, and Rui Kang. Identification of HPCAL1 as a specific autophagy receptor involved in ferroptosis. *Autophagy*, 19(1):54–74.

[397] Saad Haider and Ranadip Pal. Integrated analysis of transcriptomic and proteomic data. *Current Genomics*, 14(2):91–110, April 2013.

[398] Bijun Qiu, Junqi Wang, Yingxue Yu, Chao Zhen, Jinyang Gu, Wenjun Liu, Yankai Wen, Lili Chen, Yueqiu Gao, Qiang Xia, and Xiaoni Kong. DJ-1 promotes development of DEN-induced hepatocellular carcinoma and proliferation of liver cancer cells. *Oncotarget*, 8(5):8499–8511, December 2016. Publisher: Impact Journals.

[399] Lisa Schwarz and Julia C. Fitzgerald. Steady-State Levels of Miro1 Linked to Phosphorylation at Serine 156 and Mitochondrial Respiration in Dopaminergic Neurons. *Cells*, 11(8):1269, April 2022.

[400] Isabel Rosety, Alise Zagare, Claudia Saraiva, Sarah Nickels, Paul Antony, Catarina Almeida, Enrico Glaab, Rashi Halder, Sergiy Velychko, Thomas Rauen, Hans R. Schöler, Silvia Bolognin, Thomas Sauter, Javier Jarazo, Rejko Krüger, and Jens C. Schwamborn. Impaired neuron differentiation in GBA-associated Parkinson's disease is linked to cell cycle defects in organoids. *NPJ Parkinson's Disease*, 9:166, December 2023.

[401] Mario H. Barros and Gavin P. McStay. Modular biogenesis of mitochondrial respiratory complexes. *Mitochondrion*, 50:94–114, January 2020.

[402] Deirdre Nolfi-Donegan, Andrea Braganza, and Sruti Shiva. Mitochondrial electron transport chain: Oxidative phosphorylation, oxidant production, and methods of measurement. *Redox Biology*, 37:101674, August 2020.

[403] Luis A. Gómez, Jeffrey S. Monette, Juan D. Chavez, Claudia S. Maier, and Tory M. Hagen. Supercomplexes of the mitochondrial electron transport chain decline in the aging rat heart. *Archives of Biochemistry and Biophysics*, 490(1):30–35, October 2009.

[404] Yoshikuni Mizuno, Shigeo Ohta, Masashi Tanaka, Shinzaburo Takamiya, Keiji Suzuki, Takeshi Sato, Hiroshi Oya, Takayuki Ozawa, and Yasuo Kagawa. Deficiencies in Complex I subunits of the respiratory chain in Parkinson's disease. *Biochemical and Biophysical Research Communications*, 163(3):1450–1455, September 1989.

[405] W. Davis Parker, Janice K. Parks, and Russell H. Swerdlow. Complex I deficiency in Parkinson's disease frontal cortex. *Brain Research*, 1189:215–218, January 2008.

[406] M. Morán, H. Rivera, M. Sánchez-Aragó, A. Blázquez, B. Merinero, C. Ugalde, J. Arenas, J. M. Cuezva, and M. A. Martín. Mitochondrial bioenergetics and dynamics interplay in complex I-deficient fibroblasts. *Biochimica et Biophysica Acta (BBA) - Molecular Basis of Disease*, 1802(5):443–453, May 2010.

[407] A. H. Schapira, J. M. Cooper, D. Dexter, J. B. Clark, P. Jenner, and C. D. Marsden. Mitochondrial complex I deficiency in Parkinson's disease. *Journal of Neurochemistry*, 54(3):823–827, March 1990.

[408] Jeng-Lin Li, Tai-Yi Lin, Po-Lin Chen, Ting-Ni Guo, Shu-Yi Huang, Chun-Hong Chen, Chin-Hsien Lin, and Chih-Chiang Chan. Mitochondrial Function and Parkinson's Disease: From the Perspective of the Electron Transport Chain. *Frontiers in Molecular Neuroscience*, 14:797833, 2021.

[409] Cristina Balcells, Carles Foguet, Josep Tarragó-Celada, Pedro de Atauri, Silvia Marin, and Marta Cascante. Tracing metabolic fluxes using mass spectrometry: Stable isotope-resolved metabolomics in health and disease. *TrAC Trends in Analytical Chemistry*, 120:115371, November 2019.

[410] Xuanzhuo Liu, Fang Wang, Xinman Fan, Mingyi Chen, Xiaoxin Xu, Qiuhong Xu, Huili Zhu, Anding Xu, Mahmoud A. Pouladi, and Xiaohong Xu. CHCHD2 up-regulation in Huntington disease mediates a compensatory protective response against oxidative stress. *Cell Death & Disease*, 15(2):1–12, February 2024. Publisher: Nature Publishing Group.

[411] Manabu Funayama, Kenji Ohe, Taku Amo, Norihiko Furuya, Junji Yamaguchi, Shinji Saiki, Yuanzhe Li, Kotaro Ogaki, Maya Ando, Hiroyo Yoshino, Hiroyuki Tomiyama, Kenya Nishioka, Kazuko Hasegawa, Hidemoto Saiki, Wataru Satake, Kaoru Mogushi, Ryogen Sasaki, Yasumasa Kokubo, Shigeki Kuzuhara, Tatsushi Toda, Yoshikuni Mizuno, Yasuo Uchiyama, Kinji Ohno, and Nobutaka Hattori. CHCHD2 mutations in autosomal dominant late-onset Parkinson's disease: a genome-wide linkage and sequencing study. *The Lancet. Neurology*, 14(3):274–282, March 2015.

[412] Siddhesh Aras, Oleg Pak, Natascha Sommer, Russell Finley, Maik Hüttemann, Norbert Weissmann, and Lawrence I. Grossman. Oxygen-dependent expression of cytochrome c oxidase subunit 4-2 gene expression is mediated by transcription factors RBPJ, CXXC5 and CHCHD2. *Nucleic Acids Research*, 41(4):2255–2266, February 2013.

[413] Yuzuru Imai, Hongrui Meng, Kahori Shiba-Fukushima, and Nobutaka Hattori. Twin CHCH Proteins, CHCHD2, and CHCHD10: Key Molecules of Parkinson's Disease, Amyotrophic Lateral Sclerosis, and Frontotemporal Dementia. *International Journal of Molecular Sciences*, 20(4):908, February 2019.

[414] Teresa R. Kee, Pamela Espinoza Gonzalez, Jessica L. Wehinger, Mohammed Zaheen Bukhari, Aizara Ermekbaeva, Apoorva Sista, Peter Kotsiviras, Tian Liu, David E. Kang, and Jung-A. A. Woo. Mitochondrial CHCHD2: Disease-Associated Mutations, Physiological Functions, and Current Animal Models. *Frontiers in Aging Neuroscience*, 13, April 2021. Publisher: Frontiers.

[415] Sandra Harjuhaahto, Tiina S. Rasila, Svetlana M. Molchanova, Rosa Woldegebriel, Jouni Kvist, Svetlana Konovalova, Markus T. Sainio, Jana Pennonen, Rubén Torregrosa-Muñumer, Hazem Ibrahim, Timo Otonkoski, Tomi Taira, Emil Ylikallio, and Henna Tyynismaa. ALS and Parkinson's disease genes CHCHD10 and CHCHD2 modify synaptic transcriptomes in human iPSC-derived motor neurons. *Neurobiology of Disease*, 141:104940, July 2020.

[416] Estela Area-Gomez, Cristina Guardia-Laguarta, Eric A. Schon, and Serge Przedborski. Mitochondria, OxPhos, and neurodegeneration: cells are not just running out of gas. *The Journal of Clinical Investigation*, 129(1):34–45, January 2019.

[417] Ketki M. Hatle, Phani Gummadidala, Nicolás Navasa, Edgar Bernardo, John Dodge, Brian Silverstrim, Karen Fortner, Elianne Burg, Benajamin T. Suratt, Juergen Hammer, Michael Radermacher, Douglas J. Taatjes, Tina Thornton, Juan Anguita, and Mercedes Rincon. MCJ/DnaJC15, an endogenous mitochondrial repressor of the respiratory chain that controls metabolic alterations. *Molecular and Cellular Biology*, 33(11):2302–2314, June 2013.

[418] Lara Kroczek, Hendrik Nolte, Yvonne Lasarzewski, Thibaut Molinié, Daniel Curbelo Pinero, Kathrin Lemke, Elena Rugarli, and Thomas Langer. Stress adaptation of mitochondrial protein import by OMA1-mediated degradation of DNAJC15, March 2025. Pages: 2025.03.04.641455 Section: New Results.

[419] Shiyu Luo, C. Alexander Valencia, Jinglan Zhang, Ni-Chung Lee, Jesse Slone, Baoheng Gui, Xinjian Wang, Zhuo Li, Sarah Dell, Jenice Brown,

Stella Maris Chen, Yin-Hsiu Chien, Wuh-Liang Hwu, Pi-Chuan Fan, Lee-Jun Wong, Paldeep S. Atwal, and Taosheng Huang. Biparental Inheritance of Mitochondrial DNA in Humans. *Proceedings of the National Academy of Sciences*, 115(51):13039–13044, December 2018. Publisher: Proceedings of the National Academy of Sciences.

[420] Qianqian Ding, Yanxiang Qi, and Suk-Ying Tsang. Mitochondrial Biogenesis, Mitochondrial Dynamics, and Mitophagy in the Maturation of Cardiomyocytes. *Cells*, 10(9):2463, September 2021.

[421] Vikramjit Lahiri and Daniel J. Klionsky. Functional impairment in RHOT1/Miro1 degradation and mitophagy is a shared feature in familial and sporadic Parkinson disease. *Autophagy*, 13(8):1259–1261, August 2017. Publisher: Taylor & Francis _eprint: https://doi.org/10.1080/15548627.2017.1327512.

[422] Dzhamilja Safiulina, Malle Kuum, Vinay Choubey, Miriam A. Hickey, and Allen Kaasik. Mitochondrial transport proteins RHOT1 and RHOT2 serve as docking sites for PRKN-mediated mitophagy. *Autophagy*, 15(5):930–931, May 2019.

[423] Dajana Grossmann, Clara Berenguer-Escuder, Axel Chemla, Giuseppe Arena, and Rejko Krüger. The Emerging Role of RHOT1/Miro1 in the Pathogenesis of Parkinson's Disease. *Frontiers in Neurology*, 11:587, 2020.

[424] Yu Sun, Ajay A. Vashisht, Jason Tchieu, James A. Wohlschlegel, and Lars Dreier. Voltage-dependent Anion Channels (VDACs) Recruit Parkin to Defective Mitochondria to Promote Mitochondrial Autophagy. *The Journal of Biological Chemistry*, 287(48):40652–40660, November 2012.

[425] Seung-Min Yoo, Shun-Ichi Yamashita, Hyunjoo Kim, DoHyeong Na, Haneul Lee, Seo Jin Kim, Dong-Hyung Cho, Tomotake Kanki, and Yong-Keun Jung. FKBP8 LIRL-dependent mitochondrial fragmentation facilitates mitophagy under stress conditions. *FASEB journal: official publication of the Federation of American Societies for Experimental Biology*, 34(2):2944–2957, February 2020.

[426] Sarah Hui, Jimmy George, Minesh Kapadia, Hien Chau, Zahn Bariring, Rebecca Earnshaw, Kashfia Shafiq, Lorraine V. Kalia, and Suneil K. Kalia. Mitophagy Upregulation Occurs Early in the Neurodegenerative Process Mediated by α-Synuclein. *Molecular Neurobiology*, 61(11):9032–9042, November 2024.

[427] Sofia V. Zaichick, Kaitlyn M. McGrath, and Gabriela Caraveo. The role of Ca2+ signaling in Parkinson's disease. *Disease Models & Mechanisms*, 10(5):519–535, May 2017.

[428] Ji Wang, Jindong Zhao, Kunying Zhao, Shangpeng Wu, Xinglong Chen, and Weiyan Hu. The Role of Calcium and Iron Homeostasis in Parkinson's

Disease. *Brain Sciences*, 14(1):88, January 2024. Number: 1 Publisher: Multidisciplinary Digital Publishing Institute.

[429] Lisa Schwarz, Karan Sharma, Lorenzo D. Dodi, Lara-Sophie Rieder, Petra Fallier-Becker, Nicolas Casadei, and Julia C. Fitzgerald. Miro1 R272Q disrupts mitochondrial calcium handling and neurotransmitter uptake in dopaminergic neurons. *Frontiers in Molecular Neuroscience*, 15:966209, 2022.

[430] Victoria Vaccaro, Michael J Devine, Nathalie F Higgs, and Josef T Kittler. Miro1-dependent mitochondrial positioning drives the rescaling of presynaptic Ca2+ signals during homeostatic plasticity. *EMBO reports*, 18(2):231–240, February 2017. Num Pages: 240 Publisher: John Wiley & Sons, Ltd.

[431] Vinita Bharat, Aarooran S. Durairaj, Roeland Vanhauwaert, Li Li, Colin M. Muir, Sujyoti Chandra, Chulhwan S. Kwak, Yann Le Guen, Pawan Nandakishore, Chung-Han Hsieh, Stefano E. Rensi, Russ B. Altman, Michael D. Greicius, Liang Feng, and Xinnan Wang. A mitochondrial inside-out iron-calcium signal reveals drug targets for Parkinson's disease. *Cell Reports*, 42(12):113544, December 2023.

[432] Gaia Gherardi, Halenya Monticelli, Rosario Rizzuto, and Cristina Mammucari. The Mitochondrial Ca2+ Uptake and the Fine-Tuning of Aerobic Metabolism. *Frontiers in Physiology*, 11:554904, 2020.

[433] Elianne P. Bulthuis, Merel J. W. Adjobo-Hermans, Bastiaan de Potter, Saskia Hoogstraten, Lisanne H. T. Wezendonk, Omar A. Z. Tutakhel, Liesbeth T. Wintjes, Bert van den Heuvel, Peter H. G. M. Willems, Erik-Jan Kamsteeg, M. Estela Rubio Gozalbo, Suzanne C. E. H. Sallevelt, Suzanne M. Koudijs, Joost Nicolai, Charlotte I. de Bie, Jessica E. Hoogendijk, Werner J. H. Koopman, and Richard J. Rodenburg. SMDT1 variants impair EMRE-mediated mitochondrial calcium uptake in patients with muscle involvement. *Biochimica Et Biophysica Acta. Molecular Basis of Disease*, 1869(8):166808, December 2023.

[434] Sophia D. Staerz, Charles Anamoah, and Jetze J. Tepe. 20S proteasome enhancers prevent cytotoxic tubulin polymerization-promoting protein induced α-synuclein aggregation. *iScience*, 27(7), July 2024. Publisher: Elsevier.

[435] Alice Filippini, Veronica Mutti, Gaia Faustini, Francesca Longhena, Ileana Ramazzina, Federica Rizzi, Alice Kaganovich, Dorien A. Roosen, Natalie Landeck, Megan Duffy, Isabella Tessari, Federica Bono, Chiara Fiorentini, Elisa Greggio, Luigi Bubacco, Arianna Bellucci, Mariacristina Missale, Mark R. Cookson, Massimo Gennarelli, and Isabella Russo. Extracellular clusterin limits the uptake of α-synuclein fibrils by murine and human astrocytes. *Glia*, 69(3):681–696, March 2021.

[436] Plasma levels of Clusterin are representative of the early phase of the neurodegenerative process in Parkinson's disease | Request PDF. *ResearchGate*, December 2024.

[437] Benjamin Guy Trist, Dominic James Hare, and Kay Lorraine Double. A Proposed Mechanism for Neurodegeneration in Movement Disorders Characterized by Metal Dyshomeostasis and Oxidative Stress. *Cell Chemical Biology*, 25(7):807–816, July 2018.

[438] Amir Tahavvori, Morad Kohandel Gargari, Yalda Yazdani, Alireza Soleimani Mamalo, Elmira Aboutalebi Vand Beilankouhi, and Mohammad Valilo. Involvement of antioxidant enzymes in Parkinson's disease. *Pathology - Research and Practice*, 249:154757, September 2023.

[439] Alba Gabaldon-Albero, Sonia Mayo, and Francisco Martinez. NR4A2 as a Novel Target Gene for Developmental and Epileptic Encephalopathy: A Systematic Review of Related Disorders and Therapeutic Strategies. *International Journal of Molecular Sciences*, 25(10):5198, January 2024. Number: 10 Publisher: Multidisciplinary Digital Publishing Institute.

[440] Tushar Kamath, Abdulraouf Abdulraouf, S. J. Burris, Jonah Langlieb, Vahid Gazestani, Naeem M. Nadaf, Karol Balderrama, Charles Vanderburg, and Evan Z. Macosko. Single-cell genomic profiling of human dopamine neurons identifies a population that selectively degenerates in Parkinson's disease. *Nature Neuroscience*, 25(5):588–595, May 2022. Publisher: Nature Publishing Group.

[441] Noviana Wulansari, Wahyu Handoko Wibowo Darsono, Hye-Ji Woo, Mi-Yoon Chang, Jinil Kim, Eun-Jin Bae, Woong Sun, Ju-Hyun Lee, Il-Joo Cho, Hyogeun Shin, Seung-Jae Lee, and Sang-Hun Lee. Neurodevelopmental defects and neurodegenerative phenotypes in human brain organoids carrying Parkinson's disease-linked DNAJC6 mutations. *Science Advances*, 7(8):eabb1540, February 2021. Publisher: American Association for the Advancement of Science.

[442] L. M. A. Oliveira, L. J. Falomir-Lockhart, M. G. Botelho, K.-H. Lin, P. Wales, J. C. Koch, E. Gerhardt, H. Taschenberger, T. F. Outeiro, P. Lingor, B. Schüle, D. J. Arndt-Jovin, and T. M. Jovin. Elevated α-synuclein caused by SNCA gene triplication impairs neuronal differentiation and maturation in Parkinson's patient-derived induced pluripotent stem cells. *Cell Death & Disease*, 6(11):e1994–e1994, November 2015. Publisher: Nature Publishing Group.

[443] Kim-Ann Saal, Dagmar Galter, Sigrun Roeber, Mathias Bähr, Lars Tönges, and Paul Lingor. Altered Expression of Growth Associated Protein-43 and Rho Kinase in Human Patients with Parkinson's Disease. *Brain Pathology*, 27(1):13–25, February 2016.

[444] Shiyuan Liu, Yumin Li, Wei Chen, Pengfei Zheng, Tao Liu, Wenting He, Junqiang Zhang, and Xiangting Zeng. Silencing glypican-3 expression induces apoptosis in human hepatocellular carcinoma cells. *Biochemical and Biophysical Research Communications*, 419(4):656–661, March 2012.

[445] Atossa Shaltouki, Renuka Sivapatham, Ying Pei, Akos A. Gerencser, Olga Momčilović, Mahendra S. Rao, and Xianmin Zeng. Mitochondrial Alterations by PARKIN in Dopaminergic Neurons Using PARK2 Patient-Specific and PARK2 Knockout Isogenic iPSC Lines. *Stem Cell Reports*, 4(5):847–859, April 2015.

[446] T.-B. Ahn, S. Y. Kim, J. Y. Kim, S.-S. Park, D. S. Lee, H. J. Min, Y. K. Kim, S. E. Kim, J.-M. Kim, H.-J. Kim, J. Cho, and B. S. Jeon. alpha-Synuclein gene duplication is present in sporadic Parkinson disease. *Neurology*, 70(1):43–49, January 2008.

[447] Jens C. Schwamborn. Is Parkinson's Disease a Neurodevelopmental Disorder and Will Brain Organoids Help Us to Understand It? *Stem Cells and Development*, 27(14):968–975, July 2018. Publisher: Mary Ann Liebert, Inc., publishers.

[448] Anatole Ghazalpour, Brian Bennett, Vladislav A. Petyuk, Luz Orozco, Raffi Hagopian, Imran N. Mungrue, Charles R. Farber, Janet Sinsheimer, Hyun M. Kang, Nicholas Furlotte, Christopher C. Park, Ping-Zi Wen, Heather Brewer, Karl Weitz, David G. Camp, Calvin Pan, Roumyana Yordanova, Isaac Neuhaus, Charles Tilford, Nathan Siemers, Peter Gargalovic, Eleazar Eskin, Todd Kirchgessner, Desmond J. Smith, Richard D. Smith, and Aldons J. Lusis. Comparative analysis of proteome and transcriptome variation in mouse. *PLoS genetics*, 7(6):e1001393, June 2011.

[449] Yawwani Gunawardana and Mahesan Niranjan. Bridging the gap between transcriptome and proteome measurements identifies post-translationally regulated genes. *Bioinformatics*, 29(23):3060–3066, December 2013.

[450] Swathi Ramachandra Upadhya and Colm J. Ryan. Experimental reproducibility limits the correlation between mRNA and protein abundances in tumor proteomic profiles. *Cell Reports Methods*, 2(9):100288, September 2022.

[451] Shuzo Urata, Elizabeth Kenyon, Debasis Nayak, Beatrice Cubitt, Yohei Kurosaki, Jiro Yasuda, Juan C. de la Torre, and Dorian B. McGavern. BST-2 controls T cell proliferation and exhaustion by shaping the early distribution of a persistent viral infection. *PLoS pathogens*, 14(7):e1007172, July 2018.

[452] Shannon Jewell, Ashane M. Herath, and Richard Gordon. Inflammasome Activation in Parkinson's Disease. *Journal of Parkinson's Disease*, 12(Suppl 1):S113–S128.

[453] Linh Thi Nhat Nguyen, Huu Dat Nguyen, Yun Joong Kim, Tinh Thi Nguyen, Thuy Thi Lai, Yoon Kyoung Lee, Hyeo-il Ma, and Young Eun Kim. Role of NLRP3 Inflammasome in Parkinson's Disease and Therapeutic Considerations. *Journal of Parkinson's Disease*, 12(7):2117–2133.

[454] László Ducza and Botond Gaál. The Neglected Sibling: NLRP2 Inflammasome in the Nervous System. *Aging and Disease*, 15(3):1006–1028, May 2024.

[455] Tamara Tilburgs, Torsten B. Meissner, Leonardo M. R. Ferreira, Arend Mulder, Kiran Musunuru, Junqiang Ye, and Jack L. Strominger. NLRP2 is a suppressor of NF-B signaling and HLA-C expression in human trophoblasts†,‡. *Biology of Reproduction*, 96(4):831–842, April 2017.

[456] Ana Fontalba, Olga Gutierrez, and Jose L. Fernandez-Luna. NLRP2, an inhibitor of the NF-kappaB pathway, is transcriptionally activated by NF-kappaB and exhibits a nonfunctional allelic variant. *Journal of Immunology (Baltimore, Md.: 1950)*, 179(12):8519–8524, December 2007.

[457] Zhaohuan Zhang, Xiaohui Xu, Zhenghua Xiang, Zhongwang Yu, Jifeng Feng, and Cheng He. LINGO-1 Receptor Promotes Neuronal Apoptosis by Inhibiting WNK3 Kinase Activity *. *Journal of Biological Chemistry*, 288(17):12152–12160, April 2013. Publisher: Elsevier.

[458] Jie Zhu, Xiaolong Lin, Chen Chen, Helian Tan, Yanping Gao, Di Li, and Gang Chen. WNK3 Promotes Neuronal Survival after Traumatic Brain Injury in Rats. *Neuroscience*, 477:76–88, November 2021.

[459] F. Veríssimo, E. Silva, J. D. Morris, R. Pepperkok, and P. Jordan. Protein kinase WNK3 increases cell survival in a caspase-3-dependent pathway. *Oncogene*, 25(30):4172–4182, July 2006.

[460] Shr-Hau Hung, Gregory I Elliott, Thakku R Ramkumar, Lyubomyr Burtnyak, Callum J McGrenaghan, Sana Alkuzweny, Samia Quaiyum, Dirk Iwata-Reuyl, Xiaobei Pan, Brian D Green, Vincent P Kelly, Valérie de Crécy Lagard, and Manal A Swairjo. Structural basis of Qng1-mediated salvage of the micronutrient queuine from queuosine-5-monophosphate as the biological substrate. *Nucleic Acids Research*, 51(2):935–951, January 2023.

[461] Patti Hayes, Claire Fergus, Magda Ghanim, Cansu Cirzi, Lyubomyr Burtnyak, Callum J. McGrenaghan, Francesca Tuorto, Derek P. Nolan, and Vincent P. Kelly. Queuine Micronutrient Deficiency Promotes Warburg Metabolism and Reversal of the Mitochondrial ATP Synthase in Hela Cells. *Nutrients*, 12(3):871, March 2020.

[462] Sergio Kaiser, Luqing Zhang, Brit Mollenhauer, Jaison Jacob, Simonne Longerich, Jorge Del-Aguila, Jacob Marcus, Neha Raghavan, David Stone, Olumide Fagboyegun, Douglas Galasko, Mohammed Dakna, Bilada

Bilican, Mary Dovlatyan, Anna Kostikova, Jingyao Li, Brant Peterson, Michael Rotte, Vinicius Sanz, Tatiana Foroud, Samantha J. Hutten, Mark Frasier, Hirotaka Iwaki, Andrew Singleton, Ken Marek, Karen Crawford, Fiona Elwood, Mirko Messa, and Pablo Serrano-Fernandez. A proteogenomic view of Parkinson's disease causality and heterogeneity. *npj Parkinson's Disease*, 9(1):1–13, February 2023. Publisher: Nature Publishing Group.

[463] Rémy Liechti, Angélique D. Ducray, Pia Jensen, Stefano Di Santo, Stefanie Seiler, Charlotte H. Jensen, Morten Meyer, and Hans Rudolf Widmer. Characterization of Fetal Antigen 1/Delta-Like 1 Homologue Expressing Cells in the Rat Nigrostriatal System: Effects of a Unilateral 6-Hydroxydopamine Lesion. *PLOS ONE*, 10(2):e0116088, February 2015. Publisher: Public Library of Science.

[464] Macarena Guereño, Magali Delgado Pastore, Ana Clara Lugones, Magalí Cercato, Laura Todaro, Alejandro Urtreger, and María Giselle Peters. Glypican-3 (GPC3) inhibits metastasis development promoting dormancy in breast cancer cells by p38 MAPK pathway activation. *European Journal of Cell Biology*, 99(6):151096, August 2020.

[465] Xiufeng Zheng, Xun Liu, Yanna Lei, Gang Wang, and Ming Liu. Glypican-3: A Novel and Promising Target for the Treatment of Hepatocellular Carcinoma. *Frontiers in Oncology*, 12, February 2022. Publisher: Frontiers.

[466] Kirsten L. Moek, Rudolf S. N. Fehrmann, Bert van der Vegt, Elisabeth G. E. de Vries, and Derk J. A. de Groot. Glypican 3 Overexpression across a Broad Spectrum of Tumor Types Discovered with Functional Genomic mRNA Profiling of a Large Cancer Database. *The American Journal of Pathology*, 188(9):1973–1981, September 2018.

[467] Joon-Yong Chung, Woonghee Lee, Olivia W Lee, Kris Ylaya, Divya Nambiar, Julia Sheehan-Klenk, Stanley Fayn, Stephen M Hewitt, Peter L Choyke, and Freddy E Escorcia. Glypican-3 deficiency in liver cancer upregulates MAPK/ERK pathway but decreases cell proliferation. *American Journal of Cancer Research*, 14(7):3348–3371, July 2024.

[468] Flora Stephano, Stella Nolte, Julia Hoffmann, Samar El-Kholy, Jakob von Frieling, Iris Bruchhaus, Christine Fink, and Thomas Roeder. Impaired Wnt signaling in dopamine containing neurons is associated with pathogenesis in a rotenone triggered Drosophila Parkinson's disease model. *Scientific Reports*, 8(1):2372, February 2018. Publisher: Nature Publishing Group.

[469] Bianca Marchetti, Cataldo Tirolo, Francesca L'Episcopo, Salvatore Caniglia, Nunzio Testa, Jayden A. Smith, Stefano Pluchino, and Maria F. Serapide. Parkinson's disease, aging and adult neurogenesis: Wnt/β-catenin signalling as the key to unlock the mystery of

endogenous brain repair. *Aging Cell*, 19(3):e13101, 2020. _eprint: https://onlinelibrary.wiley.com/doi/pdf/10.1111/acel.13101.

[470] Meng Guo, Hailing Zhang, Jianming Zheng, and Yangfang Liu. Glypican-3: A New Target for Diagnosis and Treatment of Hepatocellular Carcinoma. *Journal of Cancer*, 11(8):2008–2021, February 2020.

[471] Aya Ikeda, Kenya Nishioka, Hongrui Meng, Masashi Takanashi, Iwao Hasegawa, Tsuyoshi Inoshita, Kahori Shiba-Fukushima, Yuanzhe Li, Hiroyo Yoshino, Akio Mori, Ayami Okuzumi, Akihiro Yamaguchi, Risa Nonaka, Nana Izawa, Kei-Ichi Ishikawa, Hidemoto Saiki, Masayo Morita, Masato Hasegawa, Kazuko Hasegawa, Montasir Elahi, Manabu Funayama, Hideyuki Okano, Wado Akamatsu, Yuzuru Imai, and Nobutaka Hattori. Mutations in CHCHD2 cause α-synuclein aggregation. *Human Molecular Genetics*, 28(23):3895–3911, December 2019.

[472] Gabriela Novak Kamil Grzyb Elle Wilson Carmen Lahr Anne Grünewald Carole L Linster Gunnar Dittmar Alexander Skupin Michela Bernini, Corrado Ameli. Longitudinal multiomics characterization of pink1 patient-derived ipsc differentiation reveals ubiquitin-mediated rack1 mechanism for impaired neuronal development in parkinson's disease. *in preparation*, 2025.

[473] Anindita Bose, Gregory A. Petsko, and Lorenz Studer. Induced pluripotent stem cells: a tool for modeling Parkinson's disease. *Trends in Neurosciences*, 45(8):608–620, August 2022.

[474] Sahar Avazzadeh, Jara Maria Baena, Cameron Keighron, Yajaira Feller-Sanchez, and Leo R. Quinlan. Modelling Parkinson's Disease: iPSCs towards Better Understanding of Human Pathology. *Brain Sciences*, 11(3):373, March 2021.

[475] Lucia Barazzuol, Flavia Giamogante, and Tito Calì. Mitochondria Associated Membranes (MAMs): Architecture and physiopathological role. *Cell Calcium*, 94:102343, March 2021.

APPENDIX A

Appendix

Chemical Description	Manufacturer	Catalog Reference
Accutase	Gibco	A1110501
Advanced DMEM/F-12	Gibco	12634-010
Ascorbic Acid	Peprotech	5088177
B-27 Supplement	Gibco	12587010
BDNF	StemCell Technologies	78005.3
cAMP	Sigma-Aldrich	D0627
CHIR	StemCell Technologies	73044
CyQuant - Cell Proliferation Assay Kit	Thermo	C7026
DAPT	R&D	2634/50
Fgf-8b	StemCell Technologies	78008.1
Fibronectin	R&D	1918-FN-02M
GDNF	StemCell Technologies	78058.3
Geltrex	Gibco	A1413202
GlutaMAX Supplement	Gibco	35050061
KnockOut DMEM	Gibco	10829018
KnockOut Serum Replacement	Gibco	10828010
Laminin-521	StemCell Technologies	200-0117
LDN193189	StemCell Technologies	72147
mTeSR1	StemCell Technologies	85850
mTeSR Plus	StemCell Technologies	Q-435330
N-2 Supplement (100X)	Gibco	17502001
NEAA MEM	Gibco	11140035
Neurobasal Medium	Gibco	21103049
Poly-L-Ornithin	Sigma-Aldrich	P-3655
PowerTrack™ SYBR Green Master Mix	Thermo	A46113
Puromorphamine	StemCell Technologies	72204
Puromycin	Peprotech	5855822
RNeasy Mini Kit	Qiagen	74104
Rock Inhibitor	Abcam	ab10129
Seahorse XF DMEM assay medium pack, pH 7.4	Agilent	103680-100
Seahorse XFe96/XF Pro FluxPak Mini	Agilent	103793-100
Seahorse XF Cell Mito Stress Test Kit	Agilent	103015-100
Shh	StemCell Technologies	78065.2
SB431542	StemCell Technologies	72234
SuperScript™ III First-Strand Synthesis Kit	Thermo	18080051
Synth-a-freeze	Gibco	A1371301
TGFβ3	StemCell Technologies	78131

Table A.1 Materials & reagents. Materials used in the present study, including their manufacturers and catalog references.

iPSC Line	Etiology	PD Mutation	Sex	Age	Reprogramming method	Source
ND50050	Genetic	*SNCA*-A53T	Female	51	Episomal	NINDS biobank (ND50050)
Control	Healthy control	Wild-type	Female	53	Retroviral	Reinheart et al., 2013

Table A.2 Cell line details. Details of the *SNCA*-A53T and control cell lines used for the present study.

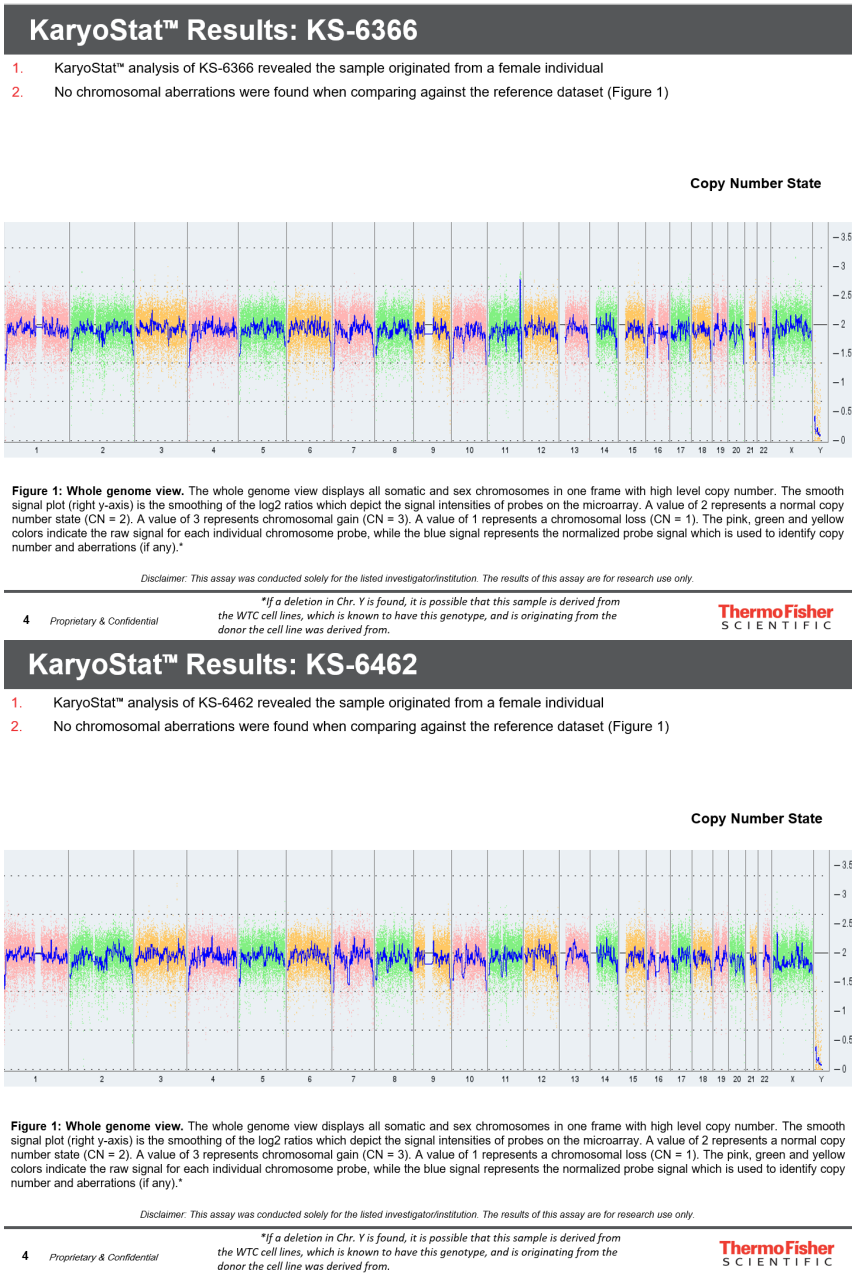

Fig. A.1 KaryoStat reports. KaryoStat reports showing normal karyotypes for *SNCA*-A53T (KS-6366) and control (KS-6462) cell lines.

Day	Procedure
Day -1	Plate iPSCs at 1.1 x 10^6 cells/well in MTeSR with ROCK inhibitor, remove ROCK inhibitor after ±8 hours.
Day 0	SRM, LDN193189 (100 nM), SB431542 (10 µM).
Day 1-2	SRM, LDN193189 (100 nM), SB431542 (10 µM), SHH (100 ng/ml), Purmorphamine (2 µM), FGF-8b (100 ng/ml).
Day 3-4	SRM, LDN193189 (100 nM), SB431542 (10 µM), SHH (100 ng/ml), Purmorphamine (2 µM), FGF-8b (100 ng/ml), CHIR (3 µM).
Day 5-6	75% SRM/25% N2 with LDN193189 (100 nM), SHH (100 ng/ml), Purmorphamine (2 µM), FGF-8b (100 ng/ml), CHIR (3 µM).
Day 7-8	50% SRM/50% N2 with LDN193189 (100 nM), SHH (100 ng/ml), CHIR (3 µM).
Day 9-10	25% SRM/75% N2 with LDN193189 (100 nM), SHH (100 ng/ml), CHIR (3 µM).
Day 11-12	NB/B27, CHIR (3 µM), BDNF (20 ng/ml), AA (0.2 mM), GDNF (20 ng/ml), cAMP (1 mM), TGFB3 (1 ng/ml), DAPT (10 µM).
Day 13+	NB/B27 with BDNF (20 ng/ml), AA (0.2 mM), GDNF (20 ng/ml), cAMP (1 mM), TGFB3 (1 ng/ml), DAPT (10 µM).
Day 21	Dissociate using Accutase and passage 1:1 onto poly-L-ornithine/fibronectin/laminin-coated dishes.
Base Media Composition	
SRM Media	Contains Knockout DMEM, Knockout Serum Replacement (18%), L-glutamine (1%), MEM NEAA (1%), and 2-mercaptoethanol (0.1%).
N2 Media	Contains Neurobasal media, L-glutamine (1%), N2 supplement (1%), and penicillin/streptomycin (1%).
NB/B27 Media	Contains Neurobasal media, B27 supplement (2%), and penicillin/streptomycin (1%).

Table A.3 mDA neuron differentiation protocol. Protocol and media compositions used for the differentiation of iPSCs to mDA neurons.

Antibody	Manufacturer	Catalog Reference
Oct3/4 (primary)	Santa Cruz	SC5279
TRA-1-60 (primary)	Merck	MAB4360
TH (primary)	Merck	AB152
MAP2 (primary)	Merck	MAB3418
LMX1A (primary)	Abcam	ab139726
OxPhos Human WB Antibody Cocktail (primary)	Abcam	ab110411
Anti-mouse 647 (secondary)	Invitrogen	A21235
Anti-mouse 488 (secondary)	Invitrogen	A21202
Anti-rabbit 488 (secondary)	Invitrogen	A32790
Anti-rat 568 (secondary)	Invitrogen	A78946
Anti-rabbit 647 (secondary)	Invitrogen	A21244
DyLight 680 (secondary)	Thermo	5366P
DyLight 800 (secondary)	Thermo	5257P
DAPI	Sigma	D9542

Table A.4 Primary & secondary antibodies. Antibodies used for immunohistochemistry, flow cytometry, and western blot analysis, including their manufacturers and catalog references.

Gene of Interest	Primer Sequence
MAP2	Forward: CAGGTGGCGGACGTGTGAAAATTGAGAGTG Reverse: CACGCTGGATCTGCCTGGGGACTGTG
TH	Forward: GGAAATTGAGAAGCTGTCCACG Reverse: GAATCTCAGGCTCCTCAGACAG
LMX1A	Forward: GCTCAGAGCAGTTCAGAGGG Reverse: CAAGCAGGAGTTTGCCCAAC
SNCA	Forward: AGAGGGTGTTCTCTATGTAGGCT Reverse: ACCCTTCCTCAGAAGGCATTT
GFAP	Forward: GAGATCCGCACGCAGTATGA Reverse: TCTGCAAACTTGGAGCGGTA
L27	Forward: CTGGTGCGGAAATTGAC Reverse: AGATGGACACTTGGTGGGC
ACTB	Forward: CGAGGACTTTGATTGCACAT Reverse: TGCGGTGCTTTTTAGGAGTG

Table A.5 Primer sequences. Forward and reverse primer sequences used for the qPCR analysis.

Parameter	Description
Non-mitochondrial Oxygen Consumption	Minimum rate measurement after Rotenone/Antimycin A injection
Basal Respiration	(Last rate measurement before first injection) – (Non-Mitochondrial Respiration Rate)
Maximal Respiration	(Maximum rate measurement after FCCP injection) – (Non-Mitochondrial Respiration)
H+ (Proton) Leak	(Minimum rate measurement after Oligomycin injection) – (Non-Mitochondrial Respiration)
ATP Production	(Last rate measurement before Oligomycin injection) – (Minimum rate measurement after Oligomycin injection)
Spare Respiratory Capacity	(Maximal Respiration) – (Basal Respiration)
Spare Respiratory Capacity as a %	(Maximal Respiration) / (Basal Respiration) × 100
Acute Response	(Last rate measurement before Oligomycin injection) – (Last rate measurement before acute injection)
Coupling Efficiency	(ATP Production Rate) / (Basal Respiration Rate) × 100

Table A.6 Seahorse parameters. Calculations used to determine mitochondrial respiration parameters based off measurements obtained from the Seahorse metabolic assay.

Day	Condition	% mt st min	% mt st max	% rb st min	% rb st max	nFeature st min	nFeature st max	nCount st min	nCount st max	% mt min	% mt max	% rb min	% rb max
0	A53T	-2	2	-2	2	-1	2	-2	1	0	100000	0	100000
0	CTL	-2	2	-2	2	-1	2	-2	1	0	100000	0	100000
6	A53T	-2	2	-2	2	-1	2	-2	1	0	100000	0	100000
6	CTL	-2	2	-2	2	-1	2	-2	1	0	100000	0	100000
15	A53T	-2	2	-2	2	-1	2	-2	1	0	100000	0	100000
15	CTL	-2	2	-2	2	-1	2	-2	1	0	100000	0	100000
21	A53T	-2	2	-2	2	-1	2	-2	1	0	100000	0	100000
21	CTL	-2	2	-2	2	-1	2	-2	1	0	100000	0	100000
30	A53T	-2	2	-2	2	-1	2	-2	1	0	100000	0	100000
30	CTL	-2	2	-2	2	-1	2	-2	1	0	100000	0	100000
40	A53T	-2	2	-2	2	-1	2	-2	1	0	100000	0	100000
40	CTL	-2	2	-2	2	-1	2	-2	1	0	100000	0	100000
60	A53T	-2	2	-2	2	-1	2	-2	1	0	100000	0	100000
60	CTL	-2	2	-2	2	-1	2	-2	1	0	100000	0	100000

Table A.7 scRNA-seq parameters. Parameters used for the filtering of the scRNA-seq data.

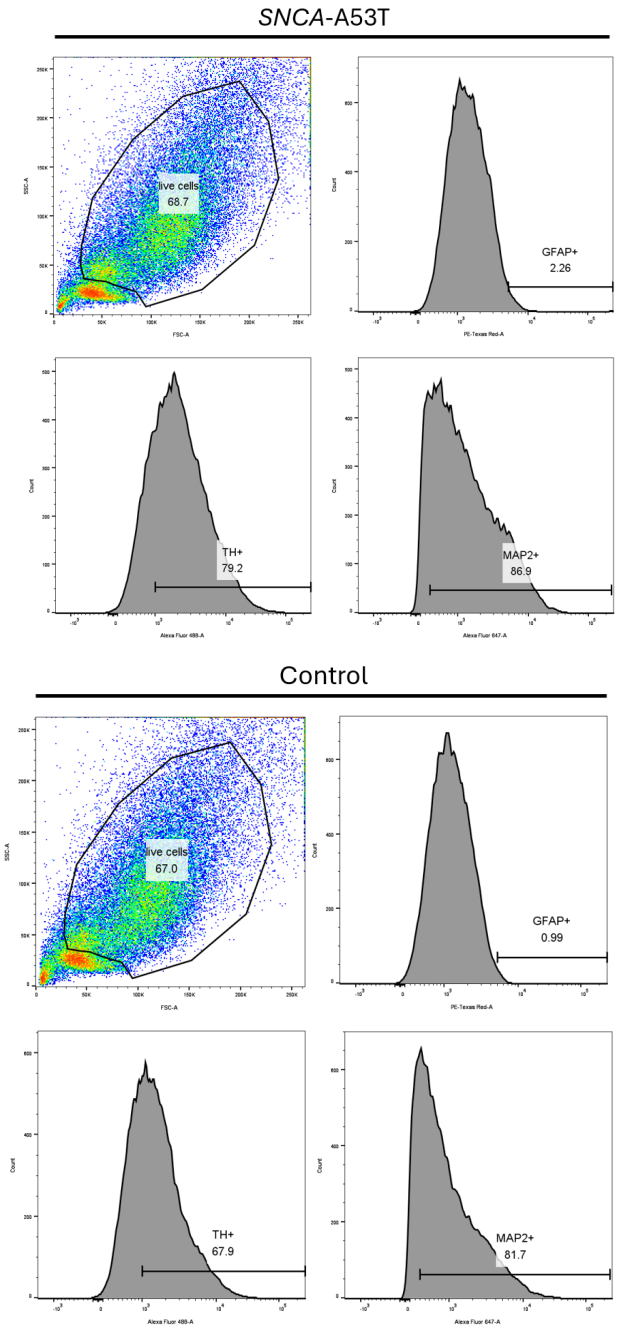

Fig. A.2 Flow cytometry analysis. Selection criteria and gating used to determine the percentage of TH, MAP2, and GFAP positive cells at day 50 in *SNCA*-A53T and control cell populations.

Timepoint	Enrichment term	Associated genes
Day 0	Parkinson's Disease	*ATP5F1D, COX7A2, COX7B, COX7C, COX8A, HSPA5, COX2, MT-ND1, MT-ND4, MT-ND4L, MT-ND5, MT-ND6, NDUFA1, NDUFA3, NDUFC2, NDUFS8, PSMB3, UQCRB, UQCR11, ADRM1, NDUFA13, NDUFA11*
Day 6	Parkinson's Disease	*ATF4, ATP5F1E, CALM1, CALM2, COX7A2, ATP8, COX1, COX2, MT-ND1, MT-ND2, MT-ND3, MT-ND4, MT-ND4L, MT-ND5, MT-ND6, NDUFB1, NDUFC2, NDUFS2, PSMA4, PSMA6, PSMA7, PSMB3, PSMD8, UBA52, SEM1, TUBA1B*
Day 15	Parkinson's Disease	*COX7A2, ATP6, COX2, COX3, MT-ND2, MT-ND3, MT-ND5, TUBA1A, SLC39A8*
Day 21	Parkinson's Disease	*ATP5F1D, ATP5MC2, ATP5MC3, COX7C, KIF5C, MAPT, CYTB, MT-ND2, MT-ND3, MT-ND5, NDUFA4, NDUFS8, PSMA3, PSMB4, SLC18A1, SOD1, TH, TXN, UBA52, UQCRB, UQCRH, XBP1, TUBA1A, COX5A, TXN2, NDUFA13, UBE2J1, SLC39A8, TUBB2B*
Day 30	Parkinson's Disease	*SLC25A5, ATP5MC2, CALM1, CALM2, CAMK2B, CAMK2D, COX5B, COX6B1, GNAI1, GNAI2, GNAL, HSPA5, KIF5A, KIF5C, KLC1, MAPT, MT-ND3, MT-ND4L, NDUFA1, NDUFA2, NDUFA7, NDUFB5, NDUFC2, PRKACB, PSMA1, SNCA, TUBB2A, UBA52, UBA1, UQCRB, UQCRH, VDAC1, XBP1, TUBA1A, SEM1, UQCR11, UQCRQ, NDUFA13, SLC39A8, TUBA1C, NDUFA11, TUBB, TUBB2B*
Day 60	Parkinson's Disease	*ATP5MC3, CALM1, CYTB, MT-ND3, MT-ND5, SNCA, TUBB2A, UCHL1, TUBA1A, TUBB2B*

Table A.8 PD genes. Genes identified in the PD annotations from the DEG enrichment analyses.

Timepoint	Enrichment term	Associated proteins
Day 0	Parkinson's Disease	SLC25A6, ATP5F1E, COX1, SLC11A2, PSMC5, VDAC2, ATP5PD, TUBB6
Day 6	Parkinson's Disease	SLC25A6, ATP5F1B, BAX, CAMK2B, COX7A2, ND2, NDUFA4, NDUFAB1, NDUFB1, NDUFB5, PSMA2, PSMA7, RPS27A, SDHB, UBA1, UQCRB, UQCRFS1, COX5A, TUBB3, CYCS, NDUFA4L2, TUBAL3, TUBB6
Day 15	Parkinson's Disease	ATP5F1E, COX7C, KLC1, COX1, ND1, PRKACB, PSMC1, UBE2G2, VDAC1, VDAC2, ATP5PD
Day 21	Parkinson's Disease	ATP5F1B, COX4I1, KIF5C, COX1, CYTB, PSMB1, PSMB3, PSMC1, PSMC5, TUBB4B, UQCR11
Day 30	Parkinson's Disease	ATP5F1E, CAMK2B, KIF5C, MAOB, CYTB, ND1, NDUFB5, NDUFC2, PSMC5, SDHC, SDHD, SNCA, TUBB2A, UQCRB, UQCRFS1, VDAC1, VDAC2, SLC39A6, TUBB6, TUBA3E
Day 40	Parkinson's Disease	SLC25A5, ATP5F1A, ATP5F1B, ATP5F1D, ATP5F1E, GNAI2, GNAI3, GNAL, GNAS, HSPA5, KLC1, ATP6, COX1, NDUFA4, NDUFB1, NDUFB5, NDUFB7, PSMA2, PSMA6, PSMB3, PSMC1, TUBA4A, TUBB2A, UBA1, VDAC2, VDAC3, SLC39A7, TUBB4A, TUBB4B, TUBB6, TUBB, TUBB2B
Day 60	Parkinson's Disease	ATP5F1E, GNAI1, MAPT, COX1, NDUFB5, SDHC, UBA1, VDAC1, VDAC2, VDAC3, ADRM1, SLC39A6

Table A.9 PD proteins. Proteins identified in the PD annotations from the DAP enrichment analyses.

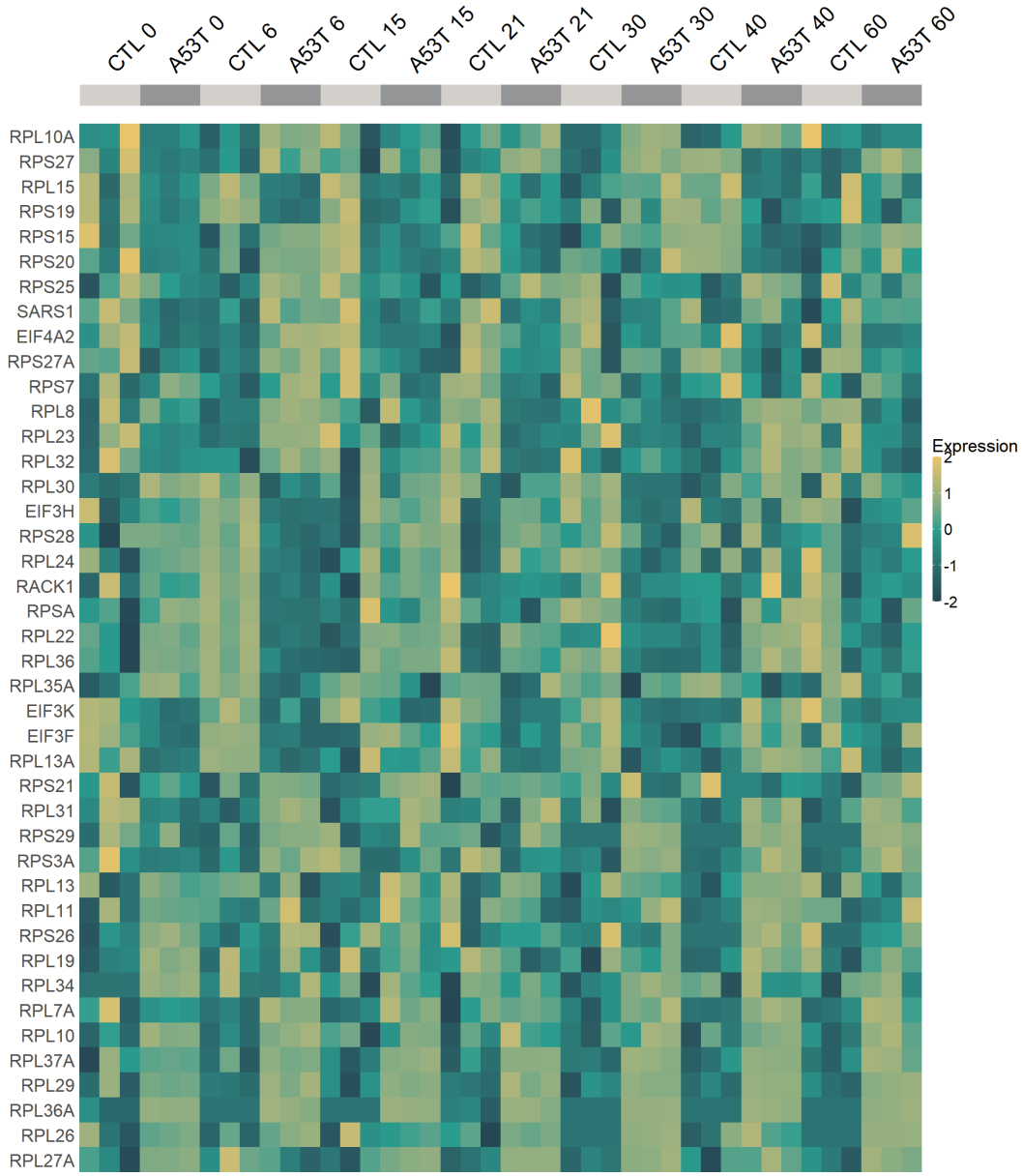

Fig. A.3 Ribosomal proteins. Heatmap showing ribosomal proteins dysregulated between *SNCA*-A53T and control cells at multiple timepoints of the differentiation ($p_{\text{adj}} < 0.05$ and |FC|>1). Colors correlate to normalized counts (z-score, centered, and scaled) of the indicated proteins.

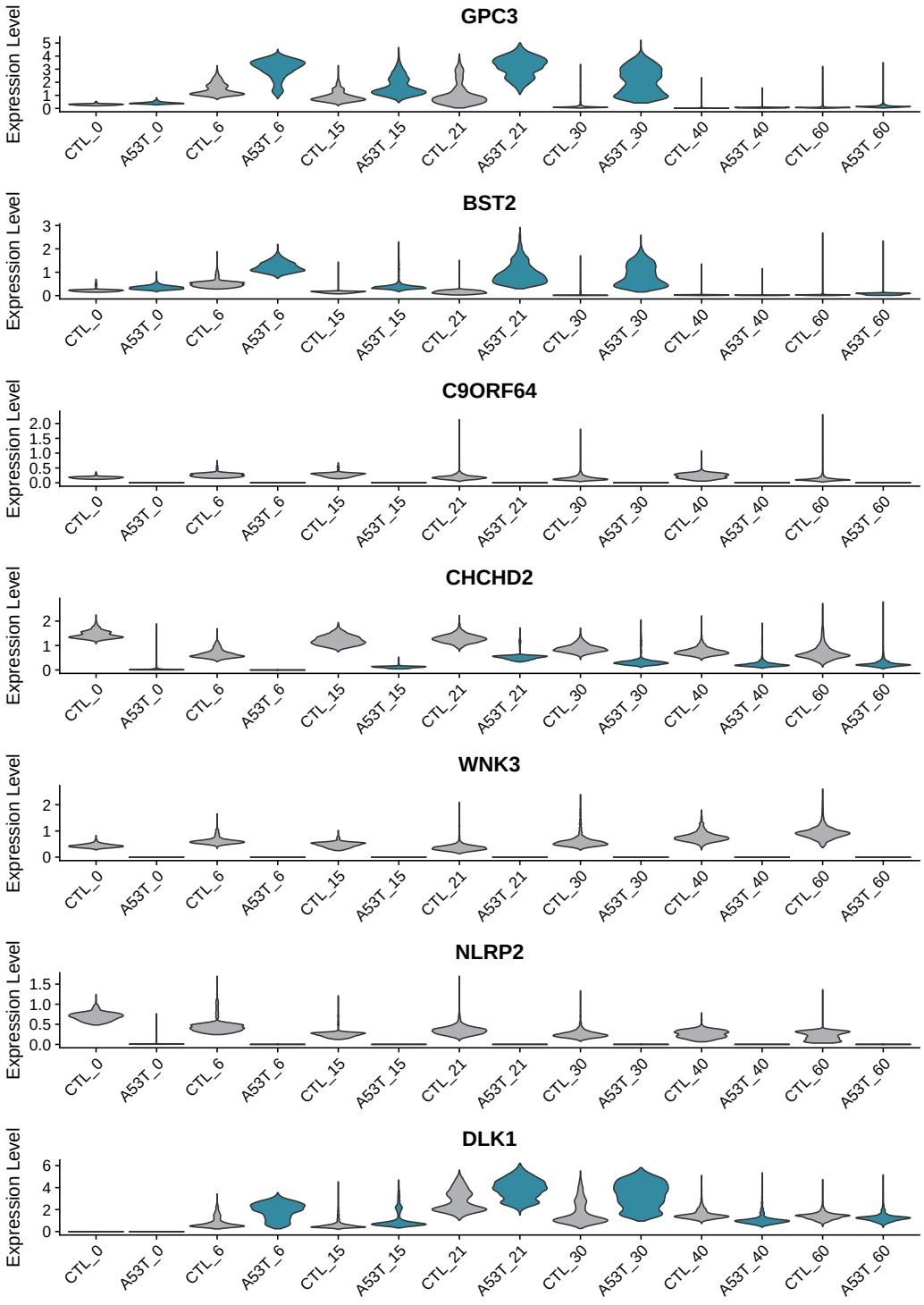

Fig. A.4 Core dysregulated genes. Violin plots depicting the most strongly dysregulated genes in *SNCA*-A53T cells compared to controls ($p_{\text{adj}} < 0.05$ and |FC|>0.4), whose corresponding proteins were also significantly dysregulated. Note, C9ORF64 is the alternate name for QNG1).

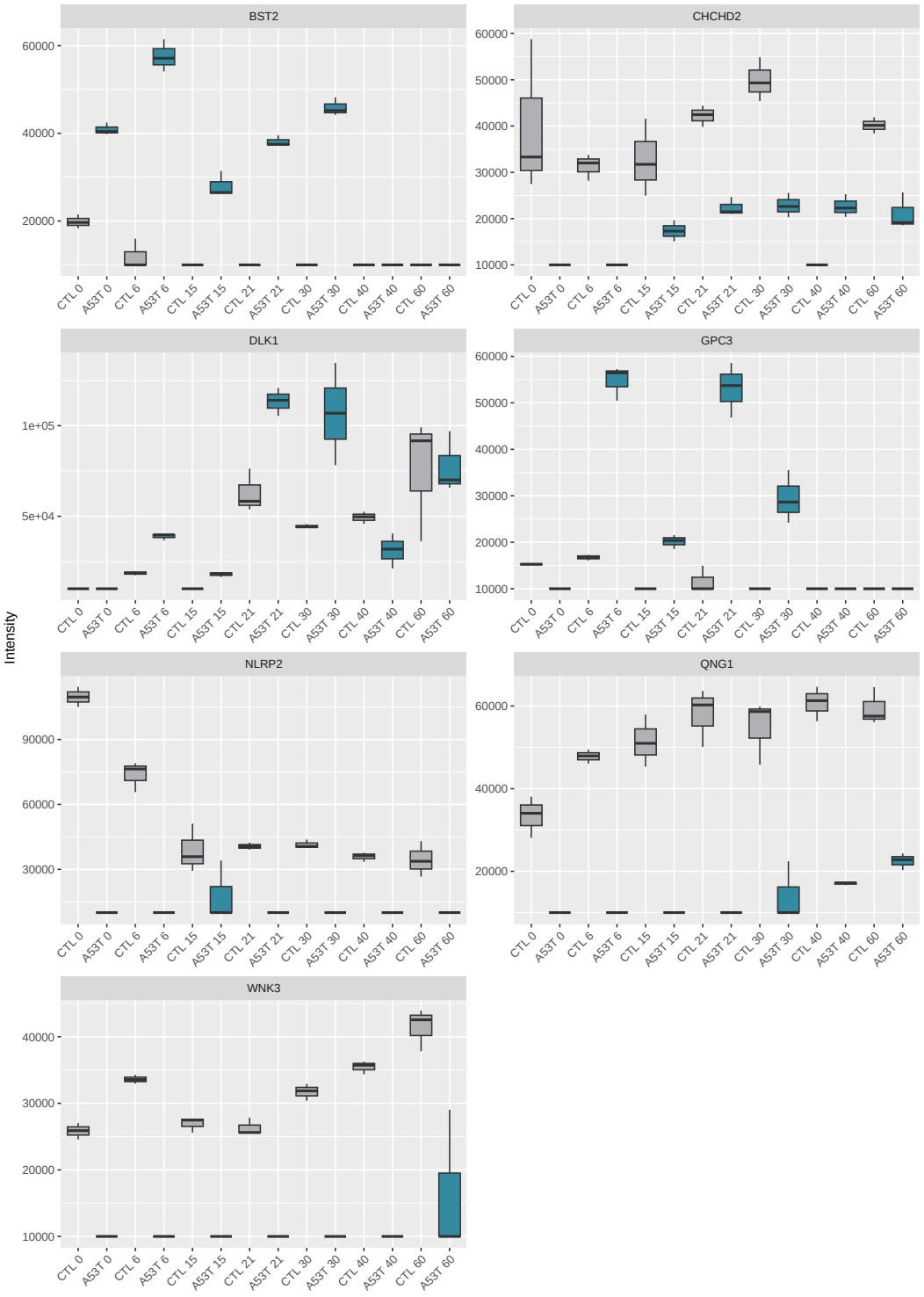

Fig. A.5 Core dysregulated proteins. Violin plots depicting the most strongly dysregulated proteins in *SNCA*-A53T cells compared to controls ($p_{\text{adj}} < 0.05$ and |FC|>1), whose corresponding genes were also significantly dysregulated.

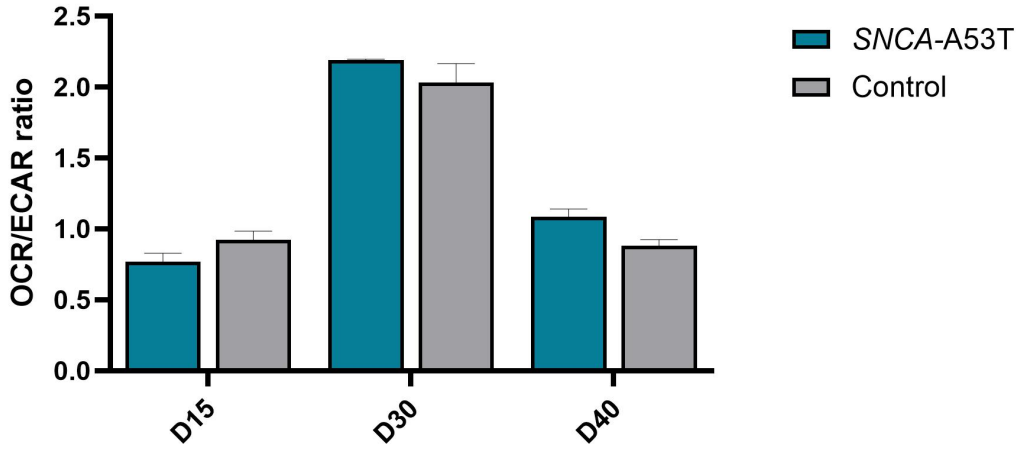

Fig. A.6 OCR/ECAR ratio. Ratio of OCR (mitochondrial metabolism) and ECAR (glycolysis) at days 15, 30, and 40 of the differentiation (N=3, mean ± SD).

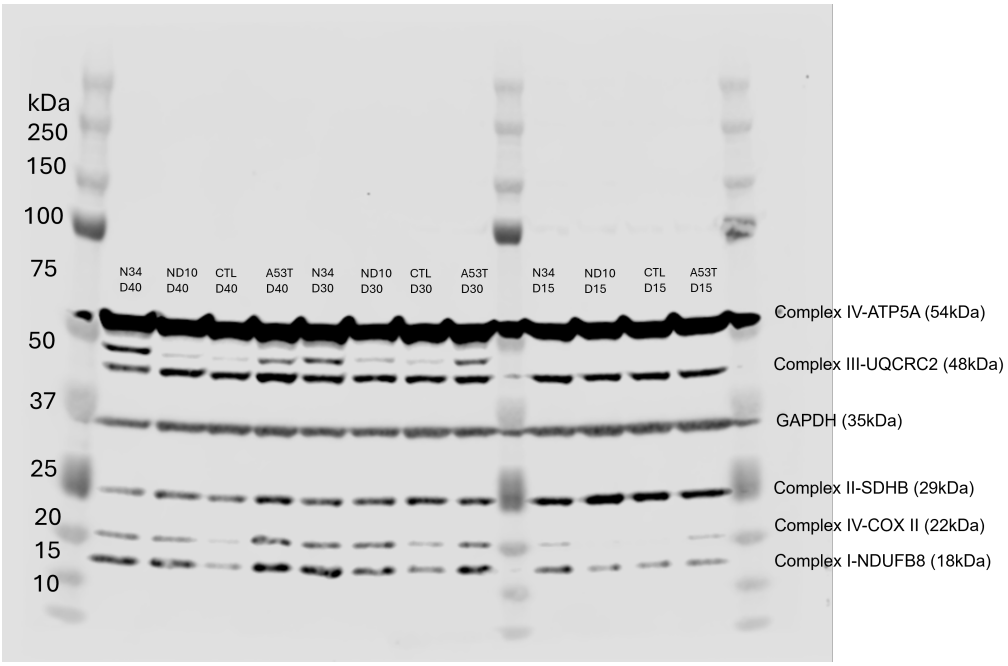

Fig. A.7 Complete western blot. Complete membrane for the western blot analysis of OXPHOS subunits and GAPDH. Note that ND10 and ND34 samples are not relevant for the present study.

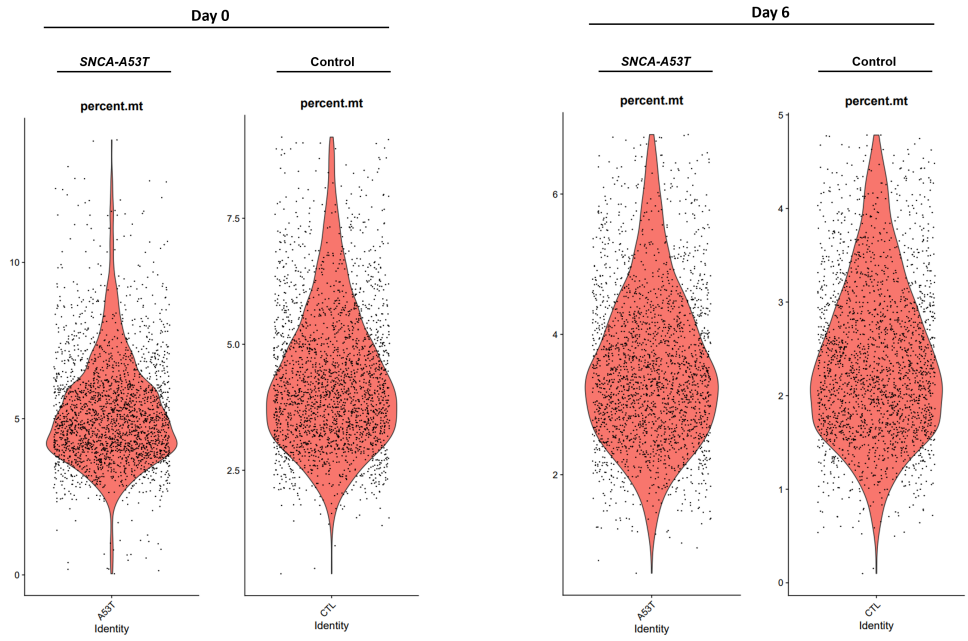

Fig. A.8 Percentage of mitochondrial transcripts. Violin plots showing a higher percentage of mitochondrial transcripts expressed in *SNCA*-A53T cells compared to control cells at days 0 and 6 of the differentiation.

A.1 Differentially expressed genes

DEGs identified at each timepoint of the differentiation ($p_{\text{adj}} < 0.05$ and |FC|>0.4). Fold changes are indicated in parentheses.

DAY 0

HSPA8 (+1.26), MT.ND6 (+1.15), BEX3 (+1.07), HMGB1P5 (+0.93), ENSG00000237550 (+0.89), MT.RNR1 (+0.88), MT.ND1 (+0.80), TCEAL9 (+0.79), GGCT (+0.75), BEX2 (+0.74), PUS7L (+0.72), MT.ND4L (+0.69), VCAN (+0.68), TCEAL8 (+0.68), CD24 (+0.67), TDGF1 (+0.65), NPM1 (+0.63), SRP14 (+0.62), FEZ1 (+0.61), SNHG17 (+0.61), TCEAL5 (+0.60), CYP51A1 (+0.60), GPC4 (+0.59), AASS (+0.58), SNRPG (+0.57), EI24 (+0.57), MT1G (+0.57), MT.CO2 (+0.57), MAT2A (+0.57), NDUFA1 (+0.56), DNAJA1 (+0.54), SKP1 (+0.53), MORF4L2 (+0.53), SKIL (+0.53), USP9X (+0.52), PSMD10 (+0.52), ID1 (+0.52), PGAM1 (+0.52), VIM (+0.51), MT1X (+0.51), IFITM3 (+0.51), RBM41 (+0.50), TOMM7 (+0.50), EEF1A1 (+0.50), ACSL4 (+0.49), POLA1 (+0.47), MT1H (+0.47), COX7B (+0.47), COX7C (+0.46), NME2 (+0.45), SNHG5 (+0.44), GJA1 (+0.43), TRIM24 (+0.43), PRPS1 (+0.43), DDX25 (+0.43), MT.RNR2 (+0.42), SNRPF (+0.42), SCGB3A2 (+0.42), IFITM1 (+0.42), CHEK1 (+0.42), ATP5MK (+0.42), PDHB (+0.41), UBE2V1 (+0.41), EPCAM (+0.41), HSPA5 (+0.40), ZNF880 (+0.40), UQCRB (+0.40), ACTG1 (+0.40), CBX3 (+0.40), GNB2 (-0.40), IGFBP2 (-0.40), NDUFC2 (-0.40), CCDC144NL.AS1 (-0.40), POLR2H (-0.40), MLF1 (-0.40), HMGB2 (-0.40), MTRFR (-0.41), DGUOK (-0.41), HLA.C (-0.41), CFL1 (-0.41), CKB (-0.41), KCNQ2 (-0.41), ANKRD12 (-0.41), ENSG00000254277 (-0.41), ADM (-0.41), SNHG3 (-0.41), ADRM1 (-0.42), KMT2A (-0.42), SNRNP70 (-0.42), DARS1 (-0.42), NPM3 (-0.42), CKS1B (-0.43), MTCO1P40 (-0.43), H1.10 (-0.43), WASF2 (-0.43), COX8A (-0.43), ENSG00000291130 (-0.43), C1ORF35 (-0.43), CHGA (-0.43), TPI1 (-0.43), NOP53 (-0.44), NACA (-0.44), NR6A1 (-0.44), SRM (-0.44), HMGA1 (-0.44), EML4 (-0.44), EDF1 (-0.44), FGFBP3 (-0.45), SEPTIN10 (-0.45), PNPLA4 (-0.45), NDUFA3 (-0.45), MT.ND5 (-0.45), HNRNPA1 (-0.45), SQLE (-0.45), ATP5F1D (-0.45), ANAPC11 (-0.46), COX7A2 (-0.46), PHF5A (-0.46), PPP1CA (-0.46), DUSP6 (-0.46), SMIM20 (-0.46), SELENOH (-0.46), LSM7 (-0.47), SRRM1 (-0.47), CCDC137 (-0.47), H1.2 (-0.48), BIRC5 (-0.48), NDUFA11 (-0.48), YBX1 (-0.48), H1.0 (-0.48), HMGN2 (-0.48), ARGLU1 (-0.49), CRABP1 (-0.49), APRT (-0.50), POLR2L (-0.50), YBX3 (-0.50), MPST (-0.50), VASP (-0.50), BCL2L12 (-0.50), IQGAP2 (-0.50), UBXN1 (-0.50), TRAPPC1 (-0.50), SC5D (-0.50), VKORC1 (-0.50), HLA.A (-0.51), KIF1A (-0.51), CYB5A (-0.51), APOBEC3C (-0.51), HMGN1 (-0.51), PKM (-0.51), LDHA (-0.52), MRPS34 (-0.52), PIH1D1 (-0.52), CAPZB (-0.53), RALBP1 (-0.53), INPP5F (-0.53), FADS2 (-0.53), POLR2I (-0.53), CNPY2 (-0.54), C4ORF3 (-0.54), SCAND1 (-0.54), ARL2 (-0.54), PNRC1 (-0.54), PPP2R1A (-0.55), DAZAP1 (-0.55), MARCKS (-0.55), POLR2E (-0.55), MRPL52 (-0.55), UQCR11 (-0.55), TMSB4X (-0.56), AP2S1 (-0.56), SH3BGRL3 (-0.56), PPP4C (-0.58), LINC01013 (-0.58), PHPT1 (-0.58), CYBA (-0.59), ENSG00000248605 (-0.59), CSNK2B (-0.60), WNK3 (-0.62), MRPL41 (-0.62), GAPDH (-0.63), MIF (-0.63), GABPB1.AS1 (-0.64), PGK1 (-0.64), S100A11 (-0.64), ENSG00000213058 (-0.64), H1.3 (-0.64), DRAP1 (-0.64), RARRES2 (-0.65), ENO1 (-0.65), SFRP2 (-0.66), EEF2 (-0.66), NDUFS8 (-0.66), ENSG00000289287 (-0.67), PKIB (-0.68), EIF4EBP1 (-0.69), PHB1 (-0.69), TMSB10 (-0.69), RRBP1 (-0.69), PSMB3 (-0.69), EDNRB (-0.70), RABAC1 (-0.70), ENSG00000289479 (-0.71), GAS5 (-0.72), HES1 (-0.73), PPDPF (-0.73), BNIP3L (-0.76), HSPB1 (-0.77), ATP5MG (-0.79), CLDN6 (-0.79), NDUFA13 (-0.80), APOE (-0.81), H1.4 (-0.82), GPX4 (-0.82), PFN1 (-0.86), NLRP2 (-0.97), MT.ND4 (-0.97), MDK (-1.00), FAM162A (-1.03), H1.1 (-1.03), SFRP1 (-1.22), DDIT4 (-1.26), LINC00551 (-1.37), DNAJC15 (-1.41), BNIP3 (-1.42), CHCHD2 (-1.88)

DAY 6

GPC3 (+2.35), MTATP6P1 (+1.83), DLK1 (+1.63), CAPN6 (+1.33), ENSG00000237550 (+1.32), MIF (+1.30), MT.ND1 (+1.26), IFITM3 (+1.26), LHX5.AS1 (+1.23), APOE (+1.20), MT.ND4L (+1.16), EPCAM (+1.10), BST2 (+1.09), MIAT (+1.05), H3.3A (+1.02), FTL (+1.02), FZD5 (+0.98), MT.ND5 (+0.97), PMEL (+0.95), XACT (+0.95), MT.CO2 (+0.94), NME2 (+0.91), SFRP2 (+0.90), EEF1A1 (+0.90), MIR302CHG (+0.90), MTND2P28 (+0.89), LMAN1 (+0.86), TNNT1 (+0.86), MT.ATP8 (+0.85), IFITM1 (+0.85), SIX6 (+0.85), GAPDH (+0.83), CRABP2 (+0.82), PGAM1 (+0.79), SOX3 (+0.79), L1TD1 (+0.78), TCF7L2 (+0.77), MT.ND2 (+0.77), NPM1 (+0.76), TCEAL5 (+0.76), TCEAL8 (+0.75), BEX3 (+0.73), UBE2V1 (+0.73), FIRRE (+0.73), MT.ND6 (+0.72), PRSS23 (+0.72), TNNI3 (+0.71), BEX2 (+0.71), FEZF2 (+0.71), EIF3L (+0.70), SELENOP (+0.70), ANXA2 (+0.70), EIF3F (+0.69), MT.CO1 (+0.68), PUS7L (+0.68), ZNF506 (+0.67), HESX1 (+0.67), FRZB (+0.66), DCX (+0.65), ENSG00000291100 (+0.64), DCAF8 (+0.63), SNHG29 (+0.63), SNHG32 (+0.63), MT.ND3 (+0.63), C6ORF141 (+0.63), S100A6 (+0.62), PPIA (+0.61), ZNF436.AS1 (+0.61), MT.RNR1 (+0.61), ZNF714 (+0.60), WFDC2 (+0.60), NGRN (+0.60), NPC2 (+0.59), LGALS1 (+0.58), CAVIN1 (+0.58), IFITM2 (+0.58), GGCT (+0.58), ACSL4 (+0.57), TCEAL3 (+0.57), SFRP1 (+0.56), TSTD1 (+0.56), ROBO2 (+0.56), SHISA2 (+0.56), SNHG17 (+0.56), EEF1B2 (+0.56), EPB41L4A.AS1 (+0.55), CHCHD10 (+0.55), CCDC18.AS1 (+0.55), BTG1 (+0.55), PSMD10 (+0.55), SKP1 (+0.54), LINC01405 (+0.54), TCEAL9 (+0.54), PUS3 (+0.53), ZFAS1 (+0.53), ENO2 (+0.53), ENSG00000290596 (+0.53), RBM41 (+0.53), PLP1 (+0.53), ARFGEF3 (+0.53), DMKN (+0.53), SYT11 (+0.53), HSPA8 (+0.52), KRT8 (+0.52), MAF (+0.52), H1.0 (+0.52), ENO3 (+0.51), HIGD2A (+0.51), PSMB3 (+0.51), SIX3 (+0.51), MRPS5 (+0.50), MORF4L2 (+0.50), CA11 (+0.50), PSMA6 (+0.50), DHRS7 (+0.50), PGK1 (+0.50), STX3 (+0.49), MAP7 (+0.49), APLP2 (+0.49), PDLIM1 (+0.49), MEA1 (+0.48), NAV1 (+0.48), FAM153CP (+0.48), UBA52 (+0.48), FAM199X (+0.48), ECHDC2 (+0.48), PAX8.AS1 (+0.48), BLVRB (+0.48), SEMA6A (+0.47), LIMCH1 (+0.47), TFF3 (+0.47), TSPYL2 (+0.47), GAS5 (+0.47), PHB1 (+0.47), SNHG8 (+0.47), NDUFS2 (+0.46), ECH1 (+0.46), EZR (+0.46), EIF3D (+0.46), SPINT2 (+0.46), ZNF880 (+0.46), ESRG (+0.46), KIZ (+0.46), TIMM10 (+0.46), C14ORF39 (+0.45), KRT19 (+0.45), ERMN (+0.45), SRPRA (+0.45), LRRC75A (+0.45), KIF1A (+0.45), CLDN6 (+0.44), PLAAT3 (+0.44), COL4A5 (+0.44), SMIM24 (+0.44), KRT18 (+0.44), HMGB1P5 (+0.44), SESN3 (+0.44), MEG3 (+0.44), ATF4 (+0.43), KRTCAP2 (+0.43), MAPKAPK5.AS1 (+0.43), VWDE (+0.43), PRPS1 (+0.43), CSNK2A1 (+0.43), LINC00173 (+0.43),

RCAN3 (+0.43), KDM5B (+0.43), PDK3 (+0.43), VPS4A (+0.42), IGBP1 (+0.42), ILF3.DT (+0.42), OTX2 (+0.42), PSMD8 (+0.41), GSC (+0.41), TXNIP (+0.41), ATP6V1F (+0.41), MT.ND4 (+0.41), UPP1 (+0.41), USP11 (+0.41), PAFAH1B3 (+0.41), ENSG00000283041 (+0.41), IGSF1 (+0.41), CDH1 (+0.41), TALAM1 (+0.41), ABCA1 (+0.41), RAD23A (+0.40), RNF213 (+0.40), MRPL52 (+0.40), ALKBH7 (+0.40), FOXRED1 (+0.40), PRPF4B (-0.40), RBM8A (-0.40), MACROH2A1 (-0.40), DPYSL2 (-0.40), NDUFB1 (-0.40), POLR2L (-0.40), G3BP1 (-0.40), SNRPF (-0.40), DENR (-0.40), CCDC80 (-0.40), VCAN (-0.41), FOXB1 (-0.41), STON2 (-0.41), HSBP1 (-0.41), RSRC2 (-0.41), NAALAD2 (-0.41), AASS (-0.41), SLC25A24 (-0.41), KHDRBS1 (-0.41), ALCAM (-0.41), DDX5 (-0.41), PAICS (-0.41), SENP6 (-0.41), SNRPD1 (-0.41), C6ORF118 (-0.42), THOC2 (-0.42), NRIP1 (-0.42), RPGR (-0.42), EIF3J (-0.42), SYT4 (-0.42), SRSF11 (-0.42), STMN1 (-0.42), HNRNPU (-0.42), BRCA2 (-0.43), PEG10 (-0.43), NUCB2 (-0.43), YBX3 (-0.43), PHLDB2 (-0.43), HP1BP3 (-0.43), CHD7 (-0.43), TGFB2 (-0.43), EIF4G3 (-0.43), ITGB1 (-0.44), SUPT16H (-0.44), LARP7 (-0.44), SLF1 (-0.44), IFT81 (-0.44), IGF2BP1 (-0.44), PSIP1 (-0.44), CCAR1 (-0.44), HELLS (-0.44), BMP7 (-0.44), SRP9 (-0.44), RDX (-0.44), CEP162 (-0.45), YWHAE (-0.45), CDKN1C (-0.45), LINC02899 (-0.45), PRMT1 (-0.45), NIN (-0.45), DLGAP5 (-0.45), LARS1 (-0.45), SORL1 (-0.45), KLHL5 (-0.45), FLRT3 (-0.46), CLIP1 (-0.46), EZH2 (-0.46), CALM1 (-0.46), PSMA4 (-0.46), SEM1 (-0.46), KHSRP (-0.46), MYLK (-0.46), SMARCA5 (-0.46), SLIRP (-0.46), EXOC5 (-0.46), MDK (-0.46), LDB2 (-0.47), RBM25 (-0.47), SMARCC1 (-0.47), MAP1B (-0.47), SOX2 (-0.47), MLF1 (-0.47), KIF20B (-0.47), MT.TP (-0.47), LPAR4 (-0.47), STT3B (-0.47), HNRNPA2B1 (-0.47), TPR (-0.47), TSPAN6 (-0.47), CRNDE (-0.47), HNRNPA1 (-0.48), KMT2A (-0.48), PCLAF (-0.48), KPNB1 (-0.48), TIA1 (-0.48), DYNC2H1 (-0.48), COX7A2 (-0.48), INPP5F (-0.48), SRSF1 (-0.48), C11ORF58 (-0.48), HIPK2 (-0.48), ATRX (-0.49), PSAT1 (-0.49), TRIM4 (-0.49), TMSB15A (-0.49), GULP1 (-0.49), FZD7 (-0.49), CCDC34 (-0.49), TOP1 (-0.49), CENPH (-0.49), TEAD1 (-0.50), CHD1 (-0.50), RFX4 (-0.51), CDK6 (-0.52), H2AZ1 (-0.52), TUT4 (-0.52), ID3 (-0.52), RAN (-0.52), HMGN1 (-0.52), MICOS10 (-0.52), NCL (-0.52), ZFP36L1 (-0.52), NDUFC2 (-0.53), TPM4 (-0.53), MYH10 (-0.53), HSPE1 (-0.53), SLTM (-0.53), HNRNPH3 (-0.53), TLE4 (-0.53), HMGB2 (-0.54), SEPTIN2 (-0.54), KLHL4 (-0.54), FUS (-0.54), CBX3 (-0.55), PCM1 (-0.55), ATP5MF (-0.55), HNRNPA0 (-0.55), CETN2 (-0.55), RFX3 (-0.55), ENSG00000224114 (-0.56), FGFBP3 (-0.56), ANKRD11 (-0.56), PDIA6 (-0.56), CENPF (-0.56), ODC1 (-0.56), NPM1P27 (-0.56), SMC4 (-0.56), SUB1 (-0.57), HSPH1 (-0.58), NUCKS1 (-0.58), CCDC14 (-0.58), QKI (-0.59), DEK (-0.59), HLA.A (-0.59), CENPE (-0.59), HSP90B1 (-0.60), MTHFD2 (-0.60), MEST (-0.61), GABPB1.AS1 (-0.61), NES (-0.61), PRKDC (-0.61), ANP32B (-0.61), ADD3 (-0.61), FKBP3 (-0.61), NLRP2 (-0.63), VIM (-0.63), ARGLU1 (-0.63), H1.1 (-0.63), H1.3 (-0.63), PLAGL1 (-0.64), PSMA7 (-0.65), TFPI (-0.65), DNAJA1 (-0.65), NCALD (-0.65), TOP2B (-0.66), EIF2S2 (-0.66), ATP1A2 (-0.66), HNRNPD (-0.66), DDIT4 (-0.67), GCC2 (-0.67), KTN1 (-0.67), PLS3 (-0.67), SSB (-0.68), FILIP1L (-0.69), LIX1 (-0.69), SFPQ (-0.69), RGS2 (-0.69), GPM6B (-0.69), HSP90AA1 (-0.69), PFN1 (-0.70), TMSB4X (-0.70), NASP (-0.70), TTC3 (-0.72), SEPTIN11 (-0.73), BCAT1 (-0.73), H4C3 (-0.74), CEP290 (-0.74), PTMS (-0.74), SLIT2 (-0.75), ATP5F1E (-0.76), CALM2 (-0.76), IQGAP2 (-0.78), FZD3 (-0.80), CCDC88A (-0.80), TUBA1B (-0.80), EFNB2 (-0.81), LGI1 (-0.81), ENSG00000213058 (-0.82), CALD1 (-0.82), PLEKHH2 (-0.83), TPBG (-0.85), WNK3 (-0.87), CRABP1 (-0.91), HNRNPM (-0.91), LPAR6 (-0.94), WLS (-0.95), CHCHD2 (-0.95), WIF1 (-0.97), TPM2 (-0.99), ATP5MG (-1.01), ZNF503 (-1.09), CDH2 (-1.10), NR2F2 (-1.11), DNAJC15 (-1.12), SLC7A11 (-1.14), DUSP6 (-1.15), LINC00551 (-1.23), PRTG (-1.28), CPE (-1.29)

DAY 15

CRABP1 (+1.89), ENSG00000237550 (+1.43), GPC3 (+1.37), BEX3 (+1.11), DLK1 (+1.11), COL1A2 (+0.93), SYT11 (+0.91), BEX2 (+0.89), TFF3 (+0.88), TGFB2 (+0.87), MIAT (+0.85), TCEAL9 (+0.79), SNHG5 (+0.77), SCG2 (+0.73), FTL (+0.71), ENSG00000176320 (+0.70), PGK1 (+0.66), NEFM (+0.64), TCEAL8 (+0.63), IGFBP5 (+0.63), TCEAL5 (+0.62), CPE (+0.61), S100A6 (+0.61), TCEAL7 (+0.58), TALAM1 (+0.58), CRABP2 (+0.55), RGS2 (+0.55), PUS7L (+0.55), PAX8.AS1 (+0.54), MT.RNR1 (+0.53), IRS4 (+0.53), TMSB10 (+0.51), C4ORF48 (+0.51), MT.ND3 (+0.50), TCEAL3 (+0.50), TCEAL1 (+0.48), PCDH9 (+0.48), MT.ATP6 (+0.47), MORF4L2 (+0.47), TFPI2 (+0.47), ENSG00000259692 (+0.47), MT.CO3 (+0.47), PET100 (+0.46), MT.CO2 (+0.46), RBM41 (+0.46), COL4A6 (+0.46), LYPD1 (+0.46), ACSL4 (+0.46), MT.ND5 (+0.46), COL4A5 (+0.45), TUBA1A (+0.44), PPDPF (+0.44), PTMA (+0.44), DMD (+0.44), PRPS1 (+0.42), MT.ND2 (+0.41), FSIP2 (+0.41), PSMD10 (+0.40), SERPINF1 (+0.40), ATP5ME (+0.40), NEXN (-0.40), SSX2IP (-0.40), CADM1 (-0.40), CCDC80 (-0.41), PNRC1 (-0.41), BZW1 (-0.42), MAGI1 (-0.42), SPON1 (-0.42), GALNT7 (-0.42), PCDHB2 (-0.42), INPP5F (-0.43), NR3C1 (-0.43), ID2 (-0.43), MAP2 (-0.43), RESF1 (-0.44), ARHGAP5 (-0.44), CCDC144NL.AS1 (-0.44), KMT2A (-0.45), LINC02899 (-0.45), KCNJ16 (-0.46), MYO1B (-0.46), IQGAP2 (-0.48), PIEZO2 (-0.49), TRIM4 (-0.50), COX7A2 (-0.50), GOLGA6L2 (-0.51), PHYH (-0.51), SLC39A8 (-0.51), LGI1 (-0.51), UBE4A (-0.53), MAMDC2 (-0.54), FHL1 (-0.54), MLF1 (-0.57), DSP (-0.60), ALCAM (-0.63), PDE5A (-0.65), H1.3 (-0.66), EGLN3 (-0.67), ATP5MG (-0.67), WNK3 (-0.68), RORA (-0.74), GPRIN3 (-0.75), LINC00551 (-0.82), CALD1 (-0.87), ADAMTS9 (-0.92), NEUROD1 (-0.96), NRCAM (-0.97), ENSG00000224114 (-0.99), TTR (-1.07), ENSG00000213058 (-1.17), DNAJC15 (-1.37), CHCHD2 (-1.52), XIST (-2.10)

DAY 21

GPC3 (+2.54), IGFBP3 (+2.20), LEFTY2 (+1.88), TBX3 (+1.75), HTR2C (+1.70), ENSG00000237550 (+1.60), CRABP2 (+1.42), BEX3 (+1.40), FGF10 (+1.37), DLK1 (+1.28), BST2 (+1.28), MGST1 (+1.20), PTH2 (+1.19), TCEAL5 (+1.19), VCAN (+1.14), SNHG5 (+1.10), ID4 (+1.07), FTL (+1.07), POMC (+1.07), SPARC (+1.04), CPE (+1.04), TGFB2 (+1.03), MDK (+1.01), IRS4 (+1.01), DIO2 (+0.99), GAS5 (+0.99), CA2 (+0.97), PCP4 (+0.97), MT.ND3 (+0.97), SYNPR (+0.97), TCEAL9 (+0.95), IFITM3 (+0.95), ITM2C (+0.95), PSMD10 (+0.94), EMX2 (+0.91), TTR (+0.90), PCSK1N (+0.88), SDC2 (+0.87), LIX1 (+0.86), TCEAL8 (+0.85), SLITRK6 (+0.85), FAU (+0.84), MT.ND2 (+0.83), PTPRZ1 (+0.83), CCND1 (+0.83), MORF4L2 (+0.82), UBA52 (+0.82), COL4A5 (+0.81), LMAN1 (+0.80), HSPB1 (+0.79), COL4A6 (+0.77), NKX2.1 (+0.77), CPNE8 (+0.76), TCEAL3 (+0.76), TXNIP (+0.74), DECR1 (+0.74), TPT1 (+0.74), SOX3 (+0.74), AKAP12 (+0.73), SESN3 (+0.72), NACA (+0.72), PLXNC1 (+0.71), MT.CYB (+0.71), GPX4 (+0.71), SYT11 (+0.71), FEZF2 (+0.70), MIF (+0.69), UQCRH (+0.69), RACK1 (+0.69), APLP2 (+0.67), ZFAS1 (+0.67), PDLIM3 (+0.65), CLU (+0.65), FGF18 (+0.64), TENT5A (+0.63), MTATP6P1 (+0.63), TXN (+0.62), NSA2 (+0.62), PDK4 (+0.62), CROT (+0.61), FGF3 (+0.61), SNHG6 (+0.60), EIF5A (+0.60), CNTN1 (+0.59), PCOLCE2 (+0.59), MTHFD2 (+0.59), TSC22D3 (+0.59), APOE (+0.59), MANF (+0.58), EIF2S3 (+0.58), MEF2C (+0.58), RBP1 (+0.58), SLITRK1 (+0.57), TCF7L2 (+0.57), ALDH7A1 (+0.57), PLD3 (+0.56), CREM (+0.56), ENO3 (+0.56), CALB1 (+0.56), KNOP1 (+0.56), SIX3 (+0.56), SSR4 (+0.55), CCDC160 (+0.55), MRPL52 (+0.55), ETV1 (+0.55), ING2 (+0.55), XACT (+0.55), C19ORF53 (+0.54), NAA38 (+0.54), CST3 (+0.54),

PGK1 (+0.54), NUCB2 (+0.54), TIMP1 (+0.54), BTG3 (+0.53), HSPA9 (+0.53), LARP7 (+0.53), MRPS6 (+0.52), SNHG32 (+0.52), TMEM14B (+0.52), SELENOP (+0.52), CWC15 (+0.52), SOD1 (+0.51), DRAP1 (+0.51), LDHB (+0.51), SNHG29 (+0.51), P3H4 (+0.51), PUS7L (+0.50), TRPM3 (+0.50), IFT57 (+0.50), BSG (+0.50), SERPINH1 (+0.50), PPIB (+0.50), TCEAL4 (+0.50), TBCA (+0.49), SPA17 (+0.49), EEF1B2 (+0.49), HNRNPC (+0.49), SMARCA1 (+0.49), UPF3A (+0.49), ATP5MC3 (+0.49), TCEAL1 (+0.48), PABPC1 (+0.48), CTSL (+0.48), COL11A1 (+0.48), HMGN2 (+0.48), NKAIN3 (+0.48), CCDC18.AS1 (+0.47), NDUFAF2 (+0.47), ATP6V0E1 (+0.47), ATP5F1D (+0.47), IMPACT (+0.47), ITM2B (+0.47), COX7C (+0.47), RSL1D1 (+0.46), SMIM30 (+0.46), TMSB10 (+0.46), ATP5MC2 (+0.46), KDELR1 (+0.46), SNRPD2 (+0.46), SCP2 (+0.45), RABAC1 (+0.45), KCNQ3 (+0.45), NPC2 (+0.45), COX5A (+0.45), TRAPPC1 (+0.45), NDUFA13 (+0.45), PSMA3 (+0.45), OPN3 (+0.44), ZNF506 (+0.44), LHX5.AS1 (+0.44), CUTA (+0.44), NOL7 (+0.44), MRPL1 (+0.44), RAD21 (+0.44), COL1A2 (+0.44), LYPD1 (+0.44), SNRNP27 (+0.43), TP53TG1 (+0.43), HADHA (+0.43), HNRNPH3 (+0.43), PRDX4 (+0.43), IFT74 (+0.43), LSM4 (+0.43), SSR3 (+0.43), IFITM2 (+0.43), SEC11A (+0.43), SELENOW (+0.43), PSAT1 (+0.43), FAM229B (+0.43), QPRT (+0.43), FRA10AC1 (+0.42), ECEL1 (+0.42), BMP4 (+0.42), ZNF593 (+0.42), CXCL14 (+0.42), NDUFA4 (+0.42), NCL (+0.42), HDAC1 (+0.42), PALMD (+0.42), ANP32B (+0.41), TXN2 (+0.41), DAD1 (+0.41), PSMB4 (+0.41), FKBP10 (+0.41), EIF1 (+0.41), NDUFS8 (+0.41), REST (+0.41), EIF2S2 (+0.41), PPP2R2A (+0.41), UBXN1 (+0.41), MRPS15 (+0.41), ELOB (+0.41), UQCRB (+0.41), PLIN2 (+0.41), PNRC2 (+0.41), HSPE1 (+0.41), BDH2 (+0.41), KHDRBS2 (+0.40), ZCRB1 (+0.40), CNPY2 (+0.40), BCAT1 (+0.40), MRPL13 (+0.40), ERP29 (+0.40), SYT13 (-0.40), USP9X (-0.41), LINC02899 (-0.41), FN1 (-0.41), RAB3B (-0.41), SIM1 (-0.41), ENSG00000286058 (-0.41), RAB3C (-0.41), NLRP2 (-0.41), POU2F1 (-0.41), NPAS3 (-0.42), KITLG (-0.42), POU2F2 (-0.42), HAPLN1 (-0.42), RIMKLA (-0.42), CXCR4 (-0.42), SHC2 (-0.43), NPL (-0.43), SPOCK1 (-0.43), LRP8 (-0.43), TNRC6B (-0.44), ENC1 (-0.45), SETBP1 (-0.45), ELOVL3 (-0.45), MAPT (-0.45), NRP1 (-0.45), PHC2 (-0.45), GADD45G (-0.46), GNG2 (-0.46), FAM13C (-0.46), PDGFD (-0.46), NSG2 (-0.47), FGD6 (-0.48), PTPRF (-0.48), NAV1 (-0.48), USP47 (-0.48), TMEM163 (-0.48), DPYSL5 (-0.48), DPYSL2 (-0.48), SAMD5 (-0.48), TH (-0.49), PCDHB2 (-0.49), GSE1 (-0.49), SOX21 (-0.49), ZEB2 (-0.49), HES6 (-0.49), FZD1 (-0.50), KIF21A (-0.50), SCN3A (-0.50), PLEKHA5 (-0.50), ANKRD36C (-0.50), CRACD (-0.51), NR4A2 (-0.51), SOX4 (-0.51), WNK3 (-0.51), GNAQ (-0.51), DOC2B (-0.51), PKIB (-0.51), NRG1 (-0.51), SRGAP3 (-0.51), PBRM1 (-0.52), PDZRN4 (-0.52), DYNC1H1 (-0.52), WNT5A (-0.52), UBE2J1 (-0.52), FRMD4A (-0.52), TULP4 (-0.53), NRSN1 (-0.53), SSX2IP (-0.53), ZNF441 (-0.53), SOX2.OT (-0.53), CHN2 (-0.54), DSP (-0.54), NEFL (-0.54), BTBD3 (-0.54), ZFHX4 (-0.54), PGM2L1 (-0.54), LINC02381 (-0.55), KIF1B (-0.55), GABPB1.AS1 (-0.55), MAP4K4 (-0.55), PUM2 (-0.55), EVL (-0.55), CASD1 (-0.56), PCSK2 (-0.56), CXADR (-0.56), SLK (-0.56), PIK3R1 (-0.57), MAP1B (-0.57), MAGI2 (-0.57), ZNF503 (-0.57), TLE4 (-0.57), H1.0 (-0.57), POU3F2 (-0.57), SLC16A9 (-0.58), CLASP2 (-0.58), BNIP3 (-0.58), MLLT11 (-0.58), LMO4 (-0.58), GRIK2 (-0.58), LMO3 (-0.59), CXXC4 (-0.59), SLC18A1 (-0.59), ZBTB20 (-0.59), DPYSL3 (-0.59), DIPK2A (-0.60), POU3F3 (-0.61), FREM2 (-0.61), NR3C1 (-0.61), CELF4 (-0.61), FSIP2 (-0.61), AUTS2 (-0.61), NR2F1 (-0.61), RGS2 (-0.62), F3 (-0.62), MIR124.2HG (-0.62), LINC00551 (-0.62), TUBB2B (-0.62), CADPS (-0.63), STMN1 (-0.63), MACF1 (-0.63), PCLO (-0.63), ASCL1 (-0.63), NPEPPS (-0.63), GRIA4 (-0.64), SATB1 (-0.64), NHLH2 (-0.64), TMTC4 (-0.65), ONECUT2 (-0.65), ARL4A (-0.65), TEAD1 (-0.65), CD24 (-0.66), DNAJC19 (-0.66), SOX11 (-0.66), FOXP1 (-0.67), PIEZO2 (-0.67), ZFHX3 (-0.67), RGS4 (-0.68), CADM1 (-0.68), KMT2A (-0.68), MYO1B (-0.68), RBFOX2 (-0.69), SMIM14 (-0.69), ATP5MG (-0.70), EBF3 (-0.70), NES (-0.70), ROBO2 (-0.70), ACSL3 (-0.70), NOS1AP (-0.70), STMN2 (-0.70), STMN4 (-0.71), PFN2 (-0.71), MIB1 (-0.71), ST18 (-0.71), SYT1 (-0.71), CORO1C (-0.72), PCBP4 (-0.72), CELF2 (-0.72), TAGLN3 (-0.72), GPM6A (-0.73), DST (-0.73), KIF5C (-0.74), TCF12 (-0.74), TFF3 (-0.74), DMRTA2 (-0.75), ENSG00000224114 (-0.75), EPHB2 (-0.75), INA (-0.75), SLC39A8 (-0.75), NBEA (-0.76), NEBL (-0.76), SLC17A6 (-0.76), PPP2R2B (-0.78), RTN4 (-0.78), TRPC5 (-0.80), NRCAM (-0.80), XBP1 (-0.81), CHD7 (-0.81), POSTN (-0.82), COL3A1 (-0.82), CADM2 (-0.83), BMP7 (-0.84), MAP2 (-0.84), ANK2 (-0.84), SRRM4 (-0.85), NIN (-0.85), PBX1 (-0.86), DNAJC15 (-0.86), CNTN4 (-0.89), ONECUT1 (-0.90), FBXW7 (-0.90), TUBA1A (-0.91), DLL1 (-0.95), EBF1 (-0.97), ALCAM (-0.97), VPS13C (-0.97), PITX2 (-0.99), SCG3 (-0.99), CRNDE (-0.99), CHCHD2 (-1.01), ENSG00000213058 (-1.01), NCAM1 (-1.03), CEMIP2 (-1.05), DCX (-1.05), FAT3 (-1.06), LMX1A (-1.06), KCNJ16 (-1.07), MAP6 (-1.08), FOXA2 (-1.09), ELAVL4 (-1.09), LINC00261 (-1.10), CACNA2D1 (-1.13), PTPRO (-1.16), SYT4 (-1.18), DDC (-1.24), GAP43 (-1.28), MIAT (-1.64)

DAY 30

IGFBP3 (+3.42), GPC3 (+3.26), TBX3 (+2.85), HTR2C (+2.75), PCP4 (+2.54), FGF10 (+2.48), PLXNC1 (+2.31), ENSG00000237550 (+2.12), DLK1 (+2.06), VCAN (+1.99), POMC (+1.96), EMX2 (+1.95), SDC2 (+1.78), MDK (+1.75), SPARC (+1.71), ZFP36L1 (+1.71), MGST1 (+1.67), XACT (+1.61), LHX2 (+1.58), SOX3 (+1.57), IGFBP2 (+1.52), LHX5.AS1 (+1.48), TGFB2 (+1.47), COL4A5 (+1.41), FEZF2 (+1.40), COL1A2 (+1.40), PTH2 (+1.40), ADAMTS9 (+1.39), BST2 (+1.38), IRS4 (+1.37), MEST (+1.37), MECOM (+1.37), TENT5A (+1.35), DIO2 (+1.34), ID4 (+1.31), CLU (+1.28), PTPRZ1 (+1.27), RBP1 (+1.27), COL4A6 (+1.26), SULF1 (+1.25), EFNA5 (+1.25), PLS3 (+1.25), LEFTY2 (+1.25), PRDX6 (+1.22), CDKN1C (+1.22), TTR (+1.21), TCEAL5 (+1.19), EMX2OS (+1.19), TCEAL9 (+1.16), SNHG5 (+1.15), CCND1 (+1.14), BTNL9 (+1.14), ID2 (+1.14), LIX1 (+1.12), NKAIN3 (+1.11), RBMS1 (+1.10), ITM2C (+1.09), TIMP1 (+1.09), GNB4 (+1.08), CALU (+1.07), TRH (+1.06), BEX3 (+1.04), FEZF1.AS1 (+1.03), COPG2IT1 (+1.02), FTL (+1.02), SLITRK6 (+1.02), HMGN3 (+1.01), SCUBE1 (+0.98), POLR2L (+0.98), FAM13A (+0.96), BDH2 (+0.95), SIX6 (+0.95), CST3 (+0.95), TCF4 (+0.95), SEPTIN6 (+0.94), CAMK2D (+0.94), NKX2.1 (+0.93), DECR1 (+0.93), AASS (+0.93), PTPRG (+0.93), SLITRK1 (+0.92), SYNPR (+0.92), ROMO1 (+0.91), REST (+0.90), NREP (+0.90), FGF18 (+0.90), P3H4 (+0.89), NPC2 (+0.89), ENSG00000270953 (+0.89), SERPINF1 (+0.89), SIX3 (+0.88), ATP6V0E1 (+0.88), PDLIM3 (+0.88), CPE (+0.87), LMAN1 (+0.87), FGFR1 (+0.87), HSPB1 (+0.85), ABAT (+0.85), GLI3 (+0.85), TBCA (+0.85), GLO1 (+0.85), ANXA5 (+0.84), CALB1 (+0.84), IL13RA2 (+0.83), GSTP1 (+0.83), SOX2 (+0.83), EMB (+0.82), MYO10 (+0.82), PDE10A (+0.82), QPRT (+0.82), HES1 (+0.82), PARM1 (+0.81), IGFBP5 (+0.81), SYNE2 (+0.81), PTP4A2 (+0.80), CPNE3 (+0.80), DZANK1 (+0.80), SSR4 (+0.79), LDHB (+0.79), SYT11 (+0.79), CSRP2 (+0.78), CHST2 (+0.78), CA2 (+0.77), UQCR11 (+0.77), NDN (+0.76), BTBD17 (+0.76), ANTXR1 (+0.76), TSC22D3 (+0.76), HMGB1 (+0.76), ADH5 (+0.76), TCF7L2 (+0.75), UNC13C (+0.75), DNER (+0.75), GPX8 (+0.75), UQCRQ (+0.75), NFIA (+0.74), GABRG3 (+0.74), QKI (+0.74), TALAM1 (+0.74), STARD4.AS1 (+0.73), FKBP10 (+0.73), ECEL1 (+0.73), LINC00461 (+0.72), SLITRK4 (+0.72), ARID5B (+0.72), PLD3 (+0.71), TXNDC17 (+0.71), PRDX4 (+0.71), NEAT1 (+0.70), PCSK1N (+0.70), JADE1 (+0.70), OTX2 (+0.70), MEG3 (+0.69), PXDN (+0.69), SESN3 (+0.69), GOLIM4 (+0.68), CACNG8 (+0.68), RBM41 (+0.68), MAGEL2 (+0.68), C4ORF48 (+0.67), CRABP2 (+0.67), HSPE1 (+0.67), MICOS10 (+0.67), CROT (+0.67), TMA7 (+0.67), PCOLCE2 (+0.66), BTG1 (+0.66), MPDZ (+0.65), LHX1 (+0.65), P4HA1 (+0.65), MARCHF1

(+0.65), ZNF83 (+0.65), FGF3 (+0.65), ASPH (+0.65), PON2 (+0.65), ANP32E (+0.65), ZNF506 (+0.65), HMGB1P5 (+0.64), ENSG00000239482 (+0.64), ATP5ME (+0.64), BCAT1 (+0.64), SEC61G (+0.64), CAPN6 (+0.64), NAA38 (+0.64), KNOP1 (+0.63), RASD1 (+0.63), SLIT2 (+0.63), NDUFA13 (+0.63), BTG3 (+0.63), UTRN (+0.63), PDE3A (+0.63), VEGFA (+0.63), RPN2 (+0.63), SPARCL1 (+0.63), CD81 (+0.63), CKB (+0.62), PRDX2 (+0.62), SEM1 (+0.62), PAICS (+0.62), PDK4 (+0.62), VPS41 (+0.62), RRBP1 (+0.62), LAPTM4A (+0.62), HDAC1 (+0.62), SLC22A17 (+0.62), GLUL (+0.61), CNPY2 (+0.61), ERBIN (+0.61), MRPS6 (+0.61), CAST (+0.61), CREB5 (+0.60), NDUFC2 (+0.60), HMGN5 (+0.60), PDLIM5 (+0.60), CCND2 (+0.60), HNRNPA1 (+0.59), CHMP2B (+0.59), IGF2 (+0.59), TCEAL8 (+0.59), FGF7 (+0.59), SLC44A5 (+0.59), ENSG00000259692 (+0.59), SERPINH1 (+0.59), KCNQ3 (+0.59), MEF2C (+0.58), SLC7A2 (+0.58), LAPTM4B (+0.58), CMTM6 (+0.58), SPA17 (+0.58), PRDX5 (+0.58), NEFH (+0.58), EZR (+0.58), LINC01833 (+0.58), FRMD6 (+0.58), GPX4 (+0.57), SNRPE (+0.57), FSCN1 (+0.57), ZNF462 (+0.57), UBL5 (+0.57), IFI27L2 (+0.57), TMEM47 (+0.57), RBIS (+0.56), DAD1 (+0.56), SEC11A (+0.56), PLIN2 (+0.56), TLE1 (+0.56), ATP5MC2 (+0.56), RAB11FIP2 (+0.56), CHD4 (+0.56), EEF1A1 (+0.56), THYN1 (+0.56), PET100 (+0.56), DLX6.AS1 (+0.55), SPART (+0.55), FAM162A (+0.55), OSBPL1A (+0.55), IFI27L1 (+0.55), ZMAT1 (+0.55), TFPI2 (+0.55), FAM217B (+0.55), STK33 (+0.55), ECHDC2 (+0.55), SLC25A5 (+0.55), NSA2 (+0.55), TBL1X (+0.55), DCT (+0.55), UQCRH (+0.54), ATF5 (+0.54), JUND (+0.54), TOX3 (+0.54), KLHDC8B (+0.54), TFDP2 (+0.54), ATRAID (+0.54), NOTCH2 (+0.54), EEF1D (+0.54), FIRRE (+0.54), TLK1 (+0.54), PUS7L (+0.54), ZBTB18 (+0.54), PTPRN2 (+0.53), PGK1 (+0.53), EMC10 (+0.53), GLG1 (+0.53), CUTA (+0.53), STK32B (+0.53), UBE2E3 (+0.53), BAZ1A (+0.53), GNB2 (+0.53), C1ORF54 (+0.53), GNAI2 (+0.52), LINC01896 (+0.52), SERF2 (+0.52), UFL1 (+0.52), LSM4 (+0.52), SCP2 (+0.52), CLIC1 (+0.52), VGLL4 (+0.52), KCNAB1 (+0.52), CEP83 (+0.52), PLEKHG4B (+0.52), YIPF4 (+0.52), UACA (+0.52), UBXN2A (+0.52), PSMA1 (+0.51), MRPL52 (+0.51), COL11A1 (+0.51), ATOX1 (+0.51), HHIP (+0.51), CLCN3 (+0.51), DNAJB4 (+0.51), ATP5MF (+0.51), SCUBE3 (+0.51), PALLD (+0.51), NDUFA11 (+0.51), YME1L1 (+0.51), DHRS7 (+0.50), UBA1 (+0.50), KDM3A (+0.50), COPS9 (+0.50), DHX40 (+0.50), OFD1 (+0.50), FGF13 (+0.50), SOX5 (+0.50), PPP1R9A (+0.50), HSP90B1 (+0.50), C19ORF53 (+0.50), SEMA3A (+0.50), TCF3 (+0.50), PAX8.AS1 (+0.50), PPIB (+0.50), LRRC75A (+0.50), NPM1 (+0.50), SRSF6 (+0.50), CCDC25 (+0.50), ITGB1 (+0.50), ANKRD44 (+0.49), YAP1 (+0.49), CKAP4 (+0.49), PCDH15 (+0.49), UBA52 (+0.49), MAP2K6 (+0.49), SNRPG (+0.49), RNF145 (+0.49), POLA1 (+0.49), PLPP5 (+0.49), BBX (+0.49), TRMT112 (+0.49), TIMM13 (+0.49), PBXIP1 (+0.49), PSAT1 (+0.49), ZNF770 (+0.49), TMEM258 (+0.48), RAB13 (+0.48), UQCRB (+0.48), LMAN2 (+0.48), COX5B (+0.48), ZNHIT1 (+0.48), RBM47 (+0.48), CCDC8 (+0.48), TNPO1 (+0.48), SELENOP (+0.48), LGI1 (+0.48), NFE2L1 (+0.48), GTF2F2 (+0.48), TYW3 (+0.48), RHOC (+0.48), CFL1 (+0.48), GPX7 (+0.48), NEGR1 (+0.48), LHX5 (+0.48), RIT1 (+0.48), MAGT1 (+0.48), CCDC136 (+0.47), SCAF11 (+0.47), C6ORF62 (+0.47), SSR2 (+0.47), SMIM30 (+0.47), SLC6A8 (+0.47), NAALAD2 (+0.47), KIAA1143 (+0.47), MZT2B (+0.47), SNRPB (+0.47), RCN2 (+0.47), HSP90AB3P (+0.47), HDLBP (+0.47), DAB2 (+0.47), ITGA2 (+0.47), ST13 (+0.47), IGF2BP1 (+0.47), OBSL1 (+0.47), GRN (+0.47), MAF (+0.47), TLE3 (+0.46), COL2A1 (+0.46), C14ORF39 (+0.46), MRPS21 (+0.46), LHX9 (+0.46), DDX21 (+0.46), DIO3 (+0.46), HSPA5 (+0.46), DESI2 (+0.46), TUBA1C (+0.46), RMI1 (+0.46), ZNF518A (+0.46), CFAP70 (+0.46), IFT74 (+0.46), HSDL2 (+0.46), TSPAN6 (+0.46), NDUFA7 (+0.46), MIDN (+0.46), ESF1 (+0.46), MIX23 (+0.46), TTC32 (+0.46), TP53TG1 (+0.46), MIF (+0.46), MAMDC2 (+0.46), LRP10 (+0.45), BBLN (+0.45), KPNB1 (+0.45), SVIL (+0.45), CETN2 (+0.45), TCEAL3 (+0.45), PDCD4 (+0.45), HNRNPUL1 (+0.45), ZSWIM7 (+0.45), PRAF2 (+0.45), CIB1 (+0.45), SSR3 (+0.45), POLR2G (+0.45), AK3 (+0.45), SMCO4 (+0.45), ACOT13 (+0.45), URI1 (+0.45), LAMTOR4 (+0.45), ZFP36L2 (+0.45), FAU (+0.45), COX6B1 (+0.45), MBIP (+0.45), LDB1 (+0.45), UPF3A (+0.45), ADGRL2 (+0.44), CPXM1 (+0.44), SPINT2 (+0.44), METRN (+0.44), GAS5 (+0.44), MXI1 (+0.44), DNPH1 (+0.44), TET1 (+0.44), TSHZ2 (+0.44), IRF2BPL (+0.44), SLC2A1 (+0.44), TMEM123 (+0.44), MIR99AHG (+0.44), FZD3 (+0.44), NPM3 (+0.44), DHX32 (+0.44), CD63 (+0.44), PDE4D (+0.44), ING2 (+0.44), GRIK1 (+0.44), ACADVL (+0.43), RASSF8 (+0.43), CUX1 (+0.43), CAPNS1 (+0.43), LAMC1 (+0.43), GNG11 (+0.43), HPF1 (+0.43), TPT1 (+0.43), TOP1 (+0.43), LAGE3 (+0.43), DMAC1 (+0.43), AHSA2P (+0.43), PGRMC2 (+0.43), TEX9 (+0.43), NDUFA2 (+0.43), DCAF16 (+0.43), ATP2B4 (+0.43), MRPL33 (+0.43), PPP1CC (+0.43), MAT2B (+0.43), KLF6 (+0.43), OST4 (+0.43), SUZ12 (+0.43), POLR2J (+0.43), ENY2 (+0.43), TMEM9B.AS1 (+0.43), DDR1 (+0.43), HADHA (+0.42), STARD3 (+0.42), PAPSS2 (+0.42), LDHA (+0.42), CACHD1 (+0.42), FAM107A (+0.42), SERPINB6 (+0.42), MSANTD2.AS1 (+0.42), CTSB (+0.42), CCDC88C (+0.42), STT3A (+0.42), ERGIC3 (+0.42), PSMD10 (+0.42), NNT.AS1 (+0.42), CD151 (+0.42), PDE1C (+0.42), PTMS (+0.42), STK39 (+0.42), PDE4B (+0.42), SLIRP (+0.41), P4HB (+0.41), SNRPF (+0.41), MT.ND3 (+0.41), NOC3L (+0.41), UROD (+0.41), PPP2R1A (+0.41), NDUFB5 (+0.41), EXOSC6 (+0.41), NDUFA1 (+0.41), USP11 (+0.41), TOX (+0.41), SH3BGRL (+0.41), MRPL22 (+0.41), DPP7 (+0.41), HMGN2 (+0.41), CNTN1 (+0.41), BSG (+0.41), ATRNL1 (+0.41), OXA1L (+0.41), SMAD9 (+0.41), CNIH4 (+0.40), APOE (+0.40), SRI (+0.40), COTL1 (+0.40), TNFRSF19 (+0.40), LPP (+0.40), KIF13A (+0.40), STK26 (+0.40), GALNT1 (+0.40), LEPROT (+0.40), SPON1 (+0.40), PRDX3 (+0.40), MUC20.OT1 (+0.40), NBPF14 (+0.40), SAP18 (+0.40), HDC (+0.40), TUBB (-0.40), ODF2L (-0.40), CAMK2B (-0.40), NCMAP.DT (-0.40), DNAJA1 (-0.40), TSPYL2 (-0.40), H2AZ1 (-0.40), HRC (-0.40), RIMS2 (-0.41), CHGB (-0.41), TNRC6C (-0.41), EVL (-0.41), CBX5 (-0.41), PKIA (-0.41), SLC16A9 (-0.41), G3BP2 (-0.41), SMC3 (-0.41), TRMT9B (-0.41), ATXN7L3B (-0.41), EPB41L4A (-0.41), ARRDC3 (-0.41), LINC02381 (-0.42), DAAM1 (-0.42), ENSG00000258757 (-0.42), SILC1 (-0.42), LRRC49 (-0.42), GNPTAB (-0.42), ICA1 (-0.42), LRRN3 (-0.42), CACNB4 (-0.42), FOXP2 (-0.42), LBH (-0.42), ETS2 (-0.42), LMO4 (-0.43), NAP1L3 (-0.43), MACO1 (-0.43), HDAC2 (-0.43), SCN9A (-0.43), DKK3 (-0.43), MYT1 (-0.43), BTBD8 (-0.43), ACSL3 (-0.43), SLIT3 (-0.43), MAP6 (-0.43), NEB (-0.43), SYP (-0.43), MBP (-0.43), OGA (-0.43), ZC3H13 (-0.43), TULP4 (-0.43), ANKRD12 (-0.43), ACTB (-0.43), VAV3 (-0.44), EHBP1 (-0.44), KIAA0232 (-0.44), ATP6V0A1 (-0.44), GLRA2 (-0.44), PAPPA (-0.44), HMGB2 (-0.44), CDH11 (-0.44), TRPC5 (-0.44), OBI1 (-0.44), CGNL1 (-0.44), NES (-0.44), AKAP8L (-0.44), SEPTIN7 (-0.44), FBXW7 (-0.44), TENM2 (-0.45), H4C3 (-0.45), CCDC82 (-0.45), C1ORF21 (-0.45), VDAC1 (-0.45), MORF4L1 (-0.45), DSTN (-0.45), TSPAN7 (-0.45), GNG2 (-0.45), FAM184A (-0.45), KLC1 (-0.45), HAPLN1 (-0.45), LCOR (-0.45), MIR100HG (-0.46), DOCK4 (-0.46), ZNF138 (-0.46), SEC14L1 (-0.46), CARTPT (-0.46), ENSG00000259203 (-0.46), STX7 (-0.46), GALNTL6 (-0.46), SACS (-0.46), ITSN1 (-0.46), SLC39A8 (-0.46), STX12 (-0.46), ZC2HC1A (-0.47), DYNC1H1 (-0.47), KIF5A (-0.47), FOXP1 (-0.47), ELAVL2 (-0.47), MAP3K13 (-0.47), ENSG00000280234 (-0.47), MAP4K3.DT (-0.47), NRN1 (-0.47), TMEM35A (-0.47), KCNMA1 (-0.47), CHD3 (-0.48), H1.4 (-0.48), KIF1B (-0.48), AHI1 (-0.48), PAFAH1B1 (-0.48), CDH20 (-0.48), AFF3 (-0.48), TRIM9 (-0.48), ZBTB20 (-0.48), SH3GL3 (-0.48), ARL6IP5 (-0.48), SMARCA2 (-0.48), PITPNB (-0.48), AASDHPPT (-0.48), PPP1R15A (-0.48), NTRK3 (-0.48), HMGCR (-0.49), RPRM (-0.49), PANK3 (-0.49), DOC2B (-0.49), VAMP2 (-0.49), ACYP1 (-0.49), RUFY2 (-0.49), UPP1 (-0.49), LGALSL (-0.49), BZW2 (-0.49), SYBU (-0.50), ATL1 (-0.50), NLGN4X (-0.50), GRIPAP1 (-0.50), NRG1 (-0.50), RGS7 (-0.50), HK1 (-0.50), CDH12 (-0.50), KCNB2 (-0.50), PRKCB (-0.50), KIFAP3 (-0.50), TUBB2B (-0.51), RTF1 (-0.51), LIN7A (-0.51), DRAXIN (-0.51), ZFHX4 (-0.51), SCAMP1 (-0.52), CDKN2D (-0.52),

NPAS3 (-0.52), SASH1 (-0.52), GREM2 (-0.52), ENSG00000288993 (-0.52), BASP1 (-0.52), KCTD16 (-0.52), XBP1 (-0.52), TSTD1 (-0.52), GUCY1B1 (-0.52), GNG4 (-0.52), FDFT1 (-0.52), LRRC4C (-0.52), TMEFF2 (-0.52), PPP3CA (-0.52), SEPTIN3 (-0.52), TAOK3 (-0.53), SFPQ (-0.53), PCDH10 (-0.53), SPTAN1 (-0.53), HIP1R (-0.53), SPTBN1 (-0.54), NRP1 (-0.54), FGF14 (-0.54), RIMS1 (-0.54), YWHAB (-0.55), KIDINS220 (-0.55), AZIN1 (-0.55), FHL1 (-0.55), AKAP9 (-0.55), SPECC1 (-0.55), B3GALT2 (-0.55), LINC03000 (-0.55), ARMH4 (-0.56), CCP110 (-0.56), PDZRN3 (-0.56), BEX1 (-0.56), ADARB2 (-0.56), SCAPER (-0.56), EPB41 (-0.56), CCDC88A (-0.56), CCDC144NL.AS1 (-0.56), NRCAM (-0.56), SLC38A1 (-0.56), CELF2 (-0.57), ADGRB3.DT (-0.57), PIK3R3 (-0.57), CHCHD2 (-0.57), LINC01322 (-0.57), GPCPD1 (-0.57), KCND3 (-0.57), LSAMP (-0.57), NRIP3 (-0.57), NOVA1 (-0.58), LRP8 (-0.58), ASAP1 (-0.58), SGCZ (-0.59), TOMM20 (-0.59), PLCB4 (-0.59), JAKMIP2 (-0.59), ANKMY2 (-0.59), PFKP (-0.59), LRRC7 (-0.60), GNAI1 (-0.60), MACF1 (-0.60), MT.ND4L (-0.60), DYNC1I1 (-0.60), ARL4A (-0.60), CAMSAP2 (-0.61), KIF3A (-0.61), IDI1 (-0.61), NR2F2 (-0.61), ST8SIA3 (-0.61), NR2F1.AS1 (-0.61), CCSER1 (-0.61), SMIM14 (-0.62), SMARCC2 (-0.62), MTSS1 (-0.62), CLVS2 (-0.62), ROBO1 (-0.62), MYO5A (-0.62), DGKB (-0.62), ZEB2 (-0.62), LINC00342 (-0.63), PLEKHH2 (-0.63), NPTN (-0.63), KLHL5 (-0.63), TMSB15A (-0.64), GRM8 (-0.64), NALF1 (-0.64), KMT2E (-0.64), GNAL (-0.64), NAV1 (-0.64), MAP2 (-0.65), CXXC4 (-0.65), PCDH11X (-0.65), PPFIA2 (-0.65), LINC02899 (-0.65), CTNNA2 (-0.65), CRACD (-0.66), TUBB2A (-0.66), SYT13 (-0.66), CEP170 (-0.67), ACSL4 (-0.67), CLASP2 (-0.67), SLC25A27 (-0.67), DPYSL3 (-0.67), SCN2A (-0.68), NSD3 (-0.68), SYT7 (-0.68), PMFBP1 (-0.68), SCG3 (-0.69), TACC2 (-0.69), MIR137HG (-0.69), TTC3 (-0.69), DNAJC12 (-0.70), TUBA1A (-0.70), DPYSL2 (-0.70), RGS4 (-0.70), CALM2 (-0.70), ENSG00000265179 (-0.70), NAV3 (-0.70), POU3F2 (-0.71), CNST (-0.71), POTEF (-0.71), LYST (-0.71), GRIN2B (-0.72), TMOD2 (-0.72), FRMD4A (-0.72), RAB2A (-0.72), F3 (-0.72), CDH10 (-0.72), TERF2IP (-0.72), CORO1C (-0.73), SNHG14 (-0.73), RUNX1T1 (-0.73), BMP7 (-0.73), ENSG00000224114 (-0.73), PLEKHA5 (-0.73), FAM13C (-0.73), ENSG00000286058 (-0.73), PAK3 (-0.73), PRKACB (-0.73), SLC8A1 (-0.74), DST (-0.74), ELL2 (-0.74), LUC7L3 (-0.74), TFF3 (-0.75), LINC01414 (-0.75), SLC1A2 (-0.76), XKR4 (-0.76), DCBLD2 (-0.76), FZD1 (-0.76), ANKRD36C (-0.77), OPTN (-0.77), CXXC5 (-0.78), CELF4 (-0.78), GABRG2 (-0.78), ZNF608 (-0.78), NFASC (-0.79), RTN3 (-0.79), NEBL (-0.79), CXADR (-0.79), KCNJ16 (-0.80), ANK2 (-0.80), GLRA3 (-0.81), C1GALT1 (-0.81), KMT2A (-0.81), NRSN1 (-0.82), SULF2 (-0.82), KIF21A (-0.83), POTEE (-0.83), DCX (-0.83), DNAJC15 (-0.83), NSG1 (-0.83), INPP5F (-0.83), TAGLN3 (-0.84), POU2F2 (-0.84), RAPGEF5 (-0.84), WNK3 (-0.85), NMNAT2 (-0.85), GPRIN3 (-0.85), HSP90AA1 (-0.86), ENSG00000213058 (-0.86), ERC2 (-0.87), TSC22D1 (-0.87), LHFPL6 (-0.87), DCLK1 (-0.87), CYP51A1 (-0.87), NBEA (-0.88), RMST (-0.88), FAT3 (-0.89), TAC1 (-0.89), SCN3A (-0.89), PCDH17 (-0.89), DNM3 (-0.89), GRB14 (-0.89), ARPC5 (-0.90), RAB3C (-0.91), NTM (-0.91), REEP1 (-0.91), H1.0 (-0.91), ENSG00000288765 (-0.92), ANKRD36 (-0.92), NOS1AP (-0.93), THSD7A (-0.93), RTN4 (-0.94), TLE4 (-0.94), MTUS2 (-0.95), MAP1B (-0.96), STMN4 (-0.97), RGS2 (-0.98), RBFOX2 (-0.98), LIMCH1 (-0.98), SAMD5 (-0.98), SRRM4 (-0.99), NAPB (-0.99), GNAO1 (-1.00), CADM1 (-1.01), PGM2L1 (-1.02), PCDH9 (-1.02), FOXA2 (-1.02), SRRM3 (-1.03), EBF3 (-1.03), NSG2 (-1.03), AKAP6 (-1.04), NRXN1 (-1.04), AUTS2 (-1.04), FNBP1L (-1.05), ENSG00000259436 (-1.06), SNAP25 (-1.06), VPS13C (-1.06), MAGI2 (-1.07), MT.RNR2 (-1.09), HMGCS1 (-1.10), SNCA (-1.10), BTBD3 (-1.10), LMO3 (-1.11), H3.3B (-1.12), NR3C1 (-1.12), INA (-1.12), GRIA4 (-1.14), PLCL1 (-1.14), RTN1 (-1.14), MLLT11 (-1.15), PBX1 (-1.15), SYT1 (-1.16), GPM6A (-1.16), ONECUT3 (-1.16), LMX1A (-1.16), STMN1 (-1.17), MAPT (-1.17), CHGA (-1.17), PTPRE (-1.17), PCLO (-1.18), ZNF385D (-1.21), GRIA2 (-1.21), ALCAM (-1.21), MIR124.2HG (-1.23), SCG2 (-1.24), LINC00261 (-1.29), POU3F3 (-1.29), EBF1 (-1.33), NR2F1 (-1.34), CNTN4 (-1.35), CALM1 (-1.36), ATP1B1 (-1.36), CRNDE (-1.36), ENSG00000289612 (-1.36), ADCYAP1 (-1.37), NR4A2 (-1.38), PTPRO (-1.44), NIN (-1.45), MYT1L (-1.46), ROBO2 (-1.50), SLC17A6 (-1.52), KIF5C (-1.53), CD24 (-1.56), NEFM (-1.56), NCAM1 (-1.59), PKIB (-1.61), ANK3 (-1.64), CHL1 (-1.67), DDC (-1.67), ONECUT2 (-1.67), PPP2R2B (-1.70), PITX2 (-1.75), GRIK2 (-1.77), NTNG1 (-1.84), STMN2 (-1.86), CADM2 (-1.87), CACNA2D1 (-1.95), PCSK1 (-2.03), ONECUT1 (-2.03), NEFL (-2.13), GAP43 (-2.15), SYT4 (-2.19), PDZRN4 (-2.23)

DAY 40

TCEAL5 (+1.54), CGA (+1.40), PDE10A (+1.19), TPH1 (+0.97), NEAT1 (+0.97), KCNQ1OT1 (+0.93), S100A6 (+0.91), PTPRT (+0.91), ENSG00000237550 (+0.89), COPG2IT1 (+0.86), DMD (+0.83), TCEAL6 (+0.81), ACSL4 (+0.79), XIST (+0.77), FTL (+0.73), ENSG00000290596 (+0.72), CPE (+0.70), TOX (+0.68), ZNF506 (+0.68), BEX3 (+0.68), PUS7L (+0.65), MORF4L2 (+0.64), PSMD10 (+0.61), BEX2 (+0.61), SYT13 (+0.60), ZFHX3 (+0.60), MSMO1 (+0.58), FAM162A (+0.57), RND3 (+0.56), EPHA5 (+0.55), TCEAL3 (+0.55), SSTR2 (+0.54), CAMK2N1 (+0.54), KCNIP4 (+0.53), TCEAL9 (+0.52), ARHGAP18 (+0.52), ZNF471 (+0.51), GRID2 (+0.50), VGF (+0.50), USP11 (+0.50), KCTD12 (+0.50), PEG10 (+0.50), PAX8.AS1 (+0.48), PGK1 (+0.48), LDHA (+0.48), MT.RNR1 (+0.47), NLGN1 (+0.47), NRN1 (+0.46), APLP2 (+0.45), P4HA1 (+0.45), DSEL (+0.44), POU2F2 (+0.43), PLCB1 (+0.43), ZNF714 (+0.43), PLEKHA5 (+0.43), LINC00662 (+0.43), TXNIP (+0.41), PTPRN2 (+0.41), KLF6 (+0.41), PCDH10.DT (+0.41), WHAMMP1 (+0.40), MT.ND6 (+0.40), RAB9B (+0.40), ESRRG (-0.40), NRG1 (-0.41), RBP1 (-0.41), SESN3 (-0.41), SPIN1 (-0.41), SOX2 (-0.41), CHD7 (-0.41), PCDH11X (-0.41), HIP1 (-0.41), NES (-0.41), ZNF37A (-0.41), PLEKHO1 (-0.42), MYO1B (-0.42), NR4A2 (-0.42), FZD3 (-0.42), DMRTA2 (-0.42), ENSG00000213058 (-0.43), DRAXIN (-0.43), BMP7 (-0.43), PIK3R1 (-0.43), CACNA2D1 (-0.43), DOC2B (-0.43), SRSF5 (-0.43), PLCL1 (-0.44), NOS1AP (-0.44), CXADR (-0.44), MTUS2 (-0.44), EIF1AX (-0.44), TDG (-0.45), SAMD5 (-0.45), ENSG00000289612 (-0.45), KCNJ16 (-0.46), NEFM (-0.46), PMFBP1 (-0.46), MIR100HG (-0.47), ZMIZ1 (-0.47), SASH1 (-0.47), SYT4 (-0.47), PCSK1 (-0.48), EBF1 (-0.49), MDK (-0.49), PITX2 (-0.50), SLC17A6 (-0.50), POTEF (-0.50), SRSF3 (-0.51), DACH1 (-0.51), DOK6 (-0.51), POTEE (-0.51), CERS6 (-0.52), SYNE2 (-0.52), DHX9 (-0.53), SC5D (-0.53), SOX4 (-0.54), PKIB (-0.54), NALF1 (-0.54), LMO3 (-0.54), HNRNPM (-0.54), PTPRE (-0.57), C1GALT1 (-0.57), ARL4A (-0.57), SLK (-0.57), PBX1 (-0.58), KLHL5 (-0.59), LINC02899 (-0.59), ENSG00000286058 (-0.60), SOX2.OT (-0.60), NR2F1 (-0.61), ATP5MG (-0.63), ONECUT3 (-0.63), ENSG00000290591 (-0.64), INPP5F (-0.64), ONECUT1 (-0.68), DLK1 (-0.68), LINC00551 (-0.68), CHCHD2 (-0.68), PDZRN4 (-0.70), ROBO2 (-0.81), CCDC144NL.AS1 (-0.82), NTM (-0.83), DNAJC15 (-0.86), WNK3 (-1.04)

DAY 60

XIST (+1.97), TCEAL5 (+1.58), S100A6 (+0.98), TTC6 (+0.96), MT.ND3 (+0.91), ZNF506 (+0.87), TCEAL6 (+0.81), TALAM1 (+0.78), XACT (+0.74), TCEAL3 (+0.74), TPH1 (+0.74), PTPRT (+0.73), MUC20.OT1 (+0.70), DNAH6 (+0.69), DMD (+0.68), FSIP2 (+0.68), VGF (+0.68), COPG2IT1 (+0.68), NEGR1 (+0.66), KCNQ1OT1 (+0.66), SULF1 (+0.64), SYNE2 (+0.61), PCDH9 (+0.60), PUS7L (+0.59), MT.RNR1 (+0.59), PCNX4 (+0.58), LCORL (+0.58), PTN

(+0.58), COL1A2 (+0.57), ENSG00000237550 (+0.56), SYT11 (+0.54), OTX2 (+0.54), GRIK1 (+0.53), ARF4 (+0.53), PAX8.AS1 (+0.53), CLU (+0.52), MEST (+0.51), FTX (+0.49), ANKRD18A (+0.49), ENSG00000270953 (+0.49), BEX2 (+0.49), PDE10A (+0.49), HTR2C (+0.48), TBX3 (+0.48), BAZ2B (+0.46), FTL (+0.44), MT.ND5 (+0.44), GRIK2 (+0.43), ATP13A3.DT (+0.42), TSIX (+0.41), SETX (+0.41), PTPRN2 (+0.41), FILIP1L (+0.41), MT.CYB (+0.41), PGM2L1 (-0.40), VASH2 (-0.40), ARMH4 (-0.40), CEP170 (-0.41), NAPB (-0.41), TUBA1A (-0.41), ATP1B1 (-0.41), DPYSL2 (-0.41), PBX1 (-0.41), CALM1 (-0.41), RFK (-0.42), ATP5MC3 (-0.42), YWHAZ (-0.42), PRDX1 (-0.42), DNAJA1 (-0.42), SOX4 (-0.42), LIMCH1 (-0.42), ENSG00000176593 (-0.42), MYO5A (-0.42), DYNLL2 (-0.43), TMPO (-0.43), SHTN1 (-0.43), SMARCA4 (-0.44), YWHAQ (-0.44), ZNF385D (-0.44), ANKMY2 (-0.44), DCBLD2 (-0.44), PCLO (-0.45), RTN1 (-0.45), GABPB1.AS1 (-0.45), TOMM20 (-0.45), TUBB2B (-0.45), MT.RNR2 (-0.45), PTGES3 (-0.46), DPYSL3 (-0.46), HMGB3 (-0.46), EID1 (-0.46), TXLNG (-0.46), SRPK1 (-0.47), SNCA (-0.47), SQLE (-0.48), HSP90AB1 (-0.48), ENSG00000213058 (-0.49), HDAC2 (-0.49), ONECUT1 (-0.49), RAPGEF5 (-0.49), APP (-0.49), GNAQ (-0.49), SET (-0.49), CDV3 (-0.50), EIF4G2 (-0.50), CISD1 (-0.50), TCEA1 (-0.50), MTPN (-0.50), FTH1 (-0.51), H3.3B (-0.51), NAP1L3 (-0.51), RBBP7 (-0.51), YWHAB (-0.51), NR2F1 (-0.51), NREP (-0.51), LINC01322 (-0.52), RHEB (-0.52), RALA (-0.52), TUBB2A (-0.52), LRCH2 (-0.52), RAB2A (-0.52), NEFL (-0.52), AUTS2 (-0.53), INPP5F (-0.53), PPA1 (-0.53), FOXA2 (-0.53), CNTN4 (-0.54), RAB10 (-0.54), ARL4A (-0.54), AASDHPPT (-0.55), SC5D (-0.55), PDZRN4 (-0.56), EEF1A1 (-0.56), TULP4 (-0.57), LINC00551 (-0.57), CEBPG (-0.57), PKIA (-0.59), ZFAS1 (-0.59), SLC38A1 (-0.59), RTN3 (-0.60), ACSL3 (-0.61), HSP90AA1 (-0.62), CCDC144NL.AS1 (-0.62), TSC22D1 (-0.63), STMN1 (-0.63), CHCHD2 (-0.63), HSPD1 (-0.63), SYT4 (-0.67), PLCL1 (-0.67), UCHL1 (-0.68), ATP5MG (-0.68), KLHL5 (-0.69), DDIT4 (-0.69), PABPC1 (-0.70), ROBO2 (-0.70), DCX (-0.71), CXADR (-0.73), EIF1AX (-0.75), KMT2A (-0.77), LMO3 (-0.77), DNAJC15 (-0.78), ATF5 (-0.81), NTM (-0.82), HMGCS1 (-0.82), LINC02899 (-0.85), POTEF (-0.86), ENSG00000290591 (-0.87), POTEE (-0.87), ENSG00000286058 (-1.12), WNK3 (-1.30)

A.2 Differentially abundant proteins

DAPs identified at each timepoint of the differentiation ($p_{\text{adj}} < 0.05$ and $|\text{FC}|>1$). Fold changes are indicated in parentheses.

DAY 0

PABPC4 (+4.23), FBLL1 (+4.00), CCDC92B (+3.87), RPL36A (+3.37), TUBB6 (+2.95), AKR1B10 (+2.91), LAMB4 (+2.89), PGM5 (+2.80), VDAC2 (+2.67), PSMC5 (+2.66), MROH2B (+2.60), SRGAP3 (+2.54), ALDH1A1 (+2.46), ZNF66 (+2.45), COL4A6 (+2.43), CCNA2 (+2.41), ATP5F1E (+2.33), UBTF (+2.30), FKBP8 (+2.30), H1-0 (+2.17), Q969Q0 (+2.17), CHMP1A (+2.09), NXPE1 (+1.98), PHGDH (+1.97), MEAF6 (+1.96), RABAC1 (+1.94), A0A0U1RQJ6;B4DDN1 (+1.81), PMPCB (+1.76), HNRNPU (+1.76), AGR3 (+1.76), PPIA (+1.73), VIP (+1.66), DCD (+1.65), MMGT1 (+1.61), TMEM160 (+1.59), Q5SU54 (+1.58), SLC11A2 (+1.51), NRAP (+1.49), VTN (+1.48), RPL34 (+1.48), PTMS (+1.46), SERPINB7 (+1.46), HLA-A (+1.41), Q04828 (+1.35), IVD (+1.35), P49335 (+1.34), CANX (+1.29), FKBP4 (+1.28), DNM1L (+1.28), RAB33A (+1.25), CCDC177 (+1.23), CHPT1 (+1.23), IKBKE (+1.23), CD47 (+1.22), P12236 (+1.20), RPL19 (+1.19), HMGA1 (+1.17), NOMO2 (+1.17), A0A5H1ZRP4 (+1.16), ALDH3A1 (+1.16), CNTRL (+1.15), P0DM35;P80294 (+1.13), MAD2L2 (+1.13), PABPC1 (+1.12), ACTG1 (+1.12), LTF (+1.11), SP1 (+1.11), CRYZ (+1.09), SNX15 (+1.09), SEZ6L2 (+1.07), CHMP2A (+1.07), SOX2 (+1.07), SCO2 (+1.06), SLC35A4 (+1.06), IST1 (+1.05), BST2 (+1.05), AKR1C2 (+1.04), HSPB6 (+1.03), SLC35B2 (+1.03), DLST (+1.03), RPL30 (+1.00), PAM (-1.00), MYH14 (-1.02), PHLDB1 (-1.02), HIP1R (-1.02), ATP5PD (-1.03), A0A140T9Q4;A0A140T9S7 (-1.03), VMP1 (-1.04), CAT (-1.04), ERRFI1 (-1.06), URM1 (-1.07), UBE2I (-1.07), ARHGAP39 (-1.08), E9PLY5 (-1.08), AGAP1 (-1.10), RACK1 (-1.11), TXNL1 (-1.11), ECHS1 (-1.12), RNASEH2C (-1.12), LSM8 (-1.16), SRSF11 (-1.17), PTDSS2 (-1.17), GALNS (-1.18), TRIM13 (-1.18), EDNRB (-1.18), CYBC1 (-1.19), TLE5 (-1.19), PANX1 (-1.20), RPS7 (-1.20), FADD (-1.22), EPN3 (-1.22), SDF2 (-1.24), GNG4 (-1.28), A0A087X0H9 (-1.28), KRT77 (-1.32), Q9Y605 (-1.33), U2AF2 (-1.33), TRMT11 (-1.37), WNK3 (-1.37), USF1 (-1.38), PGR (-1.40), INPP5F (-1.42), TSFM (-1.42), CYB5R3 (-1.44), TOR1AIP1 (-1.49), POGLUT3 (-1.55), PCBD2 (-1.60), SNRNP27 (-1.66), QNG1 (-1.73), PAFAH1B2 (-1.76), TMEM41A (-1.78), PTMA (-1.81), CHCHD2 (-1.92), MPV17 (-1.95), PRSS3 (-1.97), AP4S1 (-1.98), COX1 (-2.21), ATP5MF (-2.35), CYP2D7 (-2.45), SLC1A4 (-2.58), KPNA7 (-2.97), CCT6B (-3.10), CRYBG3 (-3.38), NLRP2 (-3.45), KRT36 (-4.17)

DAY 6

Q6PEY2 (+4.36), H3-7 (+4.08), CXCL12 (+3.39), CAMK2B (+3.34), CNIH4 (+2.73), EPHX3 (+2.53), LEFTY2 (+2.38), RPL29 (+2.34), H3C1 (+2.34), A6NCE7;Q9GZQ8 (+2.31), BST2 (+2.30), STMN2 (+2.29), ICMT (+2.21), EDF1 (+2.18), CTNND2 (+2.17), RAB1A (+2.16), HDHD2 (+2.02), DHRS13 (+1.99), FKBP8 (+1.97), GPC4 (+1.92), P32243 (+1.90), Q6P582 (+1.89), GOLT1B (+1.83), FOXRED2 (+1.83), RPL8 (+1.83), DCP1A (+1.83), POU5F1 (+1.80), NIP7 (+1.77), EHHADH (+1.76), CRABP2 (+1.74), P19012 (+1.72), Q9Y281 (+1.72), SFRP1 (+1.71), GPC3 (+1.71), SFRP2 (+1.71), TRAPPC5 (+1.65), RALA (+1.65), RPL36A (+1.64), A0A0A0MRM9 (+1.60), UTF1 (+1.60), CYP26A1 (+1.60), PGK1 (+1.59), HIGD2A (+1.59), GPI (+1.58), BTF3 (+1.56), DNAJC14 (+1.55), CCN1 (+1.55), RHBDD2 (+1.55), MFAP2 (+1.54), AHNAK2 (+1.54), H2AZ1 (+1.53), CHTOP (+1.52), OSTC (+1.49), SLC2A3 (+1.49), JAM3 (+1.47), THY1 (+1.47), DERL2 (+1.47), B3GNT7 (+1.46), ATP5F1B (+1.46), NDUFB5 (+1.46), SREK1 (+1.45), ARL1 (+1.44), DBX1 (+1.44), TMEM14C (+1.44), PSMA2 (+1.43), KRTCAP2 (+1.42), LCK (+1.41), EEF1A1 (+1.41), DPPA4 (+1.40), KRT16 (+1.40), FAM162A (+1.40), GPC2 (+1.40), HRAS (+1.40), AP4S1 (+1.39), GSTT1 (+1.39), RPL7A (+1.38), MFSD3 (+1.38), SLC23A3 (+1.38), CD9 (+1.38), SCAMP2 (+1.38), CSNK2A1 (+1.37), P43358 (+1.36), Q9BVA1 (+1.36), GSE1 (+1.36), GPALPP1 (+1.34), MAPKAPK3 (+1.34), DEPDC1B (+1.34), PHYKPL (+1.34), FANCM (+1.33), TGFBI (+1.33), NUDT12 (+1.33), CARHSP1 (+1.33), S100A10 (+1.33), POLR2L (+1.33), A0A994J4E9;A0A994J6T5;A0A994J6U9;B4DUQ1;Q5T6W2 (+1.32), RPL10A (+1.31), TMBIM6 (+1.31), GET1 (+1.30), RPS3A (+1.30), STC2 (+1.30), CMBL (+1.29), MYH14 (+1.29), XRCC5 (+1.29), GYG1 (+1.28), SYNGR3 (+1.28), YTHDC1 (+1.28), USP9Y (+1.27), Q9Y343 (+1.27), NDUFA4L2 (+1.27), C1QTNF4 (+1.27), DBT (+1.27), SIAE (+1.27), NDOR1 (+1.27), CPT1C (+1.27), TOMM5 (+1.26), CDK18 (+1.25), SCAF4 (+1.25), PDGFRL (+1.25), FHIT (+1.24), PGR (+1.23), TNC (+1.23), LSM4 (+1.22), EZR (+1.22), CNOT6 (+1.21), RPS27A (+1.21), KRT4 (+1.21), TIMM29 (+1.21), NDUFAB1 (+1.20), ALOX12 (+1.19), RPS25 (+1.19), TUBB3 (+1.19), CLN6 (+1.18), ROGDI (+1.18), Q9UKI8 (+1.18), PANX1 (+1.18), MFGE8 (+1.17), NKX2-8 (+1.17), GNG2 (+1.17), NMNAT1 (+1.16), A0A5F9YFS9 (+1.16), HIGD1A (+1.16), ZNF729 (+1.16), LMAN1 (+1.15), CYCS (+1.15), TEAD3 (+1.15), GABARAPL1 (+1.15), NOP10 (+1.15), MED27 (+1.14), HNRNPH2 (+1.14), SIGMAR1 (+1.14), KPNA3 (+1.13), DNPH1 (+1.12), SP1 (+1.12), LIN28B (+1.12), IFT25 (+1.12), XKR4 (+1.12), S100A4 (+1.12), CAPN6 (+1.12), Q7Z3J3 (+1.10), ATOX1 (+1.10), RAC3 (+1.10), DFFB (+1.10), LGALS1 (+1.09), SDHB (+1.09), DMAC2 (+1.08), TDRD7 (+1.07), HMG20A (+1.07), P06899;Q16778 (+1.07), RPUSD4 (+1.07), RBKS (+1.07), METRN (+1.07), FGFR2 (+1.06), GANAB (+1.06), DLK1 (+1.06), UBA1 (+1.06), GLDC (+1.06), FABP5 (+1.06), TPST2 (+1.05), ELMO3 (+1.05), TTC9C (+1.05), COL2A1 (+1.04), RAX (+1.04), TDRP (+1.04), TJP3 (+1.04), BLOC1S6 (+1.04), P09467 (+1.03), NIF3L1 (+1.03), Q53H12 (+1.03), HTRA3 (+1.03), MSL1 (+1.03), H3BPE1;H3BQK9 (+1.02), PTBP1 (+1.02), RAVER1 (+1.02), CBR1 (+1.02), ESCO2 (+1.02), CDH1 (+1.02), A0A0J9YVP6;A0A0J9YVR6;A0A0J9YYL3;E9PMU7;E9PN18;E9PQ56 (+1.02), DSG1 (+1.02), CZIB (+1.02), UQCRFS1 (+1.02), B3GALT5 (+1.01), CYBC1 (+1.01), ZCCHC10 (+1.01), CISD1 (+1.01), DPAGT1 (+1.01), PPIA (+1.01), HSP90AA5P (+1.00), MAPKAP1 (+1.00), SEMA4B (+1.00), SLC4A7 (-1.00), EIF3H (-1.00), RPS19 (-1.00), PSMA7 (-1.00), ARL15 (-1.01), SSRP1 (-1.01), CBX1 (-1.01), GLRX5 (-1.01), BCL9 (-1.01), NUDCD2 (-1.01), SPATA20 (-1.02), PCBP3 (-1.02), JPT2 (-1.02), STX6 (-1.02), COX7A2 (-1.02), SRP9 (-1.02), OSTM1 (-1.03), MAD2L1BP (-1.03), CDK6 (-1.03), ANKRD46 (-1.03), FKBP10 (-1.03), ZDHHC7 (-1.03), PGLS (-1.04), ATP5MG (-1.04), GPM6B (-1.05), COLEC12 (-1.05), PDLIM2 (-1.05), APOO (-1.05), TSFM (-1.05), TRMT112 (-1.05), Q15742 (-1.05), KBTBD4 (-1.06), INA (-1.06), DEPDC7 (-1.06), DES (-1.06), RNPS1 (-1.07), DTWD2 (-1.07), OLFM1 (-1.07), PHLDB1

(-1.08), TMEM263 (-1.09), NDUFA4 (-1.09), STRA6 (-1.09), FKBP1B (-1.09), MOB2 (-1.10), R3HDM1 (-1.10), MRPL54 (-1.10), NAF1 (-1.11), SEC13 (-1.11), ZNHIT2 (-1.12), NRAS (-1.12), SNX7 (-1.12), SKA2 (-1.12), JPT1 (-1.13), NDRG4 (-1.13), KNSTRN (-1.13), SEC61A2 (-1.13), UQCRB (-1.14), CETN3 (-1.14), DAD1 (-1.15), UFM1 (-1.15), STEEP1 (-1.15), FHL2 (-1.15), AURKAIP1 (-1.15), TMEM184C (-1.15), CREB1 (-1.15), TYMS (-1.16), PNPLA4 (-1.16), ADSS2 (-1.16), PCBP4 (-1.17), GSKIP (-1.17), SCAMP4 (-1.17), CRIPT (-1.17), MTHFD2 (-1.19), GPX8 (-1.20), UBE2E2 (-1.20), SRI (-1.20), SUB1 (-1.21), CCS (-1.21), UBE2V1 (-1.21), COX5A (-1.21), GSTP1 (-1.21), LAMA4 (-1.21), WRAP53 (-1.22), SDF2L1 (-1.22), ATXN7L3B (-1.23), RPSA (-1.23), RPS28 (-1.23), P12236 (-1.23), RPL35A (-1.23), RPL15 (-1.24), GSN (-1.24), NES (-1.24), Q15907 (-1.25), P24468 (-1.25), ZDHHC20 (-1.25), CALB1 (-1.25), CIR1 (-1.26), RALY (-1.26), LMCD1 (-1.26), NDUFB1 (-1.27), CKM (-1.28), EIF3F (-1.28), EFL1 (-1.28), PGGT1B (-1.28), CENPV (-1.29), ELAVL3 (-1.29), ALDH16A1 (-1.30), K7EQG2 (-1.31), UBE2E1 (-1.31), SRSF2 (-1.32), ARL6IP5 (-1.32), CNPY2 (-1.32), MYL9 (-1.32), GCSH (-1.32), VPS72 (-1.33), SMIM20 (-1.34), RMDN1 (-1.34), SEC22A (-1.35), A0A494C1T2 (-1.35), TMEM254 (-1.36), TMEM109 (-1.37), SLC35A2 (-1.37), HS3ST3B1 (-1.38), SAE1 (-1.38), FBN2 (-1.39), Q5BKY9 (-1.39), HSPA8 (-1.39), PRDX3 (-1.40), ZNF75A (-1.40), FRZB (-1.40), FGF8 (-1.40), PDLIM7 (-1.41), MRPL58 (-1.41), GFAP (-1.41), TXNL1 (-1.42), P49448 (-1.42), MRPL43 (-1.43), SMNDC1 (-1.43), LUC7L (-1.43), HPCAL1 (-1.44), ATE1 (-1.44), HEXA (-1.44), TOMM20 (-1.45), TPT1 (-1.45), NRF1 (-1.46), BAX (-1.46), ND2 (-1.46), ACTMAP (-1.46), RBM8A (-1.46), ERP29 (-1.46), USF1 (-1.47), THG1L (-1.47), SRM (-1.49), RPL36 (-1.49), CTDNEP1 (-1.50), M0R2Q4 (-1.52), DERL1 (-1.52), ACTG1 (-1.52), HSPA6 (-1.53), NHERF1 (-1.55), HKDC1 (-1.57), PELI3 (-1.57), A0A0J9YXF2 (-1.58), LSM3 (-1.58), PPP1CC (-1.58), UBE2C (-1.59), MPV17 (-1.60), CALCOCO2 (-1.61), LTF (-1.61), SSR1 (-1.62), RACK1 (-1.62), ACTN1 (-1.63), CHCHD2 (-1.64), HACD2 (-1.66), NCALD (-1.67), CLCN7 (-1.67), TMEM35B (-1.67), M0QZM1 (-1.68), P61956 (-1.71), MAX (-1.72), PDCL (-1.72), AP1S2 (-1.74), WNK3 (-1.75), OSBPL5 (-1.77), STAU1 (-1.77), TMUB1 (-1.81), HLA-A (-1.83), RPL24 (-1.84), U2AF2 (-1.87), TAGLN2 (-1.94), EIF4A2 (-1.96), GMFB (-1.96), YWHAZ (-1.99), APMAP (-2.06), TOR1AIP1 (-2.11), NOP56 (-2.13), H0YMJ0 (-2.13), TTN (-2.17), Q8WUZ0 (-2.18), PCNA (-2.20), DDA1 (-2.25), RPL22 (-2.25), QNG1 (-2.26), PHGDH (-2.27), MYL12A (-2.30), H0Y757 (-2.32), HNRNPH1 (-2.32), ALDOA (-2.41), DCTN3 (-2.42), DHCR24 (-2.51), UBE2D1 (-2.51), UBE2I (-2.76), CNN3 (-2.87), NLRP2 (-2.88), ARPC4 (-2.97), TUBB6 (-2.98), MACROH2A2 (-3.03), TUBAL3 (-3.14), KATNAL2 (-3.21), PTMS (-3.37), PPP2CB (-3.54), M0QYM7;M0R042 (-3.73), PAICS (-3.87), UBE2D3 (-4.43), PRSS3 (-4.46), HSP90AA4P (-4.87), ACTB (-4.92)

DAY 15

CCDC92B (+3.44), GAR1 (+2.93), VDAC1 (+2.86), RBBP4 (+2.84), ZNF66 (+2.57), RPL36A (+2.54), SRP14 (+2.50), ATP5F1E (+2.48), SOX2 (+2.41), PCBD1 (+2.38), SREK1 (+2.35), EBP (+2.33), NCAM1 (+2.29), PLEKHF1 (+2.29), H1-0 (+2.29), CHMP3 (+2.20), CHMP1A (+2.17), COX1 (+2.14), PCTP (+2.08), COL4A5 (+2.00), TMEM35A (+2.00), VDAC2 (+1.98), GLO1 (+1.95), ALG8 (+1.94), NAT14 (+1.93), TMEM167A (+1.91), PABPC4 (+1.88), ORMDL2 (+1.88), AURKAIP1 (+1.87), KRT6B (+1.86), RPS23 (+1.85), AKR1B10 (+1.85), PPIA (+1.80), NECAP1 (+1.79), LAMB4 (+1.72), FKBP8 (+1.71), A0A087WX23 (+1.69), USP9Y (+1.67), RIC8A (+1.67), PCBP3 (+1.66), MAPKAPK5 (+1.66), FAM32A (+1.65), SUPT4H1 (+1.61), PCBD2 (+1.60), AGPAT1 (+1.58), SEZ6L (+1.57), SYNGR2 (+1.56), FHL3 (+1.56), MACROH2A1 (+1.54), BLM (+1.53), RABAC1 (+1.52), RPL37A (+1.52), NID1 (+1.51), DAP (+1.51), EPHX3 (+1.50), CRLF1 (+1.50), A0A5H1ZRP4 (+1.49), BST2 (+1.48), JAM3 (+1.48), RABIF (+1.47), RPA3 (+1.46), NXPE1 (+1.45), PITPNM2 (+1.41), NABP2 (+1.40), TSTD1 (+1.37), CHTOP (+1.37), COL22A1 (+1.37), RHOT1 (+1.34), MRPS10 (+1.32), SLC25A29 (+1.31), TGFB2 (+1.31), UFD1 (+1.31), TMEM47 (+1.31), MBD1 (+1.30), RNF185 (+1.30), FERMT2 (+1.29), UBTF (+1.29), DHRS1 (+1.29), TLCD3A (+1.28), SEC11A (+1.28), MXRA8 (+1.27), UBE2G2 (+1.27), FZD7 (+1.27), SMDT1 (+1.26), COX7C (+1.25), HMGN4 (+1.25), ICMT (+1.24), CAMKMT (+1.23), TSC22D3 (+1.23), CANX (+1.23), SELENOH (+1.22), CRTC1 (+1.22), INTS15 (+1.22), C1orf226 (+1.21), MBD4 (+1.21), VIP (+1.21), PPA2 (+1.21), RPL7A (+1.20), BCAP29 (+1.20), A6NDN3 (+1.17), C1QTNF4 (+1.16), CCDC117 (+1.16), CIR1 (+1.16), HLA-A (+1.15), NEFL (+1.15), HIRIP3 (+1.13), PMPCB (+1.12), DPY19L4 (+1.12), HUWE1 (+1.12), TMEM33 (+1.11), RPS21 (+1.11), A8K070 (+1.11), AHNAK2 (+1.11), NEFM (+1.09), LYRM7 (+1.09), CACFD1 (+1.08), ZFYVE21 (+1.08), P35789 (+1.08), SLC25A46 (+1.07), ZKSCAN1 (+1.07), ATP1A3 (+1.06), POU5F1 (+1.06), SEC61B (+1.06), S100A13 (+1.06), THEM4 (+1.06), SFT2D2 (+1.05), MEF2C (+1.05), TRAPPC5 (+1.04), IREB2 (+1.04), STRA6 (+1.04), AMPH (+1.03), NEK5 (+1.02), FBLN1 (+1.02), CXCL12 (+1.02), CHURC1 (+1.01), GPC3 (+1.01), DCD (+1.00), SLC17A5 (+1.00), DMAC2 (+1.00), DYNC2I2 (-1.00), RIOK1 (-1.00), PELI3 (-1.00), PNPLA2 (-1.00), DDHD1 (-1.00), PARP4 (-1.01), RPS3 (-1.01), PRKAG2 (-1.01), NDST1 (-1.02), SLC35B3 (-1.02), SATB1 (-1.03), SPTY2D1 (-1.03), TGM2 (-1.03), PPCDC (-1.03), A0A3B3IRQ9 (-1.04), NTRK3 (-1.05), FYN (-1.05), VAT1L (-1.06), UFM1 (-1.07), LDAH (-1.07), Q8IVT5 (-1.08), GRIK3 (-1.08), ZDHHC4 (-1.08), DOLK (-1.08), ZNF503 (-1.08), EFCC1 (-1.09), RAP1GAP2 (-1.11), DNM3 (-1.11), TOLLIP (-1.11), ARL6IP1 (-1.11), BET1 (-1.12), CWC25 (-1.12), KLC1 (-1.13), LPIN3 (-1.13), Q9P278 (-1.13), STAU1 (-1.14), PKM (-1.14), CIC (-1.15), SMIM12 (-1.17), STARD7 (-1.17), PLIN2 (-1.18), RSPH9 (-1.18), NCALD (-1.18), APEX2 (-1.20), SLITRK6 (-1.20), TCAF2 (-1.22), ABHD5 (-1.22), LMBRD1 (-1.22), ARL8A (-1.22), JRK (-1.22), H0YC97;H0YDK8;Q5T1Z4;Q5T1Z8 (-1.23), GRK3 (-1.23), IDH3G (-1.23), ARHGEF16 (-1.24), HNRNPD (-1.24), CNIH4 (-1.24), SIX4 (-1.26), E9PBY3;H0YAH3 (-1.27), C11orf54 (-1.31), COX15 (-1.32), UBASH3B (-1.33), XPR1 (-1.33), MRGBP (-1.37), ACP6 (-1.37), ATP5PD (-1.38), POLR3H (-1.40), ND1 (-1.40), H2AZ1 (-1.40), MPV17 (-1.41), ACTN1 (-1.41), WNK3 (-1.43), PRKACB (-1.43), ARHGAP23 (-1.44), LPAR2 (-1.44), TMEM41A (-1.47), LSM1 (-1.47), PSMC1 (-1.47), MAPRE1 (-1.48), VSNL1 (-1.50), LIN9 (-1.50), TAGLN (-1.51), SPIRE1 (-1.55), PTMA (-1.58), SNRPF (-1.59), MAPRE3 (-1.63), CDK5RAP1 (-1.67), PNPLA4 (-1.70), NAA40 (-1.73), ABRACL (-1.83), HNRNPA1 (-1.88), EPN3 (-1.90), U2AF2 (-1.92), TOR1AIP1 (-1.99), YWHAZ (-2.00), ENY2 (-2.13), UBE2I (-2.26), QNG1 (-2.36), DHCR24 (-2.52), DDX5 (-2.99)

DAY 21

HNRNPU (+3.67), CA2 (+2.73), PPIA (+2.73), LEFTY2 (+2.72), DOT1L (+2.67), PRPH (+2.58), SFI1 (+2.39), CRABP2 (+2.36), ITGB6 (+2.35), CHMP1B (+2.28), GPC3 (+2.21), HMGN4 (+2.17), HTR2C (+2.14), H1-0 (+2.01), MYL1 (+1.99), COL11A1 (+1.95), CNTN1 (+1.94), BST2 (+1.93), COL4A5 (+1.90), RPL36A (+1.79), POMC (+1.77), SLITRK1 (+1.70), HMGA2 (+1.62), A0A5H1ZRP4 (+1.61), O76009 (+1.60), RABAC1 (+1.57), RPL27A (+1.57), NABP2 (+1.54), MMGT1 (+1.54), SOX2 (+1.54), AHNAK2 (+1.53), SYNGR2 (+1.51), RPL29 (+1.51), A6NDN3 (+1.49), DAP (+1.48), MEAF6 (+1.43), RAB33A (+1.41), ZNF75A (+1.41), ZNF207 (+1.37), LBR (+1.36), COL4A6 (+1.36), BLM (+1.34), MAP4 (+1.34),

C1orf226 (+1.33), MRPS6 (+1.33), A8MWD9;P62308 (+1.33), AIG1 (+1.29), PCBP3 (+1.28), SRSF5 (+1.27), DPY30 (+1.23), C1QTNF4 (+1.23), NFIA (+1.21), Q969Q0 (+1.21), PGR (+1.20), ATAD1 (+1.20), CLTA (+1.20), SELENOH (+1.19), GSTM1 (+1.19), ATRIP (+1.19), ARHGEF6 (+1.18), HNRNPL (+1.18), SLC4A4 (+1.18), YWHAB (+1.17), FBLN1 (+1.17), CRX (+1.15), BCAR1 (+1.14), COL26A1 (+1.14), EIF3J (+1.13), UBTF (+1.13), TPRKB (+1.13), HSPB1 (+1.13), BET1L (+1.13), CD99 (+1.12), IL13RA2 (+1.12), A8K070 (+1.11), HSPB6 (+1.10), PSMB1 (+1.09), RPLP2 (+1.09), CNIH2 (+1.09), CNRIP1 (+1.09), DLST (+1.08), MEF2C (+1.08), NOS2 (+1.07), PLXNC1 (+1.07), NFYB (+1.07), CTTN (+1.07), TRIR (+1.06), SSBP2 (+1.06), SSBP3 (+1.04), FSBP (+1.04), CYTB (+1.03), FKBP10 (+1.03), GAR1 (+1.03), COX4I1 (+1.03), Q04743 (+1.03), HYI (+1.02), EAPP (+1.02), FBN2 (+1.02), CCDC12 (+1.02), PSMC5 (+1.02), FH (+1.01), C7orf50 (+1.01), EDF1 (+1.01), TMEM223 (+1.00), FABP5 (+1.00), LGALSL (-1.01), UQCR11 (-1.02), STAU1 (-1.02), MSH4 (-1.04), CD81 (-1.04), PRKCD (-1.04), NAA40 (-1.04), GSTZ1 (-1.04), DERA (-1.05), O60422 (-1.06), UBE2A (-1.06), GAP43 (-1.07), DPYSL4 (-1.07), A0A140T9Q4;A0A140T9S7 (-1.07), TCAF2 (-1.08), CACNA2D1 (-1.08), P0CG29;P0CG30 (-1.08), PRSS23 (-1.08), AIDA (-1.08), NCAM1 (-1.09), LAMP2 (-1.10), DCX (-1.10), CADPS (-1.11), KIF5C (-1.12), TOLLIP (-1.13), A0A0U1RQJ6;B4DDN1 (-1.13), C12orf54 (-1.15), PANX1 (-1.17), Q9NP97 (-1.18), PSMC1 (-1.18), PRPSAP2 (-1.19), ELAVL4 (-1.20), NRCAM (-1.20), AP3B2 (-1.21), DPYSL3 (-1.22), C2orf49 (-1.23), CHN2 (-1.23), PTPN6 (-1.23), EHHADH (-1.25), NCALD (-1.25), OSBPL5 (-1.25), MAT2B (-1.26), ALCAM (-1.27), FYN (-1.27), SURF2 (-1.28), NR2F1 (-1.28), KIF21A (-1.28), GSN (-1.31), NDRG1 (-1.31), SDF2 (-1.32), MPV17 (-1.33), NAP1L1 (-1.33), ARSA (-1.33), U2AF2 (-1.34), HNRNPH1 (-1.35), HLA-C (-1.35), PNPLA4 (-1.36), M0QYM7;M0R042 (-1.37), DYNC1I1 (-1.37), CNTN2 (-1.39), MACF1 (-1.39), ZSWIM6 (-1.39), WNK3 (-1.40), AGR3 (-1.44), TMA7 (-1.45), VCP (-1.49), PFN2 (-1.61), ATP5F1B (-1.65), NME1-NME2 (-1.66), ACTN1 (-1.70), EPHB2 (-1.74), PSMB3 (-1.82), PAFAH1B2 (-1.84), COX1 (-1.85), CCDC92B (-1.86), TAGLN3 (-1.88), RIC8A (-1.91), YWHAZ (-2.00), NLRP2 (-2.02), GFAP (-2.02), ARL8A (-2.09), TOR1AIP1 (-2.12), EPB41 (-2.13), PHYHIP (-2.16), SNRPF (-2.29), QNG1 (-2.53), CYB5R3 (-2.58), VIM (-2.63), P0C0S8;P20671;Q96KK5;Q99878;Q9BTM1 (-2.69), CNIH4 (-2.76), RPLP1 (-3.10), SRP14 (-3.62), CCT6B (-3.74), H2AC8 (-4.62)

DAY 30

Q969Q0 (+4.62), SEC11A (+3.84), VDAC2 (+3.46), SERPINB7 (+3.40), HNRNPU (+3.35), LEFTY2 (+3.32), MACROH2A1 (+3.30), GAR1 (+3.11), CA2 (+3.11), UQCRFS1 (+3.03), SOX2 (+2.96), RPL26 (+2.95), A0A087WX23 (+2.95), PABPC4 (+2.92), CHMP1B (+2.82), MGST1 (+2.81), VDAC1 (+2.77), HMGN4 (+2.69), RBBP4 (+2.65), SFI1 (+2.64), SREK1 (+2.63), RBX1 (+2.62), PPIA (+2.58), RHOT1 (+2.56), TMEM123 (+2.54), TXNDC12 (+2.54), PCBD1 (+2.47), PSMC5 (+2.39), IER3IP1 (+2.35), RPL29 (+2.35), EBP (+2.31), H3-7 (+2.31), FKBP10 (+2.26), ZNF66 (+2.26), CRABP1 (+2.26), REM2 (+2.22), HMGA2 (+2.20), BST2 (+2.20), CERS6 (+2.20), DECR1 (+2.19), POMC (+2.16), CCDC92B (+2.16), HMGN2 (+2.10), RBP1 (+2.08), TLE1 (+2.08), CRABP2 (+2.07), EDF1 (+2.06), DGUOK (+2.05), RPL36A (+2.04), PYCR2 (+2.03), CAPN6 (+2.00), CPT1A (+1.98), PLXNC1 (+1.92), GIT2 (+1.92), TMEM167A (+1.91), CMBL (+1.91), MAPK15 (+1.91), NARS2 (+1.91), IL13RA2 (+1.90), AP1S2 (+1.88), MRPS28 (+1.88), FLNC (+1.88), WDR43 (+1.88), CYBC1 (+1.87), TGFB2 (+1.86), M0QYT0;M0R076 (+1.86), COL11A1 (+1.86), CHMP1A (+1.86), ATP5F1E (+1.84), RPL27A (+1.83), YIPF3 (+1.82), CALB1 (+1.81), RAB32 (+1.81), SEPTIN6 (+1.81), BAG2 (+1.79), PRPH (+1.78), CTDNEP1 (+1.77), SLITRK1 (+1.77), RPL37A (+1.77), NUDT4 (+1.76), CRTAP (+1.76), UFD1 (+1.76), ASAH1 (+1.76), AURKAIP1 (+1.75), PCBD2 (+1.74), DHRS4 (+1.74), PTPRZ1 (+1.72), SLC4A1AP (+1.72), SLC25A20 (+1.69), BLM (+1.68), RPS27 (+1.68), RPUSD3 (+1.68), ORMDL2 (+1.68), CRELD2 (+1.67), PRPS2 (+1.67), ERH (+1.66), ATAD1 (+1.65), GUSB (+1.64), FAM32A (+1.64), GPR107 (+1.64), ARAP1 (+1.63), GLO1 (+1.62), HTR2C (+1.62), TVP23B (+1.61), NKX2-1 (+1.61), PRKD2 (+1.61), NOP56 (+1.61), BCAP31 (+1.60), MRPS33 (+1.60), ND1 (+1.59), C1QTNF4 (+1.59), REEP6 (+1.59), RPS29 (+1.58), CALU (+1.56), FKBP4 (+1.56), TMEM97 (+1.56), FKBP8 (+1.55), SDC2 (+1.55), GPC3 (+1.54), USP9Y (+1.53), UNG (+1.53), MPND (+1.53), LLPH (+1.53), GSTM1 (+1.53), ABAT (+1.52), MAPKAPK5 (+1.52), TPRKB (+1.52), NUMA1 (+1.51), RAD23A (+1.51), MED18 (+1.51), AIG1 (+1.50), SPARC (+1.50), BOD1 (+1.50), CASP6 (+1.50), ATRIP (+1.49), A0A5H1ZRP4 (+1.49), ZHX2 (+1.48), PLS3 (+1.48), HADHB (+1.48), SYNGR2 (+1.47), MMP14 (+1.47), NEDD4 (+1.46), NDUFC2 (+1.46), IGSF1 (+1.46), PWP1 (+1.45), ALG3 (+1.45), VCP (+1.45), Q9H2C1 (+1.44), CD46 (+1.44), IMMT (+1.44), IREB2 (+1.44), RPL27 (+1.44), ZFYVE21 (+1.43), DERL2 (+1.43), SERPINH1 (+1.42), ALDH1A2 (+1.42), SLC17A5 (+1.41), KIF13A (+1.41), TMEM47 (+1.41), ALG8 (+1.40), MFSD10 (+1.40), THEM4 (+1.40), AKR1B1 (+1.39), MRPL58 (+1.39), ZNF516 (+1.38), NDUFB5 (+1.38), ANXA5 (+1.38), HDLBP (+1.37), GABARAPL1 (+1.37), SDHD (+1.37), TP53I3 (+1.37), IGFBP3 (+1.36), RABAC1 (+1.36), DCTPP1 (+1.36), TOR1AIP2 (+1.36), DLST (+1.36), IGDCC4 (+1.35), SUPT4H1 (+1.35), RPP25 (+1.34), MBD1 (+1.34), NABP2 (+1.34), CRLF1 (+1.34), A0A0U1RQJ6;B4DDN1 (+1.33), DNAJC18 (+1.33), MXRA8 (+1.33), NUCB2 (+1.33), MAOB (+1.32), NFIA (+1.32), ZC3HAV1L (+1.30), TMEM17 (+1.30), WASL (+1.30), CNIH2 (+1.30), CCDC9 (+1.30), PCTP (+1.30), HMGN3 (+1.29), MAP1LC3A (+1.29), PMPCB (+1.29), TCEAL5 (+1.28), AGPAT1 (+1.28), NXPE1 (+1.28), SF3A2 (+1.28), STK32B (+1.28), SLC25A29 (+1.28), MRPL3 (+1.27), MYL1 (+1.27), MROH2B (+1.27), GFER (+1.27), ITGB4 (+1.27), HIPK2 (+1.26), CZIB (+1.26), CBLL1 (+1.25), PHPT1 (+1.25), CIR1 (+1.25), A6NDN3 (+1.24), MECOM (+1.24), B3GLCT (+1.23), PKN2 (+1.23), DLK1 (+1.23), COL5A1 (+1.23), CD2AP (+1.23), RBKS (+1.22), PTPRK (+1.22), HUWE1 (+1.22), CPNE3 (+1.22), CNTFR (+1.21), GTF2H2 (+1.21), CFAP298 (+1.20), TSC22D3 (+1.20), RBM47 (+1.20), MKRN2 (+1.20), MATR3 (+1.19), A0A0A0MRX1 (+1.19), IGFBP5 (+1.19), PUM2 (+1.19), SLC39A6 (+1.19), TLCD3A (+1.19), ZNF207 (+1.18), NQO1 (+1.18), Q9H6X2 (+1.18), ZKSCAN1 (+1.18), SELENOH (+1.17), CANX (+1.17), UGGT2 (+1.17), TOP2A (+1.17), MBOAT2 (+1.17), USP22 (+1.17), PDE1C (+1.16), LXN (+1.16), PDZD11 (+1.16), ITGA2 (+1.16), MAGEL2 (+1.16), HMGB1 (+1.16), WDR12 (+1.16), NAA10 (+1.15), HGH1 (+1.15), MBD4 (+1.15), CHST2 (+1.15), MEAF6 (+1.15), DNPEP (+1.14), TMEM33 (+1.14), QPRT (+1.13), ALDH7A1 (+1.13), PGK1 (+1.13), ARHGEF7 (+1.13), PXMP2 (+1.13), BCAP29 (+1.12), PARL (+1.12), H0YBG7 (+1.12), ACYP2 (+1.12), STON1 (+1.12), STRA6 (+1.12), SEC14L2 (+1.12), LDHB (+1.12), FHL3 (+1.12), FOXP4 (+1.11), RPL15 (+1.11), CPNE2 (+1.10), Q9UKI8 (+1.10), RPL10A (+1.10), MRPL48 (+1.10), INF2 (+1.09), ICMT (+1.09), MIS12 (+1.09), ZNF268 (+1.09), Q04743 (+1.09), ABHD4 (+1.09), NUDT19 (+1.09), O60739 (+1.09), NASP (+1.09), SNX15 (+1.09), MAMDC2 (+1.08), LSM4 (+1.08), P3H4 (+1.08), SUB1 (+1.08), SRSF5 (+1.08), C1orf226 (+1.08), SEC31A (+1.07), TSTD1 (+1.07), EPS15 (+1.07), ASF1A (+1.07), NIP7 (+1.07), MED6 (+1.07), WDHD1 (+1.07), LHX2 (+1.07), PCOLCE2 (+1.07), LDHA (+1.07), MTRES1 (+1.07), PRCP (+1.07), RPS3A (+1.07), WDR73 (+1.07), CAPNS1 (+1.06), DHX37 (+1.06), PLPP6 (+1.06), Q5JXI8 (+1.06), Q9UNL4 (+1.05), P60484 (+1.05), CPNE1 (+1.05), DOCK1 (+1.05), DCPS (+1.05), PALM2AKAP2 (+1.04), THAP11 (+1.04), GPC4

(+1.04), PGK2 (+1.04), TOR1B (+1.04), FGFR1 (+1.04), PDIA6 (+1.04), GANAB (+1.04), COL4A1 (+1.03), SLC25A53 (+1.03), EPHX3 (+1.03), DPY30 (+1.03), LRATD2 (+1.03), PPP6R1 (+1.02), PYCR3 (+1.02), PLPP3 (+1.02), RPL7A (+1.02), ARL5B (+1.02), SFXN5 (+1.02), MOB4 (+1.02), DPH2 (+1.02), ASCC1 (+1.02), XRCC5 (+1.02), STAT2 (+1.02), LBR (+1.02), CYTB (+1.01), GLDC (+1.01), RPUSD2 (+1.01), HTATSF1 (+1.01), NECAP2 (+1.01), A0A499FI31 (+1.01), COLGALT2 (+1.01), O95857 (+1.01), ISCA1 (+1.01), KRTCAP2 (+1.00), NDN (+1.00), DPY19L4 (+1.00), ACO2 (+1.00), HTRA3 (-1.00), GSTP1 (-1.00), WDR47 (-1.00), TOLLIP (-1.01), GFOD1 (-1.01), ANOS1 (-1.01), C1QTNF5 (-1.01), UBE2A (-1.01), SLC25A27 (-1.01), FASTKD1 (-1.01), P24468 (-1.01), VAT1L (-1.02), GABRG2 (-1.02), POU2F1 (-1.02), MYO5A (-1.02), CFDP1 (-1.02), PTPRO (-1.02), EDIL3 (-1.02), UBE2V2 (-1.03), STX7 (-1.03), TRIM36 (-1.04), SLC22A23 (-1.04), CAMK2B (-1.04), MTCL3 (-1.04), UBASH3B (-1.04), PBX1 (-1.05), TCAF2 (-1.05), TRIM71 (-1.06), ENSA (-1.06), THSD7A (-1.06), SMPD3 (-1.06), CELF4 (-1.06), CNTNAP1 (-1.07), DHCR7 (-1.07), LIN7A (-1.08), RPS3 (-1.08), SULF2 (-1.09), ARL6 (-1.09), AP3B2 (-1.09), RAB3D (-1.09), UBL4A (-1.09), RTN1 (-1.09), PRKCB (-1.10), HKDC1 (-1.10), GPM6B (-1.10), ANK2 (-1.10), SYN1 (-1.10), CETN2 (-1.10), EFNB3 (-1.10), CD81 (-1.11), RTN4 (-1.11), A0A1C7CYX9 (-1.11), UQCRB (-1.12), SORBS1 (-1.12), AOX1 (-1.13), CHCHD2 (-1.13), APLP1 (-1.13), CTNNA2 (-1.13), SELENOF (-1.14), CELF3 (-1.14), SNCA (-1.14), GUCY1B1 (-1.14), EVL (-1.14), CRMP1 (-1.15), ACTL6B (-1.15), DCLK1 (-1.16), NDRG1 (-1.16), SYNGR1 (-1.16), GNAO1 (-1.17), ELAVL2 (-1.17), MAPRE1 (-1.17), DPYSL3 (-1.17), FAM171B (-1.17), LSAMP (-1.17), SNAP25 (-1.18), TPPP (-1.18), PIP4K2C (-1.18), SVOP (-1.19), GNG4 (-1.19), TCP11L1 (-1.19), DNM1 (-1.19), A0A994J4E9;A0A994J6T5;A0A994J6U9;B4DUQ1;Q5T6W2 (-1.20), VTN (-1.20), ABRACL (-1.20), TOR1AIP1 (-1.20), DTD1 (-1.20), TUBB2A (-1.21), GFAP (-1.21), GAP43 (-1.21), CACNG4 (-1.21), HNRNPD (-1.21), EEF1D (-1.22), MPV17 (-1.22), DNM3 (-1.22), CA11 (-1.22), NFYA (-1.22), P0CG38 (-1.22), NR2F1 (-1.22), DDA1 (-1.23), RAB5C (-1.23), RPS7 (-1.23), PELI3 (-1.24), ROBO2 (-1.24), OLFML3 (-1.25), SDHC (-1.25), Q99697 (-1.26), ALB (-1.26), H1-10 (-1.27), PRRT2 (-1.28), L1CAM (-1.28), NBL1 (-1.28), EHHADH (-1.29), GRIK3 (-1.29), NAA40 (-1.29), RAB6B (-1.29), GSTZ1 (-1.30), KCTD16 (-1.30), LRP8 (-1.31), FAM241B (-1.31), PFN2 (-1.32), PLCL1 (-1.32), ZMAT4 (-1.32), DPYSL4 (-1.33), TUBGCP5 (-1.33), CD200 (-1.34), C2CD4C (-1.34), DERPC (-1.34), PRTFDC1 (-1.34), PRPSAP1 (-1.34), TMOD2 (-1.36), REEP1 (-1.36), VMA21 (-1.36), ATP1A3 (-1.37), TMEM35A (-1.37), PTPRF (-1.37), ATP12A (-1.38), STK32C (-1.38), CHMP5 (-1.38), APOA1 (-1.39), FREM2 (-1.42), PSMG4 (-1.42), CNTNAP5 (-1.43), RAB3C (-1.44), STX12 (-1.45), CHN2 (-1.46), LINGO1 (-1.46), ELAVL3 (-1.46), NDRG4 (-1.47), SLC17A6 (-1.47), H3BSE6 (-1.48), ENO2 (-1.48), STMN2 (-1.48), CADM2 (-1.49), SYT1 (-1.49), PRRT1 (-1.49), POU2F2 (-1.50), HPCAL1 (-1.50), DPYSL5 (-1.50), RAB3A (-1.53), TAF15 (-1.53), ARL15 (-1.54), TAGLN2 (-1.54), UFM1 (-1.54), MACF1 (-1.55), DYNC1I1 (-1.56), PTPRE (-1.57), AUTS2 (-1.59), MAPRE3 (-1.59), FYN (-1.60), Q9P2P6 (-1.64), NEFL (-1.64), WNK3 (-1.66), DNAJC6 (-1.67), OPCML (-1.67), O60422 (-1.69), NCALD (-1.69), CNTNAP2 (-1.69), FDFT1 (-1.70), C1QL1 (-1.72), NAPB (-1.73), CYB5R3 (-1.75), TMEM14C (-1.75), Q9H4W6 (-1.78), CDH10 (-1.79), PPP2CB (-1.80), DNAH8 (-1.80), NCAM1 (-1.81), ARL8A (-1.84), ABTB3 (-1.85), GPM6A (-1.85), SYT7 (-1.86), A0A7P0T936 (-1.87), ATP1B1 (-1.88), Q9NP97 (-1.91), PRSS23 (-1.91), ANK3 (-1.92), ACTG1 (-1.95), ACTBL2 (-1.96), NFASC (-1.97), SNRPF (-1.97), M0QYM7;M0R042 (-2.04), NLRP2 (-2.05), QNG1 (-2.06), EIF4A2 (-2.07), EPHB2 (-2.08), SYT4 (-2.09), RRM2 (-2.10), OSBPL5 (-2.12), CACNA2D1 (-2.13), INA (-2.20), ATP1A2 (-2.20), CENPV (-2.22), DDC (-2.27), TAGLN3 (-2.34), KIF5C (-2.35), ENY2 (-2.38), TUBB6 (-2.41), GSN (-2.61), NTM (-2.71), UBE2I (-2.86), YWHAZ (-2.88), DCX (-3.26), EPB41 (-3.32), Q6PEY2 (-3.34), P0C0S8;P20671;Q96KK5;Q99878;Q9BTM1 (-3.89), H2AC8 (-5.56)

DAY 40

TUBB4B (+5.03), TUBB2A (+4.71), TUBB6 (+4.40), H3-7 (+4.08), TUBB (+3.91), RPL29 (+3.68), HSP90AB4P (+3.34), RAC3 (+3.31), A6NCE7;Q9GZQ8 (+3.29), PRPH (+3.16), FDPS (+3.05), MACROH2A1 (+2.97), EBP (+2.93), TUBB4A (+2.91), MAP1LC3A (+2.89), Q9BVA1 (+2.89), RPL11 (+2.88), IER3IP1 (+2.77), P63000 (+2.75), RHOB (+2.68), VDAC3 (+2.55), GM2A (+2.53), VMA21 (+2.51), RPL31 (+2.50), DCX (+2.47), SREK1 (+2.44), DDC (+2.41), CISD2 (+2.41), INA (+2.39), GPI (+2.34), RAB1A (+2.25), YWHAQ (+2.22), FKBP1A (+2.22), H1-0 (+2.20), SRP9 (+2.19), HNRNPL (+2.17), SSBP3 (+2.14), MDH2 (+2.12), ZNF66 (+2.11), LAMP1 (+2.10), ATE1 (+2.09), GAMT (+2.08), SH3BGRL3 (+2.07), CIRBP (+2.07), CAPZA2 (+2.07), ARF3 (+2.06), RAB3A (+2.04), CHMP1A (+2.04), GAPDH (+2.03), CD47 (+2.03), ATP5MK (+2.02), ATP5F1E (+2.01), YWHAH (+1.96), THY1 (+1.95), PFN2 (+1.95), CZIB (+1.82), GNAQ (+1.81), MGST3 (+1.81), P62879 (+1.80), TSTD1 (+1.80), PHYHIP (+1.78), HNRNPDL (+1.77), ISOC2 (+1.77), CTSB (+1.77), DDAH2 (+1.76), FSCN1 (+1.76), PGK1 (+1.76), CNRIP1 (+1.75), NAPA (+1.75), ARL8B (+1.75), SLC25A5 (+1.74), COPZ1 (+1.74), PLPPR1 (+1.73), RHOT1 (+1.73), MRPL21 (+1.73), A0A087WWU8 (+1.72), SCAMP3 (+1.72), CADM3 (+1.71), OSTC (+1.71), RPL37A (+1.69), VAMP2 (+1.68), DAD1 (+1.67), PGAM1 (+1.67), KPNA3 (+1.67), ABI1 (+1.67), ATP1B1 (+1.66), E9PN89 (+1.66), RUFY3 (+1.65), BHMT (+1.64), SNAP25 (+1.64), TTC9C (+1.62), HSPA9 (+1.62), CENPV (+1.61), DLST (+1.60), P68366 (+1.60), GNA11 (+1.60), FKBP4 (+1.59), MRPL58 (+1.59), PFDN5 (+1.57), RPL32 (+1.56), CORO1C (+1.56), MAPK15 (+1.56), NDUFB1 (+1.56), LLPH (+1.55), ATP4A (+1.54), FXYD6 (+1.53), CXADR (+1.53), TLCD3B (+1.53), MYL4 (+1.53), VAPA (+1.52), ZMYND8 (+1.51), GOT1 (+1.51), SLC6A6 (+1.51), GNAL (+1.51), RPS29 (+1.51), CSNK2A1 (+1.50), AKR7A2 (+1.50), SNRPD2 (+1.49), GLO1 (+1.49), AIG1 (+1.49), RABIF (+1.49), MARCKSL1 (+1.49), MYL1 (+1.49), TPRKB (+1.49), SLC2A3 (+1.48), PRDX1 (+1.48), EIF3K (+1.48), AURKAIP1 (+1.48), NDUFB5 (+1.47), RALY (+1.47), P06899;Q16778 (+1.47), LANCL3 (+1.46), CHMP2B (+1.46), MDP1 (+1.46), HSPA5 (+1.46), KRTCAP2 (+1.46), SLC25A29 (+1.46), U2AF2 (+1.45), SUPT4H1 (+1.45), GLUD1 (+1.44), TRAPPC3 (+1.44), CTNNA2 (+1.44), SCAF4 (+1.44), NIF3L1 (+1.43), A8MWD9;P62308 (+1.43), GNAO1 (+1.43), RAB2A (+1.43), PYCR1 (+1.42), CIT (+1.42), SNCG (+1.42), Q8TE12 (+1.42), PPP4C (+1.42), REEP5 (+1.41), UBA1 (+1.41), DRAP1 (+1.41), FAM136A (+1.41), SF1 (+1.40), CYB561 (+1.40), CASTOR2 (+1.40), NDUFB7 (+1.39), MBD3 (+1.39), CLIC1 (+1.39), RPL19 (+1.38), DHRS1 (+1.37), MED20 (+1.37), H1-4 (+1.37), ARGLU1 (+1.37), ATAT1 (+1.36), ZC2HC1A (+1.36), RELN (+1.35), G3BP2 (+1.35), ATP6V0C (+1.35), RPL13 (+1.35), DNM3 (+1.35), KCTD12 (+1.35), ATP5F1D (+1.35), SLC7A3 (+1.34), ACOT7 (+1.34), ATP6V1G2 (+1.32), PTPRT (+1.32), HNRNPA0 (+1.32), PFN1 (+1.31), YWHAG (+1.31), PDE6D (+1.31), RABAC1 (+1.31), H7C2K6 (+1.31), CYSTM1 (+1.31), CD81 (+1.30), NUMA1 (+1.30), VSNL1 (+1.30), SNURF (+1.30), ELAVL2 (+1.30), CNN2 (+1.30), RAB14 (+1.29), PRKRA (+1.29), FNTB (+1.29), GABRA3 (+1.28), Q15836 (+1.28), PRDX2 (+1.27), RPL8 (+1.27), CHTOP (+1.27), CHORDC1 (+1.27), TMEM254 (+1.27), TRAPPC5 (+1.27), BLM (+1.27), NUDT10 (+1.27), MBD4 (+1.26), DPYSL3 (+1.26), RIDA (+1.26), PORCN (+1.26), P63261 (+1.26), SBF1 (+1.26), GRIA1 (+1.25), PAICS (+1.25), LSM6 (+1.24), SARNP (+1.24), DIRAS2 (+1.23), PRRT1 (+1.23), AP1S2 (+1.23), HMGCS1 (+1.23), H0Y757 (+1.23), CAPRIN1 (+1.23), Q9Y281 (+1.23), SSBP1

(+1.23), FBXO30 (+1.22), GSKIP (+1.22), BACE1 (+1.22), EEF2 (+1.21), RAB30 (+1.21), MRPL53 (+1.21), MMGT1 (+1.21), SNRPC (+1.21), PTRHD1 (+1.21), RAB33A (+1.21), L1CAM (+1.21), CORO1A (+1.21), ALB (+1.21), MRI1 (+1.20), NOLC1 (+1.20), PMVK (+1.20), AGAP1 (+1.20), GDE1 (+1.20), NACC1 (+1.20), UBE2D1 (+1.20), MTURN (+1.20), HNRNPAB (+1.19), LSM12 (+1.19), STOML2 (+1.19), SLC2A13 (+1.18), MIEF1 (+1.18), RPL10A (+1.18), ACTG1 (+1.17), CHCHD2 (+1.17), APH1A (+1.17), GPRIN1 (+1.17), RAB5A (+1.17), O94905 (+1.17), RPS3A (+1.17), EBF1 (+1.16), SNCB (+1.16), UBA2 (+1.16), DPF3 (+1.16), RAB7A (+1.16), MPC1 (+1.16), ELFN1 (+1.16), RPS25 (+1.16), LRFN4 (+1.15), JPT1 (+1.15), PSMA2 (+1.15), EXOSC5 (+1.15), CEND1 (+1.15), ZHX2 (+1.15), TMEM258 (+1.14), NECTIN2 (+1.14), CELF5 (+1.14), COL4A5 (+1.14), SULT1A1 (+1.13), SH3GLB2 (+1.13), MATR3 (+1.13), NHP2 (+1.12), ACTN4 (+1.12), HSP90AA5P (+1.12), TSPYL5 (+1.12), TPM2 (+1.12), NDUFA4 (+1.12), HYI (+1.11), HMGB1 (+1.11), ZNF75A (+1.11), PSMA6 (+1.11), ATP6 (+1.11), SAFB (+1.10), CCT7 (+1.10), FKBP1B (+1.10), P23416 (+1.10), COPS7B (+1.09), HNRNPA2B1 (+1.09), FERMT2 (+1.09), CARS1 (+1.08), NOL7 (+1.07), PRKAR2A (+1.07), PPP2R1A (+1.07), AKT1S1 (+1.07), LASP1 (+1.07), BZW1 (+1.06), EEF1G (+1.06), ETFA (+1.06), Q08209 (+1.06), RTN4 (+1.06), MACF1 (+1.06), SHMT2 (+1.06), PPP3CB (+1.06), EIPR1 (+1.06), RPL22 (+1.05), Q9UKI8 (+1.05), DENND4B (+1.05), RNF7 (+1.05), YIF1A (+1.05), HSPA4 (+1.05), ACTMAP (+1.05), CADM1 (+1.04), RPS26 (+1.04), MAP1S (+1.04), AMDHD2 (+1.04), TP53BP1 (+1.04), NIPA1 (+1.03), ARID3A (+1.03), MRPS6 (+1.03), RAB3IP (+1.03), KLHL7 (+1.03), RPL13A (+1.03), GNAI3 (+1.03), ATP1A1 (+1.03), TRAF2 (+1.02), GHITM (+1.02), CASK (+1.02), OLFM1 (+1.02), GABBR2 (+1.02), CD200 (+1.01), XPNPEP1 (+1.01), SAP30L (+1.01), TBP (+1.00), ACVR1B (+1.00), CAP1 (+1.00), ATP5F1A (+1.00), RAB11FIP1 (-1.00), CEPT1 (-1.01), M0R2Q4 (-1.01), TMED9 (-1.01), CREB1 (-1.01), PDE5A (-1.01), CDK2 (-1.02), TOMM34 (-1.02), PLAU (-1.02), SAMD5 (-1.02), ARIH2 (-1.03), ACOT8 (-1.03), CALCOCO2 (-1.03), ATP9B (-1.03), TMEM101 (-1.03), CYGB (-1.04), PNPLA4 (-1.04), CELSR1 (-1.04), COX20 (-1.04), STX16 (-1.04), IFT70B (-1.04), ARMC1 (-1.05), MEIS2 (-1.05), REEP6 (-1.05), RAVER1 (-1.05), ADPGK (-1.06), CENPN (-1.06), RGS12 (-1.06), TTYH3 (-1.07), MKRN2 (-1.07), QRICH1 (-1.08), CKM (-1.08), WWC3 (-1.08), CDH2 (-1.08), KIAA1143 (-1.09), P63267 (-1.10), UBE2A (-1.10), WSB2 (-1.10), UBE2B (-1.10), UBE2NL (-1.11), BET1 (-1.11), HMGN1 (-1.11), CD2AP (-1.12), YY2 (-1.13), TINAGL1 (-1.13), ARR3 (-1.13), NTAN1 (-1.13), NRBF2 (-1.13), A0A0U1RQJ6;B4DDN1 (-1.13), SRR (-1.14), MMRN1 (-1.14), NAP1L5 (-1.15), GEMIN8 (-1.16), SPPL2A (-1.16), LYPLAL1 (-1.16), MTFR1L (-1.16), RPS27 (-1.17), ISY1-RAB43 (-1.17), P3H4 (-1.17), ABHD4 (-1.17), MPI (-1.18), APRT (-1.18), NPDC1 (-1.19), CCDC167 (-1.19), LDB1 (-1.19), RPS20 (-1.20), CNN3 (-1.20), EHHADH (-1.20), ARL6IP4 (-1.20), STC2 (-1.21), MRGBP (-1.21), TTF2 (-1.21), NPM1 (-1.22), COL2A1 (-1.22), SPCS3 (-1.22), GLS (-1.22), RAB6C (-1.22), BRIX1 (-1.22), CSDC2 (-1.22), NEK5 (-1.23), AJUBA (-1.24), MSH4 (-1.24), BROX (-1.24), LSM11 (-1.26), LYPLA2 (-1.26), ARSA (-1.27), MAN2B1 (-1.27), PSMF1 (-1.27), SLC16A1 (-1.27), KLC1 (-1.28), CBLL1 (-1.28), SYNGR3 (-1.28), GNB2 (-1.28), LIN28A (-1.29), ATP5MJ (-1.29), ITPRID2 (-1.29), SYVN1 (-1.31), J3KNV1 (-1.33), HAPLN3 (-1.33), RCN2 (-1.33), DOCK10 (-1.33), GNAS (-1.34), WNT10B (-1.34), GPX8 (-1.34), O60361 (-1.34), HSPB1 (-1.35), QPRT (-1.36), VCP (-1.36), RPS27L (-1.37), PARD6G (-1.38), AP1M1 (-1.40), ATP5F1B (-1.40), ALOX12 (-1.41), K7EQG2 (-1.42), PEX26 (-1.42), P19012 (-1.43), KGD4 (-1.43), TMEM201 (-1.44), A6NDN3 (-1.47), HTRA3 (-1.48), P0CG29;P0CG30 (-1.48), GSTO1 (-1.49), EMC3 (-1.49), COMMD8 (-1.50), OSBPL5 (-1.52), ACTN1 (-1.62), ANAPC7 (-1.65), RPS15 (-1.67), CD36 (-1.67), ARL8A (-1.68), WDR82 (-1.69), ERCC6L (-1.69), TPPP3 (-1.72), NAA40 (-1.73), CLN5 (-1.75), UFD1 (-1.75), HS3ST3B1 (-1.79), EFL1 (-1.82), WNK3 (-1.83), LUC7L (-1.83), QNG1 (-1.83), TMA7 (-1.83), NLRP2 (-1.84), CANX (-1.84), HRC (-1.86), COX1 (-1.87), TOR1AIP1 (-1.87), H2AC8 (-1.88), SLC39A7 (-1.90), SURF4 (-1.90), ENY2 (-1.93), RIC8A (-1.93), CLTCL1 (-1.93), CHRDL1 (-1.99), UBE2I (-1.99), NUTF2 (-2.03), CNIH4 (-2.04), PSMB3 (-2.04), PAFAH1B2 (-2.05), MYO3B (-2.05), NOP56 (-2.07), DYNLL1 (-2.08), HMGN2 (-2.11), EEF1A2 (-2.12), SRP14 (-2.13), CYP2D7 (-2.16), H3BSE6 (-2.17), TXNL1 (-2.25), HNRNPA1 (-2.25), YIPF5 (-2.29), RACK1 (-2.31), ALDOA (-2.35), MACROH2A2 (-2.35), MPV17 (-2.39), PTMA (-2.47), PSMC1 (-2.67), ATP1A2 (-2.96), GSN (-3.21), SNRPF (-3.45), DHCR24 (-3.70), PRSS3 (-4.24), CRYBG3 (-4.70)

DAY 60

Q969Q0 (+4.21), A8MWD9;P62308 (+3.38), SEC11A (+3.26), EBP (+3.22), MAPT (+3.09), VDAC1 (+2.86), PRPH (+2.80), GAR1 (+2.75), ATP5F1E (+2.72), IER3IP1 (+2.70), REM2 (+2.63), HNRNPL (+2.56), RNASEK (+2.51), RPL26 (+2.50), PABPC4 (+2.47), A0A0A0MRX1 (+2.38), ORMDL2 (+2.36), SOX2 (+2.35), PPIA (+2.33), TXNDC12 (+2.32), VDAC2 (+2.29), MAPK15 (+2.28), HMGN4 (+2.15), MPC1 (+2.13), CHMP1B (+2.12), DNM3 (+2.09), VDAC3 (+2.06), CNIH4 (+2.06), MAP1LC3A (+1.91), GABARAPL1 (+1.90), Q5JXI8 (+1.89), CHMP1A (+1.89), RPL29 (+1.88), ERC1 (+1.87), RPL36A (+1.85), NOVA2 (+1.83), FKBP4 (+1.80), CHMP3 (+1.79), FSIP2 (+1.78), NDN (+1.74), CERS6 (+1.74), CRABP1 (+1.72), B4DKF8 (+1.69), GNB1 (+1.67), CYB561 (+1.67), RABAC1 (+1.66), EDF1 (+1.64), HIPK2 (+1.64), JAM3 (+1.60), TCEAL5 (+1.60), SARS1 (+1.58), AIG1 (+1.57), COL5A1 (+1.52), FKBP8 (+1.51), PCM1 (+1.51), YIPF3 (+1.51), CCDC92B (+1.49), ALG3 (+1.49), CACFD1 (+1.49), RELN (+1.48), ACYP2 (+1.48), RPS27 (+1.48), RBM3 (+1.48), SLC39A6 (+1.47), STK26 (+1.46), HSP90AA5P (+1.44), Q9Y343 (+1.44), TLCD3B (+1.43), Q8WUZ0 (+1.43), LONP1 (+1.43), PRMT6 (+1.42), HNRNPU (+1.41), NOP10 (+1.40), PTPRT (+1.40), A6NDN3 (+1.40), PGK1 (+1.39), SUPT4H1 (+1.39), WDR43 (+1.39), NDUFB5 (+1.38), RBBP4 (+1.38), KIF11 (+1.36), HUWE1 (+1.36), RPS29 (+1.36), NME1-NME2 (+1.35), SLC4A1AP (+1.34), TMEM47 (+1.34), ZDHHC17 (+1.33), SNX15 (+1.33), FAM136A (+1.32), SLC25A29 (+1.32), GMNN (+1.32), MROH2B (+1.32), AGPAT1 (+1.31), PPT2 (+1.30), APIP (+1.29), COX1 (+1.29), RPL10 (+1.28), TOR1AIP2 (+1.28), TLE1 (+1.28), NR2F1 (+1.28), CD46 (+1.26), G3BP2 (+1.25), UQCC6 (+1.25), NOLC1 (+1.24), CCDC9 (+1.24), MAPK14 (+1.24), PAM (+1.23), SFT2D2 (+1.22), AGAP1 (+1.22), CRELD2 (+1.21), ACAT1 (+1.21), A0A994J7B0 (+1.20), MAPKAPK5 (+1.20), NKX2-1 (+1.20), PWP1 (+1.19), USP11 (+1.19), TMEM38B (+1.19), RBP1 (+1.19), CSTF2 (+1.18), MATR3 (+1.18), MED18 (+1.18), HMGN2 (+1.17), MBD4 (+1.17), ZNF24 (+1.17), ADRM1 (+1.16), A0A5H1ZRP4 (+1.16), SELENOH (+1.16), FAM118A (+1.16), ALG10 (+1.16), RAB31 (+1.16), COX18 (+1.15), GFRA2 (+1.14), NXPE1 (+1.13), DERL2 (+1.12), SULT1A1 (+1.12), CXXC4 (+1.11), TMEM123 (+1.11), FNTB (+1.11), RAB35 (+1.11), MMGT1 (+1.10), GRIA2 (+1.10), TLCD3A (+1.10), BORCS8 (+1.09), RPL27A (+1.09), UBA1 (+1.08), CD9 (+1.07), HMGA2 (+1.07), DCD (+1.07), CXXC5 (+1.07), RPS3A (+1.07), IQSEC1 (+1.06), OSBPL1A (+1.06), CYBC1 (+1.06), TIA1 (+1.05), CHTOP (+1.05), CMBL (+1.05), HDHD5 (+1.04), PTPRZ1 (+1.04), ZFYVE21 (+1.04), TSPAN4 (+1.04), TUBG2 (+1.03), HDAC3 (+1.03), HBD (+1.03), MBOAT2 (+1.02), KHDRBS3 (+1.02), ZC2HC1A (+1.01), NPTX1 (+1.01), GRIA2 (+1.01), RPS21 (+1.01), SDHC (+1.01), DPH1 (+1.00), SERINC5 (+1.00), LTF (-1.00), HSPA8 (-1.06), EFL1 (-1.07), UBE2I (-1.08), CLTC (-1.08), RAP1B (-1.13), TRIM13 (-1.14), IGHG1 (-1.15), CHMP5 (-1.17), CENPV (-1.17), ATAD3B (-1.19), MYL1 (-1.24), NCALD (-1.25), TOR1AIP1 (-1.26), PELI3 (-1.37), QNG1 (-1.40), PNPLA4 (-1.41), GLS

(-1.44), HPCAL1 (-1.46), U2AF2 (-1.49), H3BSE6 (-1.60), PHGDH (-1.63), NTM (-1.68), NLRP2 (-1.76), YWHAZ (-1.96), EIF4A2 (-2.36), DHCR24 (-3.16), MACROH2A2 (-3.38)

A.3 Persistently dysregulated genes & proteins

Gene	Day 0	Day 6	Day 15	Day 21	Day 30	Day 40	Day 60
TCEAL5	0.6	0.76	0.62	1.19	1.19	1.54	1.58
CHCHD2	-1.88	-0.95	-1.52	-1.01	-0.57	-0.68	-0.63
DNAJC15	-1.41	-1.12	-1.37	-0.86	-0.83	-0.86	-0.78
BEX3	1.07	0.73	1.11	1.4	1.04	0.68	0.26
WNK3	-0.62	-0.87	-0.68	-0.51	-0.85	-1.04	-1.3
LINC00551	-1.37	-1.23	-0.82	-0.62	-0.38	-0.68	-0.57
FTL	0.38	1.02	0.71	1.07	1.02	0.73	0.44
PUS7L	0.72	0.68	0.55	0.5	0.54	0.65	0.59
ZNF506	0.34	0.67	0.32	0.44	0.65	0.68	0.87
LINC02899	-0.32	-0.45	-0.45	-0.41	-0.65	-0.59	-0.85
PAX8.AS1	0.31	0.48	0.54	0.37	0.5	0.48	0.53
CPE	0.0	-1.29	0.61	1.04	0.87	0.7	0.29
TCEAL9	0.79	0.54	0.79	0.95	1.16	0.52	0.0
ATP5MG	-0.79	-1.01	-0.67	-0.7	0.0	-0.63	-0.68
BEX2	0.74	0.71	0.89	0.82	0.0	0.61	0.49
S100A6	0.28	0.62	0.61	0.37	0.0	0.91	0.98
KMT2A	-0.42	-0.48	-0.45	-0.68	-0.81	0.0	-0.77
TCEAL3	0.0	0.57	0.5	0.76	0.45	0.55	0.74
INPP5F	-0.53	-0.48	-0.43	0.0	-0.83	-0.64	-0.53
PSMD10	0.52	0.55	0.4	0.94	0.42	0.61	0.0
MT.RNR1	0.88	0.61	0.53	0.31	0.0	0.47	0.59
PGK1	-0.64	0.5	0.66	0.54	0.53	0.48	0.0
GAS5	-0.72	0.47	0.25	0.99	0.44	0.34	0.0
CCDC144NL.AS1	-0.4	-0.3	-0.44	0.0	-0.56	-0.82	-0.62
H1.0	-0.48	0.52	-0.31	-0.57	-0.91	-0.32	0.0
NLRP2	-0.97	-0.63	-0.36	-0.41	-0.34	-0.3	0.0
OTX2	0.28	0.42	-0.32	0.33	0.7	0.0	0.54
TCEAL7	0.32	0.29	0.58	0.38	0.33	0.35	0.0
SYT4	0.0	-0.42	0.0	-1.18	-2.19	-0.47	-0.67
PDZRN4	0.0	0.0	-0.28	-0.52	-2.23	-0.7	-0.56
SNHG5	0.44	0.0	0.77	1.1	1.15	0.3	0.0
PKIB	-0.68	0.0	-0.31	-0.51	-1.61	-0.54	0.0
TCEAL8	0.68	0.75	0.63	0.85	0.59	0.0	0.0
SYT11	0.0	0.53	0.91	0.71	0.79	0.0	0.54
PDE10A	0.0	0.0	0.38	0.56	0.82	1.19	0.49
MT.ND3	0.0	0.63	0.5	0.97	0.41	0.0	0.91
LMO3	0.0	0.0	-0.37	-0.59	-1.11	-0.54	-0.77
IFITM3	0.51	1.26	0.38	0.95	0.26	0.0	0.0
NR2F1	0.0	-0.25	0.0	-0.61	-1.34	-0.61	-0.51
PBX1	0.0	-0.26	0.0	-0.86	-1.15	-0.58	-0.41
KCNJ16	0.0	0.0	-0.46	-1.07	-0.8	-0.46	-0.26
CLU	0.28	0.28	0.0	0.65	1.28	0.0	0.52
MORF4L2	0.53	0.5	0.47	0.82	0.0	0.64	0.0
POTEF	0.0	0.0	-0.29	-0.37	-0.71	-0.5	-0.86
GPRIN3	0.0	0.0	-0.75	-0.38	-0.85	-0.3	-0.29
MT.CO2	0.57	0.94	0.46	0.28	0.32	0.0	0.0
MAP2	0.0	-0.38	-0.43	-0.84	-0.65	0.0	-0.26
CHD7	-0.38	-0.43	0.0	-0.81	-0.36	-0.41	0.0
USP11	0.0	0.41	0.49	0.48	0.41	0.5	0.0
SC5D	-0.5	-0.26	0.0	0.0	-0.34	-0.53	-0.55
SEPTIN11	-0.27	-0.73	-0.33	0.0	-0.3	0.0	-0.33
TRIM4	-0.38	-0.49	-0.5	0.0	-0.28	-0.27	0.0
MT.CO1	0.0	0.68	0.28	0.27	0.0	0.34	0.34
TIMM10	0.33	0.46	0.31	0.31	0.32	0.0	0.0
STK26	0.35	0.3	0.28	0.38	0.4	0.0	0.0
DDX11	0.0	0.26	0.28	0.29	0.25	0.28	0.0

Table A.10 Persistently dysregulated genes FC values. Genes dysregulated between *SNCA*-A53T and control cells in the same direction at five or more timepoints of the differentiation. Names and corresponding fold change (FC) values are indicated.

Protein	Day 0	Day 6	Day 15	Day 21	Day 30	Day 40	Day 60
RPL36A	3.37	1.64	2.54	1.79	2.04	1.94	1.85
QNG1	-1.73	-2.26	-2.36	-2.53	-2.06	-1.83	-1.40
TOR1AIP1	-1.49	-2.11	-1.99	-2.12	-1.20	-1.87	-1.26
YWHAZ	-0.55	-1.99	-2.06	-2.00	-2.88	-0.54	-1.96
U2AF2	-1.33	-1.87	-1.92	-1.34	-0.93	1.45	-1.49
JAM3	0.98	1.47	1.48	1.38	0.92	1.23	1.60
TBCEL	-0.54	-0.91	-0.59	-0.56	-0.70	-0.94	-0.53
NLRP2	-3.45	-2.88	0.00	-2.02	-2.05	-1.84	-1.76
VDAC2	2.67	0.59	1.98	0.00	3.46	1.93	2.29
PPIA	1.73	1.01	1.80	2.73	2.58	0.00	2.33
UBE2I	-1.07	-2.76	-2.26	0.00	-2.86	-1.99	-1.08
GSN	0.00	-1.24	-0.90	-1.31	-2.61	-3.21	-0.76
MPV17	-1.95	-1.60	-1.41	-1.33	-1.22	-2.39	0.00
WNK3	-1.37	-1.75	-1.43	-1.40	-1.66	-1.83	0.00
RABAC1	1.94	0.00	1.52	1.57	1.36	1.31	1.66
RHOT1	0.88	-0.82	1.34	0.94	2.56	1.73	0.00
AKR1B10	2.91	0.00	1.85	1.38	0.87	0.69	0.56
CHCHD2	-1.92	-1.64	0.00	-0.92	-1.13	1.17	-0.94
PNPLA4	-0.81	-1.16	-1.70	-1.36	0.00	-1.04	-1.41
SELENOH	0.00	0.80	1.22	1.19	1.17	1.83	1.16
UQCRFS1	0.61	1.02	0.85	0.96	3.03	0.83	0.00
EHHADH	-0.65	1.76	-0.95	-1.25	-1.29	-1.20	0.00
ZNF75A	0.71	-1.40	0.00	1.41	0.82	1.11	0.71
EFL1	-0.69	-1.28	-0.71	-0.53	0.00	-1.82	-1.07
DHRS1	0.00	0.77	1.29	0.80	0.84	1.37	0.82
DMAC2	0.00	1.08	1.00	0.64	0.83	0.84	0.80
CRYZ	1.09	0.76	0.71	0.00	0.82	0.86	0.88
TRIM4	-0.61	-0.68	-0.99	-0.67	0.00	-0.57	-0.63
IQGAP2	0.00	-0.62	-0.77	-0.82	-0.71	-0.71	-0.51
DHCR24	0.00	-2.51	-2.52	0.00	-0.86	-3.70	-3.16
RPL29	0.00	2.34	0.00	1.51	2.35	3.68	1.88
ATP5F1E	2.33	0.00	2.48	0.00	1.84	2.01	2.72
HNRNPU	1.76	0.00	0.00	3.67	3.35	0.88	1.41
MACROH2A2	0.00	-3.03	-0.89	0.00	-0.72	-2.35	-3.38
SOX2	1.07	0.00	2.41	1.54	2.96	0.00	2.35
ZNF66	2.45	0.78	2.57	0.00	2.26	2.11	0.00
CHMP1A	2.09	0.00	2.17	0.00	1.86	2.04	1.89
SREK1	0.00	1.45	2.35	1.05	2.63	2.44	0.00
H1-0	2.17	0.00	2.29	2.01	0.71	2.20	0.00
FKBP8	2.30	1.97	1.71	0.00	1.55	0.00	1.51
BST2	1.05	2.30	1.48	1.93	2.20	0.00	0.00
EDF1	0.00	2.18	0.00	1.01	2.06	1.83	1.64
ACTN1	0.00	-1.63	-1.41	-1.70	-0.89	-1.62	0.00
NCALD	0.00	-1.67	-1.18	-1.25	-1.69	0.00	-1.25
AIG1	0.00	0.00	0.99	1.29	1.50	1.49	1.57
BLM	0.00	0.00	1.53	1.34	1.68	1.27	0.73
PGK1	0.00	1.59	0.00	0.67	1.13	1.76	1.39
UBTF	2.30	0.00	1.29	1.13	0.85	0.71	0.00
TSTD1	0.82	0.00	1.37	0.99	1.07	1.80	0.00
TPRKB	0.94	0.88	0.00	1.13	1.52	1.49	0.00
HPCAL1	0.00	-1.44	0.00	-0.85	-1.50	-0.65	-1.46
TMEM41A	-1.78	0.00	-1.47	-0.96	-0.56	-0.99	0.00
RPS7	-1.20	-0.95	0.00	-0.79	-1.23	0.00	-0.96
A8K070	0.81	0.00	1.11	1.11	0.92	0.00	0.99
TSFM	-1.42	-1.05	-0.80	-0.81	0.00	-0.80	0.00
GLS	0.00	-0.92	-0.74	-0.53	0.00	-1.22	-1.44
TMEM258	0.00	0.00	0.79	0.97	1.00	1.14	0.82
SCO2	1.06	0.68	0.84	0.00	1.00	0.00	0.93
CD99	0.00	0.00	0.82	1.12	0.93	0.68	0.96
UBASH3B	0.00	-0.67	-1.33	-0.76	-1.04	-0.63	0.00
SLC17A5	0.85	0.00	1.00	0.55	1.41	0.53	0.00
SMDT1	0.00	0.53	1.26	0.93	0.00	0.68	0.89
IST1	1.05	0.90	0.86	0.66	0.80	0.00	0.00
MAP4	0.00	0.58	0.00	1.34	0.66	0.99	0.66
CAT	-1.04	-0.78	0.00	-0.70	-0.83	-0.87	0.00
CNOT6	0.00	1.21	0.67	0.00	0.79	0.75	0.68
LGALS1	0.86	1.09	0.00	0.78	0.00	0.57	0.78
CDH2	0.00	-0.85	-0.65	-0.67	-0.75	-1.08	0.00
COMMD10	0.00	0.00	0.83	0.95	0.75	0.56	0.80
KHDRBS3	0.00	0.55	0.00	0.58	0.79	0.84	1.02
ARL5B	0.00	0.77	0.00	0.51	1.02	0.64	0.69
LIG3	0.79	0.00	0.67	0.63	0.75	0.00	0.63

Table A.11 Persistently dysregulated proteins FC values. Proteins dysregulated between *SNCA*-A53T and control cells in the same direction at five or more timepoints of the differentiation. Names and corresponding fold change (FC) values are indicated.

A.4 Differentially abundant metabolites

Differentially abundant metabolites identified at each timepoint of the differentiation ($p_{\text{adj}} < 0.05$ and |FC|>0.4). Fold changes are indicated in parentheses.

DAY 0

Aspartic acid (+1.83), Kynurenine (-2.11), Inosinic acid (-2.40), Fructose 1,6-bisphosphate (-1.47), Indole-3-acrylic acid (+1.28), Glucose-6-phosphate (-0.97), Tryptophan (+1.26), Thymidine (+3.50), Folic acid (+3.66), Nicotinamide (+1.31), Methionine (+1.43), Cystine (+3.22), Indole-3-acetaldehyde (+3.08), Uridine monophosphate (-1.13), Galactose (+2.83), Leucine (+1.01), Guanosine monophosphate (-0.73), Betaine (-0.83), Lactic Acid (-0.55), Choline (+0.47), Phenylalanine (+0.81), Guanosine triphosphate (-1.19), Isoleucine (+0.80), Adenosine diphosphate (-1.54), Taurine (-1.54), Citric acid (-0.62), Adenosine monophosphate (-1.89), Histidine (+2.07), 2-Hydroxyglutaric acid (-0.82), Cytidine monophosphate (-0.67), Adenosine triphosphate (-0.79), Guanosine diphosphate (-1.82), Pyridoxine (+0.83), Isobutyrylglycine (-0.99)

DAY 6

(-)-Riboflavin (+1.24), Cytidine (-1.52), Betaine (+1.39), Citric acid (-0.71), 3-(4-Hydroxyphenyl)propionic acid (+1.05), Kynurenine (+2.40), Malic Acid (-0.71), Fructose (-0.53), Fumaric acid (-0.74), Pyruvic acid (-0.62), Phosphoenolpyruvic acid (-0.60), Carnitine (+0.42)

DAY 15

(-)-Riboflavin (+1.94), Citric acid (-0.66), Threonine (-1.20), Cystathionine (+1.32), D-PANTOTHENIC ACID (+1.08), Guanosine triphosphate (-1.48), Tryptophan (+0.48), gamma-Aminobutyric acid (-0.81), Carnitine (+0.66), 2-Hydroxyglutaric acid (-0.84), biotin (+2.11), Leucine (+0.55), Indole-3-acrylic acid (+0.45), Cytosine (+1.70), Isoleucine (+0.65), Cytidine triphosphate (-1.19), Lactic Acid (+0.40), Indole-3-acetaldehyde (+1.17)

DAY 21

Inosinic acid (+3.65), Citrulline (+2.61), Epinephrine (+0.89), Taurine (+1.05), Cytosine (+0.85), biotin (+1.75), Fructose 6-phosphate (+0.59), Glucose-6-phosphate (+0.59), gamma-Aminobutyric acid (-1.19), (-)-Riboflavin (+1.45)

DAY 30

Cystathionine (-3.08), Thymidine (+3.32), Citrulline (+2.70), Choline (-1.20), Uridine monophosphate (+1.05), Cytosine (+1.54)